Structural alterations in the Valosin containing protein and their mechanistic link to neurodegeneration

Dalia Halawani

Department of Anatomy and Cell Biology
McGill University
Montreal, Quebec, Canada

A thesis submitted in partial fulfillment of the requirement of the degree of

Doctor of Philosophy

© Dalia Halawani, 2009

To my beloved parents, Nabil and Nejme Halawani, for their unconditional love and insurmountable support.

Table of Contents

Acknowledgments

I am deeply in debt to my thesis supervisors, Dr. Martin Latterich, now president and CEO of The Nicholas Conor Institute for Pediatric Cancer Research in San Diego, and Dr. Andréa C. LeBlanc, James McGill professor at the Department of Neurology and Neurosurgery at McGill University, for their exceptional mentorship. Dr. Latterich provided me with invaluable opportunities to meet and network with some of the most influential people in the field of Cell Biology. His openness and collaborative spirit helped inspire the course of my research and added a unique interdisciplinary dimension to my thesis work. Dr. Latterich's mentorship style emphasized creativity in scientific thinking and planning and helped me capitalize on my own strengths and over-come my weaknesses. Simple said, Dr. Latterich helped me grow as a scientist and gain confidence as an individual.

I am also very grateful to Dr. Andréa C. LeBlanc, for welcoming me into her laboratory and facilitating the smooth continuation of my thesis work following the departure of Dr. Latterich. Dr. LeBlanc is not only a mentor, but also a true inspiration for me as a "woman" in science. From Dr. LeBlanc, I learned the importance of endurance, perseverance, and hard work in facing challenges and achieving ones personal and professional goals. I saw how independence, originality, and novelty in scientific thinking and planning could inspire great discoveries. Dr. LeBlanc is truly my inspiration to be the best scientist I could be.

I sincerely thank Dr. Isabelle Rouiller, professor at the Department of Anatomy and Cell Biology at McGill University, for directing my use of the electron microscopy imaging and critically guiding the interpretation of my biochemical data. Her guidance helped provide an important structural context to my thesis work. I am also very much in debt to Dr. Marc J. Servant, professor in the Department of Pharmacy at Université de Montréal, for his openness,

guidance and support during my work at Université de Montréal. Furthermore, I warmly thank Dr. Stephen W. Michnick, professor at the Department of Biochemistry at Université de Montréal, for facilitating my use of protein fluorescence spectroscopy, and his exceptional collaborative spirit.

I am deeply grateful for Dr. Joelle Pelletier, professor at the Department of Biochemistry at Université de Montréal, and Dr. Christopher Clouthier, post-doctoral trainee at the Department of Biochemistry at Université de Montréal, for establishing and performing the simulation annealing molecular dynamics modeling studies. My warmest thanks are due to Dr. Annie Lequerriere, professor at the Department of Neuropathology in Rouen University Hospital (Paris, France) for providing me with precious human brain tissues. My thanks are also due to Dr. Steffen Albrecht for his help in the interpretation of the immunohistochemical data in my manuscripts.

I owe my sincerest gratitude to Dr. John Bergeron, head of the Department of Anatomy and Cell Biology at McGill University, Dr. Nathalie Lamache-Vane, professor and director of the Anatomy and Cell Biology Graduate Student Program at McGill University, Dr. Maryam Taherie, post-doctoral trainee at the Department of Anatomy and Cell Biology at McGill University, for generously providing excellent antibodies and essential reagents.

I am deeply grateful to Dr. Dirk Hubmacher and Dr. Dominique Anzellotti, post-doctoral trainees at the Department of Anatomy and Cell Biology at McGill University, for introducing me to the marvels of biochemistry and protein purification. I would like to thank Mr. Sylvain Tessier, M.Sc., for sharing his expertise on Mass Spectrometry, and Mrs. Jennifer Hammond. B.Sc., for generously sharing her expertise in cell culture and immunohistochemistry. Many thanks are also due to Dr. Julie Jodoin for her invaluable critique and engaging discussions.

My warmest thanks are due to my comprehensive examination committee and thesis committee in the Department of Anatomy and Cell Biology at McGill University for their exceptional support. Many thanks are due to Miss. Paresa Giannopoulos for elegantly translating my thesis abstract into the French language. Thank you to all my colleagues and coworkers at the Department of Anatomy and Cell Biology and the Lady Davis Institute for Medical Research, whose company helped define my experience at McGill University.

First-Authored Manuscripts

This thesis is submitted in a manuscript-based format. First-authored manuscripts constituting the core of this thesis work are listed in accordance to the guidelines of the Faculty of Graduate and Postdoctoral Studies at McGill University. Copies of published manuscripts are included in the Appendix section.

Chapter 1

Halawani, D and Latterich, M.

p97: The cell's molecular purgatory?

Published in *Molecular Cell*, 2006 Jun 23;22(6):713-7.

Chapter 2

Halawani, D, LeBlanc AC, Rouiller I, Michnick SW, Servant MJ and Latterich M.

Hereditary inclusion body myopathy-linked p97 mutations in the N-domain and the D1 ring modulate p97 ATPase activity and D2 $^{+}$ ring conformation.

Published in the *Journal of Molecular and Cellular Biology*, 2009 Aug;29(16):4484-94.

Chapter 3

Halawani, D, Tessier, S, Anzellotti, D, Latterich, M and LeBlanc, AC.

Targeting of the Valosin containing protein (p97) by active Casp6 in Alzheimer Disease: implications on ubiquitin proteasome system mediated protein degradation.

To be submitted to the Journal of Neuroscience, 2009

Chapter 4

Halawani, D, Clouthier, C, Pelletier, J, Latterich, M and LeBlanc, AC.

Conformational instability of the N-domain linked to caspase mediated proteolysis in p97-linked fronto-temporal dementia

To be submitted to Human Molecular Genetics, 2009

Contributions of Authors

Chapter 1

I researched and wrote "p97: the cell's molecular purgatory?". Dr. Martin Latterich conceptualized and critically evaluated the manuscript.

Chapter 2

I planned and conducted the research, and wrote the manuscript entitled "*Hereditary inclusion body myopathy-linked p97 mutations in the N-domain and the D1 ring modulate p97 ATPase activity and D2 ring conformation*". Dr. Andréa C. LeBlanc helped conceptualize the main message of the manuscript. Dr. Isabelle Rouiller assisted in the electron microscopy imaging of Figure 1E. Dr. Stephen W. Michnick critiqued the protein fluorescence spectroscopy data. Dr. Andréa C. LeBlanc, Dr. Isabelle Rouiller, Dr. Stephen W. Michnick, Dr. Marc J. Servant and Dr. Martin Latterich, critically evaluated the manuscript.

Chapter 3

The studies in the manuscript entitled "*Targeting of the Valosin containing protein (p97) by active Casp6 in Alzheimer Disease: implications on ubiquitin proteasome system mediated protein degradation*" were planned by Dr. Andréa C. LeBlanc and I. I performed all the experiments with the exception of the following: (1) the mass spectrometry sample preparation for Figure 3, which was performed by Mr. Sylvain Tessier, (2) Dr. Dominique Anzellotti cloned the constructs for p97ND1 and p97D2C fragments, (4) Mrs, Jennifer Hammond and I both preformed the immunohistochemistry, (5) Dr. Andréa C. LeBlanc imaged, prepared, interpreted, and wrote the immunohistochemistry section of the manuscript. I wrote the reminder of manuscript under the critical evaluation of Dr. Andréa C. LeBlanc.

Chapter 4

For the manuscript, "*Conformational instability of the N-domain linked to caspase mediated proteolysis in p97-linked fronto-temporal dementia"*, I planned and conducted research with the exception of the stimulation annealing modeling, which was constructed by Dr. Christopher Clouthier and Dr. Joelle Pelletier. Dr. Christopher Clouthier wrote the methods and results sections pertaining to the simulation annealing modeling. I wrote the remainder of the manuscript, including the discussion section under the critical evaluation of Dr. Andréa C. LeBlanc.

Collaborative Publications

As part of the scientific community in Montréal, Quebec, I engaged in two collaborations to which I contributed intellectually and provided useful reagents. Both of these collaborations involved investigations on mammalian p97 or its lower homologues, but do not constitute the core of this thesis work. Copies of these manuscripts are included in the Appendix section.

Appendix

Binette J, Dubé M, Mercier J, Halawani D, Latterich M, Cohen EA.

Requirements for the selective degradation of CD4 receptor molecules by the human immunodeficiency virus type 1 Vpu protein in the endoplasmic reticulum.

Retrovirology. 2007 Oct 15;4:75.

Caruso ME, Jenna S, Bouchecareilh M, Baillie DL, Boismenu D, Halawani D, Latterich M, Chevet E.

GTPase-mediated regulation of the unfolded protein response in Caenorhabditis elegans is dependent on the AAA+ ATPase CDC-48.

Mol Cell Biol. 2008 Jul;28(13):4261-74.

Abstract

The ubiquitin-dependent ATPase, p97, extracts ubiquitinated protein from macromolecular complexes by utilizing ATP-driven conformational changes. Consequently, p97 facilitates essential cellular quality control processes upstream of the proteasome, including endoplasmic reticulum associated degradation (ERAD) and ubiquitin fusion degradation (Ufd). Mutations in p97 are linked to an unusual muti-systemic disease (IBMPFD), involving skeletal muscle degeneration, Paget disease of bone, and fronto-temporal dementia, where the accumulation of ubiquitin-rich protein aggregates suggests impairment in p97-dependent activities. Interestingly, the accumulation of ubiquitin-rich aggregates is also well documented in common neurodegenerative diseases, such as Alzheimer Disease (AD). This thesis is focused on (i) understanding the structural and biochemical consequences of p97 mutations, and (ii) substantiating whether disruption of p97 cell biological function occurs in neurodegeneration. First, we employed a variety of biochemical and biophysical approaches to show that two p97 mutations, Arg155Pro and Ala232Glu, alter the conformational state and ATPase activity. We further demonstrated that these alterations were directly related to p97 protein aggregation in solution. Secondly, we identified p97 as a target of Caspase-6 (Casp6) proteolytic activity in AD and further demonstrated that the overexpression of a Casp6 cleaved p97 fragment compromises the ubiquitin-proteasome system (UPS). Finally, considering the role of IBMPFD-linked p97 mutations in activating caspases, we used simulation annealing modeling to provide evidence that structural defects in pathogenic p97 mutants enhanced p97 susceptibility to caspase-mediated processing. We further showed that p97 was indeed cleaved in dystrophic neurites and activated astrocytes of patients diagnosed with p97-linked fronto-temporal dementia (FTD). Collectively, this work identifies caspase-mediated cleavage of p97 as a novel mechanism for UPS impairment and suggests specific inhibitors of caspase activity as putative treatment strategies in neurodegeneration.

Résumé

La p97, une ATPase ubiquitine-dépendante, extrait des protéines ubiquitinées des complexes macromoléculaires en utilisant les changements conformationnels activés par l'ATP. Conséquemment, la p97 facilite les processus essentiels du contrôle-qualité cellulaire en amont du protéasome, incluant la dégradation associée au réticulum endoplasmique (ERAD) et la voie de dégradation des fusions ubiquitinées (Ufd). Les mutations dans la p97 sont liées à une maladie multisystémique inhabituelle (IBMPFD), impliquant comme effets la dégénération musculosquelettique, la maladie osseuse de Paget et la démence fronto-temporale, où l'accumulation d'aggrégats protéiques riches en ubiquitine suggère la perturbation des activités dépendantes à la p97. Il est intéressant de noter que cette accumulation d'aggrégats riches en ubiquitine est aussi bien démontrée dans les maladies neurodégénératives, telle que la maladie d'Alzheimer (MA). Cette thèse s'intéresse à (i) comprendre les conséquences structurales et biochimiques des mutations dans la p97, et (ii) confirmer si la pertubation de la fonction cellulaire biologique de la p97 s'observe dans la neurodégénération. D'abord, nous avons utilisé une variété d'approches biochimiques et biophysiques pour révéler que les deux mutations dans la p97, Arg155Pro et Ala232Glu, modifient l'état conformationnel et l'activité ATPase. Nous avons de plus démontré que ces altérations étaient directement liées à l'aggrégation protéique de la p97 en solution. Ensuite, nous avons identifié la p97 comme étant une cible de l'activité protéolytique de la Caspase-6 (Casp6) dans la MA et ainsi prouvé que la surexpression d'un fragment p97 clivé par la Casp6 compromet le système ubiquitine protéasome (UPS). Enfin, en tenant compte du rôle des mutations dans la p97 liées à l'IBMPFD dans les caspases activatrices, nous avons utilisé un modèle de simulation de l'appariement pour prouver que les défauts structuraux des mutants pathogéniques de la p97 font augmenter sa susceptibilité au clivage caspasique. Nous avons également indiqué que la p97 était effectivement clivée dans les neurites dystrophiques et les astrocytes activés chez des patients diagnostiqués de la démence fronto-temporale liée à la p97 (FTD). Ce travail dans l'ensemble identifie le clivage médié par une caspase de la p97 comme étant un nouveau mécanisme de perturbation de l'UPS et suggère des inhibiteurs spécifiques de l'activité caspasique comme stratégie putative de traitement de la neurodégénération.

List of Abbreviations

A	Alanine
AAA	ATPases Associated with various cellular Activities
AD	Alzheimer Disease
ADP	Adenosine di-phosphate
ADP.ALF$_3$	Adenosine di-phosphate Aluminum Fluoride
AEBSF	4-(2-Aminoethyl) benzenesulfonyl fluoride hydrochloride
Ala	Alanine
ALS	Amyotrophic lateral sclerosis
AMFR	Autocrine motility factor receptor
AMP-PNP	5'-adenylyl-beta,γ-imidodiphosphate
ANOVA	Analysis of variance
aPKC	Atypical protein kinase C
Arg	Arginine
ASCE	Additional strand, catalytic E
Asn	Asparagine
ATP	Adenosine tri-phosphate
ATPase	Adenosine tri-phosphatase
BLAST	Basic local alignment search tool
BiP	Binding immunoglobulin protein
C	Cysteine
Casp1	Caspase-1
Casp3	Caspase-3

Casp6	Caspase-6
Casp7	Caspase-7
Casp8	Caspase-8
Casp9	Caspase-9
Casp10	Caspase-10
Caspase	Cysteine-dependent aspartate proteases
Cdc48p	Cell division cycle 48 protein
CDD	Conserved domains database
CDK1	Cyclin dependent kinase 1
cDNA	Complementary DNA
CFTR	Cystic fibrosis transmembrane conductance regulator
CHAPS	3-[(3-Cholamidopropyl)dimethylammonio]-1-propanesulfonate
CHIP	Carboxyl terminus of Hsc70-interacting protein
CHMP2B	Charged multivesicular body protein 2B
CJD	Creutzfeldt Jakob disease
COOH	Carboxyl
Cryo-EM	Cryo-electron microscopy
CSF-1	Colony stimulating factor-1
CVFF	Constant valence free field
D	Aspartate
Der1p	Degradation in the endoplasmic reticulum 1 protein

Derlin-1	Degradation in the endoplasmic reticulum 1 protein-like protein 1
DLS	Dynamic light scattering
DNA	Deoxyribonucleic acid
Doa10p	Degradation of alpha 10 protein
DTT	Dithiothreitol
DUB	Deubiquitinating enzyme
E	Glutamate
ECL	Enhanced chemiluminescence
EDEM	ER degradation enhancing α-mannosidase-like protein
EDTA	Ethylenediaminetetraacetic acid
ER	Endoplasmic reticulum
ERAD	Endoplasmic reticulum associated degradation
FACS	Fluorescent activated cell sorting
FPLC	Fast performance liquid chromatography
FTD	Fronto-temporal dementia
FTDP-17	Frontotemporal dementia with Parkinsonism linked to chromosome-17
FTLD-U	frontotemporal lobe dementia with tau-negative and ubiquitin-positive inclusions
G	Glycine
Glu	Glutamine
Gly	Glycine

GNE	UDP-N-acetylglucosamine 2-epimerase / N-acetylmannosamine kinase
GTP	Guanosine tri-phosphate
GTPase	Guanosine tri-phophatase
HEPES	4-(2-hydroxyethyl)-1-piperazineethanesulfonic acid
His	Histidine
Hif-1α	Hypoxia induced factor-1α
HIM-6	High induced mutagenesis-6
Hmg2p	3-Hydroxy-3-methylglutaryl-coenzyme a reductase 2 protein
HPLC	High performance liquid chromatography
HRP	Horseradish peroxidase
Hsc70	heat shock cognate protein 70
IBM	Inclusion body myopathy
IBMPFD	Inclusion body myopathy associated with early onset Paget disease of bone and fronto-temporal dementia
IBR	In between RING
IκB-α	Inhibitor of NFκB-α
IKK	IκB kinase β
IPTG	Isopropyl β-D-1-thiogalactopyranoside
K	Lysine
KLH	Keyhole limpet hemocyanin

LC-MS/MS	Liquid chromatography tandem mass spectrometry
Leu	Leucine
LGMD	Limb girdle muscular dystrophy
LMNA	Lamin A/C gene
Lys	Lysine
MAPT	Microtubule associated protein tau
MCI	Mild cognitively impaired
MEM	Minimum essential media
MESG	2-amino-6-mercapto-7-methylpurine riboside
MHC	Major histocompatibility complex
MMSE	Mini mental state exam
MYHCIIA	Myosin heavy chains type II A
NCBI	National Center for Biotechnology Information
NCI	Non-cognitively impaired
ND1	Amino-terminal domain and D1 AAA ATPase domain
NFκB	Nuclear factor κ B
NFT	Neurofibrillary tangles
N	Amino
NID	Non-ionic detergent
Npl4	Nuclear protein localization-4
NSF	N-ethylmaleimide-sensitive factor
NTP	Nucleotide tri-phosphate
NTPase	Nucleotide tri-phosphatase

OD	Optical density
Otu1p	Ovarian tumor 1 protein
P	Proline
P-loop	Phosphate-binding loop
PARP	Poly (Adenoside di-phosphate-ribose) polymerase
Pas1p	Peroxin 1 protein
PC12	rat pheochromocytoma 12
PD	Parkinson disease
PDB	Protein data bank
PDB	Paget Disease of bone
Phe	Phenylalanine
PHF	Paired helical filaments
PIPES	Piperazine-N,N'-bis(ethanesulfonic acid)
PMSF	Phenylmethanesulphonylfluoride
Pro	Proline
p97D179↓	p97 cleaved at D179
R	Arginine
Rad23p	Radiation sensitive 23 protein
RANK	Receptor activator of nuclear factor κ B
RANKL	Receptor activator of nuclear factor κ B ligand
RING	Really interesting new gene
RIPA	Radioimmunoprecipitation assay buffer
RMSD	Root mean square deviation

RNAi	RNA interference
SAXS	Small angle X-ray scattering
S-phase	DNA synthesis phase
SCFfbs1,2	Skp1p/cullin/F box proteins 1 and 2
SDS-PAGE	Sodium dodecyl sulfate polyacrylamide gel electrophoresis
Sec17p	Secretory 17 protein
Sec18p	Secretory 18 protein
Sec61p	Secretory 61 protein
SHP1	Suppressor of high-copy PP1
SNARE	Soluble NSF attachment receptor
SOD-1	Superoxide dismutase-1
SP	Senile plaques
Spt23p	Suppressor of Ty
SQSTM1	Sequestosome-1
SRH	Second region of homology
STAT3	Signal transducer and activator of transcription 3
t-SNARE	Target-soluble NSF attachment receptor
v-SNARE	Vesicle-soluble NSF attachment receptor
TARDBP	TAR DNA binding protein
Tau∆Casp6	Tau cleaved by Casp6
TCEP	Tris(2-carboxyethyl)phosphine
TDP-43	TAR DNA binding protein-43
TEAB	Tetraethylammonium

TFA	Trifluoroacetic acid
Thr	Threonine
TLCK	Nα-Tosyl-Lys-chloromethylketone·Hcl
TNF	Tumor necrosis factor
TNFRSF	Tumour necrosis factor superfamily
TRAF6	TNF receptor associated factor 6
Trp	Tryptophan
Ub	Ubiquitin
UBA	Ubiquitin-associated domain
UBX	Ubiquitin-regulatory X domain
UCH-L1	Ubiquitin carboxyl-terminal hydrolase-L1
Ufd	Ubiquitin fusion degradation
UPR	Unfolded protein response
UPS	Ubiquitin proteasome system
Usa1p	U1-Snp1 associating 1 protein
V	Valine
v-SNARE	Vesicle soluble NSF attachment receptor
Val	Valine
VCIP135	Valosin-containing protein interacting protein 135
VCP	Valosin containing Protein
VIMP	VCP interacting membrane protein
WT	Wild-type
YT	Yeast tryptone

α	alpha-helical.
α-SNAP	α-soluble NSF attachment protein

List of Tables

Page

List of Figures

Page

CHAPTER 1: Introduction and literature review

1.1 The AAA protein superfamily: a subdivision of P-loop NTPases

Virtually all-essential cell biological processes, from DNA transcription to protein degradation, are chemically fueled by nucleotide-triphosphate (NTP) hydrolysis. While mitochondrial biochemical reactions secure the cellular NTP reserves, an abundant class of enzymes widely termed "phosphate-binding loop (P-loop) NTPases" drives NTP hydrolysis. P-loop NTPases can be simplistically classified into two major groups: (1) the Kinase-GTPase and (2) the Additional Strand, Catalytic E (ASCE) (Leipe et al. 2003; Iyer et al. 2004). Together, both groups represent ~ 10 to 18 % of prokaryotic and eukaryotic genomes (Koonin et al. 2000); and therefore, it is predicted that P-loop fold is by far the most abundant protein fold throughout evolution (Wolf et al. 1999). The P-loop fold is comprised of the Walker A motif or P-loop proper [GX4GKT/S, X represents any amino acid residue], and the highly variable Walker B motif (Walker et al. 1982; Saraste et al. 1990). The most common Walker B consensus sequence is ϕ_4D, where ϕ encodes any hydrophobic amino acid residue, and is characteristic to the Kinase-GTPase class. The ASCE class, however, deviates in the substitution of the aspartic acid residue in the Walker B motif for a glutamate, ϕ_4E (Leipe et al. 2003). Another distinguishing feature between the Kinase-GTPase and the ASCE class of P-loop NTPases is the structural arrangement of the P-loop fold relative to the Walker B motif. The P-loop is positioned adjacent to the Walker B motif in kinases and GTPases, but separated by an additional strand in the ASCE class (Leipe et al. 2003). Therefore, the acronym of ASCE, Additional Strand Catalytic E, excellently relays the distinguishing feature of this novel class of P-loop

NTPase. Despite these differences, the function of the Walker A and B motifs remains conserved in all P-loop NTPases: the Walker A motif mediates NTP binding, while the Walker B motif is involved in NTP hydrolysis.

AAA proteins represent a large sub-division of the ASCE class of P-loop NTPases. Members of this protein family are classified based on the presence of the AAA cassette which is comprised of ~ 230 to 250 highly conserved amino acids encompassing the Walker A and Walker B motifs (Kunau et al. 1993) and a unique second region of homology (SRH) domain (Erdmann et al. 1991; Beyer 1997; Guenther et al. 1997; Neuwald et al. 1999). The second region of homology domain is defined by the consensus sequence, X(T/S)(N/S) XXXXXDXAXXRXXRX(D/E), where X is a variable amino acid residue (Erdmann et al. 1991; Kunau et al. 1993), and encompasses highly conserved arginine "sensor" residues, which differentially modulate ATP-binding or hydrolysis [reviewed in (Ogura et al. 2004)]. The AAA cassette was first identified in 1991 by Erdmann and colleagues, during their characterizations of Pas1p in Yeast peroxisome biogenesis (Erdmann et al. 1991). In this study, Pas1p was shown to contain sequences 'strikingly' homologous to Sec18p/NSF and the Valosin containing protein (VCP) and its respective Xenopus homologue, p97 (Erdmann et al. 1991). These sequences were later designated the AAA acronym by Kunau and colleagues in 1993 (Kunau et al. 1993). Currently, a standard search using the Conserved Domains Database (CDD) on the National Center for Biotechnology Information (NCBI) web-engine identifies 18 superfamilies and 52

families of proteins containing the AAA domain throughout all sequenced prokaryotic and eukaryotic genomes. Accordingly, AAA proteins represent some of the most ubiquitous and highly conserved proteins throughout evolution.

1.2 The discovery of Cdc48p and its higher vertebrate homologue (p97)

The discovery of Yeast Cdc48p and mammalian p97 (also named the Valosin containing protein, VCP) occurred independently. CDC48 was first discovered in 1982 by Moir and colleagues (Moir et al. 1982) in a study aimed at identifying cell cycle genes in Saccharomyces cerevisiae (*S. cervisiae*). Using a forward genetics approach combined with a yeast complementation analysis, CDC48 was identified as an affected gene in yeast mutant strains displaying defects in medial nuclear division. Five years later, in 1987, Koller and Brownstein conducted a search for a presupposed precursor of a biologically active peptide named "Valosin". Using a porcine adrenal medulla complementary DNA (cDNA) library, Koller and Brownstein showed that the peptide, "Valosin" represented amino acid resides 493-517 of an 806 amino acid precursor, and hence assigned the name, Valosin-containing protein. However, the fact that VCP tissue expression was reported to be ubiquitous, its N-domain lacked a signal peptide for secretion, and it did not contain any known protease processing sites, led to the conclusion that "Valosin" was an artifactual product of the chymotryptic digestion of VCP during purification. Nevertheless, the study established that VCP was a predominantly cytosolic protein of an unknown function.

In 1990, Peters and coworkers provided first clues to the biochemical activity of p97. In an effort to characterize macromolecular complexes within the S100 fraction of Xenopus oocyte extracts, a widespread 14.5S particle was detected (Peters et al. 1990); and it was the distinction between the 14.5S particle and the 20S proteasome that rationalized further investigation into its identity. Unlike the 20S proteasome, the 14.5S particle was predominantly comprised of a 97 kDa protein, and hence termed, p97. Importantly, Peters et al. reported for the first time that p97 formed homo-oligomeric, ring-shaped complexes with a 6-fold radial symmetry and measurable ATPase activity. Furthermore, using cloning and sequencing techniques, p97 was shown to be highly homologous to VCP, and the vesicle-fusion proteins, mammalian N-ethylmaleimide sensitive factor (NSF) and yeast Sec18p. This study was seminal since it identified p97 as an ATPase, provided clues to its structure, and pointed to its strong relationship to vesicle fusion proteins in the endocytic pathway (Peters et al. 1990).

The link between Cdc48p and p97 was first identified in 1991 by Fröhlich and colleagues (Frohlich et al. 1991) who cloned and sequenced CDC48. Fröhlich and colleagues showed that Cdc48p shared a sequence identity of 69.5% with the previously identified VCP, 46.6% with Sec18p, and 47.7% with NSF. It was concluded that VCP is the mammlian homologue of yeast Cdc48p and that Sec18p, NSF, VCP, and Cdc48p are all members of a novel ATPase superfamily. Furthermore, based on the phenotype of CDC48 mutant strains, it

was proposed that Cdc48p may regulate cell division through some "vesicle-related" biochemical activity. While these results confirmed what Erdmann and colleagues had previously reported on the evolutionary relationship between these proteins, it was not until 1995 that the first cell biological role of Cdc48p was identified in endoplasmic reticulum (ER) membrane fusion (Latterich et al. 1995).

1.3 p97 biochemical activities

1.3.1 p97 in the post-mitotic biogenesis of the endoplasmic reticulum and Golgi apparatus

Cell division requires not only the faithful duplication and transfer of genetic material between two daughter cells, but also the partitioning of organelles between the two newly defined cytoplasmic compartments. Unlike the Golgi apparatus, which fragments at the onset of mitosis, the ER remains relatively intact and polarizes at the spindle poles. Depending on the cell type, the cortical ER network flanking the plasma membrane could also pinch off into two daughter cells during cytokinesis. Once partitioned, ER membranes serve as templates for further membrane expansion and growth (Warren 1993; Powell and Latterich 2000). The minimal biochemical requirements for ER membrane fusion were first resolved in elegant studies by Latterich and Schekman, where ER membrane fusion was reconstituted in vitro (Latterich and Schekman 1994). The fusion of donor and acceptor ER derived microsomes was shown to be protein dependent and to occur only in the presence of ATP and an ATP regeneration

system. Surprisingly, NSF/Sec18p, an important mediator of vesicle transport within the Golgi stalks (Malhotra et al. 1989) and the endocytic pathway (Diaz et al. 1989), and its associated receptor, α-Soluble NSF Attachment Protein, SNAP/Sec17p (Weidman et al. 1989; Clary et al. 1990), were both not required for ER-membrane fusion. In an attempt to identify the components of the ER-membrane fusion machinery, Cdc48p represented a likely candidate based on its strong homology with NSF and the mitotic defect associated with its mutation in yeast strains (Latterich et al. 1995). Indeed, using the in vitro ER membrane fusion reconstitution assay, Latterich and colleagues demonstrated that (1) cell cycle arrested Cdc48p mutant yeast strains were indeed defective in ER membrane fusion, (2) Cdc48p blocking antibodies inhibited ER membrane fusion in wild-type yeast strain, (3) concentrated cytosol of wild-type, but not mutant, Cdc48p yeast strains rescued the membrane fusion defect, and (4) purified Cdc48p restored ER membrane fusion in a dose dependent manner (Latterich et al. 1995). Accordingly, the first biochemical function of Cdc48p was identified in ER-membrane fusion.

Parallel studies on the mammalian homologue, p97, demonstrated its involvement in Golgi stack reformation following mitotic vesiculation (Acharya et al. 1995; Rabouille et al. 1995). These studies initiated a debate on whether p97's role in Golgi biogenesis was functionally redundant with NSF. On the one hand, Acharya and colleagues proposed that Golgi biogenesis occurred in two steps: fusion of small vesicles into larger ones followed by stalk and cisternae

formation. In this process, NSF mediated the fusion of larger vesicles, while p97 was involved in the morphogenesis of the stalk and cisternae structures characteristic to the Golgi (Acharya et al. 1995). Conversely, parallel studies by Rabouille and coworkers demonstrated that both NSF and p97 could support stalk and cisternae formation, however, each resulted in morphologically distinct structures (Rabouille et al. 1995). While the discrepancy between both studies could be due to the type and nature of the membrane preparations used in the fusion assays, both studies confirmed a role for p97 in the biogenesis of the Golgi from vesiculated membrane components.

1.3.1.1 Biochemical requirements of p97 fusogenic activity

The soluble NSF Attachment receptor (SNARE) hypothesis has been proposed to explain the mechanism of membrane fusion (Sollner et al. 1993). It postulates that membrane fusion is enabled by the pairing of a vesicle SNARE (v-SNARE) with a cognate SNARE on a target membrane (t-SNARE) thereby forcing the lipid bi-layers to interact and fuse. Structurally, SNAREs interact in a leucine-zipper-like manner facilitated by the pairing of their alpha-helical domains (Sutton et al. 1998) which extend into the length of the lipid bi-layer (Stein et al. 2009). The specificity of SNARE pairing, in turn, determines the fusogenic capacity of two membranes. However, prior to pairing, docked v-SNARE-t-SNARE complexes must be dissociated by an energy-driven reaction mediated by NSF and its SNARE receptor, α-SNAP. The dissociation reaction forces the

antiparallel v-SNARE-t-SNARE complex to adapt a parallel conformation favouring pairing and subsequent lipid bi-layer fusion (Sollner et al. 1993).

Analogous to the role of α-SNAP in NSF recruitment to SNARE-complexes, p47/SHP1 was identified as an essential cofactor of p97 in membrane fusion (Kondo et al. 1997). Interestingly, p97-p47 complex is in competition with the NSF-α-SNAP complex for the engagment of the t-SNARE, syntaxin-5 (Rabouille et al. 1998; Roy et al. 2000) on ER and Golgi membranes. This mutually exclusive interaction mode is reflected in the fact that p47 and α-SNAP utilize the same binding sites on syntaxin-5. Surprisingly, unlike the NSF-SNAP complex, which utilizes ATP-hydrolysis in dissociating from syntaxin-5 (Sollner et al. 1993), the p97-p47/syntaxin-5 trimer remains stable in the presence of ATP (Rabouille et al. 1998), and an additional cofactor, VCP interacting protein 135 (VCIP135) interacts with both p97 and syntaxin-5 to dissociate the complex (Uchiyama et al. 2002) in an ATP-dependent manner.

Golgi membrane fusion must be timely orchestrated at the onset of telophase and precluded during mitosis. Accordingly, the interaction between p97-p47, syntaxin-5 and VCIP135 is necessarily highly regulated throughout the cell-cycle. In interphase, p47 localization is usually nuclear and fragmentation of the nuclear envelope during mitosis is accompanied by CDK1-mediated phosphorylation of p47 (Uchiyama et al. 2003). Phosphorylation of p47, in turn, prevents p47 untimely recruitment to Golgi membranes following nuclear membrane fragmentation. Interestingly, p47 phosphorylation occurs in parallel

with the ubiquitination of unknown targets on the Golgi membranes during fragmentation. Considering that p47 employs an N-terminal ubiquitin-associated domain (UBA) in binding to Golgi membranes (Meyer et al. 2002), p47 phosphorylation likely prevents the association of p47 with a ubiquitinated Golgi membrane target. Conversely, in telophase, p47 is dephosphorylated and subsequently recruited along with p97 to its ubiquitinated Golgi membrane receptor (Uchiyama et al. 2003), however, membrane fusion only occurs in the presence of VCIP135 (Wang et al. 2004). VCIP135 plays several important roles in p97-mediated membrane fusion. First, both VCIP135 and p47 utilize similar highly conserved ubiquitin-regulatory X (UBX) domains and likely compete for the same binding site on p97 (Uchiyama et al. 2002). Second, VCIP135 is hypothesized to release the conformational "grip" of the p47 trimer on p97 (Kondo et al. 1997) which inhibits p97 ATPase activity (Meyer et al. 1998). In doing so, VCIP135 allows p97 to hydrolyse ATP and thereby dissociate the complex (Wang et al. 2004). Lastly, VCIP135 also precludes the reassembly of the p97 complex by catalyzing the removal of the regulatory ubiquitin moiety on the Golgi apparatus (Wang et al. 2004). These findings indicate that the role of p97 in membrane fusion is highly regulated by p47 phosphorylation and VCIP135 deubiquitination activity.

Recently, a novel p97-dependent pathway has been identified and demonstrated to be essential for Golgi and ER maintenance during interphase as well as in membrane reassembly at exist of mitosis (Latterich 2006; Uchiyama et

al. 2006). p97 forms a complex with VCIP135 and p37, a newly identified orthologue of p47, which distinctly target the SNARE, GS15. Similar to p47, p37 also interacts with p97 via a UBX domain, however, p37 lacks a UBA domain and shows no evidence of interactions with any form of ubiquitin. In addition, VCIP135 facilitates p97-p37 role in membrane fusion independent of its deubiquitinating activity and the role of p97-p37-VCIP135 in membrane fusion is known to be ubiquitin independent (Latterich 2006; Uchiyama et al. 2006). Interestingly, the total cellular ubiquitination activity is least prominent during interphase, a fact which may explain the necessity for a ubiquitin-independent pathway in organellar maintenance in this resting phase of the cell cycle. Accordingly, it is not surprising that p37 expression is most abundant in post-mitotic tissues, such as the brain (Latterich 2006; Uchiyama et al. 2006). Therefore, it appears that ubiquitination is required for the temporal regulation of p97 activity in membrane fusion and that p97 is mechanistically able to mediate membrane fusion independent of ubiquitination.

1.3.1.2 p97 as a molecular motor in the retrotranslocation of misfolded proteins from the ER lumen into the cytosol

Considerable progress has been made in characterizing the role of p97 in ERAD, a process involving the ATP-powered transport of misfolded proteins from the ER lumen, through a protein channel, and into the cytosol (Tsai et al. 2002). In ERAD, p97 functions at the cytosolic phase of the retrotranslocation channel and couples substrate retrotranslocation to its ubiquitination and subsequent

degradation by the proteasome (Ye et al. 2001; Jarosch et al. 2002). The role of p97 in ERAD is mediated by several adaptor proteins: (1) a heterodimeric complex comprised of nuclear localization protein 4 (Npl4) and ubiquitin fusion degradation protein 1 (Ufd1) (Ye et al. 2001), (2) VCP interacting membrane protein (VIMP), a transmembrane protein with a lengthy cytosolic COOH-terminal domain (Ye et al. 2004), and (3) Derlin-1 (Lilley and Ploegh 2004; Ye et al. 2004), a candidate ER-retranslocation channel analogous to Sec61p (Lilley and Ploegh 2004). Accordingly, a model is proposed in which the cytosolic tail of VIMP is utilized in baiting the N-domain of p97Ufd1/Npl4, and thereby recruiting the extraction machinery to the membrane. Meanwhile, on the luminal side, a rigorous quality control system of ER luminal chaperones is thought to shuttle misfolded proteins to Derlin-1 for subsequent retrotranslocation across the ER membrane. As substrates emerge from the ER, they are subjected to ubiquitination- a post-translational modification required for interaction with the Ufd1/Npl4 heterodimer (Ye et al. 2004). However, in other instances, p97 can aid in substrate retrotranslocation independent of ubiquitination (Rodighiero et al. 2002). In either case, non-ubiquitinated proteins are released into the cytosol, while ubiquitinated proteins are quickly shuttled to the proteasome.

The novel role of p97 in the retrotranslocation of misfolded proteins across the ER membrane, as opposed to the remodeling of integral membrane proteins as in membrane fusion, is supported by several findings. First, the mode of p97 interaction with VIMP is independent of ATP and Ufd1/Npl4 binding, and

therefore, the possibility of VIMP serving as a substrate for p97 is ruled-out (Ye et al. 2004). Secondly, the fact that VIMP and Derlin-1 are found to associate transiently with poly-ubiquitinated proteins is consistent with a role in protein degradation and not the refolding of newly synthesized secretory proteins (Ye et al. 2004). Furthermore, RNAi-mediated knockdown of Derlin in *C. elegans* elicits a moderate unfolded protein response (UPR) (Ye et al. 2004), and Derlin protein expression is upregulated in response to ER stress (Oda et al. 2006). While the mechanism of Derlin-mediated substrate recognition in the ER lumen is hitherto unclear, it is possible that Derlin is gated by ER chaperones in a manner analogous to BiP gating of the Sec61 translocation channel (Alder et al. 2005). Alternatively, Derlin could interact with a specific subset of ER transmembrane proteins, such as the ER degradation enhancing α-mannosidase-like (EDEM) protein or other lectins, which could confer the specificity of the targeted substrates (Hosokawa et al. 2001; Gnann et al. 2004). Also, the lack of VIMP homologues in invertebrates is somewhat perplexing considering that the ERAD machinery is a highly conserved cellular apparatus (Ye et al. 2004). It is tempting to speculate the VIMP may have evolved to further stabilize p97 on the membranes, thereby representing an added specialization in more complex systems. Alternatively, other novel and highly conserved luminal and transmembrane components may need to be identified.

1.3.2 The role of ubiquitination in p97-mediated retro-translocation across the ER membrane

The role of ubiquitination in p97-mediated ERAD has been subject to recent intense investigation. Since the identification of Hrd1p, an E3 ubiquitin ligase, as part of the Cdc48p retrotranslocation complex, it became evident that p97/Cdc48p actively coupled substrate retrotranslocation with ubiquitination to ensure the efficient degradation of misfolded proteins (Bays et al. 2001). p97/Cdc48p was subsequently established as a central convergence point for interaction with specific E3 ubiquitin ligase complexes in specialized ERAD pathway (Ye et al. 2005; Grou et al. 2009). For example, misfolded luminal ER proteins are degraded by the Hrd1p/Hrd3p ligase complex through the ERAD-L pathway. Proteins with misfolded intramembrane domains are degraded through the ERAD-M pathway, which uses the same Hrd1p/Hrd3p complex, albeit in a manner independent of Der1p and the linker protein, Usa1p. The third pathway is ERAD-C, which specializes in the degradation of membrane proteins with misfolded cytosolic domains using the Doa10p ligase (Carvalho et al. 2006). However, it is important to note that the distinction amongst the three pathways is not definitive, as Doa10p is also involved in the degradation of proteins with misfolded transmembrane domains in the ERAD-M pathway (Nakatsukasa et al. 2008). In addition to coupling ubiquitination with retrotranslocation, it is postulated that Cdc48p actively facilitates the extraction of misfolded transmembrane proteins from the ER and the maintenance of their soluble state in the cytosol (Nakatsukasa et al. 2008).

While ubiquitination facilitates and improves the efficiency of retrotranslocation, evidence suggests that p97-mediated retrotranslocation is also possible in the absence of ubiquitination (Abujarour et al. 2005; Kothe et al. 2005). For example, Cholera toxin displays two characteristics : (1) it is intrinsically a poor substrate for ubiquitination due to the scarcity of lysine residues in its primary amino acid sequence, and (2) it demonstrates a high intrinsic capacity for refolding following denaturation (Rodighiero et al. 2002). In spite of these characteristics, cholera toxin is retrotranslocated in a p97 dependent manner and expression of dominant negative p97 halts its transport (Abujarour et al. 2005; Kothe et al. 2005). Accordingly, whether ubiquitination serves as a prerequisite for retrotranslocation likely depends on the identity of the ERAD substrate. p97 is known to interact with ubiquitinated proteins as well as non-modified polypeptide chain. For ubiquitinated substrates, interaction with p97 is likely reinforced by the recruitment of its ubiquitin-binding partners, Ufd1/Npl4. This in turn may facilitate the retrotranslocation process by stabilizing the unfolded conformation of the substrate (Ye et al. 2003).

1.3.3 p97 in the regulation of protein stability

The well-established requirement for p97 in ERAD strongly hints at a mechanistic role in substrate ubiquitination, extraction, and subsequent delivery to the proteasome. However, this ascribed function is in striking contrast to the apparent role of p97 in organelle membrane fusion, which implicates p97 in substrate deubiquitination rather than degradation. A number of recent studies

now establish a novel paradigm where p97 could positively or negatively regulate substrate stability through manipulation of the ubiquitin conjugation and deconjugation machineries.

It is commonly preconceived that substrates must first be processed by the ubiquitin-conjugation machinery prior to their recognition and recruitment by p97 ubiquitin-dependent adaptors. Emerging data, however, point to an active role for p97 in substrate recognition and presentation to ubiquitin ligases. Cdc48p is able to function in a novel ubiquitin-fusion degradation pathway, along with its binary partner, Ufd1p/Npl4p, and the specialized E3/E4 ligase, Ufd2p. These proteins form a stable complex that catalyzes the extension of oligo-ubiquitinated chains. Importantly, complex stability appears contingent on the simultaneous assembly of all components, hinting that Cdc48p may mediate substrate presentation to the ubiquitin conjugation machinery (Richly et al. 2005). Consistently, several recent reports highlight functional interactions between p97 and various E3 ligases (Table 1.1), including the ERAD-linked SCFfbs1,2 (Skp1p/cullin/F box protein), and Dorfin, a RING-IBR ligase that is elevated in neurodegenerative conditions (Ishigaki et al. 2004; Yoshida et al. 2005). For example, SCF employs two F box protein receptors (fbs1 and fbs2) to link misfolded N-glycosylated ERAD substrates to p97. Surprisingly, active ATP hydrolysis by the p97 D2 ring is necessary for Fbs1-mediated substrate recognition, suggesting that p97 is mechanistically required prior to SCFfbs1,2 complex recruitment. Similarly, an ATPase-deficient p97 mutant abolishes Dorfin-mediated recognition and ubiquitination of superoxide dismutase-1 (SOD-1). Therefore, it appears that

substrate accessibility to p97 is a prerequisite for coupling E3 ligase activity to select target substrates.

The mechanistic basis of p97 participation in substrate ubiquitination remains elusive. The fact that Cdc48p interaction with ubiquitinated substrates and Ufd2p is concomitantly reduced in *ufd1-2* and *npl4-1* mutant strains indicates that some target substrate must first be recruited by adaptor proteins prior to E3 complex assembly (Richly et al. 2005). Given that Ufd2p has an unusual role in catalyzing the elongation of preassembled oligo-ubiquitinated chains, it is possible that to ensure the timely degradation of substrates, p97 may couple an extraction step with the multiubiquitination process, whereby target substrates are already oligo-ubiquitinated and present as an integral part of a larger macromolecular assembly. Remarkably, Cdc48p has been shown to restrict the length of Ufd2p-assembled ubiquitin chains in vitro. This is especially important considering that the length of the multiubiquitin chain has a modulating effect on the efficiency of recognition and degradation by the 20S proteasome. Once processed, arrested degradation substrates are then channeled to the trimeric Ufd2p/Dsk2p/Rad23p complex, which in turn mediates their transfer from Cdc48p to the proteasome (Richly et al. 2005).

Just as it is able to interact with the ubiquitin conjugation machinery, Cdc48p is now identified as a constituent of distinct complexes that either inhibit E3 interaction or actively deubiquitinate the substrate. Strikingly, both Ufd2p and

the WD40-motif protein Ufd3p compete for interaction with Cdc48p and share the same docking site on its COOH-terminal domain, with Ufd3p having preferentially the higher binding affinity (Rumpf and Jentsch 2006). Consequently, depending on the cofactor associated with the complex, Cdc48p can either promote or inhibit the ubiquitination process for a common substrate. For example, the degradation of Ub-proline-β-galactosidase is accelerated with Ufd2p overexpression but conversely repressed by Ufd3p upregulation. Similarly, an Ufd3p deletion mutant, containing only its Cdc48p binding site, dominantly inhibits the degradation of model UFD substrates. Better yet, even if the substrate is already ubiquitinated, Cdc48pUfd1/Npl4 is able to assemble a deubiquitinating complex with both Otu1p (yeast homologue of VCIP135), a member of the Ovarian Tumor family with a ubiquitin-hydrolase activity, and Ufd3p. This complex, in turn, competes with Ufd2p in the processing of its well-characterized substrate in the OLE pathway, the transmembrane transcription factor Spt23p. Therefore, depending on the cellular metabolic demands, Cdc48p is able to participate in opposing functions, which can either involve the ubiquitination and activation of Spt23p or its deubiquitination and stabilization on the ER membrane. Interestingly, in addition to Cdc48p activity, the common denominator in this process is the requirement of the Ufd1p/Npl4p heterodimer, which helps bridge Cdc48p to its substrate (Rumpf and Jentsch 2006).

These findings together establish a novel role for p97/Cdc48p in regulating substrate turnover and raise more questions surrounding the underlying

biochemical basis of its mechanism. The fact that p97 is considerably more abundant than its partners suggests that cofactor expression, stability, or localization may all be important determinants of the identity of the assembled complexes. Alternatively, p97 and its cofactors may be subject to a dynamic post-translational modification process that determines the identity of the assembled complex within pockets of cellular microdomains and according to specific metabolic demands. This would not be surprising considering that the cell cycle dependent phosphorylation of p47 by Cdc2 regulates its localization on the ER and Golgi membranes and may subsequently affect its interaction with p97 (Uchiyama and Kondo 2005). Similarly, AKT-mediated phosphorylation regulates p97 interaction with ubiquitinated substrates, although it is unclear whether this is a direct effect on substrate binding or a mere consequence of abolishing cofactor binding (Klein et al. 2005). Furthermore, p97 may also assume the role of a protein-proofing chaperone that has coevolved to alleviate the metabolic pressures of protein synthesis and degradation. Depending on conformational recoverability, a crucial decision must be made to either ubiquitinate and degrade or deubiquitinate and recycle target substrates (Fig. 1.1). A better mechanistic understanding of p97 function, especially its potential role in protein unfolding or complex disassembly, is evermore pressing considering the scope and complexity of its interaction with the ubiquitin modification machinery (Halawani and Latterich 2006).

1.3.4 p97 in the regulation of apoptotic cell death

1.3.4.1 Overview of apoptosis and the role of the Caspase protease family in its execution.

The word “apoptosis” describes a highly regulated and energy demanding process undergone by the cell to initiate its own death in response to intrinsic or extrinsic stimuli (Kerr et al. 1972). Morphological markers of apoptosis include chromatin condensation, nuclear DNA fragmentation, cytoplasmic vacuolization, membrane blebbing, and phosopholipid phophatidylserine translocation from the inner to the outer lipid bilayer (Galluzzi et al. 2009). The cysteinyl proteases, caspases, are crucial mediators of both the intrinsic and extrinsic apoptotic pathways (Li et al. 1997; Zou et al. 1999). The human genome contains 11 genes encoding Caspase-1 to Caspase-10 and Caspase-14 (Li and Yuan 2008). Generally, the caspase genes are translated into inactive single polypeptide chains encompassing a prodomain, a large subunit containing the catalytic site, and a small subunit. Activation occurs through the proteolytic processing of the three subunits and the subsequent assembly of two large and two small subunits into tetramers (Fuentes-Prior and Salvesen 2004). Caspases can be simplistically classified into initiator caspases (Caspase-1, -2, -4, -5, -8, -9, -10, -11, -12), and effector caspases (Caspase-3,-6,-7) (Li and Yuan 2008). Initiator caspases have very few identified substrates, which generally include their own precursors and/or other caspases and are therefore deemed responsible for initiating the apoptotic cascade. On the other hand, effector caspases are responsible for the massive proteolysis of cellular proteins or “executing” apoptosis (Li and Yuan 2008).

Apoptotic cell death can be initiated through either an intrinsic or an extrinsic pathway. The intrinsic apoptotic pathway involves the release of mitochondrial cytochrome c into the cytosol and its subsequent incorporation into a complex with apoptotic peptidase activating factor 1 (APAF-1) and the initiator caspase, Caspase-9 (Casp9). Casp9 in turn processes and activates the latent effector caspases, Caspase-3 (Casp3) and Caspase-7 (Casp7), and thereby initiates a cascade of proteolytic degradation of essential cellular proteins. Conversely, the extrinsic apoptotic pathway involves the activation of the death-inducing signaling complex though the engagement of the FAS receptor and activation of the initiator caspases, Caspase-8 (Casp8) or Caspase-10 (Casp10). As for Casp9, Casp8 and Casp10 are indirectly responsible for executing apoptosis through the activation of Casp3 and Casp7 (Vercammen et al. 1998; Scaffidi et al. 1999).

The classification of caspases as either initiators or effectors of apoptosis is rather simplistic. For example, effector Casp6 activation in primary human neurons leads to an alternate form of cell death that is distinct from apoptosis (LeBlanc et al. 1999 and Zhang et al. 2000). Moreover, the functional distinction amongst effector caspases in apoptosis was recently highlighted in a study by Nikolaev and colleagues, where Casp3 activation was found to be associated with neuronal cell body death, while Casp6 activation initiated axonal degeneration without cell body death (Nikolaev et al. 2006). These results are consistent with earlier report by Guo and colleagues where Casp6 activation was demonstrated in pathological hallmark of Alzheimer Disease, where neuronal

degeneration also occurs in the absence of apoptotic cell death (Guo et al. 2004 and Albrecht et al, 2009). Accordingly, caspases may have proteolytic roles independent of apoptosis.

1.3.4.2 Evidence for p97 involvement in apoptotic cell death

The first evidence for p97 involvement in the regulation of cell survival emerged from a study by Shirogane and colleagues who identified p97 as a mediator of cell survival in the STAT3 antiapoptotic pathway. In this study, p97 expression was strongly upregulated in response to Pim-1, a serine/threonine kinase involved in the regulation of STAT3, expression and p97 overexpression partially mimicked the prosurvival effects of Pim-1. Interestingly, the role of p97 in mediating cell survival was also shown to be dependent on p97 ATPase activity (Shirogane et al. 1999). This observation merited analysis of the role of p97 in cell survival. Indeed, transfection of an ATPase deficient p97 variant, p97K524A, in PC12 cells induces vacuolization of the rough ER and apoptosis (Hirabayashi et al. 2001; Kobayashi et al. 2002). Furthermore, RNAi-mediated depletion of p97 also leads to ER vacuolization, p53 induction, Casp3 and Casp7 activation, and PARP cleavage (Wojcik et al. 2004; Wojcik et al. 2006). These studies suggest that functional p97 is necessary for cell survival. Exactly how p97K524A mutant induces apoptosis remains elusive. Studies on Cdc48p suggest that impairment in ATPase activity induces apoptosis through a mitochondrial pathway involving oxidative stress, mitochondrial membrane depolarization and activation of the yeast metacaspase protein (Madeo et al.

1997; Madeo et al. 1999). Accordingly, it is possible that dysfunction in mammalian p97 ATPase activity may lead to apoptotic cell death through the activation of the intrinsic apoptotic pathway.

1.3.5 Other less characterized cellular roles for p97 in DNA replication and repair

In addition to its participation in membrane fusion, ERAD, and ubiquitin fusion degradation (Ufd), p97 also facilitates mitotic exit by regulating mitotic spindle disassembly (Cao et al. 2003) and chromatin decondensation (Ramadan et al. 2007). In mitotic spindle disassembly, p97 interacts with spindle assembly factors and chaperones their release from the microtubules at the end of mitosis (Cao et al. 2003). Furthermore, Cdc48 is required for the stability of the separase proteolytic complex during anaphase and is therefore an indirect facilitator of the separation of sister chromatids during mitosis (Ikai and Yanagida 2006). On the other hand, chromatin decondensation is indirectly promoted by p97-mediated extraction of the ubiquitinated Aurora B kinase (Ramadan et al. 2007). p97 is also implicated in DNA replication since its depletion delays S-phase progression and reduces the total DNA content (Mouysset et al. 2008). The involvement of p97 in DNA replication and repair is also supported by its interaction with the human Werner RecQ helicase (Partridge et al. 2003; Indig et al. 2004) and the Bloom Syndrome helicase homogue, HIM-6, in *C. elegans* (Caruso et al. 2008). Nevertheless, the exact mechanisms regulating p97 participation in these activities remain elusive.

1.4. The structure of p97 and its relationship to function

1.4.1 The general structural features of p97

p97 is comprised of 806 amino acids encompassing an N-domain (residues 1-187), two homologous AAA domains, D1 (residues 208-459) (Zhang et al. 2000) and D2 (residues 481-761), and a COOH-terminal domain (residues 761-806) (DeLaBarre and Brunger 2003) (Fig. 1.2). p97 also contains two short linkers, N-D1 (residues 188-207) (Zhang et al. 2000) and D1-D2 (residues 460-480) which ensure the flexible interconnectivity of all domains (DeLaBarre and Brunger 2003) (Fig. 1.2). Intermolecular interactions between the AAA domains of a p97 monomer and their counterpart AAA domains in other monomers enable the assembly of a hexameric ring-shaped structure (DeLaBarre and Brunger 2003) (Fig. 1.3) . Within the hexamer, the D1 and D2 rings are vertically stalked in a "head to tail" arrangement with six flexible N-domains protruding out of the D1 AAA ring (DeLaBarre and Brunger 2003) (Fig. 1.3). The orientation of the COOH-terminal domain relative to the D2 AAA ring is not currently known considering its disordered structure and lack of sufficient resolution by X-ray crystallography (DeLaBarre and Brunger 2003). The D1 and D2 rings form a central pore spanning the vertical axis of the hexamer (Fig. 1.3). The shape of this pore mimics two cones joined through their bottom and flaring out towards the top and bottom of the hexamer (DeLaBarre and Brunger 2003). The hexameric assembly of p97 is highly favoured and likely occurs spontaneously following translation (Wang et al. 2003). p97 hexameric structure is also highly resistant to acid and alkaline denaturation and requires concentrations as high as

6 M urea for disassembly (Wang et al. 2003). Furthermore, p97 hexamerization is required for its ATPase activity as monomeric p97 has negligible activity (Wang et al. 2003).

1.4.2 The N-domain

The N-domain of p97 forms two equally sized subdomains, with the distal subdomain encompassing a double-ψ β-barrel fold (residues 25-106) and the proximal subdomain forming a β-clam fold (residues 112-186) (Fig. 1.4A-D). The interphase between the two subdomains represents a putative hydrophobic protein binding pocket which also contains a short linker of six amino-acids, 107DVKYGK111 (Zhang et al. 2000) (Fig. 1.4 A-D). Functionally, the N-domain of p97 carries a nuclear localization sequence, 59LKGKKRR65 (Fig. 1.4 B), and mediates p97 interaction with many adaptor protein complexes, such as VCIP135, Ufd1/Npl4, Ubx-domain proteins (p47, p37, and UBX-2), and Werner RecQ helicase (Dr. Dominique Anzellotti, unpublished data). Furthermore, p97 N-domain also interacts with ubiquitin and polyubiquitin chains. Mechanistically, it is postulated that cofactor binding to p97 is ATP-independent, whereas substrate binding is ATP-dependent (Ye et al. 2003; Ye et al. 2004); however, as of yet, only a few proteins have been proposed to be true physiological substrates of p97 (ie. synaptotagmin-1 and HIF-1α) and thereby further investigation into the validity of this hypothesis is necessary (DeLaBarre et al. 2006; Alexandru et al. 2008). Interestingly, while the N-terminal domain is not required for ATPase activity (Rouiller et al. 2002; Ye et al. 2003; Rothballer et al. 2007), adaptor

protein complex could regulate p97 ATPase activity through its N-domain (Meyer et al. 1998).

1.4.3 The D1 and D2 AAA rings

The D1 and D2 domains are each comprised of an N-terminal α/β-fold and a COOH-terminal α-helical domain and are flexibly interconnected in a head to tail arrangement (DeLaBarre and Brunger 2003; DeLaBarre et al. 2006) (Fig. 1.5). The D1 domain is necessary for hexamerization and, in the absence of the D2 ring, the flexible D1-D2 linker represents the minimal requirement for nucleotide independent hexamerization (Wang et al. 2003). On the other hand, the D2 ring is responsible for p97 major ATPase activity and when crystallized without the D1 ring, the D2 ring adapts a heptameric structure (Davies et al. 2008). Examination of the nucleotide occupancy state indicates that the D1 ring is consistently and, perhaps irreversibly, bound to ADP, where as the D2 ring can exist in an unbound (Huyton et al. 2003), AMP-PNP, ADP.AlF3, and ADP bound states (DeLaBarre and Brunger 2005). The differences in the nucleotide binding capacities between the D1 and D2 rings can be attributed to the high affinity of the D1 ring for ADP, especially considering that both rings have the same affinity for ATP (Briggs et al. 2008). Furthermore, recent evidence suggests that all six nucleotide binding sites in the D1 ring can bind ADP simultaneously, while about only 3-4 nucleotide binding sites can be occupied at the same time in the D2 ring (Briggs et al. 2008). Nucleotide hydrolysis in the D2 ring initiate movements which propel protomers by their neighboring protomers (Davies et al. 2008).

These movements are, in turn, relayed through the D1-D2 linker to the α-helical domains of the D1 ring and subsequently the flexible N-domain (DeLaBarre and Brunger 2005). Thus far, it is clear that the ATP hydrolysis does not occur simultaneously in the D2 ring and that the mechanism is likely rotational or stochastic (Briggs et al. 2008). In either case, the D1 and D2 rings are also subject to post-translational modifications that could regulate their activity *in vivo* (Klein et al. 2005; Vandermoere et al. 2006).

1.4.4 The COOH-terminal domain

The structure of the COOH-terminal domain of p97 (residues 761-806) is unknown for the reason that it is characteristically flexible and therefore irresolvable by X-ray crystallography. Functionally, the COOH-terminal domain mediates p97 binding to the E3/E4 ligase, Ufd2, and Ufd3. Furthermore, Serine784 (Livingstone et al. 2005) and tyrosine 805 (Madeo et al. 1998) are targets of phosphorylation events which regulate p97 subcellular localization (Madeo et al. 1998; Lavoie et al. 2000; Livingstone et al. 2005).

1.5 Conformational changes in p97 during its ATPase cycle

Cryo-electron microscopy (cryo-EM) represents an ideal technique to study conformational changes in p97 during its ATPase cycle. Firstly, it allows the resolution of the hydrated structure of a protein in its native state (ie. without staining or fixation), which could be more representative of its physiological state *in vivo*. And secondly, cyro-EM enables the visualization of large multi-protein

complexes that could be difficult to resolve by X-ray crystallography. Using cryo-EM, pioneering studies by Rouiller and coworkers demonstrated drastic conformational changes in p97 upon ATP-binding (Rouiller et al. 2000), and in all nucleotide binding states (Rouiller et al. 2002). p97 conformational changes were also elucidated using X-ray crystallography (DeLaBarre and Brunger 2005) and small angle X-ray scattering (SAXS) (Davies et al. 2005). Except for the X-ray crystallography structures, p97 conformational changes were generally defined in the movement of the N-domain relative to the D1 ring, the opening and closure of the D1 and the D2 ring pores, and in vertical shifts of the surface densities on the sides of the hexamer (Rouiller et al. 2000; Rouiller et al. 2002; Davies et al. 2005). Many of these conformational changes were not observed on the crystal structure probably due to the structural constraints imposed by the crystallization process. Interestingly, the conformational changes in p97 were dependent on the N-domain, as its deletion abolished all the changes observed by cryo-EM, without impairing p97 ATPase activity (Rouiller et al. 2002). Nevertheless, it is proposed that p97 conformational changes mechanistically drive its role in the "extraction" or "remodeling" of protein substrates.

1.6 The denaturation collar model for substrate processing

By exploiting the homology between p97 and the proteasomal Rpt regulatory proteins, DeLaBarre and colleagues identified two loops (residues Arg586/Arg599 and Trp551/Phe552) guarding the aperture of the D2 ring as essential for substrate interaction (DeLaBarre et al. 2006). Importantly,

DeLaBarre and colleagues identified, synaptotagmin-1, a calcium sensor for synaptic neurotransmission, as a physiological candidate for a putative p97 unfoldase function (DeLaBarre et al. 2006). Synaptotagmin-1 crosslinks specifically to D2 Lys565, indicating that it interacts with residues at the distal end of p97. Mutations affecting the D2 loops, Arg586/Arg599, and, Trp551/Phe552, all lead to severe attenuation of p97 ATPase activity, disruption of its cooperativity, and impairment in ERAD function (DeLaBarre et al. 2006). Furthermore, mutation of Trp551 leads to a pronounced defect in ERAD, without affecting p97 ATPase activity and hydrolysis kinetics. This behavior combined with reduced co-immunoprecipitation and cross-linking with synaptotagmin-1, suggests that Trp551 is essential for substrate binding and that ERAD impairment can be attributed to the abolition of substrate binding (DeLaBarre et al. 2006). Although this model is indeed attractive, caution must be taken in its interpretation. A plausible alternative scenario is that synaptotagmin-1 may stimulate p97 activity, subsequently enabling its interaction with a yet unidentified substrate at the N-terminal end of the complex. Synaptotagmin-1 could then represent a membrane receptor for the recruitment of p97 activity (Halawani and Latterich 2006).

Although these findings pose the possibility of D2 involvement in substrate binding, the molecular mechanism of substrate processing remains to be elucidated. In the "denaturation-collar" model DeLaBarre and colleagues proposed that secondary structures in protein substrates are unfolded through the guanidyl-rich denaturing milieu of the arginine double ring (Arg586/Arg599) that

guards the p97 D2 pore (DeLaBarre et al. 2006). Subsequently, substrates are either threaded out through transient grooves at the D1/D2 interphase or reversibly channeled out from the entry port (Fig. 1.6 A-B). In contrast to other AAA proteins, which thread substrates through their symmetry axis, p97 has a narrow D1 pore that is unlikely able to accommodate a polypeptide chain (DeLaBarre and Brunger 2003). In this case, the D1 ring function seems to be limited to correct hexameric assembly and proper interprotomer communication. Furthermore, this model does not rule out the mechanistic involvement of the N-domain and adaptor proteins in substrate recruitment to the COOH-terminal pore or substrate release from the D2 ring (Halawani and Latterich 2006).

1.7. The role of p97 in human diseases

1.7.1 Hereditary inclusion body myopathy associated with Paget disease of bone and fronto-temporal dementia

In 2004, Watts and colleagues identified mutations in the p97 gene as causative for a rare and progressive disease with an autosomal dominant pattern of inheritance named, hereditary inclusion body myopathy associated with Paget disease of bone and fronto-temporal dementia (IBMPFD). Presentation of first clinical symptoms usually occurs in the late third or early fourth decade of life with all patients developing inclusion body myopathy (IBM). Fifty percent of patients also develop Paget Disease of Bone (PDB) and 30-40% are also diagnosed with fronto-temporal dementia (FTD) (Watts et al. 2004). However, considering the recent documentation of subclinical brain pathology in several IBMPFD patients

displaying no symptoms of dementia, it is likely that the low penetrance of FTD is due to the premature mortality of patients due to muscle-specific complications (Forman et al. 2006). Similarly, the variation in the diagnosis of PDB could be attributed to either early mortality, or the effect of modifier genes that have yet to be identified. To date, all identified patients carry single amino acid substitutions in highly conserved residues within the N-domain and the D1 ring of p97 (Fig. 1.7). Fourteen mutations have been identified: nine substitutions affecting five residues within the N-terminal domain (Arg93, Arg95, Arg155, Gly157, Arg159), with Arg155 being the most frequently affected residue; two substitution affecting residues Arg191 and Leu198 within the N-D1 linker region; and three additional substitutions interfere with D1 residues, Ala232, Thr262 and Asn387 (Fig. 1.7) (Watts et al. 2004; Schroder et al. 2005; Bersano et al. 2007; Watts et al. 2007; Spina et al. 2008; Djamshidian et al. 2009). Some of these mutations were also identified in sporadic forms of IBM, but not sporadic PDB (Lucas et al. 2006) or FTD (Schumacher et al. 2009). Often, patients are misdiagnosed with other diseases such as limb girdle muscular dystrophy (LGMD) and amyotrophic lateral sclerosis (ALS) as well as other forms of dystrophies, which make it difficult to accurately estimate the prevalence of these mutations in the population (Kimonis et al. 2008). Currently, the recommended criteria meriting a genetic screen of the VCP gene is the concurrent diagnosis of myopathy with PDB (Kimonis et al. 2008).

1.7.2 p97-linked inclusion body myopathy

Autosomal dominant and recessive forms of inclusion body myopathies can be caused by mutations in a large number of genes summarized in Table 1.2. Only p97-linked IBM is also associated with early onset PDB (Kimonis et al. 2000; Waggoner et al. 2002). Examination of muscle biopsy tissue of patients with p97-linked IBM reveal nonspecific changes, including high variability of muscle fiber size, muscle fiber atrophy and hypertrophy, myopathic grouping, vacuolization, and fatty replacement of muscle tissue (Hubbers et al. 2007; Kimonis et al. 2008). Immunohistochemical analyses of advanced disease cases show large disperse sarcoplamic aggregates plaguing normal and atrophic muscle fibers and comprised of p97, ubiquitin and TAR DNA binding protein-43 (TDP-43) (Watts et al. 2004; Weihl et al. 2008). p97 also colocalizes with ubiquitin in filamentous structures and granular aggregates in both the nuclei and the sarcoplasm of affected muscle fibers (Hubbers et al. 2007). In one report, there was evidence of nuclear accumulation of paired helical filaments (PHF), phosphorylated microtubule binding protein, tau, and amyloid precursor protein (APP), which is reminiscent of Alzheimer Disease pathology (Alvarez 1998). However, these finding have yet to be substantiated in the majority of cases with p97-linked IBM (Djamshidian et al. 2009). Alzheimer-like pathology is also well documented in inclusion body mystic, which is distinguished from hereditary IBM by its underlying inflammatory component (Asians and Engel 2005; Asians and Engel 2006). Inflammatory cell infiltration is notably absent in the muscles of patients with hereditary-type myopathies, including p97-linked IBM (Kimonis et al. 2000). Generally, the morphological features of the myopathy associated with

p97 mutations are shared by all hereditary-type myopathies. The vast heterogeneity in the genetic causes of hereditary-type myopathies makes the possibility of common pathophysiological pathway unlikely in spite of the overlapping clinical presentation.

1.7.2.1 The role of p97 in myosin assembly

Proper myofibril alignment in myotubes requires the activity of the myosin motors and their specific chaperone, UNC-45 (Ao and Pilgrim 2000). UNC-45 protein levels are critically regulated throughout development by the concerted actions of two E3 ubiquitin ligases: Ufd2 and the carboxyl terminus of Hsc70-interacting protein, CHIP (Hoppe et al. 2004). Either a reduction or an increase in UNC-45 protein levels leads to reduced myosin contents and myofibril disorganization thereby resulting in paralysis (Janiesch et al. 2007). Here, p97 is implicated in the direct regulation of UNC-45 protein turnover. In C elegans, p97 two homologues, CDC-48.1 and CDC-48.2, form a complex with Ufd2 and CHIP homologue, CHN-1, and together they catalyze the ubiquitination and degradation of UNC-45 (Janiesch et al. 2007). A null allele of CDC-48.1 or CDC48.2 results in the accumulation of UNC-45 protein levels and paralysis due to sarcomere disorganization (Janiesch et al. 2007). Given (1) the role of p97 in UNC-45 protein degradation, and (2) the accumulations of polyubiquitinated protein in IBMPFD, Janiesch and coworkers, investigated whether IBMPFD mutations impaired UNC-45 protein degradation in human myotubes derived from patients with IBMPFD (Janiesch et al. 2007). Compared to healthy myotubes, IBMPFD-

derived myotubules accumulated UNC-45 and displayed disorganized sarcomeric structures (Janiesch et al. 2007). These results imply that IBMPFD-linked p97 mutations induce their pathogenic effects by interfering with UNC-45 protein degradation; however the mechanism remains unclear. Recent evidence indicates that excess UNC-45 promotes the unfolding or aggregation of the myosin motors which leads to their UPS-mediated degradation (Landsverk et al. 2007). Accordingly, it remains to be seen if there is a reduction in myosin protein level in IBMPFD. Furthermore, failure in UNC-45 protein degradation is predicted to result in a developmental defect, which is not currently observed in IBMPFD patients. On the contrary, aging appears to be a critical prerequisite for the pathogenesis of IBMPFD. Therefore, it is plausible that ageing may increase the demand on p97 function in mediating protein degradation and facilitating regeneration associated membrane fusion, which in turn could present a challenge for the mutant p97 complexes. Alternatively, p97 activity may be necessary for the regulation of UNC-45 protein levels only in adult muscle stem cells (satellite cells), and not in embryonic muscle progenitors. In support of this view, UNC-45 protein levels were found to accumulate in myotubes generated from satellite cells of adult IBMPFD patients (Janiesch et al. 2007). Furthermore, recent evidence suggests that the genetic requirements for muscle differentiation in adult stem cells and embryonic muscle progenitors may be distinct (Lepper et al. 2009). Further studies are indeed necessary to identify the biochemical roles of p97 in muscle development and regeneration.

1.8. Paget Disease of Bone

Paget disease of bone (PDB) is the second most common bone disorder following osteoporosis with approximately 15-40% of all cases having an underlying genetic component (Hocking et al. 2000) (Table 1.3). This ailment is characterized by increased osteoclast-mediated bone resorption, followed by a compensatory increase in osteoblast-mediated bone formation. The woven and disorganized nature of new bone formation renders the bone susceptible to fractures and deformities (Paget 1877). Abnormal osteoclast differentiation, nucleation, and activation are thought to be key mediators of this complex disease. PDB affects both the axial and appendicular skeletons in patients with IBMPFD mutations where focal lesions are reported in the skull, spine, clavicles, pelvis, and the scapulae. The accelerated rate of bone resorption is caused by an increase in the number and activity of osteoclasts; however, unlike the healthy multinucleated osteoclasts, pagetic cells can encompass up to 100 nuclei per cell which leads to their metabolic hyper-activation (Rebel et al. 1980). In response to increased resorption, osteoblasts compensate by accelerating bone formation and deposition, which often results in fragile and disorganized bone structure.

1.8.1 Osteoclastogenesis

Typically, osteoclastogenesis is mediated by two osteoblast-derived factors: (1) the secreted colony stimulating factor-1 (CSF-1), which stimulates the expression of a cell surface receptor, the receptor activator of nuclear factor κ B (RANK), in osteoclast progenitors; and (2) the extracellular membrane protein,

RANK ligand (RANKL), which mediates the activation of the nuclear factor κ B (NFκB) pathway and thereby the initiation of the full osteoclastogenic differentiation program. Therefore, osteoclastogenesis requires both, the physical interaction between osteoblasts and osteoclastprogenitor cells, and the subsequent activation of the NFκB pathway (Nakagawa et al. 1998; Yasuda et al. 1998). Osteoblasts also secrete the decoy receptor, osteoprotegrin, which binds to RANKL and prevents its interaction with RANK on osteoclasts (Simonet et al. 1997; Burgess et al. 1999). Accordingly, osteoclastogenesis is dependent on the proper integration and fine-tuning of complex cell-to-cell signaling.

RANK signaling is connected to the NFκB pathway through the E3 ubiquitin ligase, tumor necrosis factor receptor associated factor 6 (TRAF6) and the ubiquitin-binding protein p62 (also known as sequestosome-1) (Duran et al. 2004; Gohda et al. 2005; Lamothe et al. 2007; Bai et al. 2008). TRAF6 mediates its own polyubiquitination in response to RANK activation (Deng et al. 2000; Lamothe et al. 2007) and forms a complex containing p62 and atypical protein kinase C (aPKC) (Duran et al. 2004). TRAF6 mediated signaling downstream of RANK mediates osteoclastogenesis (Kobayashi et al. 2001; Kadono et al. 2005; Bai et al. 2008) and its homozygous deletion leads to severe osteopetrosis in mice (Lomaga et al. 1999). On the other hand, p62 interacts with both aPKC and IκB kinase (IKKβ) and mediates the activation of the NFκB pathway (Sanz et al. 1999) in a TRAF6 dependent manner (Sanz et al. 2000). In animal models,

mutations in p62 do not lead to PDB, but rather lower the threshold for osteoclast differentiation in the bone microenvironment (Hiruma et al. 2008; Chamoux et al. 2009). Therefore, the activation of the NFκB pathway and the transcription of osteoclast-specific differentiation genes require RANK signaling through TRAF6 and p62.

1.8.2 Putative mechanisms for p97 involvement in osteoclastogenesis

The manifestation of PDB in 50% of patients diagnosed with IBMPFD implicates p97 in the regulation of osteoclast differentiation or activation or both. At this stage, the mechanisms of p97 involvement in osteoclastogenesis are speculative at best with all proposed mechanisms centering on putative roles for p97 in the regulation of the NFκB pathway. For example, p97 is involved in the degradation of the ubiquitinated inhibitory subunit of the NFκB transcriptional complex, IκB-α (Dai et al. 1998), however, it is unclear if p97-mediated degradation of IκB-α is necessary for NFκB activation. IκB-α is found mainly in complex with the NFκB transcriptional complex, but can also exist in a free cytosolic state (Dai et al. 1998). Considering that p97 does not associate with the NFκB transcriptional complex, p97 may be involved in the degradation of ubiquitinated free IκB-α. p97 is also known to interact with TRAF6, although little is known about the relevance of this interaction in the NFκB pathway (Bouwmeester et al. 2004). TRAF6 polyubiquitination activity promotes osteoclastogenesis by functioning downstream of RANK and the NFκB pathway

(Lamothe et al. 2007; Lamothe et al. 2007). Interestingly, TRAF6 interaction with p62 facilitates its catalytic activation (Wooten et al. 2001; Wooten et al. 2005). Future studies will establish whether TRAF6 polyubiquitination activity is a convergence point for p62 and VCP in the regulation of osteoclastogenesis through RANK and the NFκB pathway.

1.9. Fronto-temporal dementia

FTD is characterized by severe personality changes including loss of inhibition, initiation, judgment, and interest in the surrounding environment. It can be accompanied by alcoholism, delusions, aggression, and negligence of personal hygiene and well being (Neary et al. 1998). Unlike Alzheimer disease (AD), which is characterized by severe memory loss and degeneration of the hippocampus and the entrorhinal cortex, the memory in FTD remains intact and most of the degenerative changes occurs in the cerebral cortex including the frontal and temporal lobes. Accordingly, FTD and AD are viewed as very distinct forms for neurodegeneration caused by different neuropathological pathways. Treatments alleviating AD symptomology could lead to severe side effects in FTD (Cummings 2000).

FTD can be subdivided into two types: Frontotemporal dementia with Parkinsonism linked to chromosome-17 (FTDP-17), and frontotemporal lobe dementia with tau-negative and ubiquitin-positive inclusions (FTLD-U). FTDP-17 is caused by mutations in the microtubule associated protein tau (MAPT) on

chromosome 17 and is accompanied by the accumulation of neurofibrillary tangles (NFT). Although NFT are also observed in AD, these tangles are not associated with the senile plaque pathology characteristic to AD. Furthermore, MAPT mutations are not associated with hereditary forms of AD. While both types of FTD share the accumulation of ubiquitin-positive inclusions, tau dysfunction evident in the accumulation of NFT is only observed in FTDP-17 (reviewed in Gotz and Ittner 2008).

1.9.1 p97-linked fronto-temporal dementia

Hereditary forms of FTD can be caused by mutations in several seemingly unrelated genes (Table 1.4) indicating that the mechanisms of pathogenesis are likely diverse. FTD caused by p97 mutations is classified as a FTLD-U due to the absence of the tau pathology. Only 30 to 40 % of all patients carrying the p97 mutations are diagnosed with FTD, but this is likely due to premature death in subclinical stages of FTD (Forman et al. 2006). Histological assessment of the neuropathology in p97-linked FTD reveals novel ubiquitin pathology where ubiquitinated inclusions are mostly intranuclear and devoid of p97. Furthermore, there is currently no evidence of cytosolic inclusions or p97-containing aggregates in neurons (Forman et al. 2006; Guyant-Marechal et al. 2006), which is in striking contrast to the sequestration of p97 in muscle-specific inclusion bodies in the same patients (Watts et al. 2004). Overall, IBMPFD brains show extensive cerebral atrophy (Schroder et al. 2005; Forman et al. 2006) with severe degeneration and vacuolization of neurons. The neuropathology is most severe

in the upper cortical layers, where Caspase-9 (Casp9) is activated (Guyant-Marechal et al. 2006). Considering that active Casp9 is a central component of the apoptosome, downstream effector caspases, Caspase-3 (Casp3), Caspase-6 (Casp6), and Caspase-7 (Casp7), may also be activated. Interestingly, p97 has been identified as a putative target of Casp3 and Casp7 in apoptotic cells (Jang et al. 2008), and of Casp6 in primary human neurons (Klaiman et al. 2009); however, p97 proteolysis in IBMPFD remains to be substantiated. The fact that caspases are also activated in response to overexpression of p97 IBMPFD-linked mutants in neuronal cell models (Gitcho et al. 2009) suggests a positive feedback mechanism by which p97 mediates its own proteolysis in p97-linked FTD. Further studies are necessary to investigate if caspase mediated proteolysis of p97 is a plausible mechanism for neurodegeneration in p97-linked FTD.

Recently, TDP-43 was found to be hyperphosphorylated, ubiquitinated, and C-terminally truncated in p97-linked FTD. It also colocalizes with ubiquitin in intranuclear inclusions and accumulates within the insoluble fractions of affected brains (Neumann et al. 2007). Interestingly, mutations in TDP-43 are also associated with various sporadic and hereditary forms of FTD and amyotrophic lateral sclerosis (ALS) (Neumann et al. 2007; Sreedharan et al. 2008). Furthermore, overexpression of p97 mutant variants in cell culture alters the localization of TDP-43 by promoting its translocation from the cytoplasm to the nucleus (Gitcho et al. 2009). These findings imply that p97 and TDP-43 neuronal functions may be linked. However, the fact that post-translationally modified

TDP-43 is also present in AD poses the possibility that the processing of TDP-43 may be consequential to neuronal stress (Uryu et al. 2008; Arai et al. 2009; Kadokura et al. 2009). Future investigations of the cell biological function of TDP-43 and the relevance of its post-translational modification should shed light on the mechanism of its involvement in neurodegeneration.

1.10 Understanding the molecular pathogenesis of IBMPFD.

1.10.1 Rationale

The multisystemic nature of IBMPFD implicates p97 in the generalized pathogenesis of inclusion body diseases. p97 involvement in protein aggregation can be reconciled in two mutually exclusive possibilities: Firstly, p97 may be positively involved in the sequestration of misfolded proteins into insoluble aggregates; or alternatively, p97 may mediate the solubilization and clearance of misfolded protein from the cellular microenvironment. Therefore, it is essential to address the question of whether p97 IBMPFD-linked mutations are associated with a deleterious gain-of-function or loss-of-function phenotype. Furthermore, aging is an important prerequisite in the pathogenesis of many inclusion body diseases, including IBMPFD. The adult onset of IBMPFD and apparent lack of developmental defects point to a subtle effect on p97 cell biological activities and implicate age-related stress in the full manifestation of the disease. Elucidation of the molecular consequences of p97 IBMPFD-linked mutations may help identify the mechanism by which the wild-type protein usually circumvents or neutralizes age-related stresses in the cellular microenvironment. Accordingly, this thesis

work will further our current understanding of the pathogenic mechanisms mediating proteinopathies and age-related disorders.

1.10.2 Thesis objectives:

1. While p97 IBMPFD-linked mutations localize to the N-domain or its regulatory D1 ring, the effect of these mutations on p97 structure and biochemical activity remains unclear. This objective aims at characterizing the effect of two mutations, Arg155Pro and Ala232Glu, on p97 structure and ATPase activity, using a variety of biochemical and biophysical approaches.

2. Considering that p97 has been identified as a putative target of Casp6 activity in primary human neurons, this objective aims at addressing if p97 is cleaved by Casp6 in AD, where Casp6 activity is upregulated and implicated in mediating neurodegeneration. Accordingly, this objective will help address the question of whether p97 cell biological function is compromised in common neurodegenerative diseases not associated with p97 mutations, such as Alzheimer disease (AD).

3. The accumulation of polyubiquitinated protein in IBMPFD indicates that p97 function in UPS-mediated protein degradation could be impaired. This objective aims at identifying a putative mechanism of how IBMPFD-linked p97 mutations may lead to UPS impairment in p97-linked FTD.

Table 1.1. p97-interacting ubiquitin modification enzymes and their associated cellular pathways

Process	E3 Ligase	Interaction	Substrate	Adaptor	Reference
Quality Control (ERAD)	Hrd1	Complex Ubx2p mediated	CPY*, MHC class I, Hmg2p	Ufd1p Npl4p	(Neuber et al. 2005; Schuberth and Buchberger 2005)
	Ufd2p	Direct	Spt23p	Ufd1p Npl4p	(Richly et al. 2005)
	AMFR/ gp78	Direct	CD3delta	N/A	(Zhong et al. 2004)
	$SCF^{fbs1,2}$	Complex	B1 integrin N - glycosylated proteins	N/A	(Yoshida et al. 2005)
	Dorfin	Direct	Calcium sensing receptor	N/A	(Huang et al. 2006)
UPS	Ufd2p	Direct	Ub-Proβgal Ub-ProtA Ub-GST	Ufd1p Npl4p	(Richly et al. 2005)
	E4B	Direct	Ataxin-3	N/A	(Matsumoto et al. 2004)
	Dorfin	Direct	Superoxide Dismutase-1	N/A	(Ishigaki et al. 2004)
Process	**DUB Enzyme**	**Interaction**	**Substrate**	**Adaptor**	**Reference**
ERAD (UPS)	Otu1p	Direct	Spt23p	Ufd1p Npl4 Ufd3p Shp1p	(Rumpf and Jentsch 2006)
UPS	Ataxin-3	Direct	Ub-Proβgal	N/A	(Doss-Pepe et al. 2003)
Membrane fusion	VCIP135	Direct	Unidentified	p47	(Uchiyama et al. 2002)

An asterisk (*) represents unidentified substrates; Abbreviation: N/A: not assessed

Table 1.2. Genes implicated in the pathogenesis of hereditary forms of inclusion body myopathies

Gene	Biological Role of Encoded Protein	Inheritance Pattern	OMIM*	Reference
Desmin & related proteins	Type III intermediate filament cytoskeletal protein	Dominant	#601419	(Goldfarb and Dalakas 2009)
GNE	Sialic acid biosynthesis	Recessive	#600737, #605820	(Eisenberg et al. 2001; Hinderlich et al. 2003)
VCP	Encodes p97-a AAA ATPase involved in Protein degradation and membrane fusion	Dominant	#167320	(Watts et al. 2004)
MYHCIIA	Myosin heavy chains type IIA	Recessive	#605637	(Martinsson et al. 1999; Martinsson et al. 2000)
Myotilin	Thin filaments associated structural protein	Dominant	#159000	(Hauser et al. 2000)
Caveolin-3	Muscle-specific membrane protein	Dominant	#607801	(Minetti et al. 1998)
LMNA	Lamin A/C-Nuclear membrane proteins	Dominant	#159001	(Muchir et al. 2000)
Calpain 3	Calcium activated protease	Recessive	#253600	(Richard et al. 1995)
Dysferlin	Calcium dependent transmembrane protein implicated in membrane fusion	Recessive	#254130	(Liu et al. 1998)
Dystrophin-glycoprotein complex components	Links extracellular matrix with cytoskeletal proteins	Recessive	#253700, #604286, #608099	(Roberds et al. 1994; Noguchi et al. 1995; Piccolo et al. 1995; Trabelsi et al. 2008)
Telethonin	sarcomeric protein	Recessive	#601954	(Moreira et al. 2000)

*__OMIM__, Online Mendelian Inheritance in Man, National center for biotechnology information

Table 1.3. Genes implicated in the pathogenesis of hereditary forms of Paget disease of bone

Gene	Encoded Protein	Mutational region	Inheritance pattern	OMIM*	Reference
SQSTM1	p62-a ubiquitin interacting scaffold protein	UBA domain	Dominant	#167250	(Laurin et al. 2001; Laurin et al. 2002)
TNFRSF11A	Receptor Activator of NfkB (RANK) receptor	Signal peptide	Dominant	#174810	(Hughes et al. 2000)
TNFRSF11B	Osteoprotegrin-negative regulator or RANK signaling	Ligand binding region	Recessive	#239000	(Cundy et al. 2002; Whyte et al. 2002)
VCP	p97-a AAA ATPase involved in Protein degradation and membrane fusion	N-Domain and its regulatory D1 domain	Dominant	#167320	(Watts et al. 2004)

*__OMIM__, Online Mendelian Inheritance in Man, National center for biotechnology information

Table 1.4. Genes implicated in the pathogenesis of fronto-temporal dementia

Gene	Encoded protein & Its Biological Role	Inheritance Pattern	OMIM*	Reference
MAPT	Tau-microtubule associated protein	Dominant	#600274	(Hutton et al. 1998)
GRN	Granulin-a pleiotropic protein with a proposed neurotrophic function in the brain	Dominant	#607485	(Baker et al. 2006)
VCP	p97-a AAA ATPase involved in Protein degradation and membrane fusion	Dominant	#167320	(Watts et al. 2004)
TARDBP	TDP-43- a DNA binding protein	Dominant	#612069	(Sreedharan et al. 2008) Neumann M and 2006)
CHMP2B	Chromatin-modifying protein/ charged multivesicular body protein 2B-functions in endosomal sorting	Dominant	#600795	(Skibinski et al. 2005)

*__OMIM__, Online Mendelian Inheritance in Man, National center for biotechnology information

Figure 1.1. Proposed mechanisms for p97/Cdc48p substrate recognition and processing. Oligoubiquitylated substrates are first recruited to p97/Cdc48p via its diverse adaptors (**A**). Alternatively, p97/Cdc48p can bind to misfolded proteins (**B**) and oligoubiquitylated substrates (**C**) directly and chaperone against their aggregation. Once the substrate is bound (**D**), complex will stabilize the binding of either, an E4 ligase, which catalyzes substrate ubiquitylation (**F**), or a deubiquitylating complex (Otu1p/Ufd3p), which subsequently removes the attached ubiquitin moieties (**E**). Ubiquitylated substrates, depending on the type of attached ubiquitin moieties, can be channeled for degradation or, like deubiquitylated substrates, extracted and released into the cytosol.

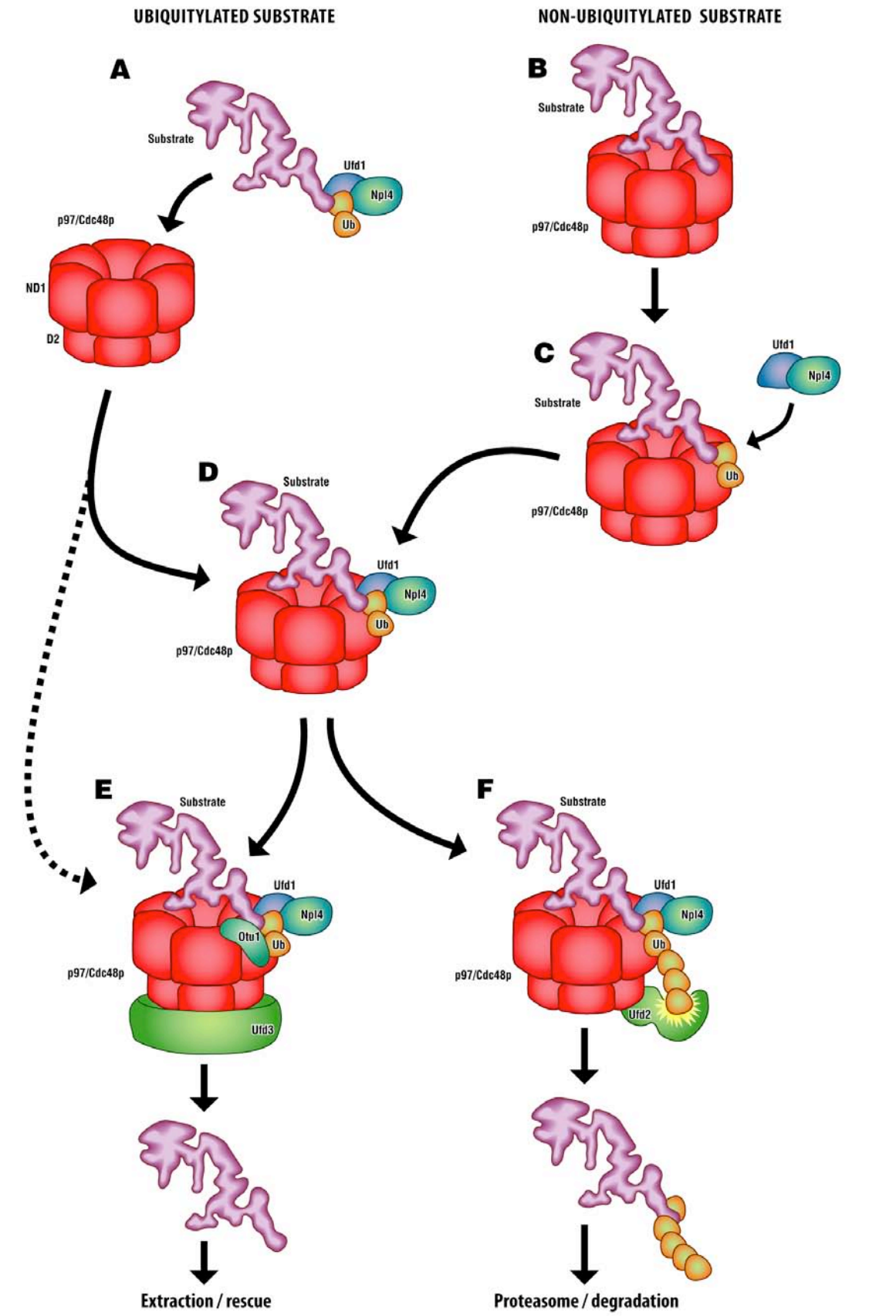
UBIQUITYLATED SUBSTRATE
NON-UBIQUITYLATED SUBSTRATE
A
Substrate
Ufd1
Npl4
Ub
p97/Cdc48p
ND1
D2
B
Substrate
p97/Cdc48p
C
Ufd1
Npl4
Substrate
Ub
p97/Cdc48p
D
Substrate
Ufd1
Npl4
Ub
p97/Cdc48p
E
Substrate
Ufd1
Npl4
Otu1
Ub
p97/Cdc48p
Ufd3
F
Substrate
Ufd1
Npl4
Ub
p97/Cdc48p
Ufd2
Extraction / rescue
Proteasome / degradation

Figure 1.2. The crystal structure of the p97 monomer. The N-domain represents amino acid residues, 1-187, in gray. The D1 AAA domain, amino acid residues 208-459, is depicted in purple. The D2 AAA domain, amino acid residues 481-761, are coloured in green. The connecting N-D1 linker, amino acid residues 188-207, and the D1-D2 linker, amino acids 460-480, are outlined red. Structures are PyMOL visualizations of PDB file 1R7R (Huyton et al. 2003).

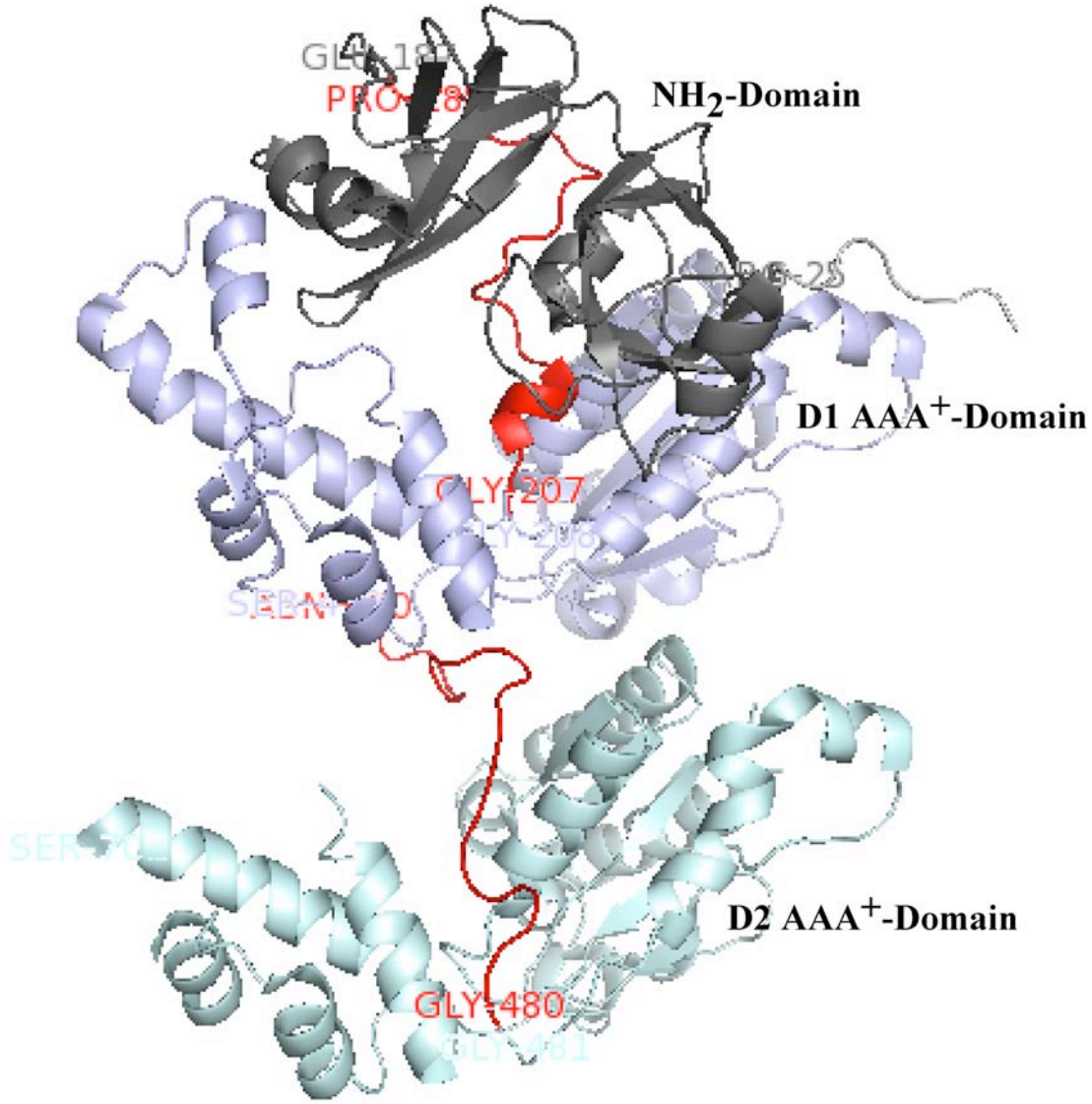
NH2-Domain
D1 AAA+-Domain
D2 AAA+-Domain
GLY-207
GLY-480

Figure 1.3. The crystal structure of the p97 hexamer. A. Top view of the D1 ring. **B.** Bottom view of the D2 ring. **C.** Side view with the D1 ring arranged on top of the D2 ring. The N-domain is represented in gray. The D1 is depicted in purple. The D2 is coloured in blue. The connecting linkers are outlined in red. Structures are PyMOL visualizations of PDB file 1R7R (Huyton et al. 2003).

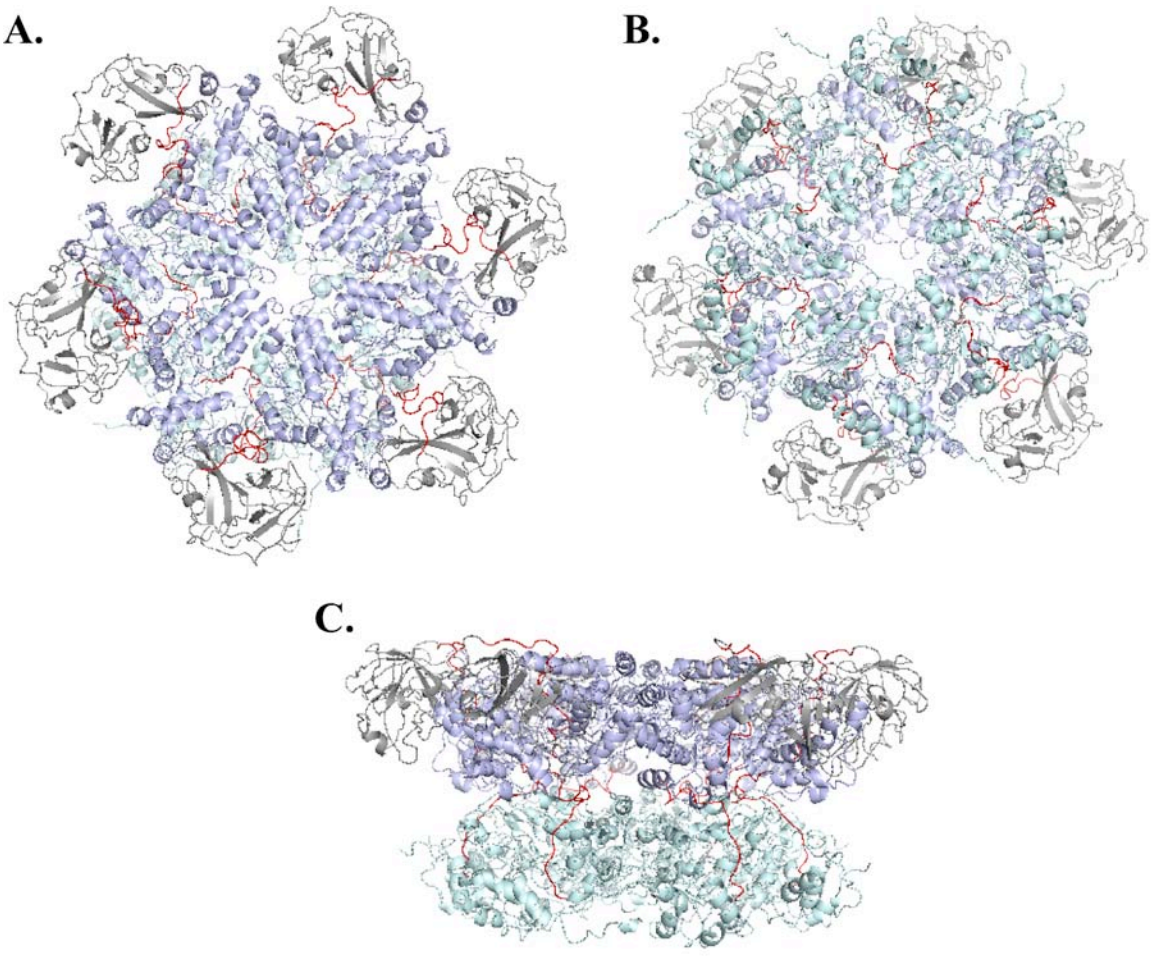
A.
B.
C.

Figure 1.4. Structural features of the p97 N-domain. A. The crystal structure of the N-domain, amino acid residues 1-187. The distal double-ψ β- barrel fold, amino acids 25-106, is depicted in red, the proximal β-clam fold, amino acids 112-186, is represented in gray. **B.** The arrangement of the double-ψ β-barrel with the starting and ending amino acid residues Arg 25 and Pro 106 indicated. The nuclear localization signal, amino acid residues 59-65 is outlined in yellow. **C.** The arrangement of the β-clam fold starting with amino acid residue Lys 112 and ending with Glu 187. **D.** Illustration of the putative protein binding groove encompassed between the double-ψ β-barrel fold and the β-clam fold and represented in amino acid residues 107-111 in green. Structures are PyMOL visualizations of PDB file 1R7R (Huyton et al. 2003).

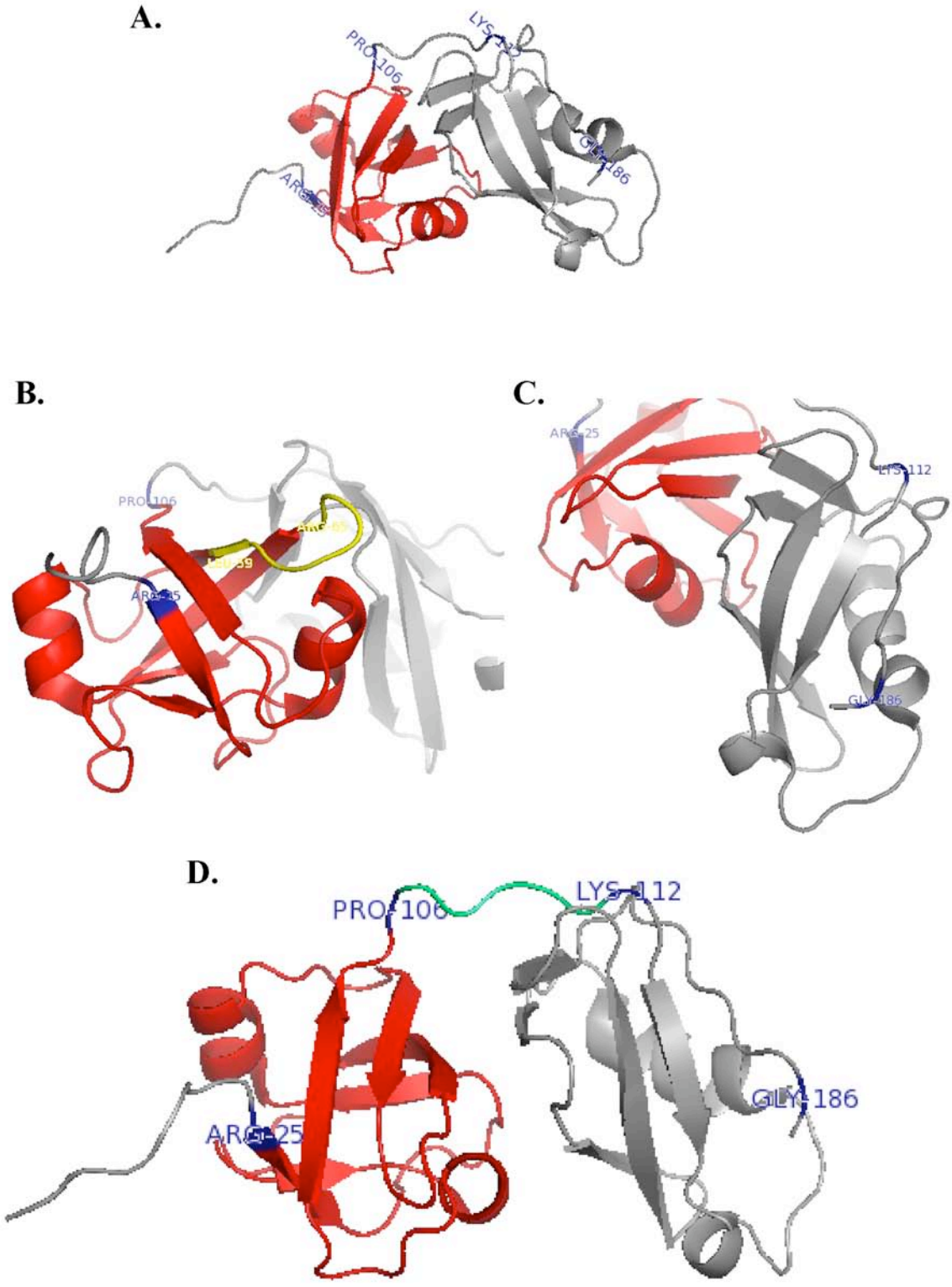
A.
PRO 106
LYS 112
GLY 186
ARG 25
B.
PRO 106
ARG 25
C.
ARG 25
LYS 112
GLY 186
D.
PRO 106
LYS 112
ARG 25
GLY 186

Figure 1.5. The structural arrangement of the D1 and D2 AAA domains in the p97 monomer. The D1 and D2 AAA domains are depicted in gray, with the D1-D2 linker outlined in red. Both domains are arranged in an almost exact replicate fashion. The ATP-binding, Walker A motifs, represented in amino acid residues, 245-252 and 518-525, of the D1 and D2 domains respectively are outlined in green. The ATP hydrolysis, Walker B motifs, amino acids 300-305 of the D1 domain and 573-578 of the D2 domain are depicted in yellow. Structures are PyMOL visualizations of PDB file 1R7R (Huyton et al. 2003).

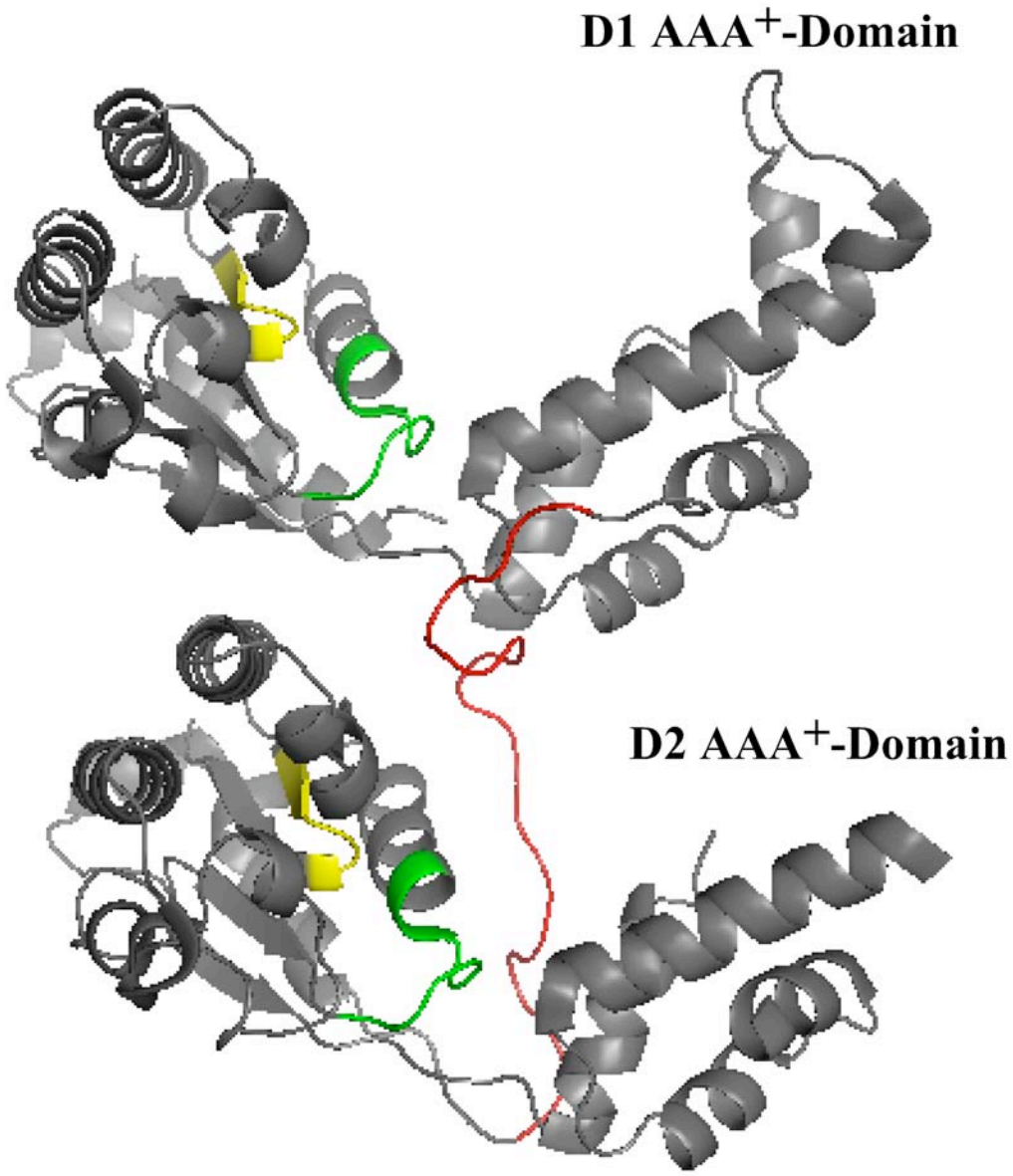
D1 AAA+-Domain
D2 AAA+-Domain

Figure 1.6. The "Denaturation-Collar" Model for D2-Mediated Substrate Processing. DeLaBarre et al. (2006) propose the D2 ring as an entry port. Guarding the D2 pore is an arginine double ring (Arg586/Arg599) and, thus, the collar, which provides a guanidyl-rich environment theoretically sufficient for unwinding tertiary structures. Once denatured, the substrate is either funneled back through the entry port (**A**) or threaded through transient pores are the D1/D2 interphase (**B**). Structures are PyMOL visualizations of PDB file 1R7R (Huyton et al. 2003).

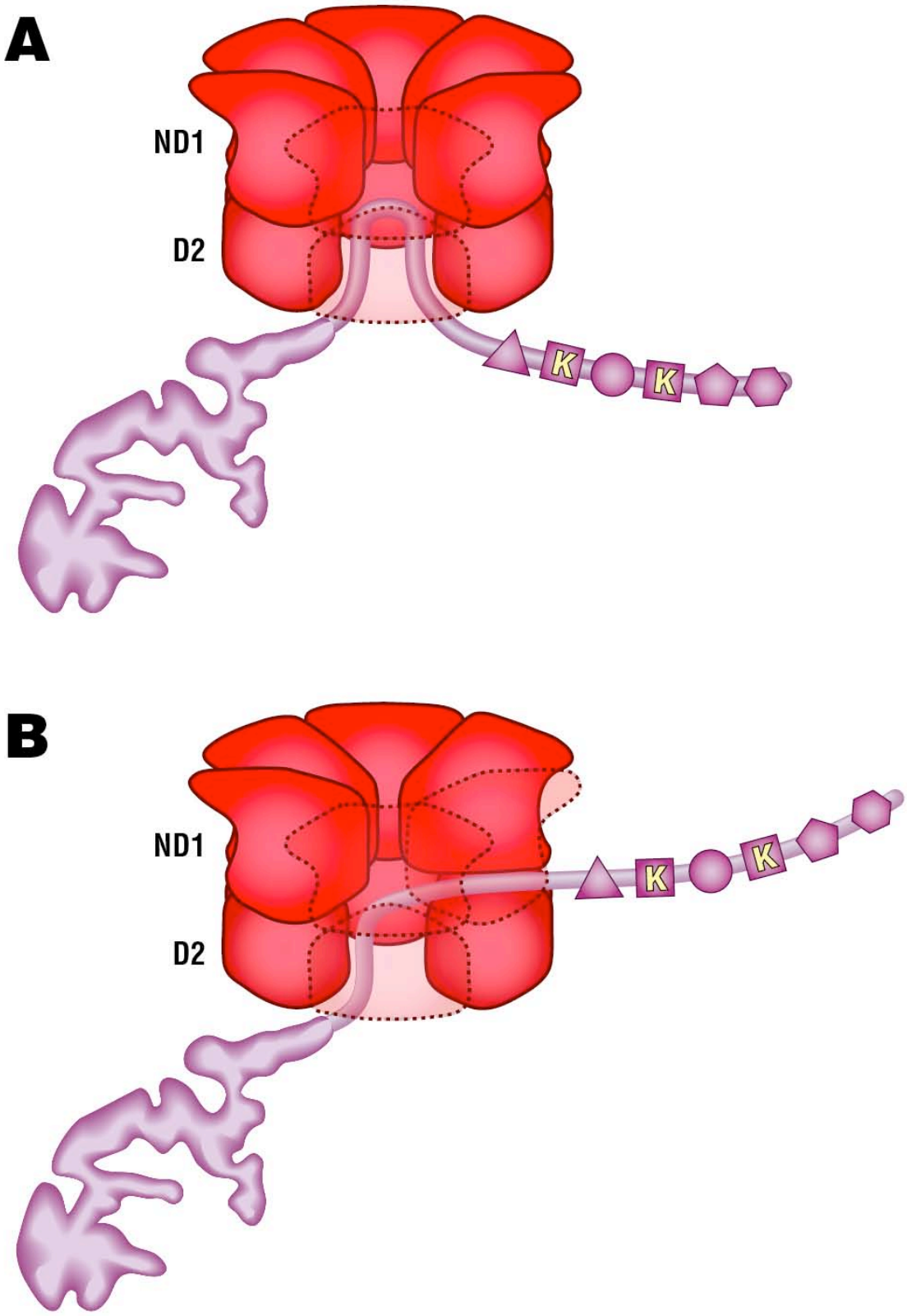
A
ND1
D2
K
K
B
ND1
D2
K
K

Figure 1.7. Localization of IBMPFD-linked p97 mutations. Schematic illustration of p97 functional domains with the mutated amino acid residues identified below the domain to which they localize. Abbreviations: N; amino-terminal domain, L1; N-D1 linker, D1; D1 AAA Domain, L2; D1-D2 linker, D2; D2 AAA Domain, COOH; Carboxyl-terminal domain. Arrows indicate the amino acid substitutions and the slashes are used to separate other possible substitution.

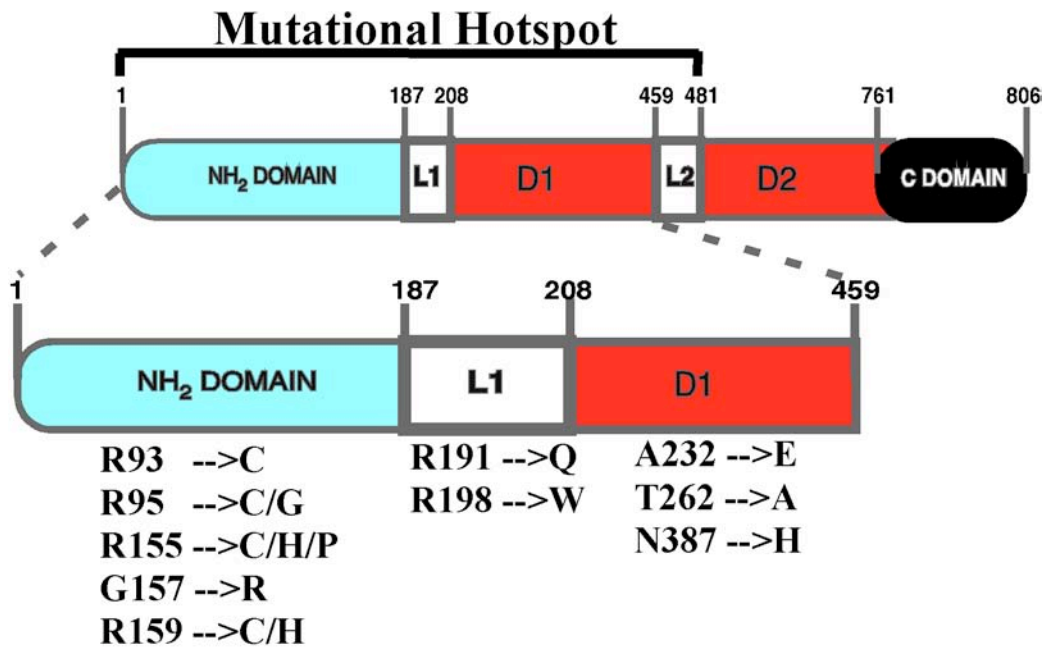

R93 -->C
R95 -->C/G
R155 -->C/H/P
G157 -->R
R159 -->C/H

R191 -->Q
R198 -->W

A232 -->E
T262 -->A
N387 -->H

CHAPTER 2: Characterization of structural defects in hereditary inclusion body myopathy-linked p97 mutant variants

Preface

Although it is evident that the expression of IBMPFD-linked p97 mutations leads to impairment in ERAD and ubiquitin-mediated protein degradation, it is unclear if these defects are related to structural alterations in p97. Interestingly, all IBMPFD mutations cause the same pathogenic phenotype, irrespective of whether they localize to the N-terminal substrate binding domain or its regulatory D1 ring. Given that (1) the N-domain is necessary for p97 conformational changes during the ATPase cycle and that (2) the D1 ring is responsible for relaying conformational changes between the D2 ring and the N-domain, it is hypothesized that IBMPFD mutations lead to conformational defects in p97. In this work, a multitude of biochemical approaches were utilized to investigate the effects of the IBMPFD-linked p97 mutations on the structural integrity and biochemical activity of p97.

2.1 Abstract

Hereditary inclusion body myopathy associated with Paget disease of bone and frontotemporal dementia is a degenerative disorder caused by single substitutions in highly conserved residues of p97. All mutations identified thus far cluster within the N-domain or the D1 ring, which are both required for communicating conformational changes to adaptor protein complexes. In this report, biochemical approaches were used to identify consequences of mutations, R155P and A232E, on p97 structure. Assessment of p97 oligomerization revealed that p97R155P and p97A232E formed hexameric, ring-shaped structures of ~600 kDa. p97R155P and p97A232E exhibited ~3X increase in ATPase activity compared to p97WT and displayed increased sensitivity to heat-induced upregulation of ATPase activity. Protein fluorescence analysis provided evidence for conformational differences in the D2 ring of both IBMPFD mutants. Furthermore, both mutations increased the proteolytic susceptibility of the D2 ring. The solution structure of all p97 proteins revealed a di-disperse distribution of a predominant hexameric population, and a minor population of large diameter complexes. ATP binding significantly increased the abundance of large diameter complexes for p97R155P and p97A232E, but not p97WT or ATP-binding mutant p97K524A. Therefore, we propose that IBMPFD p97 mutants, p97R155P and p97A232E, possess structural defects which may compromise the mechanism of p97 activity within large multi-protein complexes.

2.2 Introduction

The ubiquitous Valosin containing protein (p97) is a prominent member of the highly conserved AAA+ (ATPases-Associated with diverse cellular Activities) proteins, which are distinctly known for their oligomeric structure and chaperone-like activities. p97 is an essential biochemical component of a wide-range of ubiquitin-linked cell biological reactions, including ubiquitin-proteasome system (UPS)-mediated protein degradation (Halawani and Latterich 2006), Golgi and endoplasmic reticulum (ER) membrane fusion (Acharya et al. 1995; Rabouille et al. 1995), transcription factor activation (Rape et al. 2001), and DNA repair (Partridge et al. 2003; Indig et al. 2004). Within these processes, p97 acts as a molecular segregase that utilizes ATP-powered conformational changes in the assembly and disassembly of macromolecular machineries (Halawani and Latterich 2006; Jentsch and Rumpf 2007).

p97 ATPase activity is contingent on the assembly of an inherently stable hexamer (Song et al. 2003), comprised of two highly homologous D1 and D2 nucleotide-binding rings and regulatory N- and COOH-terminal domains (DeLaBarre and Brunger 2003). ATP hydrolysis in the D2 ring mediates p97 major ATPase activity, while the D1 ring is involved in the regulation of p97 hexamerization (Song et al. 2003). Recently, p97 has been linked to a severe degenerative disorder identified as hereditary inclusion body myopathy associated with early onset Paget disease of bone and frontotemporal dementia (IBMPFD). The pathogenesis of IBMPFD is attributed to autosomal dominant

single amino acid substitutions in highly conserved residues within p97 N-domain and D1 ring (Watts et al. 2004). Patients present with hallmark features of a 'protein conformational' disorder, where proteinaceous inclusions accumulate in the cytoplasm and nuclei of degenerating myofibrils (Kimonis et al. 2008) and dystrophic neurites (Schroder et al. 2005; Forman et al. 2006; Neumann et al. 2007). Transgenic expression of IBMPFD p97 mutants in a murine animal model sufficiently recapitulates these inclusions (Weihl et al. 2007). While the ultrastructure and composition of IBMPFD inclusions are poorly defined, several reports have identified p97 and ubiquitin as major constituents (Watts et al. 2004; Ju et al. 2008; Weihl et al. 2008). Furthermore, overexpression of IBMPFD mutants in C2C12 skeletal myoblasts results in p97 localization to cytoplasmic inclusions and fractionation with insoluble proteins (Weihl et al. 2006). One possibility is that misfolding or misassembly directly mediates p97 accumulation in inclusion bodies which, in turn, nucleates the entrapment of its interacting proteins. Alternatively, the biogenesis of p97-containing inclusions could represent an indirect consequence of failure in other p97-dependent pathways upstream of the UPS. To date, the mechanisms by which IBMPFD p97 mutants induce the biogenesis of inclusion bodies in cell culture models are not well-understood (Weihl et al. 2006; Hubbers et al. 2007).

Despite current progress in resolving more refined p97 crystal structures in various nucleotide-binding states (DeLaBarre and Brunger 2005; Davies et al. 2008), clues on how IBMPFD mutations impact p97 structure or conformation

remain elusive. Cryo-electron microscopy (Rouiller et al. 2000; Rouiller et al. 2002) and crystallography studies (DeLaBarre and Brunger 2003; DeLaBarre and Brunger 2005) on p97 in various nucleotide-binding states reveal extensive communication between the tripartite, N-D1-D2 domains (Pye et al. 2006). Conformational changes first initiated in the D2 ring are relayed through a D1-D2 linker region to the D1 (-subdomain. The D1 (-subdomain, in turn, communicates these motions to the flexibly-linked N-domain, thereby regulating its conformation (DeLaBarre and Brunger 2005). Ultimately, these ATP-powered conformational changes are utilized in remodeling macromolecular complexes. One hypothesis is that IBMPFD mutations interfere with p97 biochemical activity by altering its conformation or interdomain communication. For example, structural analysis of p97 in the pre-activated ATP-occupied state revealed communication between Arg155 and Arg159 within the N-terminal domain and the D1 residue asparagine387-all that are now identified as mutated residues in IBMPFD (DeLaBarre and Brunger 2005; Hubbers et al. 2007). However, it remains to be seen whether IBMPFD mutations do indeed induce structural or conformational defects in p97.

In this report, we specifically focused on studying IBMPFD p97R155P and p97A232E mutants because Arg155 is the most commonly affected amino acid residue, and mutation of Ala232 is associated with increased severity of the disease. (Watts et al. 2004; Kimonis et al. 2008). A series of biochemical approaches were employed to characterize the oligomeric assembly, ATPase

activity, and solution structure of wild-type (p97WT) and mutant p97. Our results indicate that recombinant p97R155P and p97A232E assembled into ~600 kDa complexes similar to p97WT. Both mutants showed a 3 fold increase in ATPase activity and increased sensitivity to heat induced upregulation in ATPase activity. Analysis of the intrinsic protein fluorescence and proteolytic susceptibility provided evidence for conformational defects in the D2 ring. These effects correlated with increased propensity for aggregation in the presence of ATP. Based on these data, we propose that IBMPFD p97 mutations induce structural defects, which may underlie the mechanism of pathogenesis in biological systems.

2.3 Results

IBMPFD p97 mutants, p97R155P and p97A232E, form hexameric complexes similar to p97WT *in vitro*.

To investigate the oligomerization pattern of p97R155P and p97A232E, recombinantly expressed p97 proteins, first purified on a metal affinity column, were size-fractionated by gel filtration chromatography (Fig. 2.1 A and B). p97WT, IBMPFD mutants, p97R155P and p97A232E, and an ATPase deficient mutant, p97K524A, all eluted in two peaks: a minor peak within the void volume (Fig. 2.1 A & B , Peak 1, ~37-43 ml), and a major peak overlapping with the 670 kDa thyroglobulin complex (Fig. 2.1 A & B, Peak 2, ~47-63 ml). Further analysis of the major peak fraction by native gel electrophoresis also demonstrated that both p97R155P and p97A232E comigrated with p97WT and the thyroglobulin complex (Fig. 2.1 C). Interestingly, p97K524, which encompasses a mutation abolishing ATP binding in the D2 ring, could not be resolved under the native gel electrophoresis conditions used. These results indicate that p97WT and IBMPFD mutants formed ~ 600 kDa complexes consistent with hexameric assembly. To confirm ring-shaped assembly, the hexameric protein peaks (Fig. 2.1 D) were analyzed by negative-staining electron microscopy. At 160,000 X magnification, p97R155P, p97A232E, and p97K524A showed relatively homogenous populations of ring-shaped particles notably similar to p97WT (Fig. 2.1 E, upper panel). ATP-binding had no effect on the ring-shapped assembly of p97WT or mutant variants (Fig. 2.1 E, lower panel). Furthermore, all p97 protein samples contained some misfolded aggregates (not shown); however, there were no

apparent differences in the structure or abundance of these aggregates between p97WT and mutant variants. All together, these results confirm that IBMPFD p97 mutants, and p97K524A, assemble into hexameric, ring-shapped complexes similar to p97WT and display no inherent propensity for misassembly or aggregation.

IBMPFD mutants, p97R155P and p97A232E, confer a gain-of-function phenotype on p97 total ATPase activity and alter its intrinsic fluorescence profile.

The ATPase activity of p97WT, p97R155P, and p97A232E was monitored under physiological temperature and saturating ATP concentrations. At 37 ºC, p97R155P and p97A232E displayed significantly higher ATPase activity than p97WT (Fig. 2.2 A and C, Table 2.1). The ATP hydrolysis rates of p97R155P and p97A232E were similar, and about three times higher than the rate of p97WT (Fig. 2.2 C, Table 2.1). At 42ºC, there was no significant increase in p97WT ATPase activity; however, p97R155P and p97A232E displayed a significant 1.7 and 1.4 fold increase, respectively (Fig. 2.2 B and C, Table 2.1). Furthermore, p97R155P's heat-induced ATPase activity was significantly higher than p97A232E (Fig. 2.2 C and Table 2.1). In contrast, p97K524A, displayed no measurable ATPase activity at both temperatures (Fig. 2.2 A-C and Table 2.1). Collectively, these data show that IBMPFD mutants, p97R155P and p97A232E, display not only elevated ATPase activity, but also increased sensitivity to heat-induced upregulation of ATPase activity.

To investigate if the upregulation in p97 ATPase activity correlated with changes in the conformational state of the AAA+ rings, a qualitative analysis was performed using intrinsic protein fluorescence spectroscopy (Fig. 2.3 and Table 2.2). In this assay, the change in protein fluorescence is inversely related to the hydrophobicity of tryptophan 476 (Trp476) within the D2 ring (Wang et al. 2003). In the absence of ATP-binding, only p97R155P showed significantly higher total fluorescence emission than p97WT, which is indicative of increased basal accessibility of Trp476 (Table 2.2, Fig. 2.3 A). Both p97A232E and p97K524A also displayed higher total fluorescence emission than p97WT, although it did not reach statistical significance (Table 2.2, Fig. 2.3 A). Upon ATP-binding, p97R155P and p97A232E displayed significantly higher total fluorescence compared to p97WT, which reflects increased solvent accessibility of Trp476 (Table 2.2, Fig. 2.3 B). On the other hand, p97K524A displayed significantly lower total fluorescence than p97WT and both IBMPFD-linked mutants, which is consistent with its inability to bind ATP in the D2 ring (Fig. 2.3 B&C and Table 2.2). Comparison of the ATP-dependent change in total fluorescence showed that p97R155P underwent the largest change in protein fluorescence (Fig. 2.3 C, Table 2.2). All together, these data suggest that p97R155P undergoes the largest conformational change in response to ATP-binding and that both, p97R155P and p97A232E, display ATP-dependent conformational alternations in the local region surrounding Trp476 within the D2 ring.

IBMPFD mutants, p97R155P and p97A232E, display a loss in the protective effect of ATP-binding on D2 ring proteolysis.

We further analyzed conformational differences between p97WT and IBMPFD mutants using a limited-proteolysis approach. Trypsin-mediated digest of full-length p97 generated two predominant cleavage products, p87 and p58, both retaining a large N-terminal epitope (residues 9-130, Fig. 2.4 A). Silver stain analysis ruled out the presence of additional cleavage products (Fig. 2.4 B). Thus, p87 reflected the cleavage of the COOH-terminal domain, while p58 resulted from additional proteolysis of the D2 ring. Comparison of proteolysis kinetics between p97WT and p97R155P revealed similar susceptibility patterns in the absence of ATP addition, while p97A232E and p97K524A were more prone to proteolysis (Fig. 2.4 A, left panel). Specifically, p87 proteolysis was completed at 90 minutes for p97A232E and p97K524A, compared to 120 minutes for p97WT and p97R155P (Fig. 2.4 A&B, left panels). These data indicate that the conformation of the COOH-terminal domain and the D2 ring are more 'labile' in p97A232E and p97K524A. Furthermore, p97WT showed an ATP-dependent delay in p87 and p58 degradation where both cleavage products could be detected 120 minutes after the initiation of the reaction (Fig. 2.4 A, right panel). In contrast, p87 showed increased susceptibility to proteolytic cleavage in all p97 mutants, with p97A232E and p97K524A having the most accelerated degradation kinetics. Conversely, p58 was most strongly protected in p97R155P relative to all other p97 variants.

To identify the approximate sites of proteolysis, p97, p87, and p58 were sequenced using mass spectrometry (Table 2.3, Fig. 2.5). p97 sequencing resulted in the generation of peptides covering 58% of its total amino acid sequence. The most N-terminal amino acid residue was determined to be Gly9, while Arg772 was identified as the last COOH-terminal residue. A large part of the COOH-terminal domain of p97 (residues 773-806) did not contain trypsin cleavage sites and therefore likely generated a peptide too large for detection by mass spectrometry (Data not shown). Sequencing of p87 identified Leu26 at the N-terminal domain and Arg709 at the COOH-terminal end, while the peptide coverage was determined to be 51% of p97 total amino acid sequence. p58 sequencing covered 39% of p97 amino acid sequence, starting with Met46 and ending with Lys524 (Table 2.3, Fig. 2.5). These results suggest that the increased proteolytic susceptibility of p87 in p97R155P and p97A232E is due to D2 ring destabilization between residues Lys524 and Arg709 (Fig. 2.4 C).

IBMPFD p97 mutants, p97R155P and p97A232E, undergo ATP-dependent alteration in solution structure.

In the absence of ATP, p97 particle size distribution consisted of two populations: a population of ~ 20 nm particles corresponding to assembled p97 (Fig. 2.6 A, Table 2.4, Peak 1), and a minor population reflecting large diameter species (Fig. 2.6 A & Table 2.4, Peak 2). p97R155P and p97A232E showed similar distributions to p97WT (Fig. 2.6 A) and displayed no significant differences in the diameter estimates of either assembled p97 or the large diameter species

(Table 2.4). In all cases, the most abundant population reflected hexameric p97 and accounted for at least 80% of the total light scattering intensity (Table 2.4, Peak 1). Interestingly, assembled p97K524 and its large diameter species both displayed significantly higher diameter estimates, with the assembled population accounting for at least 90% of the light scattering intensity (Fig. 2.6 A, Table 2.4, Peak1 and Peak 2).

In the presence of physiologically relevant ATP concentrations, there were no significant changes in the solution structure of p97WT. In comparison, the light scattering intensity of assembled p97R155P was significant reduced and this effect correlated with an increase in the scattering intensity of the large diameter population (Fig. 2.6 B, Table 2.4). These results show an ATP-dependent shift towards increased abundance of the large diameter population in p97R155P. Furthermore, the diameter estimate of assembled p97R155P was significantly reduced compared to p97WT (Table 2.4). Similarly, p97A232E displayed a pronounced increase in the abundance of the large diameter population, which correlated with a significant reduction in particle size (Fig. 2.6 B, Table 2.4). However, unlike p97R155P, assembled p97A232E diameter was significantly reduced compared to the ATP-unbound state as well as assembled p97WT(Table 2.4). These effects correlated with a significant increase in the heterogeneity of the population's size distribution profile, as reflected by the increased polydispersity index estimate (Table 2.4). Therefore, ATP-binding changed the solution structure of p97A232E and promoted the formation of large diameter

complexes. Moreover, the large diameter population in p97K524A displayed changes similar to p97A232E; however, despite the increased abundance of the large diameter population in p97K524A, both the size and light scattering intensity were not significantly different from p97WT (Table 2.4). Interestingly, compared to p97WT, ATP-binding significantly reduced the diameter of assembled p97R155P and p97A232E, but increased the diameter of p97K524A (Table 2.4). All together, these data provide evidence for ATP-dependent alterations in the solution structure of IBMPFD mutants and indicate that ATP-binding may facilitate the formation of large diameter species.

2.4 Discussion

IBMPFD is a degenerative disorder caused by single substitutions in highly conserved amino acid residues in the N-domain and the D1 ring of p97 (Watts et al. 2004; Kimonis et al. 2008). Affected residues are proposed to play a role in relaying conformational changes initiated in the D2 ring to adaptor protein complexes (DeLaBarre and Brunger 2005). These ATP-powered conformational changes (Rouiller et al. 2000; Rouiller et al. 2002), in turn, provide the mechanistic basis for p97 cell biological activity. In this study, we provide evidence for structural defects in IBMPFD p97 mutants, p97R155P and p97A232E. We show that both mutations up-regulate p97 ATPase activity and increase sensitivity to heat-induced upregulation of ATPase activity. Using protein fluorescence analysis and a limited proteolysis assay, we provide evidence for altered conformational states and destabilization of the D2 ring. We further show that these defects correlated with a propensity for nucleotide-dependent aggregation of both mutants in solution. Based on these data, we propose that structural defects in p97 may underlie the pathogenesis of IBMPFD.

IBMPFD p97 mutations in Arg155 and Ala232 do not impair spontaneous self-assembly. Using size-exclusion chromatography and native gel electrophoresis, we showed that IBMPFD mutants, p97R155P and p97A232E, assembled into hexameric complexes and ruled out the possibility of misassembly or de-oligomerization. Visualization by electron microscopy further confirmed the ring-shaped structure of the pathogenic p97 mutants. These

results are in agreement with previous finding that p97R155H does not display an oligomerization defect (Weihl et al. 2006) and are consistent with the N-domain being dispensable for hexamerization (Rouiller et al. 2002; Ye et al. 2003). We also show that p97 mutation, A232E, does not impair hexamerization, in spite of its localization in the D1 ring, which is necessary for p97 self-assembly (Wang et al. 2003). Residue Ala232 is positioned at the junction between the D1 domain and the N-D1 linker region (Watts et al. 2004). This peripheral localization is inconsistent with a role in regulating inter-protomer interaction within the D1 ring. Other works have demonstrated that p97 oligomerization is spontaneous, and that nucleotide binding to the D1 ring stabilizes the hexamer (Wang et al. 2003). The only single amino acid mutations, known to prevent p97 assembly affect the D1 walker A residue, Lys251 (Wang et al. 2005; DeLaBarre et al. 2006) or the D1 second region of homology (SRH) residue, Arg362 (Wang et al. 2005). Mutations of residues lining the D1 pore (Arg313, Lys315, Thr316, His317, Glu319, and Arg322) also do not influence oligomerization (DeLaBarre et al. 2006). Together, our results suggest that the disease severity associated with mutation in Ala232 in IBMPFD is likely unrelated to an oligomerization defect in p97. Interestingly, our data also suggest that p97K524A may be forming higher ring-shaped oligomers than p97WT or IBMPFD mutant variants. This is evident in its migration pattern on native gel electrophoresis and its significantly larger diameter estimate in solution. Recent work demonstrated that the D2 ring adopts a heptameric structure with a 7-fold symmetry when purified independent of the N-domain and the D1 ring (Davies et al. 2008). It is possible that disrupting

nucleotide binding in the D2 ring may also alter the fold symmetry of p97. Alternatively, p97K524A mutation may alter the shape of the hexamer in a way that influences its native gel migration and increases its apparent diameter in solution.

IBMPFD p97 mutants, p97R155P and p97A232E, show increased ATPase activity. Under the conditions used, the specific ATPase activity of p97WT was lower than the values previously reported (Meyer et al. 1998; Song et al. 2003; DeLaBarre et al. 2006), although different expression, purification, and assay conditions were used. Nevertheless, our data show ~ 3 fold increase in p97R155P ATPase activities. In another report, p97R155H mutant, displayed ATPase activity levels comparable to p97WT, whereas heat-induced upregulation in ATPase activity was not assessed (Weihl et al. 2006). One explanation for this discrepancy is the nature of the amino acid change associated with Arg155. For example, DeLaBarre and colleagues showed that different amino acid substitutions of the D1 pore residue His317 could have opposing effects on p97 ATPase activity, in spite of the fact that His317 is not directly involved in ATP-binding or hydrolysis (DeLaBarre et al. 2006). Nevertheless, our results pose the possibility that p97 N-domain is involved in the positive regulation of p97 basal ATPase activity. The strong ATP-dependent protection of the p58 N-terminal fragment of p97R155P in the limited proteolysis assay suggests increased affinity for ATP binding in the D1 ring. Changes in nucleotide binding affinity may alter the cooperativity between the D1 and D2 rings. Furthermore, previous studies

demonstrated that some adaptor protein binding to p97 N-domain (ie. p47) down-regulate p97 ATPase activity (Meyer et al. 1998), while others had no effect (ie. Npl4/Ufd1) (Bruderer et al. 2004). To date, it remains to be determined whether any of p97 ubiquitous N-domain binding proteins could play a role in the positive regulation of its ATPase activity. Interestingly, deletion of the N-terminus does not influence p97 ATPase activity (Rouiller et al. 2002; Ye et al. 2003; Rothballer et al. 2007).

Like p97R155P, our results also show that p97A232E displayed up-regulated ATPase activity. The contribution of the D1 ring to p97 basal ATPase activity is unclear (Song et al. 2003; Ye et al. 2003); however, it is known to be activated in response to heat stimulation (Song et al. 2003). Our data show that the ATPase activity of both mutants is significantly up-regulated at 42°C, but do not rule out the ectopic activation of the D1 ring at 37°C. Accordingly, this increase in basal ATPase activity could be attributed to either D1 ring activation at 37°C, or increased activity of the D2 ring, or both. On the other hand, the increased sensitivity to heat stimulation suggests alteration in D1 ring function. Nevertheless, an increase in ATPase activity may be detrimentally alter p97 cell biological activities by destabilize p97-mediated protein interactions, or alternatively, leading to the gain of new toxic functions (ie. increasing the binding affinity or promiscuity of p97-substrate interaction). Further studies are needed to address the mechanism by which IBMPFD mutations up-regulate p97 ATPase activity and the possible implications on biological systems.

Evidence of structural defects in IBMPFD p97 mutants, p97R155P and p97A232E. Our results indicate that Arg155 and Ala232 mutations influence distant residues within p97 structure, a fact consistent with the dynamic nature of p97 inter-domain communication (Rouiller et al. 2000; Rouiller et al. 2002). Considering that Trp476 fluorescence has been previously used to report ATP-dependent conformational changes within the D2 ring (Wang et al. 2003), our data suggest that p97R155P and p97A232E display different D2 ring conformations than p97WT. We further defined the affected region between residues Lys524 and Arg709, which covers part of the D2 ring and the COOH-terminal domain. The tryptic proteolysis assay showed that this region is more susceptible to proteolysis. Wang et al. previously demonstrated that p97WT showed a large increase in protein fluorescence in response to ATP-binding and that this correlated with protection of the D2 ring from proteolysis (Wang et al. 2003). While this is consistent with the results reported here, both p97R155P and p97A232E showed significantly higher ATP-dependent shifts in protein fluorescence than p97WT with only partial D2 ring protection during the limited proteolysis assay. It is possible that an elevated rate of nucleotide exchange may account for the increased proteolytic susceptibility of the D2 ring, especially since p97 D2 ring adapts a flexible state directly following nucleotide release (DeLaBarre and Brunger 2005). Alternatively, the increased ATPase activity may be consequential to structural defects imposed by mutations in residues Arg155 and Ala232. In either case, the results indicate that the ATP-bound D2 ring adapts a relaxed conformation in p97R155P and p97A232E compared p97WT.

Interestingly, while p97R155P displayed a larger change in protein fluorescence compared to p97A232E, this did not correlate with faster proteolysis kinetics.

A possible explanation is that the Arg155 mutation increases the affinity for nucleotide binding as suggested by the strong protection of p58 during the limited proteolysis assay. Nevertheless, both p97R155P and p97A232E show increased proteolytic susceptibility in the region between residues Lys524 and Arg709. Importantly, this region contains residues central for p97 function in ER-associated degradation (ERAD), specifically Arg586 and Arg599 as well as Phe551 and Trp552 (DeLaBarre et al. 2006). Arg586/Arg599 have been suggested to form a 'denaturation collar' for the processing of misfolded ERAD substrates, and Phe551/Trp552 have been proposed to bind to misfolded substrates through hydrophobic interactions (DeLaBarre et al. 2006; Halawani and Latterich 2006). It is also known Arg586/Arg599 adapt different localizations relative to the D2 pore during the ATPase cycle (DeLaBarre and Brunger 2005). Accordingly, the conformational integrity of the D2 ring is necessary for proper substrate processing and its perturbation in IBMPFD mutations may represent a possible mechanism of pathogenesis. Although it is yet unclear if IBMPFD-linked p97 mutations influence the accessibility or function of the 'denaturation collar', our data indicate that the overall conformational state of the D2 ring is altered in mutant p97 complexes. Indeed, IBMPFD-linked mutation in residues Arg155 (R155H) has been shown to impair the degradation of ERAD substrate, (F508-CFTR, in C2C12 skeletal myoblasts (Weihl et al. 2006). Future studies are necessary to substantiate if all IBMPFD-linked p97 mutations result in similar

alteration in D2 ring conformation and if this is indeed a relevant mechanism of pathogenesis *in vivo*.

Consequences of IBMPFD mutations on p97 solution structure-Dynamic light scattering (DLS) is a technique used to resolve particle size distribution in solution. Our analysis clearly showed a di-disperse distribution consisted of assembled p97 and large diameter species. The hydrated diameter of p97, estimated at 20-25 nm, is consistent with published structural data (Rouiller et al. 2002). Remarkably, we showed an ATP-dependent increase in the light scattering intensity of the large diameter population in samples containing p97R155P and p97A232E, but not p97WT or p97K524A. Considering that there was no significant increase in diameter size, the increase in light scattering intensity should be attributed to increased abundance of the large diameter species. This finding appears at odds with our EM images, which show assembled, ring-shaped p97 in presence of ATP. However, it is important to note that the percent intensity measurements in DLS do not reflect the actual proportion of the large diameter species versus hexameric p97 particles, and that DLS detects large diameter species with high sensitivity. Overall, based on the EM study and the ATPase activity analyses, we conclude that hexameric p97R155P and p97A232E remain the predominant populations. However, in solution, p97R155P and p97A232E show an ATP-dependent propensity to assemble into large diameter particles. The fact that the estimated diameter of these particles was ~ 10 X larger than the diameter of the assembled hexamers

pose the possibility of ATP-mediated aggregate formation. Alternatively, the large diameter particles may represent a population of transiently interacting p97 hexamers.

Together, these biochemical data provide the first evidence of structural defects associated with IBMPFD p97 mutations. Importantly, these defects correlated with increased ATPase activity and alterations in mutant p97 solution structure. It remains unclear whether these defects could be generalized to other IBMPFD p97 mutations, especially since both mutations, R155P and A232E, are relatively rare (Kimonis et al. 2008). It is known that some p97 mutants, such as p97R95G and p97R155H, show reduced solubility in cell culture models (Weihl et al. 2006). Consistently, our initial analysis of p97R95G expression in recombinant expression systems also showed reduced solubility (unpublished data). Accordingly, it remains to be seen if this effect is secondary to structural and biochemical defects such as these reported here. We propose that IBMPFD mutations influence D2 ring conformation by increasing its flexibility and reducing its compactness upon ATP-binding. Considering the newly proposed role of the D2 ring in the processing of protein substrate (DeLaBarre et al. 2006; Halawani and Latterich 2006), these defects may have detrimental consequences on p97 cell biological functions.

2.5 Materials and Methods

Generation of p97 recombinant expression constructs.

Wild-type murine p97 cDNA clone in pBluescript SK+ was a kind gift of Dr. Fred Indig (National Institute on Aging/NIH, Baltimore, USA). To introduce IBMPFD mutations, p97cDNA was subjected to site-directed mutagenesis using the GeneTailor(kit according to manufacturer's instructions (Invitrogen, Carlsbad, CA). For the R155P mutation, G464 in codon 463CGG465 was substituted with C using the following primers: 5' AGGAGATATTTTTCTTGTCCCGGGTGGGATG 3', and 5' GGACAAGAAAAATA TCTCCTTTACGGATGGGCC 3'. For the A232E mutation, C695 in codon 694GCG696 was mutated to A using primers 5' ACATCCTGCGCTCTTCAAGGAGATTGGTGTA 3' and 5' CCTTGAAGAGCGCAGGATGTCTCAGTGGCAGCT 3'. cDNA of the ATP-binding deficient mutant p97K524A in pQE9 vector was a kind gift of Dr. Tom Rapoport (Harvard University, Boston, USA). Subsequently, all constructs were subcloned into the pTrcHis2C vector backbone (Invitrogen, Carlsbad, CA) for COOH-terminal polyhistidine tagging by PCR. Briefly, cDNA was amplified using primers:5' CCGAGCTCGGCCTCTGGAGCCGAT 3',and 5' ATGGTACCAGCGGC ATACAGGTCATC 3', which contained the Sac I and Kpn I restriction sites, respectively. Following restriction digests, the PCR products were ligated into the pTrcHis2C multiple cloning site. Insertion of cDNA was verified by restriction digest, which was followed by full sequencing (McGill University and Genome Quebec Innovation Center, Montreal, QC).

Expression and purification of Recombinant p97.

Wild-type p97 and mutant variants were expressed in the TOP10 E. coli strain. Overnight starter cultures were diluted 50 X in 2 L of 2 X YT media, with 100 μg/ml ampicillin, and grown at 37 °C until reaching an OD of 600 nm. Cultures were subsequently induced with 300 (M IPTG and further grown for 4 hours. Cells were pelleted by centrifugation (4,000 g for 20 minutes) and lysed in buffer A (20 mM HEPES pH=7.5, 300 mM NaCl, 5 mM $MgCl_2$, 2.5 mM DTT, and 20 mM imidazole), supplemented with 1 mg/ml lysozyme and complete protease inhibitors (Roche, Mississauga, ON). Following sonication, the lysates were cleared by centrifugation at 26,000 g for 45 minutes. The supernatant was then loaded on a 5 ml Ni2+ affinity column (GE Healthcare Bio-sciences, Uppsala, Sweden) pre-equilibrated with 10 X column volume of buffer A. Following a first wash with 10 X column volume of buffer A, bound proteins were subjected to an additional wash with 10 X column volume of buffer B (20 mM HEPES pH 7.5, 300 mM NaCl, 5 mM $MgCl_2$, 2.5 mM DTT, and 35 mM imidazole). The proteins were eluted with 35-500 mM imidazole gradient over 5 X column volume. Peak fractions containing p97 were pooled, concentrated on Amicon Ultra column, MWCO 15,000 kDa, and loaded on a pre-calibrated 10 ml Superose-6 gel-filtration column (GE Healthcare Bio-sciences, Uppsala, Sweden). Size-fractionated proteins were eluted as 1 ml fractions in buffer C (20 mM HEPES pH 7.5, 150 mM NaCl, 5 mM $MgCl_2$, and 2.5 mM DTT). All purifications were performed at 4 °C using the UKTA FPLC purification system (GE Healthcare Bio-

sciences, Uppsala, Sweden). Protein concentrations were determined using the Bradford assay (BioRad, Mississauga, ON).

Native Gel Electrophoresis

Ten micrograms of purified recombinant wild-type p97 or mutant variants were loaded on a 6 % Tris-polyacrylamide gel (pH 8.0). Electrophoresis was performed at 4 °C using 200 V and ice-cold 1 X Tris-glycine buffer (pH 8.0) to prevent heat-induced denaturation.

Negative Staining Electron Microscopy

p97 proteins were diluted to a concentration of 50 μg/ml in buffer containing 20 mM HEPES pH 7.5, 150 mM NaCl, 10 mM $MgCl_2$, and 1 mM DTT, in the presence or absence of 1 mM ATP (Sigma, Oakville, ON). For each protein, a 5 μl sample was spotted on a glow discharged carbon-coated copper grid. The grids were then stained for 60 seconds with 5 μl of uranyl acetate and visualized using a FEI Tecnai 12 120 KV electron microscope. Digital images were collected with a Gatan 792 Bioscan 1k x 1k wide angle multiscan CCD camera. Images were cropped at the level of the scale bar to show ~25% of the full image.

Dynamic Light Scattering (DLS) Measurements

p97 protein samples were diluted to 100 μg/ml in buffer containing 20 mM HEPES pH 7.5, 150 mM NaCl, 10 mM $MgCl_2$, and 1 mM DTT in the presence or absence of 2 mM ATP. Measurements were performed using the Zetasizer Nano ZS (Malvern) at 20 ºC.

ATPase activity assays

p97 ATPase activity was assessed using the EnzCheck phosphate assay kit (Molecular Probe, Oregon, USA) as previously described (DeLaBarre et al. 2006). This assay is based on the inorganic phosphate-dependent conversion of 2-amino-6-mercapto-7-methylpurine riboside (MESG) to ribose-1-phosphate and 2-amino-6-mercapto-7-methylpurine, which results in a shift of the maximum absorbance from 330 nm to 360 nm (Webb 1992). For assessment of p97 ATPase activity, 50 nM of p97 (based on the ~600 kDa hexamer) were incubated in 100 μl reaction buffer (20 mM HEPES pH 7.5, 150 mM NaCl, and 10 mM $MgCl_2$) containing 200 μM of ATP. Parallel reactions were set without the addition of ATP to correct for background absorbance values. Absorbance at 360 nm was then measured at 20 seconds intervals for a total of 20 minutes at the physiological temperature of 37 °or 42 °C for heat induction. The amount of inorganic phosphate released was quantified based of a KH_2PO_4 standard curve of 0-80 μM set in 100 μl reaction buffer. All reactions were preformed in duplicates for each experiment.

Protein fluorescence spectroscopy

The intrinsic protein fluorescence was determined using the Edinburgh FLS-920 fluorometer. Protein samples were diluted to 62.5 μg/ml in buffer containing 20 mM HEPES pH 7.5, 150 mM NaCl, 10 mM $MgCl_2$, and 1 mM DTT in the presence or absence of 2 mM ATP. The excitation wavelength was set at 295 nm while fluorescence emission was monitored between 305 nm and 450 nm. The excitation and emission slits were set at 5 nm and the measurements were performed using a high PMT voltage setting. All measurements were performed at 20°C and corrected for background emission values. Four independent measurements were performed, each in triplicates, for each p97 protein variant.

Limited proteolysis assay and western blot detection

Proteolysis reactions were performed at 37 °C in a total volume of 50 μl containing 5 μg of p97, 250 ng of trypsin, and reaction buffer (20 mM HEPES pH 7.5, 150 mM NaCl, 10 mM $MgCl_2$, and 1 mM DTT) in the presence or absence of 1 mM ATP, for the indicated time intervals. Reactions were terminated by the addition of 0.5 mM PMSF and boiled in 1 X SDS loading buffer. Samples were subsequently subjected to SDS-PAGE and transferred to polyscreen© PVDF membranes (Perkin Elmer, Zaventem, Belgium). Following blocking in 5 % non-fat milk, membranes were incubated in a monoclonal anti-p97 antibody at a dilution of 1:1000 (BD Transduction Laboratories(tm), San Jose, CA) for 1 hour at room temperature. The blots were then incubated in HRP-conjugated anti-mouse

secondary antibody and subsequently developed using the ECL Plus detection system. Visualization was performed using the Storm 840 scanner (GE Healthcare, Baie d'Urfé, QC).

LC/MS-MS sequencing of full-length p97 and limited proteolysis products

Proteolysis reactions were performed by incubating 5 μg of wild-type p97 with or without 250 ng of trypsin in buffer containing 20 mM HEPES pH 7.5, 150 mM NaCl, 10 mM $MgCl_2$, 1 mM DTT, and 1 mM ATP. Reactions were set in 50 μl volumes and incubated at 37 ºC for 60 minute. Following termination with 0.5 mM PMSF, samples were boiled in 1 X SDS loading buffer and subjected to SDS-PAGE followed by coomassie staining. Stained bands were excised and analyzed at the Institut de recherches cliniques de Montréal proteomics discovery platform (Montréal, QC).

Statistical Analysis

An analysis of variance (ANOVA) was conducted followed by the Scheffé post hoc test or Tukey/Kramer analysis. Data was designated as statistically significant only if the p value was equivalent to or less than 0.05. All tests were conducted using the StatView 5.0 software (SAS Institute Inc., Cary, NC).

2.6 Acknowledgments

We gratefully acknowledge Dr. Tom Rapoport (Harvard University, Boston, MA, USA) and Dr. Yihong Ye (NIDDK/NIH, Bethesda, MD, USA) for the initial cloning of the ATPase deficient p97K524A construct and for their generous advice on the expression and purification of recombinant p97. We also would like to thank Dr. Julie Jodoin (McGill University, Montréal, QC, Canada) for advice on the statistical analysis and critical reading of the manuscript, Dr. Julia Guy (University of Montréal, QC, Canada) for assistance with the fluorometeric analysis, and Archana Srivastava for assistance with the EM imaging. Part of this work was supported by grants from the HFSP, Genome Canada, Silicon Kinetics and Genocean to ML, CIHR grant #MOP-86693 to I.R, CIHR grant #MOP-53282 to M.S., and CIHR grand #MOP-81146 to ALB. I.R. is recipient of a CIHR New Investigator award and M.S. is the recipient of a Rx&D/CIHR Health Research Foundation Career Awards in Health Sciences. ML wishes to acknowledge support from the Canada Research Chair Program.

Table 2.1: Quantification of p97/VCP ATPase Activity

	37 °C (nmole Pi $ug^{-1}min^{-1}$)	**42 °C** (nmole Pi $ug^{-1}min^{-1}$)
p97WT	0.0289±0.0065	0.0412±0.0048
p97R155P	0.0885±0.0098*	0.1471±0.0309*#
p97A232E	0.0742±0.0058*	0.1036±0.0156*
p97K524A	0.0016±0.0024*	0.0010±0.0017*

Statistically significant from $p97^{WT}$ (*) or $p97^{A232E}$ (#), Tukey /Kramer Test, $p \leq 0.05$.

Table 2.2: Comparison of p97/VCP total protein fluorescence emission.

	-ATP	+ATP	Δ		-ATP	+ATP
p97WT	2485.5±89.6	3025.9±98.2	+540			
p97R155P	2775.8±126.9*	3493.7±99.0*	+717.9	**p97R155P vs. p97WT**	+290.3 ±99.8	+467.9 ±48.9
p97A232E	2699.8±169.3	3141.3±46.1*	+441.5	**p97A232E vs. p97WT**	+214.3 ±84.4	+115.4 ±68.4
p97K524A	2663.1±14.9	2650.9±76.6 *	- 12.2	**p97K524A vs. p97WT**	-177.6 ±94.5	-374.9 ±34.3

* Statistically significant from $p97^{WT}$ at $p \leq 0.05$ (Scheffe)

Table 2.3: LC/MS-MS sequencing of p97 tryptic fragments.

Gel Band	% Coverage of p97	Start Residue	End Residue	Theoretical MW	Functional Domains
p97	58%	Gly^{9}	Arg^{772}	85.4 kDa	N-D1-D2
p87	51%	Lys^{26}	Arg^{709}	75.9 kDa	N-D1-partial D2
p58	39%	Met^{45}	Lys^{524}	53.5 kDa	N-D1-partial D2

Table 2.4: Comparative analysis of p97 particle-size distribution in solution using dynamic light scattering.

	-ATP					+ATP				
		Peak 1		Peak 2			Peak 1		Peak 2	
	PDI (a.u.)	Diameter (nm)	Intensity (%)	Diameter (nm)	Intensity (%)	PDI (a.u.)	Diameter (nm)	Intensity (%)	Diameter (nm)	Intensity (%)
p97WT	0.380±0.04	22.73±1.89	84.1±2.5	413.5±92.5	15.9±2.5	0.343±0.013	25.25±0.97	87.4±1.9	311.4±116.2	12.5±1.9
p97R155P	0.433±0.03	21.80±0.37	81.9±2.7	384.1±99.9	18.1±2.7	0.459±0.122	22.13±0.70*	71.1±1.7*	236.5±26.06	28.8±2.1*
p97A232E	0.453±0.01	23.47±0.43	80.8±0.7	345.1±21.8	19.1±0.8	0.954±0.080*	20.11±0.12*	35.0±2.0*	239.5±16.65	65.0±2.0*
p97K524A	0.329±0.02	30.75±1.49*	95.8±4.2*	734.0±148*	4.20±1.1*	0.333±0.013	34.55±0.66*	87.2±1.1	403.3±130.0	12.8±1.1

* Statistically significant from p97WT at $p \leq 0.05$ (Scheffe)

Figure 2.1. Oligomeric assembly of p97 and IBMPFD mutants. A. Size-exclusion chromatography of recombinant p97 and mutant variants. Elution peaks for calibration controls, thyroglobulin (670 kDa) and gamma-globulin (158 kDa), are shown. Relative absorbance represents measured absorbance values at 280 nm adjusted for background absorbance. **B.** Coomassie-blue staining of peak elutions from A. 50 μl of 1 ml elution fractions were loaded on 10 % gels and subjected to SDS-PAGE. **C.** Coomassie-blue staining of p97WT or indicated mutants (5 μg) following native gel electrophoresis. **D.** Coomassie-blue staining of eluted p97 proteins following size-exclusion chromatography. p97WT or mutant variants (5 μg) were loaded on a 10 % gel and resolved by SDS-PAGE . **E.** Digital images of representative carbon-grid fields containing p97 particles, with (lower panel) or without (upper panel) 1 mM ATP, at 160,000 X magnification (Scale bar: 100 nm). Inserts: digitally enlarged p97 particles.

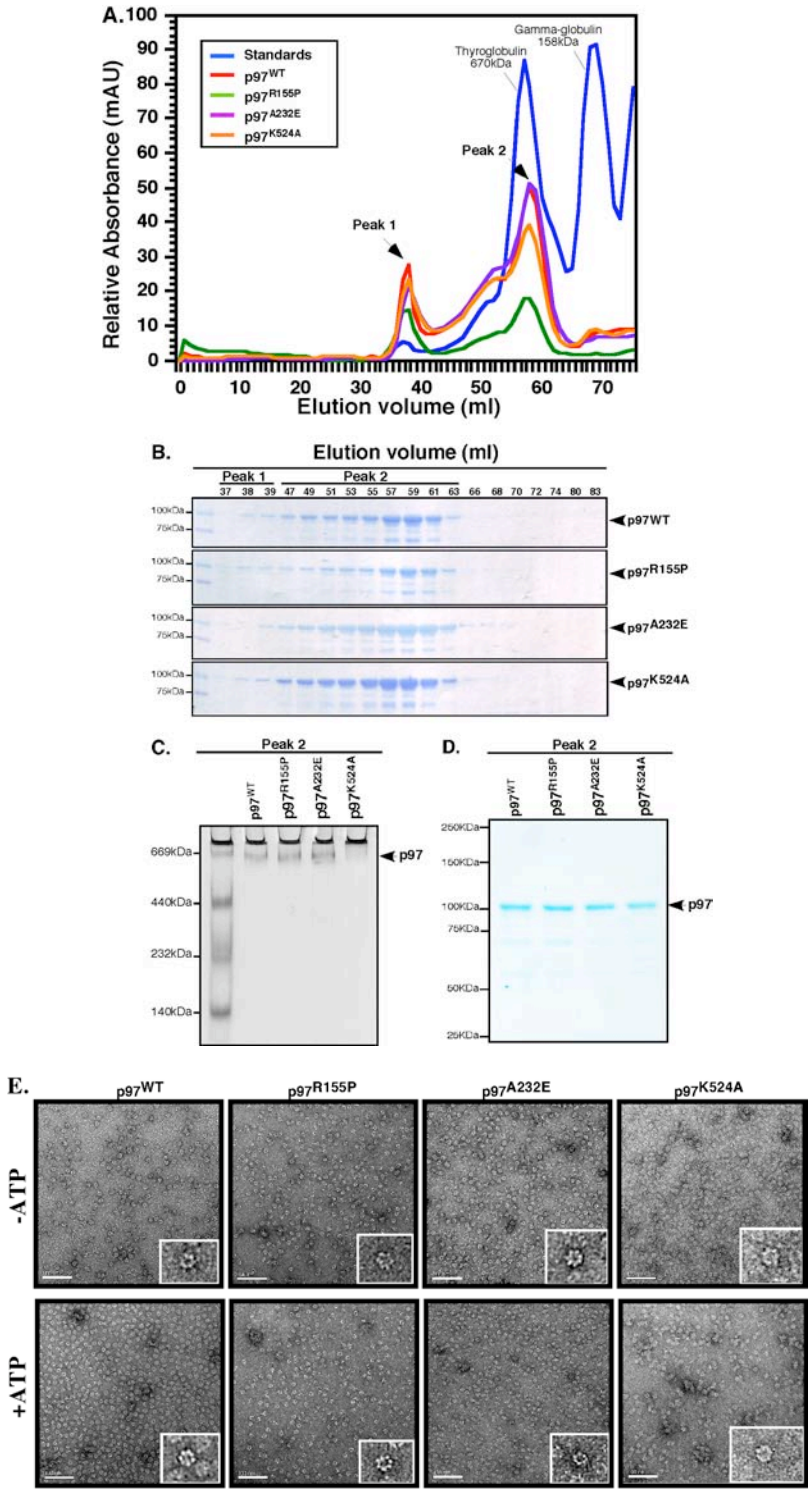
A.
Relative Absorbance (mAU)
Elution volume (ml)
Standards
p97WT
p97R155P
p97A232E
p97K524A
Gamma-globulin 158kDa
Thyroglobulin 670kDa
Peak 1
Peak 2
B.
Elution volume (ml)
Peak 1
Peak 2
p97WT
p97R155P
p97A232E
p97K524A
C.
Peak 2
669kDa
440kDa
232kDa
140kDa
p97
D.
Peak 2
250KDa
150KDa
100KDa
75KDa
50KDa
25KDa
p97
E.
p97WT
p97R155P
p97A232E
p97K524A
-ATP
+ATP

Figure 2.2. ATPase activity of p97WT and IBMPFD mutants. A&B. uantification of ATP hydrolysis of p97WT or indicated mutants at select time points. Measurements were performed at 37 °C (**A**), or 42 °C (**B**). **C**. Quantification of the average ATP hydrolysis rates of p97WT or mutant variants. Data represents an average of at least 4 independent measurements.

* Statistically significant from p97WT ($p \leq 0.05$).

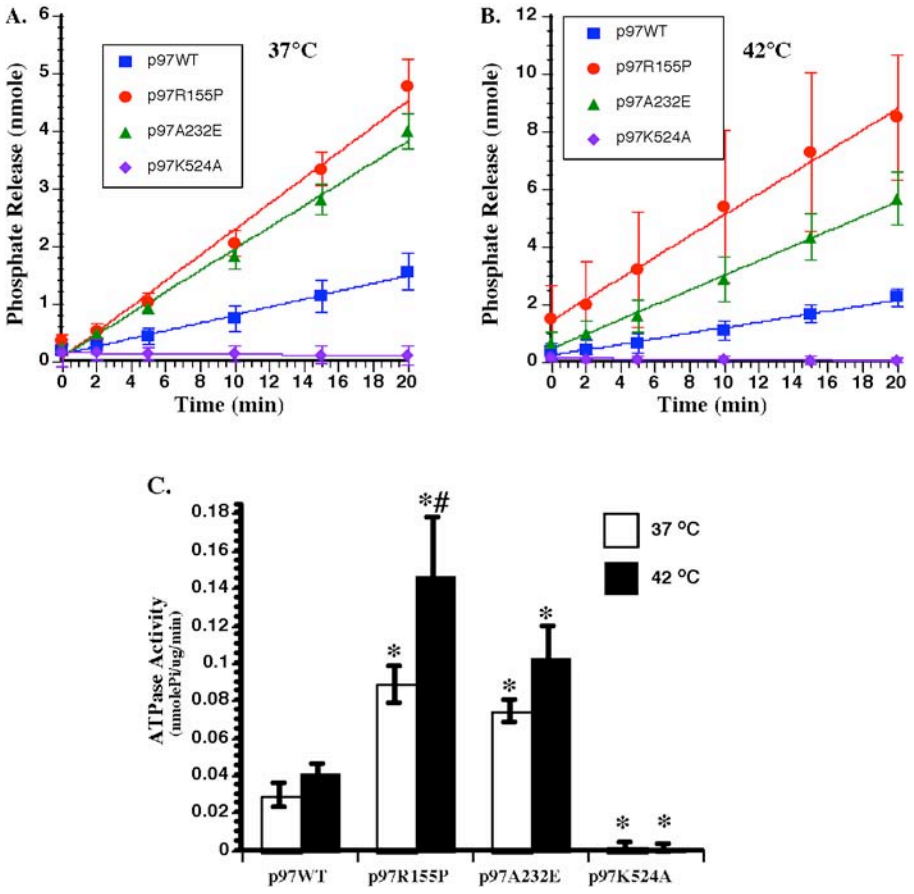
A.
37°C
p97WT
p97R155P
p97A232E
p97K524A
Phosphate Release (nmole)
Time (min)
B.
42°C
p97WT
p97R155P
p97A232E
p97K524A
Phosphate Release (nmole)
Time (min)
C.
37 °C
42 °C
ATPase Activity
(nmolePi/ug/min)
p97WT
p97R155P
p97A232E
p97K524A

Figure 2.3. Analysis of the intrinsic fluorescence properties of p97 and IBMPFD mutants. A. Fluorescence emission of p97WT or indicated mutants (62.5 μg/ml) between 305 to 450 nm, without nucleotide addition or in the presence of 2 mM ATP. B. comparison of p97WT or mutant p97 fluorescence emission without nucleotide addition. C. Comparison of p97WT or mutant p97 fluorescence emission with 2 mM ATP. Data is representative of four measurements each performed in triplicates. All measurements were corrected for background absorbance.

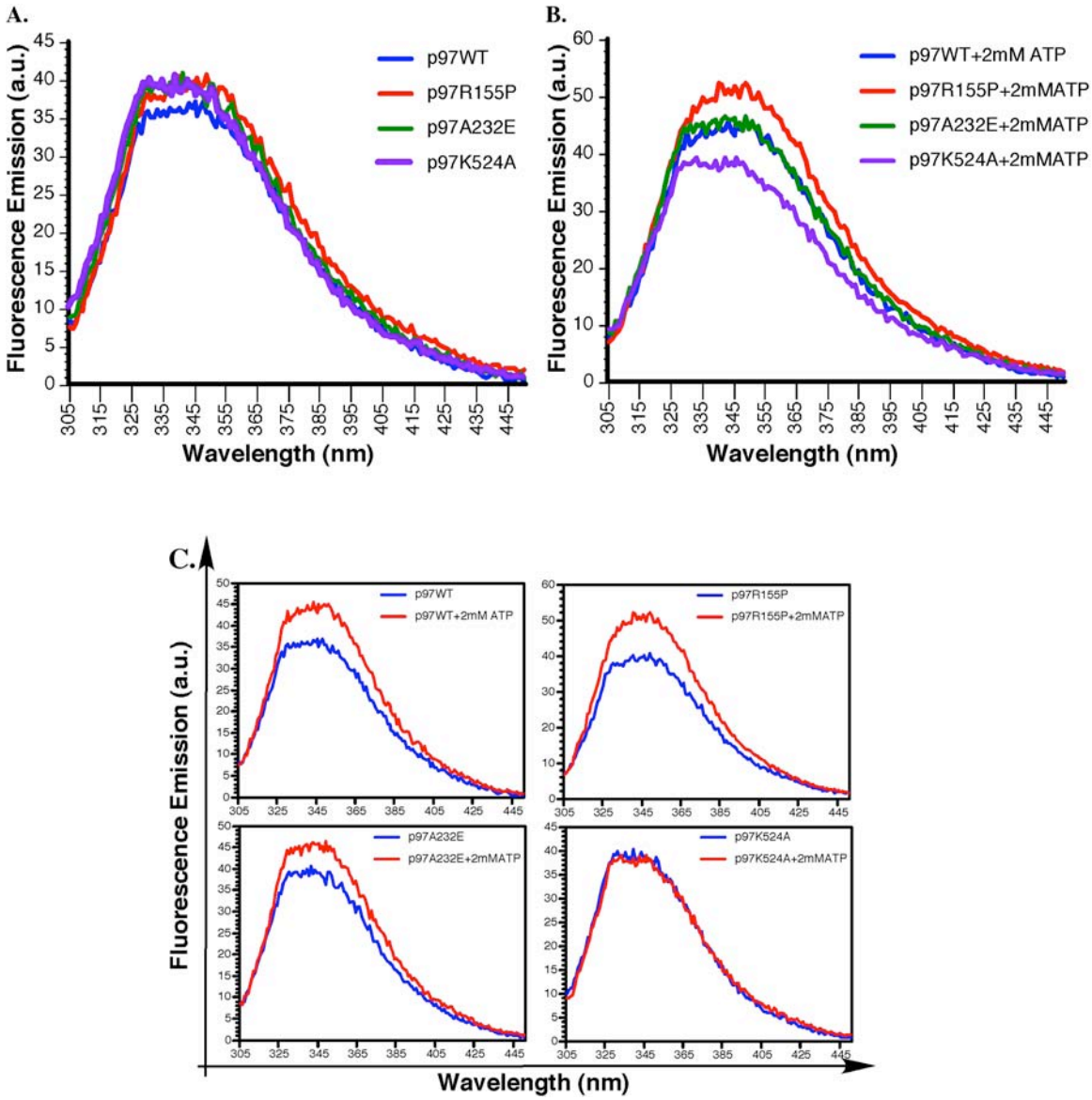
A.
Fluorescence Emission (a.u.)
Wavelength (nm)
p97WT
p97R155P
p97A232E
p97K524A
B.
Fluorescence Emission (a.u.)
Wavelength (nm)
p97WT+2mM ATP
p97R155P+2mMATP
p97A232E+2mMATP
p97K524A+2mMATP
C.
Fluorescence Emission (a.u.)
Wavelength (nm)
p97WT
p97WT+2mM ATP
p97R155P
p97R155P+2mMATP
p97A232E
p97A232E+2mMATP
p97K524A
p97K524A+2mMATP

Figure 2.4. Proteolysis kinetics of p97WT and IBMPFD mutants in limited proteolysis assay. A. Western blot analysis of p97WT or mutant variants subjected to trypsin digestion for the indicated times, using a monoclonal anti-N-terminal antibody (residues 9-130). Left panel: Trypsin digestion without nucleotide addition. Right panel: Trypsin digestion with 1 mM ATP. **B.** Schematic representation of p97 fragments generated from trypsinization. Abbreviations: ab; antibody, N; N-terminal domain, D1; D1 cassette, D2; D2 cassette, COOH; Carboxyl-terminal domain. **C.** Silver stain analysis of p97 trypsinization kinetics with (right panel) or without 1 mM ATP (left panel).

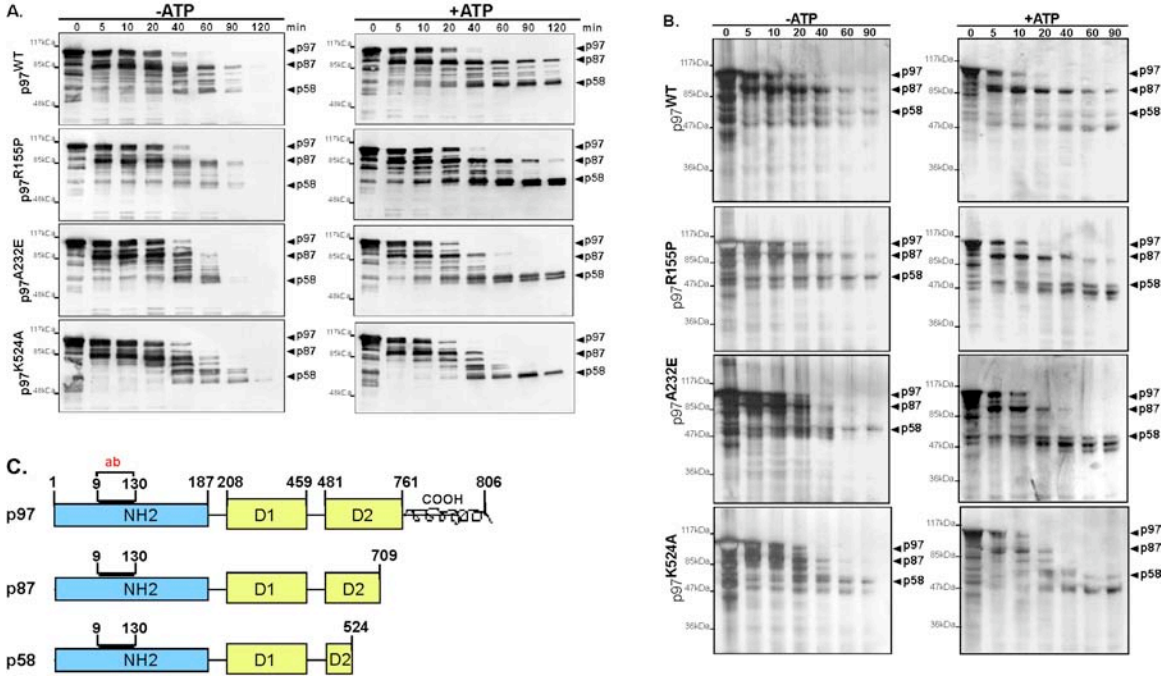
A.
-ATP
+ATP
0 5 10 20 40 60 90 120 min
p97WT
p97R155P
p97A232E
p97K524A
p97
p87
p58
B.
-ATP
+ATP
0 5 10 20 40 60 90
C.
ab
1 9 130 187 208 459 481 761 806
p97
NH2
D1
D2
COOH
9 130 709
p87
9 130 524
p58

Figure 2.5. Identification of the regions of proteolytic susceptibility in IBMPFD mutants. **A.** Coomassie-blue staining of p97WT subjected to trypsin digestion for 60 minutes in the presence of 1 mM ATP. **B.** Summary of full-length p97, and tryptic fragments, p87 and p58, LC/MS-MS sequencing results. **C.** Sequenced peptides identified by LC/MS-MS within the p97 full-length amino acid sequence.

A.

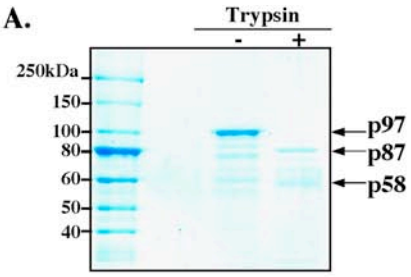

B.

Gel Band	Coverage	Start residue	End residue	Theoratical MW	Domains
p97	58%	Gly^{9}	Arg^{772}	85.4 kDa	N-D1-D2
p87	51%	Lys^{26}	Arg^{709}	75.9 kDa	N-D1-D2
p58	39%	Met^{16}	Lys^{524}	53.5 kDa	N-D1-partial D2

C.

Sample p97

Matched peptides shown in **Bold Red**

```
   1 MASGADSKGD DLSTAILKQK NRPNRLIVDE AINEDNSVVS LSQPKMDELQ
  51 LFRGDTVLLK GKKRREAVCI VLSDDTCSDE KIRMNRVVRN NLRVRLGDVI
 101 SIQPCPDVKY GKRIHVLPID DTVEGITGNL FEVYLKPYFL EAYRPIRKGD
 151 IFLVRGGMRA VEFKVVETDP SPYCIVAPDT VIHCEGEPIK REDEEESLNE
 201 VGYDDVGGCR KQLAQIKEMV ELPLRHPALF KAIGVKPPRG ILLYGPPGTG
 251 KTLIARAVAN ETGAFFFLIN GPEIMSKLAG ESESNLRKAF EEAEKNAPAI
 301 IFIDELDAIA PKREKTHGEV ERRIVSQLLT LMDGLKQRAH VIVMAATNRP
 351 NSIDPALRRF GRFDREVDIG IPDATGRLEI LQIHTKNMKL ADDVDLEQVA
 401 NETHGHVGAD LAALCSEAAL QAIRKKMDLI DLEDETIDAE VMNSLAVTMD
 451 DFRWALSQSN PSALRETVVE VPQVTWEDIG GLEDVKRELQ ELVQYPVEHP
 501 DKFLKFGMTP SKGVLFYGPP GCGKTLLAKA IANECQANFI SIKGPELLTM
 551 WFGESEANVR EIFDKARQAA PCVLFFDELD SIAKARGGNI GDGGGAADRV
 601 INQILTEMDG MSTKKNVFII GATNRPDIID PAILRPGRLD QLIYIPLPDE
 651 KSRVAILKAN LRKSPVAKDV DLEFLAKMTN GFSGADLTEI CQRACKLAIR
 701 ESIESEIRRE RERQTNPSAM EVEEDDPVPE IRRDHFEEAM RFARRSVSDN
 751 DIRKYEMFAQ TLQQSRGFGS FRFPSGNQGG AGPSQGSGGG TGGSVYTEDN
 801 DDDLYG
```

Sample p87

Matched peptides shown in **Bold Red**

```
   1 MASGADSKGD DLSTAILKQK NRPNRLIVDE AINEDNSVVS LSQPKMDELQ
  51 LFRGDTVLLK GKKRREAVCI VLSDDTCSDE KIRMNRVVRN NLRVRLGDVI
 101 SIQPCPDVKY GKRIHVLPID DTVEGITGNL FEVYLKPYFL EAYRPIRKGD
 151 IFLVRGGMRA VEFKVVETDP SPYCIVAPDT VIHCEGEPIK REDEEESLNE
 201 VGYDDVGGCR KQLAQIKEMV ELPLRHPALF KAIGVKPPRG ILLYGPPGTG
 251 KTLIARAVAN ETGAFFFLIN GPEIMSKLAG ESESNLRKAF EEAEKNAPAI
 301 IFIDELDAIA PKREKTHGEV ERRIVSQLLT LMDGLKQRAH VIVMAATNRP
 351 NSIDPALRRF GRFDREVDIG IPDATGRLEI LQIHTKNMKL ADDVDLEQVA
 401 NETHGHVGAD LAALCSEAAL QAIRKKMDLI DLEDETIDAE VMNSLAVTMD
 451 DFRWALSQSN PSALRETVVE VPQVTWEDIG GLEDVKRELQ ELVQYPVEHP
 501 DKFLKFGMTP SKGVLFYGPP GCGKTLLAKA IANECQANFI SIKGPELLTM
 551 WFGESEANVR EIFDKARQAA PCVLFFDELD SIAKARGGNI GDGGGAADRV
 601 INQILTEMDG MSTKKNVFII GATNRPDIID PAILRPGRLD QLIYIPLPDE
 651 KSRVAILKAN LRKSPVAKDV DLEFLAKMTN GFSGADLTEI CQRACKLAIR
 701 ESIESEIRRE RERQTNPSAM EVEEDDPVPE IRRDHFEEAM RFARRSVSDN
 751 DIRKYEMFAQ TLQQSRGFGS FRFPSGNQGG AGPSQGSGGG TGGSVYTEDN
 801 DDDLYG
```

Sample p58

Matched peptides shown in **Bold Red**

```
   1 MASGADSKGD DLSTAILKQK NRPNRLIVDE AINEDNSVVS LSQPKMDELQ
  51 LFRGDTVLLK GKKRREAVCI VLSDDTCSDE KIRMNRVVRN NLRVRLGDVI
 101 SIQPCPDVKY GKRIHVLPID DTVEGITGNL FEVYLKPYFL EAYRPIRKGD
 151 IFLVRGGMRA VEFKVVETDP SPYCIVAPDT VIHCEGEPIK REDEEESLNE
 201 VGYDDVGGCR KQLAQIKEMV ELPLRHPALF KAIGVKPPRG ILLYGPPGTG
 251 KTLIARAVAN ETGAFFFLIN GPEIMSKLAG ESESNLRKAF EEAEKNAPAI
 301 IFIDELDAIA PKREKTHGEV ERRIVSQLLT LMDGLKQRAH VIVMAATNRP
 351 NSIDPALRRF GRFDREVDIG IPDATGRLEI LQIHTKNMKL ADDVDLEQVA
 401 NETHGHVGAD LAALCSEAAL QAIRKKMDLI DLEDETIDAE VMNSLAVTMD
 451 DFRWALSQSN PSALRETVVE VPQVTWEDIG GLEDVKRELQ ELVQYPVEHP
 501 DKFLKFGMTP SKGVLFYGPP GCGKTLLAKA IANECQANFI SIKGPELLTM
 551 WFGESEANVR EIFDKARQAA PCVLFFDELD SIAKARGGNI GDGGGAADRV
 601 INQILTEMDG MSTKKNVFII GATNRPDIID PAILRPGRLD QLIYIPLPDE
 651 KSRVAILKAN LRKSPVAKDV DLEFLAKMTN GFSGADLTEI CQRACKLAIR
 701 ESIESEIRRE RERQTNPSAM EVEEDDPVPE IRRDHFEEAM RFARRSVSDN
 751 DIRKYEMFAQ TLQQSRGFGS FRFPSGNQGG AGPSQGSGGG TGGSVYTEDN
 801 DDDLYG
```

Figure 2.6. Analysis of p97 particle size distribution in solution using dynamic light scattering. A &B. Average intensity size distribution of p97WT or mutant variant (100 μg/ml) without nucleotide addition (**A**) or with 1 mM ATP (**B**). Data represents average of four measurements. Arrows point to high molecular weight intermediates statistically significant from p97WT ($p \leq 0.05$).

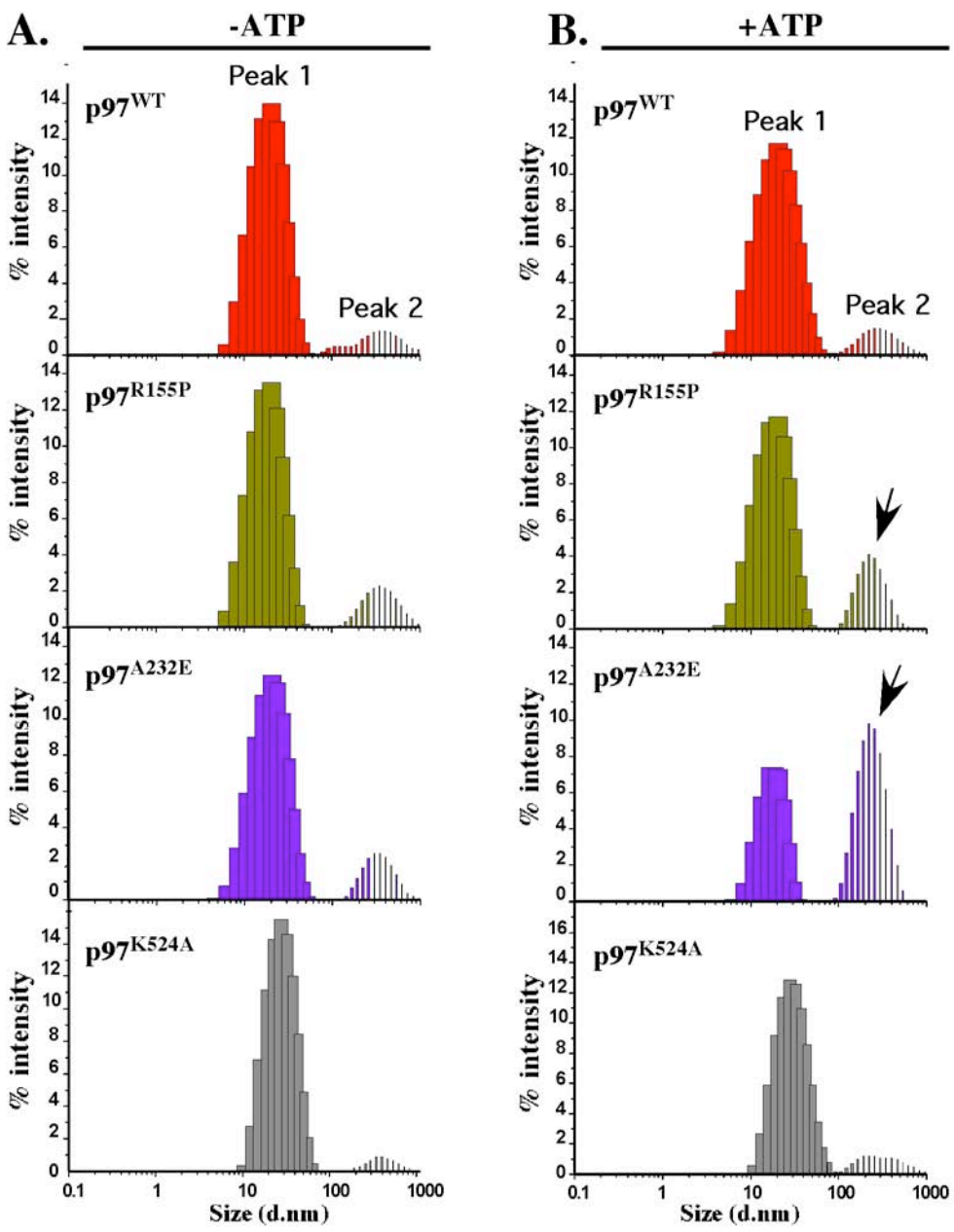
A.
-ATP
Peak 1
Peak 2
p97WT
p97R155P
p97A232E
p97K524A
% intensity
Size (d.nm)
B.
+ATP
Peak 1
Peak 2
p97WT
p97R155P
p97A232E
p97K524A
% intensity
Size (d.nm)

CHAPTER 3: Targeting of the Valosin containing protein (p97) by active Caspase-6 in Alzheimer Disease: implications on ubiquitin proteasome system mediated protein degradation

Preface

In Alzheimer Disease (AD), there is well-documented evidence of accumulation of ubiquitin epitopes in hippocampal neurons, where ubiquitin is found covalently linked to neurofibrillary tangles (NFT) and neuritic plaques (NP). The fact that ubiquitin immunoreactivity is also enhanced in neurons devoid of protein aggregates suggests that UPS impairment is an early event in AD. The cysteinyl protease, Casp6, has been described as a putative instigator of neurodegeneration in AD. Importantly, Casp6 activation is observed early in AD and correlates with the extent of cognitive impairment in subclinical stages of AD. Considering that p97 was identified as a target of Casp6 activity in primary human neurons, in this chapter, we investigate if p97 is cleaved by Casp6 in AD. Our results support a role for Casp6 in the proteolytic processing of p97 and the subsequent impairment of the UPS in AD.

3.1 Abstract

The accumulation of polyubiquitinated proteins is a common feature of many neurodegenerative diseases and is associated with UPS impairment. The Valosin containing protein (also known as p97) is a ubiquitin dependent ATPase which plays central roles in UPS-mediated protein degradation pathways. p97 has been recently identified as a putative target of Casp6 activity in primary human neurons. Considering that Casp6 is activated in mild-cognitive impairment (MCI) and AD, the targeting of p97 by Casp6 may represent an important mechanism for UPS impairment in AD. Here, we show that p97 is a Casp6 substrate *in vitro* and *in vivo*. Casp6 cleavage of recombinant p97 generated two N-terminal fragments of 28 and 20 kDa, which were not generated by Casp3 or Casp7. ATP binding to the D1 ATPase ring protected against Casp6 mediated proteolysis of p97 N-domain. Mass spectrometric analysis identified five Casp6 cleavage sites: VAPD179, DELD307, ETID438, TWED478, and VEED725, with only VAPD179 localizing to the N-domain. P97 cleavage at VAPD179 (p97D179↓) was further demonstrated in AD using a polyclonal neoepitope antibody. Cleaved p97 localized to the cytoplasm of hippocampal neurons and to large neurites that likely represent axons. Furthermore, overexpression of p97D179↓ fragment in N2a cells led to a significant accumulation of the ubiquitin fusion degradation reporter, UBG76V-GFP and proteolysis of endogenous p97. Collectively, these results suggest that caspase cleavage of p97 may represent a relevant mechanism of UPS impairment in AD.

3.2 Introduction

The accumulation of polyubiquitinated proteins and the sequestration of UPS components into protein aggregates are two common manifestations of many neurodegenerative diseases, including AD, Parkinson Disease (PD), and Creutzfeldt-Jakob Disease (CJD). In AD, ubiquitin is found associated with neurofibrillary tangles (NFT) and neuritic plaques (NP) in hippocampal brain tissue (Perry et al. 1987; Perry et al. 1989; Dickson et al. 1990; Tabaton et al. 1991). Paired helical filaments (PHF), the principal component of NFT, are known to be ubiquitinated (Mori et al. 1987; Tabaton et al. 1991), and their composite, the microtubule binding protein, tau, is a major target of ubiquitination (Morishima-Kawashima et al. 1993). Immunoreactivity to ubiquitin is also selectively observed in hippocampal neurons of AD patients in the absence of NFT and NP, suggesting that impairment in global UPS functions may occur early in AD (Perry et al. 1987; Ii et al. 1997). Multiple pathways have been implicated in UPS dysfunction in AD: First, the expression of an aberrant variant of the ubiquitin protein, UBB+, which acts as an inhibitor of the UPS (van Leeuwen et al. 1998; Lindsten et al. 2002); second, the oxidation of the ubiquitin carboxyl-terminal hydrolase, UCH-L1 (Choi et al. 2004); and third, direct proteasomal impairment by PHF (Keck et al. 2003). These findings imply that proteasome dysfunction is secondary to alterations in protein translation, oxidative stress, and PHF formation.

Recently, the cysteinyl protease, Casp6, has been proposed to be an important effector of the neurodegenerative changes observed in AD (LeBlanc 2005). Casp6 activation is observed in the hippocampus of aged individuals and those diagnosed with mild cognitive impairment (MCI), a condition that usually precedes AD (Albrecht et al. 2007). The cleaved subunit of Casp6 (p20) localizes to characteristic features of AD brains, including NFT, neuritic plaques (NP), and neuropil threads (NPT) (Guo et al. 2004). Furthermore, Casp6 activation is evident by the abundant presence of Casp6 cleaved Tau, in AD brains (Guo et al. 2004; Albrecht et al. 2007). Approximately 40% of Casp6 targets in primary human neurons are cytoskeletal proteins, which include Tau, α-Tubulin, Drebrin, Spinophilin, and α-Actinin-4 (Klaiman et al. 2008). These results raise the possibility that Casp6 activation in AD disrupts the cytoskeletal system (Klaiman et al. 2008). Indeed, in primary cell culture models, neurotrophic factor deprivation is known to activate Casp6 (LeBlanc et al. 1999; Nikolaev et al. 2009) and to result in axonal degeneration independent of cell body death (Nikolaev et al. 2009). Accordingly, active Casp6 may be a critical mediator of axonal injury in neurons during the prolonged course of AD.

In search of other consequences of Casp6 activation, we had previously identified the Valosin containing protein, p97, as a putative target of Casp6 activity in primary human neurons (Klaiman et al. 2008). p97 is a ubiquitin dependent ATPase which utilizes ATP-driven conformational changes in dismantling multiubiquitinated protein complexes (Shcherbik and Haines 2007).

p97 biochemical activities are not only confined to multiubiquitinated protein disaggregation or extraction, but also include direct participation in protein ubiquitination and deubiquitination (Halawani and Latterich 2006; Rumpf and Jentsch 2006). Regulation of substrate ubiquitination is enabled by p97 interaction with a variety of E3 ubiquitin ligases and deubiquitinating enzymes (Halawani and Latterich 2006). These interactions mediate p97 activity in multiple proteasome dependent pathways (Halawani and Latterich 2006), including ERAD (Ye et al. 2001; Braun et al. 2002; Ye et al. 2003), UFD (Richly et al. 2005; Rumpf and Jentsch 2006), and transcription factor activation (Hoppe et al. 2000). Furthermore, mutations abolishing p97 ATPase activity lead to ER vacuolization and accumulation of polyubiquitinated proteins in differentiated PC12 cells (Hirabayashi et al. 2001; Kobayashi et al. 2002). Single nucleotide missense mutations in the p97 gene are also linked to the pathogenesis of a hereditary form of inclusion body myopathy, where approximately ~ 38% percent of patients also develop FTD (Watts et al. 2004; Kimonis et al. 2008). p97 linked FTD is characterized by widespread cerebellar neuronal dystrophy with ubiquitin- (Forman et al. 2006) and TDP-43 positive intranuclear inclusions (Neumann et al. 2007). In cell culture models, p97 mutations have been shown to impair ERAD (Weihl et al. 2006) and UPS dependent protein degradation (Janiesch et al. 2007), alter TDP-43 localization (Cairns et al. 2007), and activate caspases (Guyant-Marechal et al. 2006; Cairns et al. 2007). All these results indicate that p97 cell biological activity is vital for UPS function in neurons. Therefore, the

possible targeting of p97 by Casp6 may represent an important link between Casp6 activation and UPS dysfunctions in AD.

In this report, we demonstrated that p97 is a substrate of Casp6 in vitro and in vivo. We further showed that p97 can be cleaved by effector Casp3 and Casp7, but not initiator caspase-8 (Casp8). Casp6 cleavage of p97 released a 28 kDa N-terminal cleavage product not generated by Casp3 or Casp7. Moreover, nucleotide binding to p97 modulated the accessibility of the Casp6 cleavage sites. Using a neoepitope antibody recognizing p97 cleaved within the N-domain, we demonstrated that p97 is cleaved in the hippocampal neurons of AD patients, but not healthy controls. Overexpression of the cleaved p97 fragment (p97D179↓) in N2a neuroblastoma cells compromised the degradation of model substrates in the UFD pathway and led to proteolysis of endogenous p97. All together, these results show that p97 is cleaved in AD and suggest that caspase mediated cleavage of p97 may lead to UPS dysfunction in AD.

3.3 Results

p97 is cleaved by Casp6 in vitro.

Analysis of p97 primary amino acid sequence based on combinatorial chemistry identified 15 putative Casp6 cleavage sites (Fig. 3.1 A). To examine whether p97 is indeed cleaved by Casp6, p97 ND1 (residues 1-480, Fig. 3.1 A) or D2C (residues 481-806, Fig. 3.1 A) fragments were incubated with active Casp6. The 54 kDa p97 ND1 fragment (p54) generated 50 kDa (p50), 28 kDa (p28), and 20 kDa (p20) cleavage products which were immunoreactive with a monoclonal antibody raised against the N-domain of p97 (Fig. 3.1 B, top panel). A 38 kDa (p38) N-terminal fragment was also observed, however it likely represented an N-terminal truncation product in the purified p97 ND1 protein preparation (Fig 3.1 B, top panel). Conversely, the 43 kDa p97 D2C (p43) fragment resulted in a 30 kDa (p30) cleavage product, which was immunoreactive with a polyclonal antibody against the COOH-terminal domain of p97 (Fig. 3.1 C, top panel). p97 ND1 and D2C cleavage was dependent on Casp6 concentration (Fig. 3.1 B&C, top panels) and inhibited by Casp6 peptide inhibitor, Z-VEID-FMK (Fig. 3.1 B&C, lower panels). These results indicate that p97 contains caspase consensus sites that are recognized and cleaved by Casp6 in vitro.

To confirm that assembled p97 is also a substrate of Casp6, full-length hexameric p97 was incubated with active Casp6 in vitro. Purified hexameric p97 contained minor COOH-terminal truncations produced either by proteolysis, premature termination of translation, or alternate start codons in *E coli* expression systems. These truncations were readily detected in the absence of Casp6

treatment using an anti-N-terminal antibody for p97 (Fig. 3.1 D). Casp6 processed assembled p97 within 30 minutes of incubation, generating a 75 kDa (p75), 28 kDa (p28), and 20 kDa (p20) N-terminal cleavage products (Fig. 3.1 D). At 30 minutes of incubation, p75 was the predominant cleavage product followed by p28. Within four hours of incubation, p75 was destabilized and p28 became the major N-terminal cleavage product. We next used an antibody against the COOH-terminal polyhistidine-tag for p97. Within 30 minutes of incubation, this antibody detected multiple COOH-terminal cleavage products for p97: p80C, p50C, p28C, p27C, p7C (Fig. 3.1 E). All together, these results indicate that full-length hexameric p97 is a substrate of Casp6 in vitro.

ATP-dependent conformational changes in p97 modulate the accessibility of the Casp6 cleavage sites.

Given that p97 protein conformation can be modulated by its nucleotide binding state, we assessed the role of nucleotide binding on p97 susceptibility to Casp6 mediated cleavage. As previously shown, in the absence of ATP, p97ND1 cleavage by Casp6 generated the predominant cleavage product p28 kDa (Fig. 3.2 A). In the presence of ATP, Casp6 mediated cleavage generated a 50 kDa product, p50, indicating that p97ND1 was truncated within the COOH-terminal end (Fig. 3.2 A). To investigate the effect of Casp6 concentration on p97ND1 processing, p97ND1 was incubated with increasing concentrations of Casp6 in the presence or absence of ATP. Consistent with our previous finding, there was a Casp6 dependent generation of p28 in the absence of ATP (Fig. 3.2 B) and p50

in the presence of ATP (Fig. 3.2 B). Moreover, using high concentrations of Casp6 in the presence of ATP did not increase the generation of p28, indicating that the N-domain of p97 remained resistant to proteolysis. Furthermore, p50 generation was positively dependent on the ATP concentration in solution (Fig. 3.2 C), indicating that increasing the concentration of ATP enhances p97ND1 proteolysis at the COOH-terminal end. Collectively, these results suggest that the nucleotide binding state of the D1 ring influences p97 N-terminal susceptibility to Casp6 mediated processing.

We next investigated if Casp6 mediated processing of full-length p97 is also modulated by nucleotide binding. Full-length p97 incubated with buffer alone (Fig. 3.2 D, lane 1) or with heat-denatured Casp6 (Fig. 3.2 D, lane 2) both contained the N-terminal truncation products usually observed in the purified protein preparation. Addition of the Casp6 inhibitor, Z-VEID-FMK, had no effect on the stability of these N-terminal truncations (Fig. 3.2 D, lane 3). In contrast, incubation of full-length p97 with active Casp6 generated p28 in the absence of ADP (Fig. 3.2 D, lane 4); however, in the presence of ADP, p75 was the predominant cleavage product (Fig. 3.2 D, lane 5). In addition, a 60 kDa fragment was irreproducibly observed (Fig. 3.2 D, lane 5), and probably resulted from the proteolysis of a noncanonical Casp6 consensus sequence. These results show that, as for p97ND1, nucleotide binding to full-length p97 also modulates the susceptibility of the N-domain to Casp6 mediate proteolysis.

p97 is also cleaved by effector Casp3 and Casp7, but not initiator Casp8 in vitro.

To determine whether p97 is also a substrate of other caspases, full-length hexameric p97 was incubated with effector Casp3 and Casp7, and initiator Casp8. Casp3 and Casp7 both partially processed p97 into p75 and p40 N-terminal fragments (Fig. 3.3 A. top panels). Furthermore, the p40 fragment appeared as a doublet when cleaved by Casp3 compared to Casp7 (Fig. 3.3 A, top panels). Unlike Casp3 and Casp7, Casp8 did not cleave p97 (Fig. 3.3 A, lower right panel). Interestingly, only cleavage by Casp6 generated the low molecular weight N-terminal cleavage products, p28 and p20 (Fig. 3A). Unlike Casp6, nucleotide binding to p97 had no protective or modulatory effects on its processivity by Casp3 and Casp7 (Fig. 3.3 B, top panels). Moreover, p97 remained uncleaved by Casp8 irrespective of its nucleotide binding state (Fig. 3.3 B, lower panel). These results indicate that p97 is a substrate of effector Casp3 and Casp7, but not initiator Casp8. In addition, Casp6 mediated processing of p97 generates a cleavage pattern distinct from that generated by Casp3 and Casp7.

Identification of the Casp6 cleavage site in p97.

Considering the role of Casp6 in mediating neuronal degeneration in AD, we sought to identify the Casp6 cleavage sites in p97 using LC-MS/MS. Digestion of recombinant p97 ND1 fragment with active Casp6 resulted in the identification of four semi-tryptic peptides of a total of 50 sequenced peptides (Table 3.1). All

semi-tryptic peptides contained an aspartic acid residue at the COOH-terminus (Fig. 3.4 A). Two peptides contained the consensus sites, 176VAPD179 and 304DELD307, which were previously predicted (Fig. 3.1 A). Two additional peptides contained the unique cleavage sites, 435ETID438 and 475TWED478, both of which were not predicted (Fig. 3.4 A). Cleavage of the p97 D2C fragment with active Casp6 yielded a single semi-tryptic peptide of 41 sequenced peptides (Fig. 3.4 B). Unlike the ND1 semi-tryptic peptides, the D2C derived peptide contained an aspartic acid residue at the N-terminal end (Fig. 3.4 B). Analysis of the sequence immediately preceding the peptide revealed the predicted cleavage site 722VEED725 (Table. 3.1, Fig. 3.4 B and Fig. 3.1 A). As expected, no semi-tryptic peptides were identified in p97 ND1 or D2C fragments treated with heat-inactivated Casp6 (Fig. 3.4 A & B). All together, the results indicate that p97 contains at least five Casp6 cleavage sites.

VAPD179 is not the only N-terminal cleavage site in p97.

Given that the predominant p97 N-terminal cleavage product is p28, we next assessed whether p28 is generated from p97 cleavage at VAPD179, the only N-terminal cleavage site identified by mass spectrometry (Table 3.1). The VAPD179 consensus site was mutagenized to VAPA179 and the recombinant protein (p97D179A) was incubated with active Casp6. As p97WT (Fig. 3.5 A), p97D179A cleavage also generated p28 and p20 suggesting that VAPD179 is not the targeted cleavage site (Fig. 3.5 C). Another putative caspase cleavage site, VETD169, was previously identified in the p97 primary amino acid sequence (Fig.

3.1 A). Since p97 ND1 is cleaved at VAPD179 (Fig. 3 A), additional cleavage at VETD169 would have generated a peptide too small for detection by mass spectrometry. Therefore, we considered the possibility that full-length p97 is preferentially cleaved at VETD169. Unexpectedly, cleavage of p97D169A by Casp6 also generated p28 and p20 (Fig. 3.5 C). Furthermore, the p97D169A mutation promoted more efficient generation of the p20 fragment compared to p97WT and p97D179A. These results suggest that neither VAPD179 nor VETD169 are the cleavage sites leading to p28 generation and that p20 is possibly generated from cleavage at both sites. Further work is necessary to identify the Casp6 cleavage site(s) responsible for p28 generation *in vitro*.

p97 is cleaved at VAPD179 in Alzheimer Disease.

Considering that VAPD179 is the only N-terminal cleavage site consistently identified by mass spectrometry, we generated a neoepitope antibody recognizing this cleavage site in p97 (p97D179↓). To determine if p97D179↓ accumulated in Alzheimer disease brains, we performed immunohistological staining of 4 non-cognitively impaired (NCI), 5 mild cognitively impaired (MCI) and 14 AD hippocampal tissue sections. The results showed strong immunopositive neurons in AD brains, negative or faint staining in most MCI cases and negative staining in most NCI cases (Fig. 3.6 A). One case of MCI and one case of the NCI showed stronger immunopositive neurons for p97D179↓. Interestingly, these immunopositive cases had lower mini mental

state exam (MMSE) scores. Furthermore, p97D179↓ immunoreactivity localized to the same hippocampal region where active Casp6 and TauΔCasp6 were detected. These observations suggest possible co-localization of the active Casp6 with the p97D179↓ fragment (Fig. 3.6 B). Double immunostaining is required to confirm the co-localization of the active Casp6 and p97D179↓ in AD neurons. Interestingly, the immunoreactivity of p97D179↓ in neurons had a granulous appearance and was localized to the cytoplasm of the neuronal cell body and to large neurites that likely represent the axons (Fig. 3.6 C). No immunoreactivity was observed in the nuclei of neurons.

Overexpression of the p97D179↓ fragment compromises the ubiquitin fusion degradation (UFD) pathway and destabilizes endogenous p97.

Given the presence of the p97D179↓ fragment in AD brains, we next assessed the effects of its expression on p97-mediated cell biological pathways. We co-expressed vector only, p97WT, p97K524A, or p97D179↓ (Fig. 3.7 A) with either one of two previously characterized reporters in the UPS: the UFD reporter, UBG76V-GFP, and the N-end rule pathway reporter, R-GFP. Quantification of the number of GFP positive cells showed no significant differences between cells expressing vector only, p97WT, p97K524A, or p97VAPD179, for both UBG76V-GFP and R-GFP (Fig. 3.7 B, upper panel). Cells expressing p97VAPD179 consistently showed the highest number of GFP positive cells, although it was not statistically significant (Fig. 3.7 B, upper panel). GFP accumulation, as reflected

by the mean fluorescence intensity, showed a significant accumulation of UBG76V-GFP, in p97D179↓ expressing cells compared to vector, p97WT, and p97K524A expressors (Fig. 3.7 B, lower panel). Interestingly, there was no significant difference in the accumulation of R-GFP in p97D179↓ expressors compared to vector only or p97WT transfected cells (Fig. 3.5 B, lower panel). Furthermore, expression of p97K524A led to marked apoptosis of UBG76V-GFP and R-GFP expressors within 48 hours of transfection (data not shown). Collectively, these data show that the overexpression of the p97D179↓ fragment impairs the UFD pathway in cell culture. Considering the high variability of the data, more experiments are necessary to substantiate if the N-end rule pathway is also impaired by p97D179↓ expression.

Considering the role of p97K524A mutation in inducing apoptosis and activating caspases, endogenous p97 protein level was assessed in transfected cells using an antibody against the COOH-terminal domain of p97. While no p97 cleavage fragments could be detected in cells expressing either vector only, p97WT, or p97K524A, cells transfected with p97D179↓ showed two cleavage products of 55 and 38 kDa (Fig. 3.7 C). Moreover, these proteolysis products could be detected irrespective of whether the cells were co-transfected with UBG76V-GFP or R-GFP. These results show that the overexpression of p97D179↓ fragment impairs the stability of endogenous p97.

3.4 Discussion

While the accumulation of ubiquitinated proteins in Alzheimer Disease is well documented, our knowledge of how this accumulation is linked to UPS impairment is rudimentary at best. UPS impairment has been attributed to several pathogenic pathways, including mistranslation of the intracellular ubiquitin moiety available for conjugation (UBB+) (van Leeuwen et al. 1998; Lindsten et al. 2002), reduced deubiquitination due to oxidative damage of ubiquitin hydrolases (Choi et al. 2004), and direct proteasomal blockage by neurofibrillary structures (Keck et al. 2003). In this study, we propose that the targeting of p97, a central player in UPS mediated protein degradation pathways, by active Casp6 represents an additional mechanism for UPS impairment in AD. In support of this hypothesis, we show that p97 is cleaved by Casp6 *in vitro*, but unlike Casp3 and Casp-7, Casp6 generated a 28 kDa and 20 kDa N-terminal fragments. Using a neoepitope antibody with specificity for N-terminally cleaved p97, we show that p97 is cleaved in AD brains. Furthermore, we found that the mere overexpression of p97D179↓ impaired the UFD pathway and led to the proteolysis of endogenous p97 in N2a neuroblastoma cells. These data provide evidence that p97 targeting by active Casp6 may represent a novel mechanism of UPS impairment in AD.

p97 cleavage by Casp6 in vitro.

Our in vitro analysis clearly demonstrates that p97 contains caspase consensus sites that are recognized and cleaved by Casp6. p97 cleavage

occurred at an equimolar concentrations of hexameric p97 to tetrameric Casp6 and was evident within two hours of co-incubation. In agreement with other reports (Jang et al. 2008), p97 was also cleaved by effector Casp3 and Casp7, using similar conditions - a fact which indicates that p97 can be targeted by all members of the effector class of caspases (ie. Casp3, Casp6, and Casp7). Interestingly, our data also ruled out the involvement of Casp8 in the processing of p97 in vitro. Although Casp3 and Casp7 both conferred a similar proteolysis pattern on p97, Casp6 mediated proteolysis was distinguished by the generation of low molecular weight N-terminal cleavage products (p28 and p20) not generated by Casp3 or Casp7. Accordingly, we can infer that Casp6 targets unique consensus sites not shared by either Casp3 or Casp7. Importantly, this finding provides further evidence for the specificity of Casp6 mediated proteolysis of p97 *in vitro*.

p97 susceptibility to N-terminal proteolysis is modulated by nucleotide binding to the D1 AAA+ ring.

Given that p97 undergoes drastic conformational changes in response to nucleotide binding (Rouiller et al. 2000; DeLaBarre and Brunger 2003; DeLaBarre and Brunger 2005), our data indicate that ATP-driven conformational changes could alter either the structure or the accessibility of the Casp6 cleavage site within the N- domain. Indeed, p97 was preferentially cleaved within the N-domain in the absence of nucleotide binding, and within the COOH-terminal end in the presence of ATP. Furthermore, our data suggest that D1 ring regulates the

conformation of the N-domain, especially considering that the N-domain was protected in the p97ND1 fragment lacking the D2 ring. Interestingly, the presence of an active D2 ring in p97WT reduced the protective effect of nucleotide binding on N-terminal proteolysis. Our data suggest that the conformation of the N-domain is modulated by nucleotide binding to the D1 ring, and that in full-length p97, the ATPase activity of the D2 ring may influence the nucleotide occupancy state of the D1 ring (Beuron et al. 2003; Ye et al. 2003). Furthermore, these results imply that the accessibility of the Casp6 consensus sites in p97 can be dynamically modulated by its conformational state. In a cell biological system, p97 conformational state is likely influenced by multiple factors including adaptor protein binding (Meyer et al. 1998) and posttranslational modifications, such as ubiquitination (Hitchcock et al. 2001) and phosphorylation (Klein et al. 2005). Other studies have demonstrated that phosphorylation could modulate the susceptibility of a substrate to caspase mediated processing, either positively or negatively. For example, Bid phosphorylation by Casein Kinase I and II decreases its sensitivity to Casp8 mediate cleavage (Desagher et al. 2001). Similarly, mutant Huntington phosphorylation by Cdk5 reduced its cleavage by Casp3 (Luo et al. 2005). In other cases, phosphorylation, such as Mitogen Activated Protein Kinase (MAPK) mediated phosphorylation of the androgen receptor, enhances substrate cleavage by caspases (LaFevre-Bernt and Ellerby 2003).

The physiological relevance of the modulation of p97 N-terminal proeolysis remains unclear. Unlike Casp6, our results indicate that Casp3 and Casp7 mediated cleavage of p97 is not modulated by nucleotide binding. While activation of Casp3 and Casp7 is associated with apoptosis, activation of Casp6 occurs in the absence of apoptosis or cell death (LeBlanc et al. 1999; Klaiman et al. 2009; Nikolaev et al. 2009). For example, in AD, Casp6 activation is widely observed in the hippocampus in the absence of apoptotic neuronal morphology or neuronal cell death (Guo et al. 2004; Albrecht et al. 2007). Accordingly, it is tempting to speculate that Casp6-mediated proteolysis of p97 may serve a regulatory function in vivo.

The use of mass spectrometry in the identification of the Casp6 cleavage sites in p97.

Our mass spectrometric analysis identified five Casp6 cleavage sites within p97, with only p97VAPD179 localizing to the N-terminal domain. A limitation of this analysis is that some of the generated semi-tryptic peptides may be too short, too long, or too hydrophobic for detection by LC-MS/MS. Accordingly, we cannot exclude the presence of additional Casp6 cleavage sites within the N-domain, or other domains of p97. Indeed, our results show that neither 166VETD169 nor 176VAPD179 are the Casp6 cleavage sites responsible for p28 generation in vitro. Accordingly, it is possible that Casp6 is capable of cleaving p97 at both sites and that the mutagenesis of one site does not impede cleavage at the alternate site. Interestingly, 304DELD307 within the D1 ring was

previously identified as a Casp3 and Casp7 cleavage site within the D1 ring-a fact which indicates that some caspase consensus sites in p97 can be shared by multiple caspases. Cleavage at 304DELD307 predicts the generation of ~ 34 kDa N-terminal fragment, not observed in our in vitro analysis. It is possible that p28 is generated by consecutive cleavage at an unidentified site close to extreme N-terminal end (ie. 71VLSD74) followed by cleavage at 304DELD307. Only one cleavage site was identified within the D2 ring, 722VEED725, although our western blots analysis indicated that presence of multiple sites. Considering that the COOH-terminal domain of p97 is more prone to proteolysis (during purification and cell lysis), we opted to focus our subsequent analysis of the only Casp6 N-terminal cleavage site identified with certainty by mass spectrometry. Future experiments will concentrate on the identification of the Casp6 cleavage sites responsible for p28 generation in vitro.

p97 cleavage at VAPD179 in vivo.

Our results demonstrate that p97 is cleaved at Asp179 in AD and likely in subclinical stages of AD. These findings merit further investigation of whether cleaved p97 also colocalizes with active Casp6 in the hippocampal neurons of AD patients. We also cannot rule out the involvement of others caspases or proteases in p97 proteolysis in vivo, although the immunoreactivity of active Casp3 is limited in AD (Stadelmann, 1999 and Selznick, 1999) and Casp3 mediated cleavage of p97 does not generate a low molecular weight N-terminal fragment *in vitro*. Furthermore, considering the prominent role of p97 in the

regulation of the UPS system, our results suggest that p97 cleavage may lead to the accumulation of polyubiquitinated proteins in AD. Co-immunostaining studies with the neoepitope antibody and a ubiquitin antibody are necessary to substantiate UPS impairment in neurons containing cleaved p97. Interestingly, immunoreactivity against cleaved p97 was cytoplasmic and not nuclear, which is consistent with the exclusion of active Casp6 from the nuclei of hippocampal neurons in AD brains (Guo et al. 2004). Moreover, neurons immunostained with the neoepitope antibody did not display morphological evidence of apoptosis. Consistently, heterozygous deletion of p97 results in fully viable mice that are virtually indistinguishable from the wild-types (Muller et al. 2007). Accordingly, it is likely that p97 cleavage precedes the accumulation of polyubiquitinated proteins in AD and that substantial cleavage has to occur before the induction of ER stress or apoptosis due to p97 loss of function (Wojcik et al. 2004; Wojcik et al. 2006). Furthermore, neurons displaying strong immunoreactivity with the neoeopitope antibody also displayed a granular staining pattern. While the significance of this observation is unclear, loss of p97 function is known to prevent aggresome formation in the presence of UPS impairment (Wojcik et al. 2004). It is therefore possible is that the p97 N-terminal cleavage product may be sequestered within dispersed ubiquitinated protein aggregates as a result of loss of p97 function.

p97 N-terminal cleavage is linked to UPS impairment in cell culture.

The presence of p97D179↓ in AD brains prompted investigation of the physiological consequences of its expression. Our data indicate that the overexpression of p97D179↓ compromised the degradation of a model substrate in the UFD pathway. It is possible that p97D179↓ sequesters p97 N-terminal binding partners, such as Ufd1/Npl4 and p47 (Meyer et al. 2002), and out competes endogenous p97 for their binding. Alternatively, overexpression of p97D179↓ may have cytotoxic consequences independent of p97 cell biological functions. Indeed, unlike p97K524A which is known to impair p97 mediated pathways (Hirabayashi et al. 2001; Kobayashi et al. 2002), p97D179↓ destabilized endogenous p97 protein levels. Further studies are necessary to investigate whether endogenous p97 cleavage is caspase mediated. Nevertheless, our results suggest that the generation of p97 N-terminal fragments may compromise the UPS in AD. Interestingly, Casp6 also targets mammlian UFD2a (E4B) (Mahoney et al. 2002), an E3 ubiquitin ligase that is necessary for the proper development of the nervous system (Kaneko-Oshikawa et al. 2005) and a binding partner of p97 in the UFD pathway (Koegl et al. 1999). These findings suggest that Casp6 may target multiple p97 dependent pathways. Collectively, our data suggest that Casp6 is an important effector of UPS dysfunction in AD.

3.5 Material and Methods

Protein Expression Vectors

All vectors were generated from a murine p97 cDNA in pBluescript SK+ vector, kindly provided by Dr. Fred Indig (National Institute on Aging/NIH, Baltimore, USA). p97ND1 (residues 1-480) and p97D2C (residues 481-806) were subcloned into the pTrcHis2A vectors (Invitrogen, Carlsbad, CA) to allow for COOH-terminal polyhistidine tagging. The p97ND1 fragment was amplified by PCR using the primers: 5' AGCTCGAGAATGGCCTCTGGAGCCGAT3', and 5' CCATATGTACCTTATCCAATATCTTCCCAGGT 3', which contained the restriction sites, Xho I and Kpn I, respectively. Similarly p97D2C fragment was amplified using the primers: 5' AGCTCGAGAGGTGGCCTGGAGGATGTC 3', and 5' ATATGGTACCAGGCCATACAGGTCATCGTC 3', containing the restriction sites Xho I and Kpn I, respectively. Subsequent to restriction digest, both PCR products were ligated into the pTrcHis2A vectors. Full-length p97WT in pTrcHis2C was generated as previously described (Halawani et al., 2009). Full-length p97D169A and p97D179A mutants were both generated using the GeneTailor™ site-directed mutagenesis system with p97WT-pTrcHis2C as a starting template (Invitrogen, Carlsbad, CA). Aspartate 169 in p97 was mutagenized to alanine by changing the codon, 505GAT507 to 505GCT507 using the primers: 5' AGTTCAAAGTTGTAGAGACAGCTCCCAGCCCTT 3' and 5' TGTCTCTACAA CTTTGAACTCCACAGCACGC 3'. Aspartate 179 was mutagenized to Alanine by changing codon, 535GAC537 to 535GCC537 using

the primers: 5' CCTTACTGTATTGTTGCTCCAGCCACAGTGATCCAC 3' and 5' TGGAGCAAC AATACAGTAAGGGCTGGGATCTGT 3'.

Mammalian p97WT expression vectors were generated by cloning full-length murine p97WT cDNA into the p3X-FLAG-CMV10™ vector for N-terminal tagging or p3X-FLAG-CMV14™ vector for COOH-terminal tagging with the FLAG peptide (Sigma, St. Louise, MO, USA). Full-length p97 was amplified using the primers: 5' CTTGCGGCCGCGGCCTCTGGAGCCGATTCAAAA 3' and 5' GGGGATCCTTA GCCATACAGGTCATCGTCATT 3', containing the restriction sites NotI and BamHI for cloning into the p3X-FLAG-CMV10™. Similarly, primers: 5' CTTGCGGCCGCGGCCGCCACCATGGCCTCTGGAGCC GAT 3' and 5' GGGGATCCGCCATACAGGTCATCGTCATT 3' with the restriction sites, NotI and BamHI, were used for cloning into the p3X-FLAG-CMV14™. Subsequent to restriction digest, the inserts were ligated into the appropriate vector. FLAG-tagged p97K524A was generated as described for p97WT except that the cDNA was supplied in the pQE9 vector (kind gift of Dr. Tom Rapoport, Harvard University, Boston, USA). The FLAG- p97D179↓ vector was constructed using site-directed mutagenesis as described above. Briefly, the codon 538ACA540 was changed to 538TAA540 using the primers: 5' TACTGTATTGTTGCTCCAGACTAAGTGATCCACTGT 3' and 5' GTCTGGAGCAACAATACAGTAAGGGCTGGGATC 3'. The untagged p97 fragment encoding residues 180-806 was subcloned into the pBudCE2.1 vector (Invitrogen, Carlsbad, CA, USA) under the CMV promoter using the restriction

sites Hind III and BamHI. The PCR was performed using the following primers: 5' CCCAAGCTTGCGCGCCATGACAGT GATCCACTGTGAG 3' and 5' GACGATGACCTGTATGGCTAATAAGGATCCGAA 3'. All constructs were verified by sequencing at the McGill University and Genome Quebec Innovation Center Platform (Montreal, QC, Canada).

Caspase expression constructs: pET23b-Casp3-His (Addgene plasmid 11821), pET23b-Casp6-His (Addgene plasmid 11823), pET23b-Casp7-His (Addgene plasmid 11825), pET15b-Casp8ΔDED (Addgene plasmid 11827), were kindly provided by Dr. Guy Salvesen (The Burnham Institute, La Jolla, CA, USA).

Protein Expression and Purification

p97 proteins were expressed and purified as previously described with minor modifications (Halawani et al. 2009). Briefly, p97WT, p97D169A, p97D179A, p97ND1, and p97D2C were expressed in Top10 E.coli strain. Overnight starter cultures were diluted 50X in 2X YT media (16 g/L Tryptone, 10 g/L Yeast Extracts, 5 g/L NaCl) and grown at 37 ºC to an OD at 600nm of 0.6 with vigorous shaking. Following induction with 300 μM IPTG, cell were grown for 4-5 hours and harvested by centrifugation at 4,000 g for 20 minutes. Pelleted cells were lysed in buffer containing 20 mM HEPES pH 7.5, 300 mM NaCl, 5 mM $MgCl_2$, 2.5 mM DTT, and 20 mM imidazole and supplemented with 1 mg/ml lysozyme and complete protease inhibitors (Roche, Mississauga, ON). Lysates were sonicated and cleared by centrifugation at 26,000 g for 45 minutes. Cleared supernatants

were filtered with 0.2 μm filters (Millipore, Bedford, MA) and loaded on a pre-equilibrated Ni^{2+} affinity column (GE Healthcare Bio-sciences, Uppsala, Sweden). Bound proteins were washed with 10 times column volume of lysis buffer, followed by a second wash with 10 times column volume of lysis buffer with 35 mM imidazole. Proteins were eluted with a 35 to 500 mM imidazole gradient over 5 times column volume. For the p97ND1 and p97D2C protein fragments, eluted proteins were dialyzed against buffer containing 20 mM HEPES pH 7.5, 150 mM NaCl, 5 mM $MgCl_2$, and 2.5 mM DTT, using Slide-A-lyzer® dialysis cassettes with a molecular weight cut-off of 10 kDa (Fisher, Nepean, ON, Canada). Full-length p97 proteins were further purified on a pre-calibrated 25 ml Superdex-200 size-exclusion chromatography column (GE Healthcare Bio-sciences, Uppsala, Sweden). Peak fractions corresponding to hexameric p97 were eluted as 1ml fractions in buffer containing 20 mM HEPES pH 7.5, 150 mM NaCl, 5 mM $MgCl_2$, and 2.5 mM DTT. Final protein concentrations were determined using the Bradford assay (BioRad, Mississauga, ON). Purified proteins were snap frozen and stored at -80°C. All purifications were performed using the UKTA FPLC system (GE Healthcare Bio-sciences, Uppsala, Sweden).

Caspase protein expression was conducted using the BL21(DE3)pLysS E.coli stain using the following IPTG induction conditions: 200 μM IPTG was used for Casp3 and expression was allowed for 4-6 hrs at 30 ºC, Casp6 was induced with 50 μM IPTG and expressed overnight at 16 ºC, 200 μM IPTG was used for

Casp7 expression at 30 ºC for 12-16 hrs, and Casp8 was induced with 200 μM IPTG for 4-6 hrs at 30 ºC. Protein expression was preformed from overnight starter cultures in 2 times YT media (16 g/L Tryptone, 10 g/L Yeast Extracts, 5 g/L NaCl). Cell lysis and Ni^{2+} affinity purification were performed as described above for p97 using the following buffer conditions: lysis buffer (50 mM Tris-HCL pH 8.0, 100 mM NaCl, and 10 mM imidazole supplemented with 1 mg/ml lysozyme), wash buffer (50 mM Tris-HCL pH 8.0, 500 mM NaCl, 10 mM imidazole), elution buffer (50 mM Tris-HCL pH 8.0, 100 mM NaCl using 10-500 mM imidazole gradient). Eluted proteins were dialyzed against buffer containing 50 mM Tris-HCl pH 8.0 and 100 mM NaCl as described above. Protein concentrations were quantified using the Bradford assay (BioRad, Mississauga, ON). Caspase activity was verified using the appropriate fluorogenic substrates as previously described in Zhang et al., 1999.

In vitro p97 protein cleavage assay

p97ND1, p97D2C, p97WT, p97D169A, and p97D179A were digested in HEPES buffer (0.1 M HEPES, pH 7.5, 10% sucrose, 0.1% CHAPS, 10 mM DTT) or Stennicke's buffer (20mM PIPES pH 7.4, 30 mM NaCl, 1 mM EDTA, 0.1% CHAPs, 10% sucrose, and 10 mM DTT) as indicated in the figure legends. Reactions were incubated at 37°C in 50 μl volume using the indicated concentrations of p97 and caspase. Reactions assessing the effect of ATP on p97 proteolysis were also supplemented with 5 mM $MgCl_2$. p97 proteolysis was assessed using SDS-PAGE followed by either coomassie staining or western blot

analysis. Western blotting was performed using a monoclonal anti-p97 antibody raised using a p97 fragment containing residues 9-130 (BD Transduction Laboratories™, San Jose, CA), or a polyclonal anti-p97 antibody raised against the carboxyl-terminal residues 786 to 806 (generous gift of Dr. Maryam Taheri, McGill University, Montreal, Quebec, Canada). The monoclonal antibody was used at a dilution of 1:1000, while the polyclonal antibodies were used a dilution of 1:3000. Following incubation with the appropriate HRP-conjugated secondary antibodies, the blots were visualized using the Storm 840 scanner (GE Healthcare, Baie d'Urfé, QC) or standard autoradiography.

Identification of the Casp6 cleavage sites in p97 using LC-MS/MS analysis.

One microgram of p97ND1 or D2C fragments were digested with 320 ng of active recombinant Casp6 as indicated above. In parallel, similar digest reactions were setup as controls with heat-inactivated Casp6. Ten replicates of each sample or controls were subsequently pooled and prepared for MS/MS analysis. Briefly, the CHAPS component of the reaction buffer was first removed using a non-ionic detergent (NID) exchange cartridge (MICHROM Biosources Inc Auburn, CA) according to the manufacturer's instruction. The eluted sample was dried in a speed vacuum and resolubilized in 20 μl 1M TEAB, 2 μl 2% SDS, and 2 μl 50 mM TCEP for one hour at 60 °C. Following treatment with 1μl of 84mM TCEP, trypsin was added and samples were further incubated overnight in a thermomixer at 37 °C and 700 rpm. On the following day, samples were dried and resolubilized in buffer containing 0.1 % TFA, and 2% acetonitrile in HPLC

grade water and loaded on an SDS removal column (MICHROM Biosources Inc Auburn, CA). The flow-through containing the peptides was subsequently speed vacuumed to dryness and submitted for LC-MS/MS analysis. LC-MS/MS and peptide identification was conducted at the Institute for Research in Immunology and Cancer (University of Montreal, Montreal, Qc, Canada).

Generation of a neopitope antibody for p97 cleaved at Asp179.

Casp6 cleaved p97 neoepitope antibody was generated using the six amino acid peptide, 174CIVAPD179, N-terminally conjugated to the keyhole limpet hemocyanin protein. Prior to peptide synthesis, a BLAST search was conducted against the human genome to ensure uniqueness of this peptide sequence to human p97. All steps involved in antibody production (ie. Peptide synthesis, conjugation, immunization, bleed production and antisera collection) were performed by SIGMA GENOSYS (The Woodlands, TX, USA). The antibody bound the 174CIVAPD179 peptide at a dilution of 1: 300,000 in an ELISA assay. The immunohistochemistry was performed as previously described (Guo et al. 2004).

Transient Transfections, protein expression, and flow cytometry

N2a neuroblastoma cells were plated in 6-well plates at a density of 500, 000 cell/well in MEM media (Invitrogen, Carlsbad, CA, USA) supplemented with 10% fetal bovine serum (Fisher, Ottawa, ON, Canada) and allowed to adhere overnight. Transfection was performed using 3.5 μg of p3X-FLAG-CMV14™

vector or p97 vectors: p97WT-FLAG, p97K524A-FLAG, FLAG-p97D179↓, p97ΔN) and 0.5 μg of either the ubiquitin fusion degradation reporter, UbG76V-GFP (Addgene plasmid 11941), or the N-end rule reporter, Ub-R-GFP (Addgene plasmid 11939). The transfection complex contained 100 μl of serum free MEM (Invitrogen, Carlsbad, CA, USA), 20 μg of polyethyleneimine (Polysciences, Inc. Warrington, PA, USA), and 4.0 μg DNA. After 20-30 min incubation, the complex mix was added to cells and culture media was changed 6 hrs post-transfection. Expression was allowed for 48 hrs, and cell were trypsinized and harvested in 1ml of culture media. Cell suspension was split in two: 0.5 ml for flow cytometry and 0.5 ml for the protein expression analysis. Flow cytometery was performed on at least 20 000 live cells using the FACS Calibur flow cytometer (Becton Dickinson Biosciences). The data was analyzed using the CellQuest software (Becton Dickinson Biosciences). For protein expression, cells were lyzed in RIPA buffer containing protease inhibitors (TLCK, 0.1 μg/ml, 0.5 μg/ml leupeptin, 38 μg/ml AEBSF, and 0.1 μg/ml pepstatin A). Protein concentrations were quantified with the BCA protein assay (Fischer, Ottawa, ON, Canada). 30 μg of protein were loaded on SDS-PAGE gels and analyzed by western blotting using either a monoclonal anti-FLAG antibody (Sigma, Oakville, ON, Canada) or a polyclonal anti-carboxyl terminal antibody for p97 (kind gift of Dr. Maryam Taheri, McGill University, Montreal, Quebec, Canada). Quantification of protein expression levels was performed using the ImageQuant TL 7.0 software (GE Healthcare, Baie d'Urfé, QC).

Statistical analysis

All statistics were conducted using the Stat View 5.0 software (SAS Institute Inc., Cary, NC). The variance was analyzed from three independent experiments using a one-way ANOVA followed by the Scheffé post hoc test. Significance was determined at a p value < 0.05.

3.6 Acknowledgment

We gratefully acknowledge Jennifer Hammond for assistance with the immunohistochemistry, Dr. Steffen Albrecht (The Department of Pathology, McGill University, Montréal, QC, Canada) for assisting in the interpretation of the Immunohistochemical data, and Dr. Guy Klaiman (The Department of Neurology and Neurosurgery, McGill University, Montréal, QC, Canada) for initial guidance with the early purification of Casp6. We would like to thank Dr. Guy Salvesen (The Burnham Institute, La Jolla, CA, USA) for providing the caspase recombinant expression constructs, Dr. David A Bennett (Rush University Medical Center, California, USA) for providing precious AD human brain tissue, Dr. Nico Dantuma (Karolinska Institutet, Stockholm, Sweden) for providing the UPS GFP model substrates, and Dr. John Bergeron and Dr. Maryam Taheri (The Department of Anatomy and Cell Biology, McGill University, Montréal, QC, Canada) for generously providing the polyclonal antibody against the C-terminal domain of mammlian p97. Part of this work was supported by grants from the HFSP, Genome Canada, Silicon Kinetics and Genocean to ML and CIHR grant #MOP-81146 to ALB.

Table 3.1. Semi-tryptic peptides of Casp6 cleaved p97 identified using mass spectrometry

Identified Semi-tryptic Peptide	Consensus site	p97 domain localization	Theoretical Molecular Weight from the N domain (kDa)	Theoretical Molecular Weight from the prior caspase cleavage site (kDa)
^{165}VVETDPSPYCIVAPD^{179}	VAPD^{179}	N Domain	20.0	20.0
^{296}NAPAIIFIDELD^{307}	DELD^{307}	D1 AAA+ ring	34.1	20.0, 14.1
^{426}KMDLIDLEDETID^{438}	ETID^{438}	D1 AAA+ ring	48.7	20.0, 14.1, 14.6
^{466}ETVVEVPQVTWED^{478}	TWED^{478}	D1-D2 Linker	53.2	20, 14.1, 14.6, 4.5
^{714}QTNPSAMEVEED DPVPEIR^{732}	VEED^{732}	D2 AAA+ ring	80.4	20.0, 14.1, 14.6, 4.5, 27.2

Figure 3.1. p97 cleavage by Casp6 *in vitro*. A. Schematic representation of p97 structural domains with the localization of the antibody binding sites and putative Casp6 cleavage sites indicated. Abbreviations: ab; antibody, N; amino-terminal domain, L1; linker-1, D1; D1 AAA+ Domain, L2; linker-2, D2; D2 AAA+ Domain, COOH; Carboxyl-terminal domain. **B&C.** Western blot analysis of p97ND1 (**B**) or p97D2C (**C**) incubated with Casp6 using a monoclonal anti-N-terminal antibody (**B**) or a polyclonal anti-COOH terminal antibody (**C**) for p97. Digest reaction was performed with the indicated amounts of p97 fragments and Casp6 in Stennicke's buffer for 4 hours. Upper panels: digestion reaction in the absence of inhibitor. Lower panels: digestion reaction in the presence of the inhibitor, Z-VEID-FMK at 10 μM concentration. **D&E.** Western blot analysis of hexameric p97 incubated with active Casp6, using a monoclonal anti-N-terminal antibody for p97 (**D**) or a monoclonal anti-His tag antibody (**E**). Digestion was performed in HEPES buffer using 100 nM p97 and 300 nM Casp6 incubated for the times indicated.

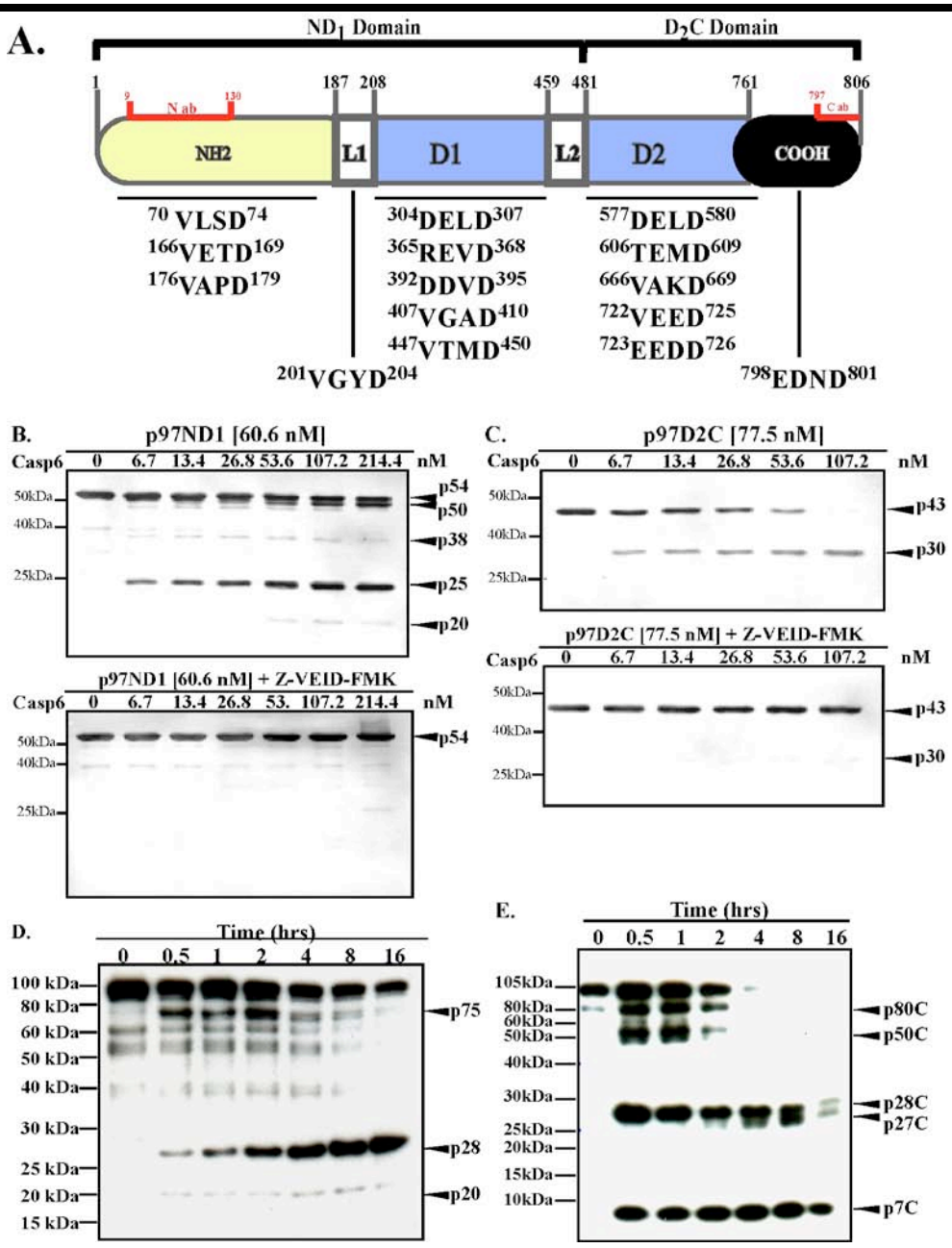
A.
ND1 Domain
D2C Domain
1
187 208
459 481
761
806
9
130
N ab
797
C ab
NH2
L1
D1
L2
D2
COOH
70 VLSD 74
166 VETD 169
176 VAPD 179
304 DELD 307
365 REVD 368
392 DDVD 395
407 VGAD 410
447 VTMD 450
577 DELD 580
606 TEMD 609
666 VAKD 669
722 VEED 725
723 EEDD 726
201 VGYD 204
798 EDND 801
B.
p97ND1 [60.6 nM]
Casp6 0 6.7 13.4 26.8 53.6 107.2 214.4 nM
50kDa
40kDa
25kDa
p54
p50
p38
p25
p20
p97ND1 [60.6 nM] + Z-VEID-FMK
Casp6 0 6.7 13.4 26.8 53. 107.2 214.4 nM
50kDa
40kDa
25kDa
p54
C.
p97D2C [77.5 nM]
Casp6 0 6.7 13.4 26.8 53.6 107.2 nM
50kDa
40kDa
25kDa
p43
p30
p97D2C [77.5 nM] + Z-VEID-FMK
Casp6 0 6.7 13.4 26.8 53.6 107.2 nM
50kDa
40kDa
25kDa
p43
p30
D.
Time (hrs)
0 0.5 1 2 4 8 16
100 kDa
80 kDa
60 kDa
50 kDa
40 kDa
30 kDa
25 kDa
20 kDa
15 kDa
p75
p28
p20
E.
Time (hrs)
0 0.5 1 2 4 8 16
105kDa
80kDa
60kDa
50kDa
40kDa
30kDa
25kDa
20kDa
15kDa
10kDa
p80C
p50C
p28C
p27C
p7C

Figure 3.2. ATP-dependent modulation of p97 cleavage by Casp6. A-C. Western blot analyses using a monoclonal anti-N-terminal antibody for p97. Reaction was prepared in Stennicke's buffer using 33 nM p97ND1, indicated concentration of Casp6, with or without 2.5 mM ATP (**A&B**). The ATP concentration was titrated in (**C**). **D.** Western blot analysis using a monoclonal anti-N-terminal antibody for p97. Reaction was performed in HEPES buffer using 100 nM p97 and 300 nM Casp6, and incubated for 16-18 hrs at 37°C. (*) indicates a no reproducibly observed band. $Casp6^{HD}$ refers to heat-denatured Casp6.

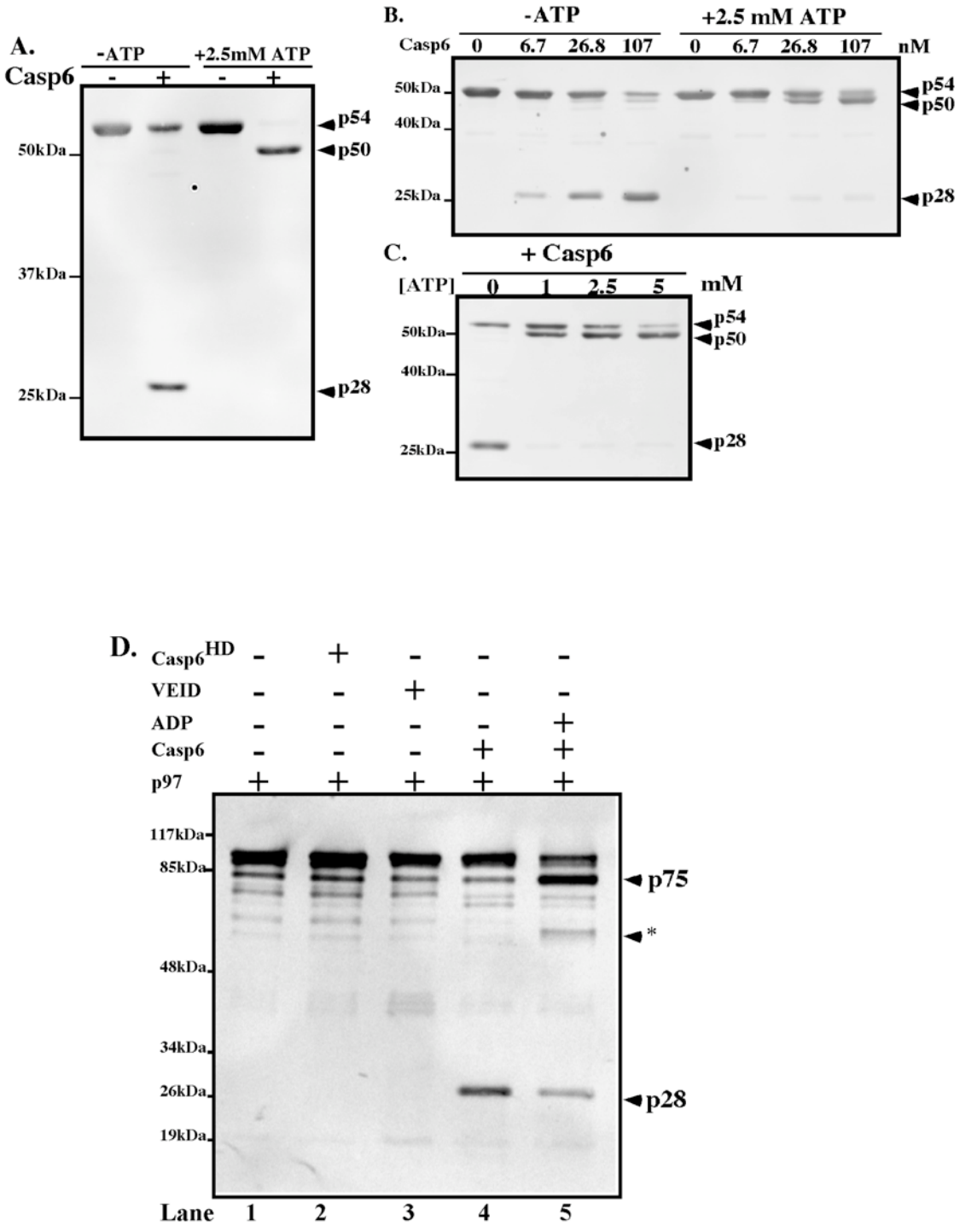
A.
-ATP
+2.5mM ATP
Casp6
- + - +
50kDa
37kDa
25kDa
p54
p50
p28
B.
-ATP
+2.5 mM ATP
Casp6 0 6.7 26.8 107 0 6.7 26.8 107 nM
50kDa
40kDa
25kDa
p54
p50
p28
C.
+ Casp6
[ATP] 0 1 2.5 5 mM
50kDa
40kDa
25kDa
p54
p50
p28
D.
Casp6HD - + - - -
VEID - - + - -
ADP - - - - +
Casp6 - - - + +
p97 + + + + +
117kDa
85kDa
48kDa
34kDa
26kDa
19kDa
p75
*
p28
Lane 1 2 3 4 5

Figure 3.3. p97 cleavage by effector Casp3 and Casp7 and initiator Casp8 *in vitro*. A. Western blot analysis of 100 nM hexameric p97 incubated with 300 nM active Casp3, Casp7, Casp6, or Casp8 for 4 hrs, using a monoclonal anti-N-terminal antibody for p97. **B.** Western blot analysis of 100 nM p97 digested with 300 nM active Casp3, Casp7, and Casp8 without nucleotide addition or in the presence of 1 mM ADP or ATP.

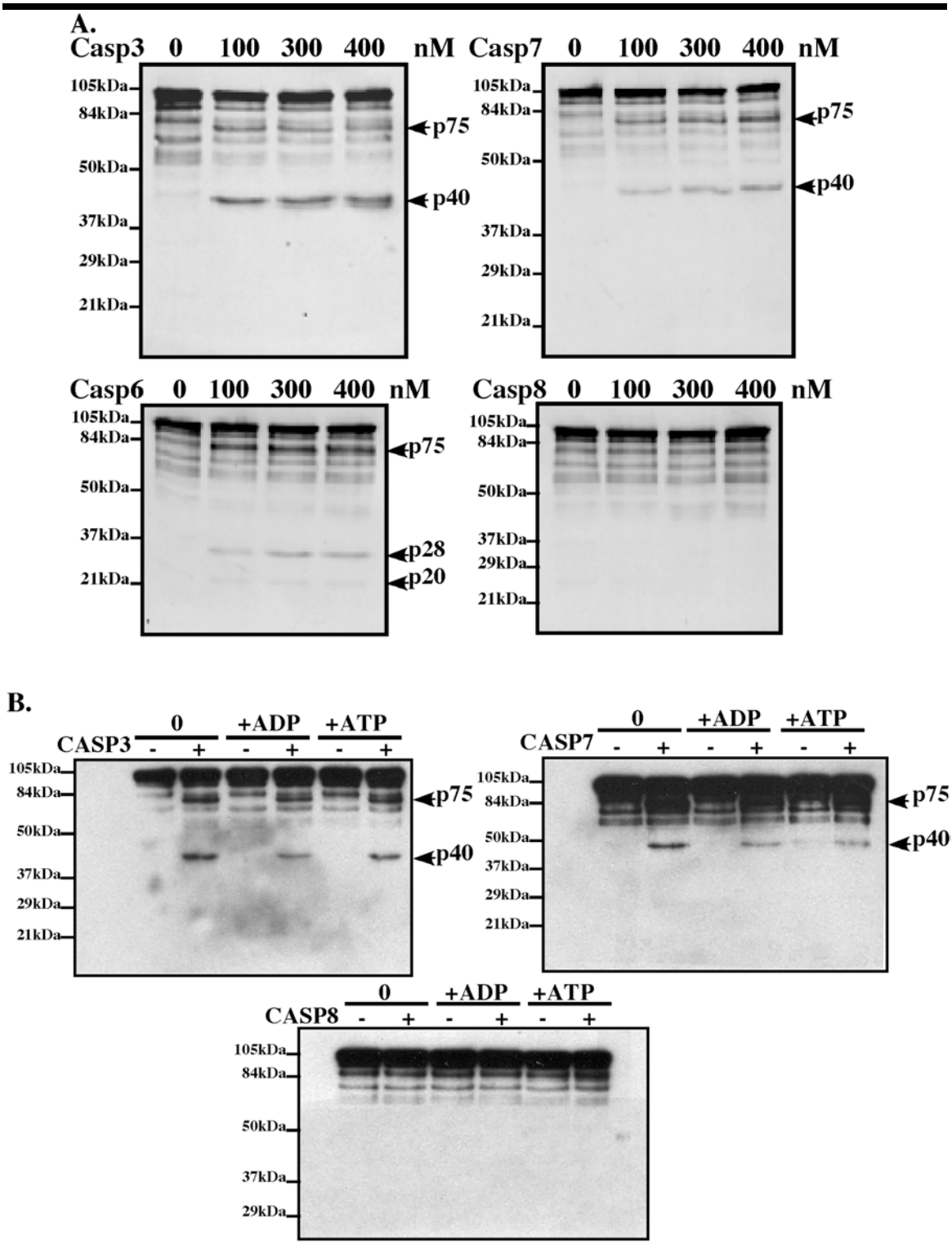
A.
Casp3 0 100 300 400 nM
105kDa
84kDa
50kDa
37kDa
29kDa
21kDa
p75
p40
Casp7 0 100 300 400 nM
105kDa
84kDa
50kDa
37kDa
29kDa
21kDa
p75
p40
Casp6 0 100 300 400 nM
105kDa
84kDa
50kDa
37kDa
21kDa
p75
p28
p20
Casp8 0 100 300 400 nM
105kDa
84kDa
50kDa
37kDa
29kDa
21kDa
B.
0 +ADP +ATP
CASP3 - + - + - +
105kDa
84kDa
50kDa
37kDa
29kDa
21kDa
p75
p40
0 +ADP +ATP
CASP7 - + - + - +
105kDa
84kDa
50kDa
37kDa
29kDa
21kDa
p75
p40
0 +ADP +ATP
CASP8 - + - + - +
105kDa
84kDa
50kDa
37kDa
29kDa

Figure 3.4. Identification of the Casp6 cleavage sites in p97 by mass spectrometry. A&B. LC-MS/MS chromatograms of semi-tryptic peptides detected in p97ND1 (**A**) or p97D2C (**B**) samples treated with active (lower panels) or heat-inactivated (top panels) of Casp6. Arrowheads point to the peak corresponding to the identified semi-tryptic peptide. The Casp6 recognition site is underlined. The shadowed peptide in **B** was not detected by LC-MS/MS.

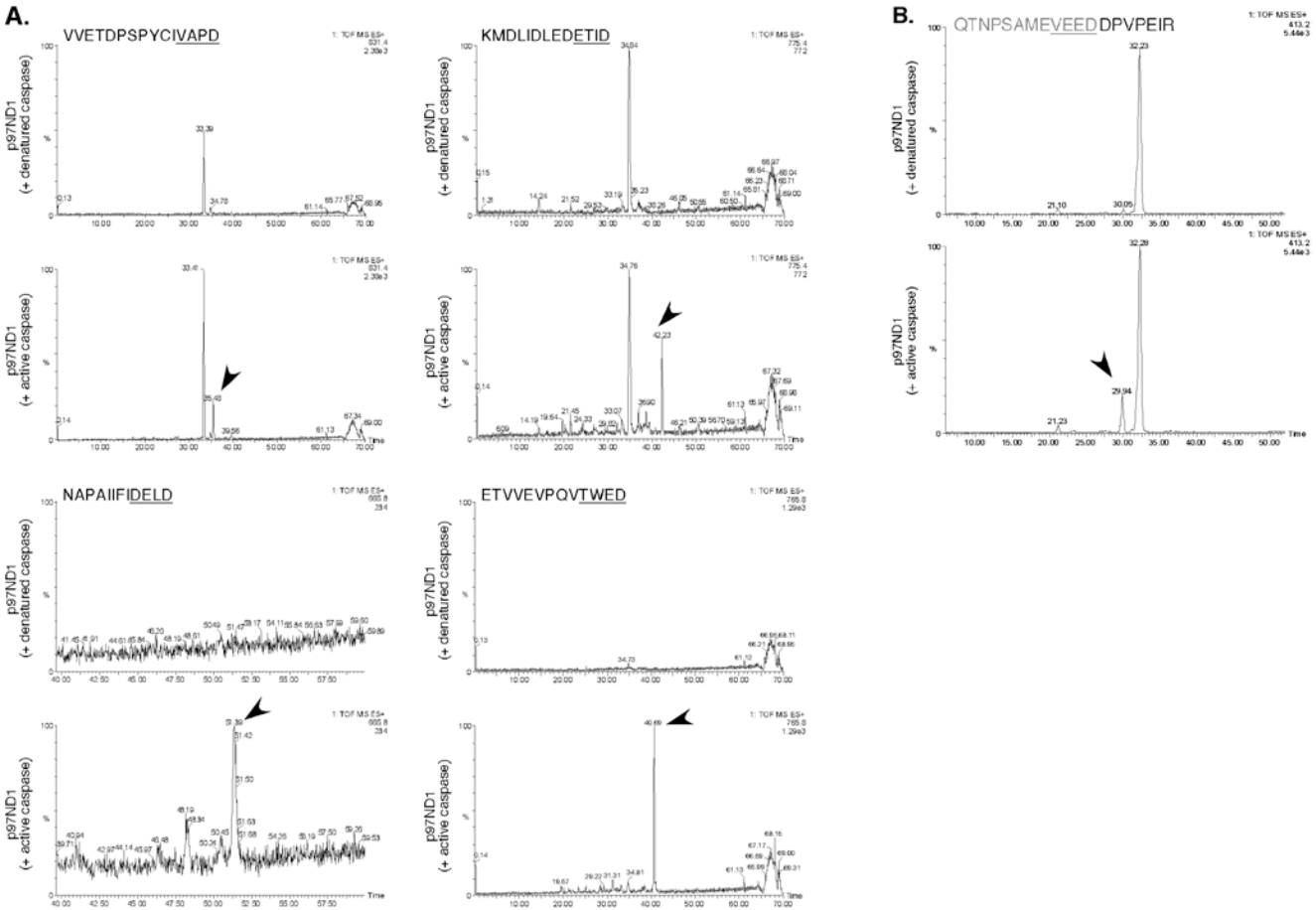
A.
VVETDPSPYCIVAPD
KMDLIDLEDETID
NAPAIIFIDELD
ETVVEVPQVTWED
p97ND1
(+ denatured caspase)
(+ active caspase)
B.
QTNPSAMEVEEDDPVPEIR
p97ND1
(- denatured caspase)
(- active caspase)
Time

Figure 3.5. Cleavage of p97D179A and p97D169A by Casp6. A-C. Western blots with a monoclonal anti-N-terminal antibody for p97. Reaction was performed in HEPES buffer containing 100 nM hexameric p97, and 300 nM Casp6 incubated for the indicated times.

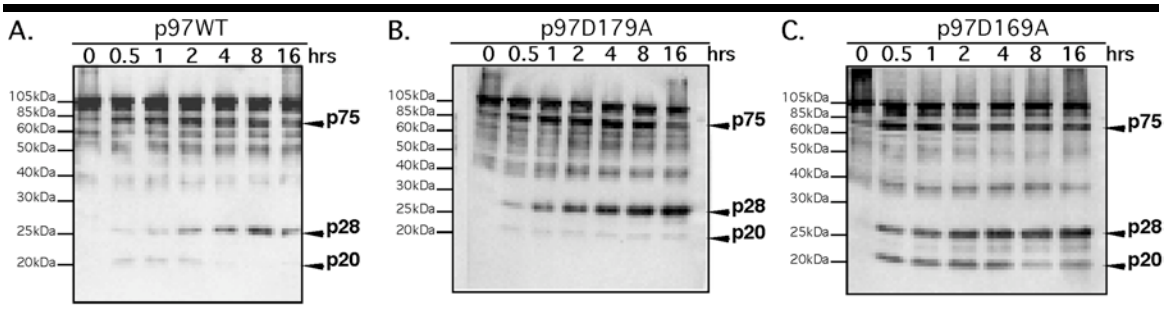
A.
p97WT
0 0.5 1 2 4 8 16 hrs
105kDa
85kDa
60kDa
50kDa
40kDa
30kDa
25kDa
20kDa
p75
p28
p20
B.
p97D179A
0 0.5 1 2 4 8 16 hrs
105kDa
85kDa
60kDa
50kDa
40kDa
30kDa
25kDa
20kDa
p75
p28
p20
C.
p97D169A
0 0.5 1 2 4 8 16 hrs
105kDa
85kDa
60kDa
50kDa
40kDa
30kDa
25kDa
20kDa
p75
p28
p20

Figure 3.6. Positive immunoreactivity to p97 cleaved by Casp6 (p97D179↓) in AD brains. A. Micrographs of p97D179↓ neoepitope antibody (1/1000) immunostaining developed with diaminobenzidine in the dentate gyrus of one representative case of non-cognitively impaired (NCI), mild cognitively impaired (MCI) and Alzheimer disease (AD). **B.** Micrographs of the CA2/CA3 area of the hippocampus of tissue sections from an AD individual stained consecutively with p97D179↓, anti-active Casp6, and Tau cleaved by Casp6 (TauΔCasp6). All micrographs were taken from the same areas for comparison. **C.** Magnified micrograph of a neuron showing the granularity of the p97D179↓ positive staining in the cytoplasm and neurite of neurons (+N) and a few neurons that were p97D179↓ negative (-N).

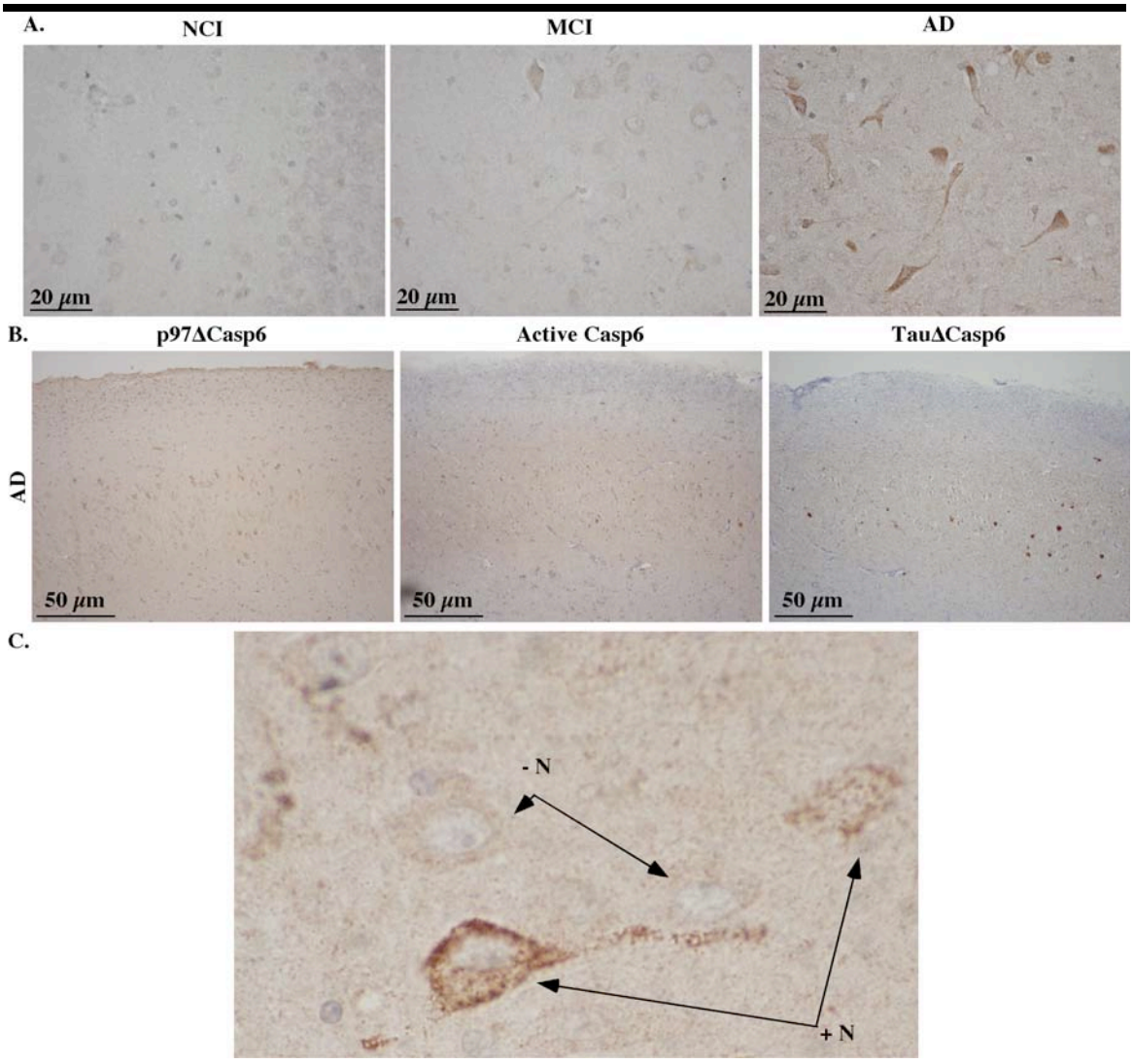
A.
NCI
MCI
AD
20 μm
20 μm
20 μm
B.
p97ΔCasp6
Active Casp6
TauΔCasp6
AD
50 μm
50 μm
50 μm
C.
- N
+ N

Figure 3.7. Monitoring of UPS function in cells over-expressing the p97VAPD179 fragment. **A.** Western blot analyses of N2a extracts co-expressing vector only, p97WT, p97K524A, p97VAPD179 (also referred to as p97D179↓) with UBG76V-GFP or R-GFP. Blots were probed with an anti-FLAG antibody. **B.** Quantitative analysis of the number of GFP positive cells (top panel), or the mean fluorescence intensity normalized against p97 overexpression levels (lower panels). Error bars represent the standard deviation of three independent experiments. **C.** Western blot analyses of N2a extracts co-expressing FLAG vector only, or FLAG-tagged p97WT, p97K524A, and p97VAPD179 with UBG76V-GFP or R-GFP. Blots were probed with an anti-COOH terminal antibody for p97. (*) indicates statistical significance compared to $p97^{WT}$ at $p \leq 0.05$ (Scheffe)

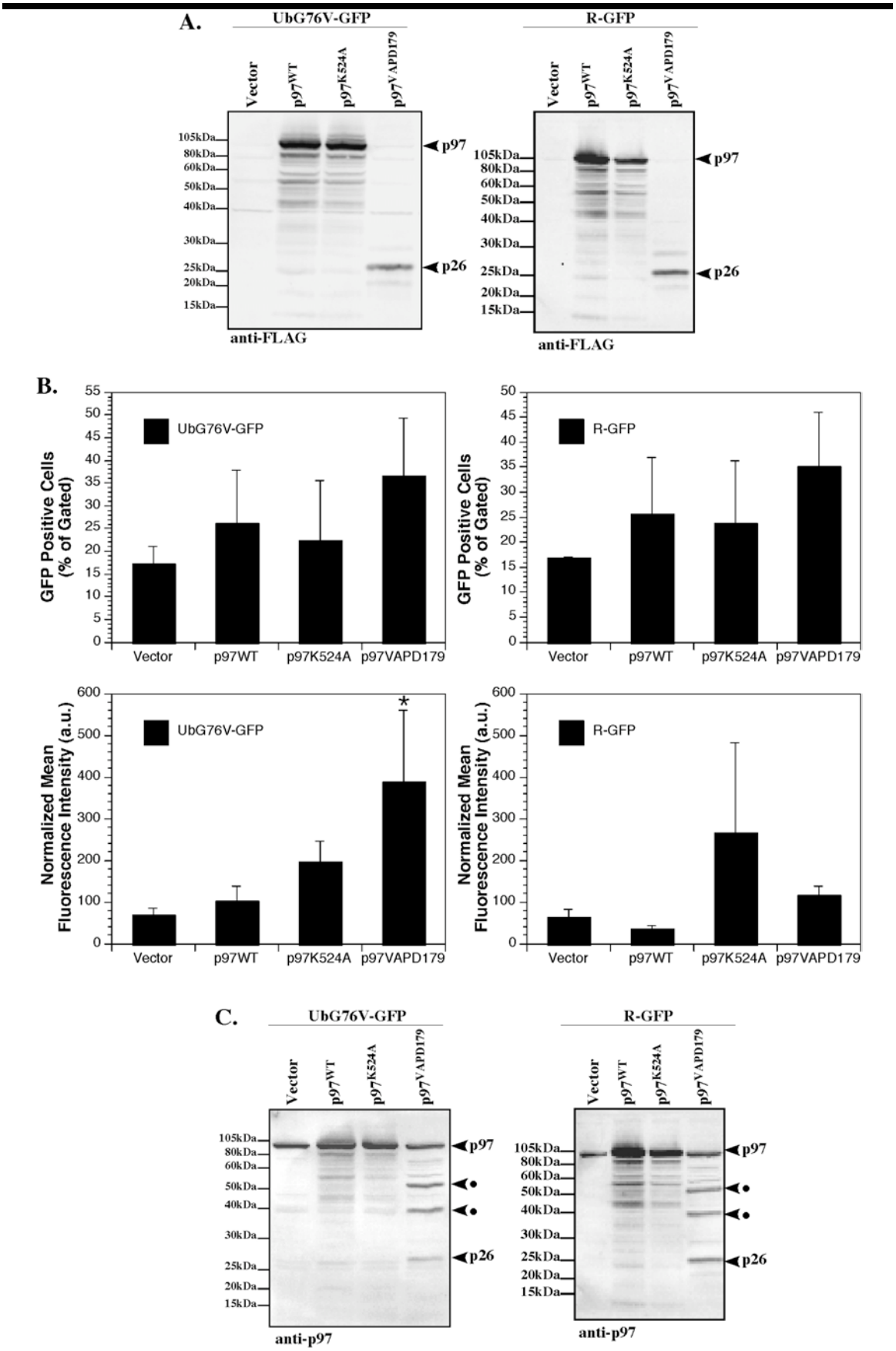
A.
UbG76V-GFP
R-GFP
Vector
p97WT
p97K524A
p97VAPD179
105kDa
80kDa
60kDa
50kDa
40kDa
30kDa
25kDa
20kDa
15kDa
p97
p26
anti-FLAG
B.
GFP Positive Cells (% of Gated)
UbG76V-GFP
R-GFP
Normalized Mean Fluorescence Intensity (a.u.)
*
C.
anti-p97

CHAPTER 4: Conformational instability of the N-domain linked to caspase mediated proteolysis in p97-linked fronto-temporal dementia

Preface

Although we previously demonstrated that two IBMPFD-linked mutations, p97R155P and p97A232E, alter p97 ATPase activity and D2 ring conformation, the structural consequences of these mutations on the p97 N-domain remain unclear. In this chapter, we utilized molecular dynamics modeling to investigate the potential effects of the Arg155Pro mutation on the conformation of the p97 N-domain. Subsequently, we utilized Casp6 activity to assess the structural integrity of the N-domain. Our findings implicate the Arg155Pro and Ala232Glu mutations in enhancing the conformational flexibility of the N-domain, and consequently increasing the accessibility of the Casp6 cleavage site. We further show that p97 is abundantly cleaved in p97-linked FTD. Collectively, our results pose the possibility that IBMPFD mutations may enhance the proteolytic susceptibility of p97 *in vivo*.

4.1 Abstract

Hereditary inclusion body myopathy associated with Paget disease of bone and fronto-temporal dementia is an autosomal dominant disease linked to mutations in highly conserved amino acid residues of p97. While all identified mutations localize to the N- terminal domain or the D1 ATPase ring, how these mutations influence p97 structure or conformation remains unclear. In this study, we used simulation annealing to model the Arg155Pro (R155P) mutation on the structure of the N-terminal domain and the D1 AAA ring (ND1). The R155P substitution enhanced the overall conformational flexibility of the N-terminal domain *in silico*. Using Casp6 mediated cleavage of the ND1 domain, we show that p97R155P ND1 fragment displayed increased susceptibility to Casp6-mediated processing compared to p97WT ND1. Substitution of Ala232Glu (A232E), was also associated with enhanced susceptibility to Casp6 mediated processing. While ATP-binding protected p97WT ND1 and p97A232E ND1 from N-terminal proteolysis, p97R155P ND1 remained susceptible. Furthermore, full-length p97A232E, but not p97R155P, showed increased susceptibility to Casp6 mediated proteolysis compared to p97WT*, in vitro*. Using a neoepitope antibody raised against p97 cleaved at 176VAPD179, we showed abundant p97 cleavage in the dystrophic neurites and activated astrocytes of patients carrying an Arg155Cys (R155C) mutation, p97R155C. Collectively, these results show conformational defects in the ND1 domain of IBMPFD-linked p97R155P and p97A232E mutants and suggest that these defects may predispose mutant complexes to caspase mediated proteolysis *in vivo*.

4.2 Introduction

p97 is one of the most intensively studied members of the AAA protein family due to its participation in a remarkable number of vital cell biological processes ranging from organellar biogenesis to protein degradation (Wang et al. 2004). p97 shares two hallmark features with other members of the AAA family: (i) it forms a homohexameric ring-shaped structure (DeLaBarre and Brunger 2003), and (ii) it utilizes ATP-driven conformational changes (Rouiller et al. 2000; Rouiller et al. 2002) in performing chaperone-like biochemical activities such as protein extraction or disaggregation (Thoms 2002; Shcherbik and Haines 2007) and macromolecular complex assembly and disassembly (Richly et al. 2005; Rumpf and Jentsch 2006). Each p97 monomer is comprised of an amino (N)-terminal protein-binding domain, which is flexibly linked to two homologous and highly conserved AAA cassettes (D1 and D2) (DeLaBarre and Brunger 2003). Each AAA cassette encompasses ~250 amino acid residues containing the Walker A and Walker B motifs, which mediate ATP binding and hydrolysis, respectively, as well as a SRH domain (Kunau et al. 1993). Within the hexamer, the D1 and the D2 AAA cassettes interact with their counterpart domains in adjacent protomers to form the D1 and the D2 ATPase rings (DeLaBarre and Brunger 2003). While the D1 ring is largely responsible for p97 oligomerization (Wang et al. 2003), the D2 ring mediates p97 major ATPase activity (Song et al. 2003). ATP-binding and hydrolysis within the D2 ring initiate conformational changes which are relayed through the D1-D2 linker residues to the D1 ring (DeLaBarre and Brunger 2005). The D1 ring subsequently communicates these

motions to the N-domain (DeLaBarre and Brunger 2005). The N-domain of p97 mediates its interaction with a wide array of cofactors, including p47 (Kondo et al. 1997) , Npl4-Ufd1 (Meyer et al. 2000), VCIP135 (Uchiyama et al. 2002), and multiubiquitin chains in protein substrates (Meyer et al. 2002). While deletion of the N-domain has no effect on p97 ATPase activity (Rouiller et al. 2002; Ye et al. 2003; Rothballer et al. 2007), it is predicted to comprise its interaction with its essential cofactors.

Recently, single point mutations affecting highly conserved residues within p97 N-domain and the D1 AAA ring have been linked to the pathogenesis of IBMPFD (Watts et al. 2004). IBMPFD is a rare autosomal dominant disorder characterized by myopathy with sarcoplasmic inclusions, neuronal dystrophy, and abnormal bone remodeling (Watts et al. 2004). The fact that this disease manifests itself only in fourth or fifth decade of life suggests the IBMPFD-linked mutations have a subtle effect on p97 cell biological activities (Watts et al. 2004). Indeed, loss of p97 function is detrimental, as overexpression of an ATPase deficient mutant of p97 in cell culture systems leads to apoptosis (Hirabayashi et al. 2001). Similarly, a homozygous null allele in murine animal models leads to early embryonic lethality (Muller et al. 2007). Nevertheless, the mechanism by which IBMPFD interferes with p97 cell biological activities remains unclear. Overexpression studies in cell culture models show accumulation of polyubiquitinated protein (Weihl et al. 2006), increased p97 localization in insoluble cell extracts (Weihl et al. 2006), altered localization of TDB-43 (Gitcho

et al. 2009), and caspase activation (Gitcho et al. 2009). Transgenic animals expressing IBMPFD-linked p97 mutant variants show an accumulation in polyubiquitinated proteins and evidence of defects in UPS mediated protein clearance (Janiesch et al. 2007; Weihl et al. 2007). Interestingly, it has been recently shown that IBMPFD-linked mutations do not impair p97 interaction with several N-terminal binding partners, including UFD1 and ataxin-3 (Hubbers et al. 2007).

We recently demonstrated that two IBMPFD-linked mutations, Arg155Pro (R155P) and Ala232Glu (A232E), altered p97 structure and ATPase activity (Halawani et al. 2009). Both p97R155P and p97A232E displayed higher ATPase activity than p97WT and showed evidence of conformational defects in the D2 ring (Halawani et al. 2009). These defects also correlated with an ATP-dependent propensity to form higher molecular weight oligomers in solution (Halawani et al. 2009). Therefore, we proposed that conformational alterations in p97 may underlie mechanism of pathogenesis in IBMPFD.

In this study, we used simulated annealing modeling to further investigate the potential effects of IBMPFD-linked p97 mutation, R155P, on the structure of the N-domain and the D1 AAA ring (ND1). Substitution of Arg155 by Pro enhanced the overall conformational flexibility of the ND1 domain *in silico*. We next utilized the availability of Casp6 (Casp6) consensus sites in p97 to assess the validity of this model. Our results show that IBMPFD-linked mutants,

p97R155P and p97A232E, display conformational defects in the ND1 ring which may increase the accessibility of the Casp6 consensus sites. Furthermore, we provide evidence that p97 is abundantly cleaved at 176VAPD179 in patients carrying the Arg155 to Cys substitution. Considering the role of IBMPFD-linked mutants in activating caspases, our results suggest that conformational defects in p97 may predispose mutant complexes to caspase mediated proteolysis *in vivo*.

4.3 Results

Computational Modeling of the Arg155 to Pro p97ND1 mutation

To better understand the structural effects of the Arg155 to Pro p97 mutations, a molecular dynamics simulated annealing protocol was developed to widely sample the conformational space of the p97WT ND1 and p97R155P ND1. The backbone atoms of a minimized structure of the WT or Arg155Pro mutant of p97 ND1 domain were tethered with a force constant of 1200 kcal·mol-1·Å-2. Next, the entire protein was rapidly heated to 1000 K, equilibrated at this temperature, cooled down to 300 K, and energy-minimized without constraints. This new energy-minimized structure was used as a starting point for the next round of simulated annealing, with a total of nine iterations per trial. This process was performed twice (2 trials) for each of the p97WT ND1 and p97R155P ND1 resulting in a total of 20 minimized structures for each protein variant.

Overall, the 20 resulting conformers for the p97WTND or p97R155P ND1 displayed a global average backbone RMSD of ≤ 1.8 Å and ≤ 1.9 Å, respectively, with respect to the starting structural coordinates. Each of these 20 minimized structures was then subjected to a validation protocol using the MolProbity suite of software (Guex and Peitsch 1997) to eliminate conformations of Arg155 in p97WT ND1 or Pro155 in p97R155P ND1 which displayed atomic clashes, unlikely rotamers, abnormal Cβ deviations, and unfavorable ϕ and ψ angle values. As a further, more stringent control, the aforementioned analysis was also performed for neighboring Val154 as well as two residues, Val166 and

Thr168 (see Supplemental Data, Tables S4.1-S4.4 for a summary of the results). Based on the results of the MolProbity analysis, 15 conformers for p97WT ND1 and 19 conformers for p97R155P ND1 were retained.

Visual inspection of the p97WT ND1 domain revealed that Arg155 lies in a α-helical region connecting two anti-parallel β-sheets, with the Casp6 consensus site (166VETD169) located at the "head region" of the second sheet. In order to assess the potential dynamic nature of this region, and the degree of influence the Arg155Pro mutation might have on the overall structural integrity or dynamic nature of this secondary structural region, backbone RMSDs for two regions was analyzed. The first region spanned Asp150 to Tyr173 (region 1), which contained, both the mutational site, Arg155Pro, and the Casp6 consensus site, 166VETD169 (Table 4.1). The second region was comprised of Phe163 to Tyr173 (region 2) to focus on the Casp6 consensus site, 164VETD169 (Table 4.1). For p97WT ND1, the averaged RMSD values for the 15 retained conformers (in the focused regions 1 and 2) were in agreement with the RMSD for the entire structure suggesting this region lacks inherent instability or dynamic nature. Similar analysis for regions 1 and 2 in the 19 retained conformers of p97R155P ND1 revealed a more pronounced shift in backbone RMSD values compared to the same regions in p97WT ND1 (Table 4.1).

To further assess the influence of the Arg155Pro mutation on the α-helical region where it is located, an RMSD analysis was performed on a second Casp6

consensus site (176VAPD179) lying 10 residues downstream of 166VETD169 (region 3). Compared to p97WT ND1, p97R155P ND1 displayed a pronounced shift in the backbone RMSD values for region 3 (Table 4.1). These results provide additional evidence for the potential role of Pro155 in the destabilization of this region. Therefore, the introduction of a proline residue at position 155 may destabilize the entire α-helical region, with the most prominent effect felt at or near the Casp6 consensus site (Fig. 4.1).

To investigate if the potential effects of the Arg155Pro mutation on the protein structure were localized or also observable elsewhere in the structure, an RMSD comparison between the retained simulated annealing conformations for p97WT ND1 and p97R155P ND1 and the starting structural coordinates was performed for a forth region within the p97ND1 domain. This control region, spanning 10 residues from Val57 to Glu66, is located approximately 23 Å away from Pro155 and comprises an α-helical structural scaffold similar to that of Pro155 (region 4). An analysis of this region resulted in an overall averaged RMSD value of 1.7±0.5 Å and 2.2±0.5 Å for p97WT ND1 and p97R155P ND1, respectively (Table 4.1**)**. Interestingly, as with the previously considered regions (1 and 2), region 4 displayed an overall RMSD similar to the global overall RMSD obtained for the p97WT ND1 structure, while p97R155P ND1 conformation showed a more pronounced structural shift. The mutation Arg155Pro thus appears to influence local and distal regions of the protein without having an overall disruptive effect on the structure (Fig. 4.1).

p97R155P and p97A232E ND1 AAA ring display increased susceptibility to Casp6 mediated processing

To investigate the effect of p97R155P and p97A232E mutations on the p97 ND1 structure, we utilized putative caspase cleavage sites in the N-terminal domain and the D1 AAA ring (Fig 4.2). Using purified p97ND1 protein preparations (Fig. 4.3 A) and active Casp6 as the proteolytic agent, cleavage of p97WT ND1 generated a predominant p50 and p28 N-terminal fragments and a minor p47 band (Fig. 4.3 B). Compared to p97WT ND1, p97R155P ND1 cleavage generated predominantly p28 and a minor 38 kDa (p38) product, but not the p50 product observed in p97WT (Fig. 4.3B). Similarly, p97A232E ND1 cleavage generated predominantly p47 and p28, but minor amounts of p50 and p38. Furthermore, a substantial amount of p97WT ND1 remained resistant to proteolysis, while p97R155P and p97A232E, both showed increased susceptibility to N-terminal cleavage. These results suggest that while p28 is the predominant cleavage product of p97WT ND1 and IBMPFD-linked mutants, p97R155P ND1 and p97A232E ND1 show altered susceptibility to Casp6 mediated cleavage.

To further assess if IBMPFD-linked p97 mutations increase the proteolytic susceptibility of the ND1 AAA ring, p97WT ND1, p97R155P ND1 and p97A232E ND1 mutants were incubated with increasing concentrations of Casp6 (Fig. 4.3 C). p97WT ND1 displayed Casp6 dependent generation of p20, p28, p38, p47, and p50 (Fig. 4.3 C, top panel). Quantitation of p97WT ND1 cleavage by 213 nM

of active Casp6 demonstrated that ~ 60% of the protein remained unprocessed after 4 hours of incubation (Fig. 4.3 D). Unlike p97WT ND1, p97R155P ND1 cleavage generated only p38, p28, and p20, but not p47 or p50 (Fig. 4.3 C, middle panel), with only ~20% of the protein remaining unprocessed by Casp6 (Fig. 4.3 D). Similarly, p97A232E ND1 cleavage generated p38, p28, and p20, with only a minor amount of p47, and no p50 (Fig. 4.3 C, lower panel). Only ~30% of p97A232E ND1 remained unprocessed by Casp6 (Fig. 4.3 D). These results indicate that p97R155P and p97A232E ND1 AAA ring displays increased susceptibility to Casp6-mediated cleavage.

To examine the overall proteolysis pattern of p97WT ND1 and IBMPFD-linked mutant variants, coomassie stain analysis was performed following incubation with increasing concentrations of Casp6. Cleavage of p97WT ND1, p97R155P ND1, p97A232E ND1 generated two predominant products p28 and p30; however, p28 was generated more readily in p97R155P ND1 and p97A232E ND1 compared to p97WT ND1 (Fig. 4.3 E). These results suggest that although the overall proteolysis pattern of p97A232E ND1 and p97R155P ND1 is similar to p97WT ND1, the cleavage site(s) responsible for p28 generation is more accessible in IBMPFD-linked mutants.

p97R155P ND1 AAA ring show altered susceptibility to N-terminal cleavage in the presence of ATP.

Considering that nucleotide-binding to the D1 AAA ring have been previously shown to protect the N-terminal domain from Casp6 mediated proteolysis, we investigated if ATP-binding has the same effect on p97R155P ND1 and p97A232 ND1 proteolysis by Casp6. As previously shown, in the absence of ATP, p97WT ND1 cleavage generated the predominant cleavage product, p28 in a Casp6 dependent manner. In the presence of ATP, p50 became the predominant cleavage product (Fig. 4.4 A, upper panel). Similarly, cleavage of p97R155P ND1 and p97A232E ND1 by Casp6 generated p28 as the predominant cleavage product, however, in the presence of ATP, p97R155P ND1 generated both p28 and p50, while p97A232E ND1 generated mostly p50 (Fig 4.4 B, middle and lower panels). We next investigated whether the N-terminal domain of p97R155P ND1 is protected in the presence of higher ATP concentrations. Using concentrations as high as 5 mM ATP led to the consistent production of the p50 fragment in p97WT ND1 and p97A232E ND1, however, p97R155P ND1, consistently generated both p28 and p50 (Fig. 4.4 B). These results indicate that, unlike p97WT ND1 and p97A232E ND1, the N-terminal domain of p97R155P ND1 retains a conformation accessible to Casp6 in the presence ATP.

Full-length p97A232E, but not p97R155P, displays faster proteolysis kinetics by Casp6 compared to p97WT *in vitro*.

To investigate whether full-length p97R155P and p97A232E also display increased susceptibility to Casp6 mediated processing, recombinant hexameric p97WT, p97R155P, p97A232E, and an ATPase deficient mutant, p97K524A were coincubated with active Casp6. All proteins contained minor COOH-terminal truncation, usually occurring from either cleavage by bacterial proteases or premature termination of translation during expression that are incorporated within hexameric p97. Cleavage of p97WT generated the predominant cleavage products, p75, p28, and p20, all which could be detected with an anti-N-terminal antibody for p97 (Fig. 4.5 A). Similar cleavage products were detected for p97R155P and p97A232E, however p97A232E displayed faster proteolysis kinetics (Fig. 4.5 B&C). Conversely, p97K524A cleavage produced p28 and p20, but not p75 (Fig. 4.5 D). These results suggest that p97 IBMPFD-linked D1 mutation in alanine 232 to glutamate modulates the accessibility of the Casp6 N-terminal cleavage sites in p97.

p97 is cleaved at 176VAPD179 *in vivo*.

Considering the role of IBMPFD-linked p97 mutations in caspase activation, we next investigated whether p97 cleavage by caspases represents a relevant pathogenic mechanism in IBMPFD patients. Immunostaining of frontal lobe sections of three patients carrying p97R155C mutation with the p97 neoepitope antibody (p97D179↓) showed marked immunostaining in the

dystrophic neurites, and activated astrocytes of affected brain tissue (Fig. 4.6 B-C). No immunoreactivity was observed in healthy control hippocampal brain sections (Fig. 4.6 A). The immunostaining intensity correlated well with the pattern of cerebral degeneration observed in these patients. These results provide evidence for p97 N-terminal cleavage in patients diagnosed with IBMPFD.

4.4 Discussion

Hereditary IBMPFTD is a debilitating degenerative disorder caused by a single amino-acid substitution in the N-terminal domain or the D1 AAA+ ring of p97. The fact that eight of thirteen identified mutations localize to the N-terminal domain further reinforces the importance of this domain in mediating p97 cell biological activities (Kimonis et al. 2008). The most commonly affected residues is arginine 155, with several reported substitutions, proline, histidine, and cysteine, all resulting in the same phenotype. Five mutations have been reported either in the D1 AAA+ ring or the N-D1 linker domain, with the A232E mutation being associated with a particularly severe disease progression (Watts et al. 2004). In this study, we focused on R155P and A232E, two mutations known to affect p97 ATPase activity and D2 ring conformation (Halawani et al. 2009). We used simulated annealing modeling to examine how the substitution of arginine 155 to proline might influence the local structure or conformation of the N-terminal domain. Using the ND1 structure of p97, we found that R155P increases the overall conformational flexibility of the N-terminal domain. In support of this model, p97R155P ND1 displayed increased susceptibility to Casp6-mediated processing compared to p97WT ND1. Similarly, the D1 AAA+ mutation, A232E, also showed increased proteolytic susceptibility in the absence of ATP binding. While ATP binding protected p97WT ND1 and p97A232E ND1 from N-terminal processing, the N-terminus of p97R155P ND1 remained accessible to Casp6. Furthermore, using a neoepitope antibody raised against a cleaved N-terminal fragment of p97, we demonstrate that p97 is cleaved in the dystrophic neurites

and activated astrocytes of the frontal lobe of patients carrying the R155C mutation. Our results show that IBMPFD mutations alter the conformational state of the N-terminal domain and suggest that these alternations may be relevant to p97 cleavage *in vivo*.

Substitution of Arginine 155 to proline increases the conformational flexibility of the N-terminal domain *in silico*.

Our analysis using simulated annealing modeling predicts that Arginine 155 substitution to proline increases the conformational flexibility of the N-terminal domain, without affecting the overall structure of the ND1 ring. This analysis is based on the assumption that the R155P mutation leads to subtle, rather than drastic, structural alterations in the N-terminal domain. The general preservation of mutant p97 function is inferred from the ability of full-length recombinant p97R155P to form active, ring-shaped hexamers as p97WT (Halawani et al. 2009). Moreover, IBMPFD is characterized by its late onset in adults and is not accompanied by any developmental defects (Watts et al. 2004). Accordingly, it is plausible to assume that the structure of ND1 ring will be largely affected by the R155P mutation.

In principle, the simulated annealing modeling is based on homology modeling in that it employed what is known about the published structure of the p97WT ND1 domain in predicting the local and distal consequences of the R155P mutation assuming that the overall structure will be largely unaffected . The

general agreement between the RMSD values of the 15 p97WT ND1 conformers predicted by the model and the published structure of the ND1 domain (Zhang et al. 2000) is indicative of the stringency of the applied annealing protocols and validation analyses. Furthermore, the global RMSD value for p97R155P ND1 was comparable to p97WT ND1, which supports the fact that the p97R155P ND1 mutation did not alter the overall structure of the ND1 domain; however, p97R155P ND1 showed greater variation in the RMSD values of 19 conformers for several N-terminal regions compared to p97WT ND1. The affected regions where within the vicinity of the mutation and extended to distant regions of the N-terminal domain, with the largest variation observed for distant regions rather than the area surrounding the mutation. One explanation is the rigidity of the proline residue at position 155- the strain induced by the proline residue may be readily relayed to the entire length of the N-domain thereby producing larger conformational variations in flexible or unconstrained regions. Furthermore, the largest RMSD variation was noted for region 3 (Pro170-Glu180). Coincidently, region 3 lies adjacent to the flexible N-D1 linker, which is spanned by two highly conserved glycine residue, Gly186 and Gly208, proposed to act as flexible pivots to relay conformational changes from the D1 ring to the N-terminal domain (Zhang et al. 2000). Interestingly, as would be expected, region 3 also displayed the largest RMSDs variation in p97WT ND1.

Biochemical evidence of conformational defects in IBMPFD-p97ND1 mutant variants, p97R155P ND1 and p97A232E ND1.

Our biochemical analysis using Casp6 mediated proteolysis of the ND1 domain clearly shows substantial conformational defects in p97R155P ND1 fragment and suggests that arginine 155 substitution for proline uncouples D1 regulation of the N-domain. We showed enhanced susceptibility of p97R155P ND1 to Casp6-mediated proteolysis in the absence of ATP. While ATP-binding protected the N-terminal domain of p97WT ND1 from Casp6-,mediated proteolysis, the N-domain of p97R155P ND1 remained susceptible. Interestingly, the simulation annealing modeling predicts that arginine 155 substitution to proline would increase the conformational flexibility of the N-terminal domain. It is therefore plausible that the increased flexibility would be accompanied by increased accessibility of the Casp6 consensus site. In fact, two Casp6 cleavage sites, 166VETD169 and 176VAPD179, indeed localized to the regions examined in the simulation annealing modeling, Phe163-Tyr173 and Pro170-Glu180, and found to be perturbed by the mutation. Furthermore, our data suggest that the structure of p97R155P ND1 and p97A232E ND1 was less compact and more accessible to proteolysis compared to p97WT ND1. p97WT ND1 was partially resistant to Casp6 mediated proteolysis and generated high molecular weight N-terminal fragment, p50. In comparison, cleavage of both p97R155P ND1 and p97A232E ND1 resulted in almost complete proteolysis in the absence of ATP-binding.

p97 cleavage by caspases in IBMPFD

Our results show that p97 is targeted by caspases in IBMPFD and are consistent with previous reports implicating caspases in p97 cleavage. For example, p97 was identified as a putative target of Casp6 activity in primary human neurons (Klaiman et al. 2008) and we recently found that p97 is cleaved in Alzheimer Disease (to be submitted). p97 was also reported to be cleaved by Casp3 and Casp7 during apoptosis (Jang et al. 2008). Thus far, it is unclear if the abundant immunoreactivity against caspase-cleaved p97 is the result of increased predisposition of IBMPFD-linked p97 complexes to caspase-mediated proteolysis *in vivo*. At least, full-length p97A232E showed marginally higher susceptibility to Casp6 mediated cleavage than p97WT or p97R155P *in vitro*. Many factors, such as post-translational modification and protein-protein interactions, could modulate the accessibility of the caspase-cleavage sites *in vivo*. On the other hand, it is equally possible that both wild-type and mutant p97 complexes are cleaved indiscriminately by the robust activation of caspases in IBMPFD. In either case, p97 down-regulation has detrimental effects on cell viability since it leads to the accumulation of polyubiquitinated proteins independent of direct inhibition of proteasome activity, and causes ER and Golgi fragmentation, effector Casp3 and Casp7 activation, and p53 upregulation (Wojcik et al. 2004). Many of these defects are indeed paralleled in IBMPFD. Affected tissue shows accumulation of polyubiquitinated proteins (Forman et al. 2006) in the absence of reduced proteasome activity (Guyant-Marechal et al. 2006) and vacuolization of the Golgi apparatus (Guyant-Marechal et al. 2006).

Furthermore, down-regulation of p97 protein expression by caspase-mediated proteolysis may explain the lack of colocalization between p97 and polyubiquitinated protein in the brains of patients diagnosed with p97-linked frontotemporal dementia (Forman et al. 2006). Our data indicate the p97 is cleaved in dystrophic neurites and the activated astrocytes of the frontal lobe of patients carrying the arginine 155 to cysteine substitution. The immunoreactivity pattern against cleaved p97 was most prominent in the upper layer of the cerebral cortex, which parallels the pattern of ubiquitin pathology reported by Forman and colleagues (Forman et al. 2006).

Together our data show that substitution of arginine 155 to proline and alanine 232 to glutamate lead to conformational defects in p97ND1 ring. These defects in turn increased the proteolytic susceptibility of the ND1 ring to Casp6 mediated cleavage *in vitro*. Considering the role of IBMPFD-p97 in caspase activation, we used an antibody neoepitope antibody against Casp6 cleaved p97, and showed that p97 is cleaved in the frontal lobe of patients carrying the arginine 155 to cysteine substitution. Collectively, our results suggest that conformational defects induced by IBMPFD-linked p97 mutations may be directly linked to susceptibility to caspase-mediated proteolysis *in vivo*.

4.5 Materials and Methods

Simulated Annealing Modeling

All molecular modeling was done using the Insight II package, version 2000.1 (Accelrys, San Diego, CA) implemented on a Fuel Silicon Graphics Workstation running Irix 6.5. The Biopolymer module was used to modify molecular structures and the Analysis and Decipher modules were used to analyze molecular dynamics simulated annealing trajectories. Energy minimizations and simulated annealing calculations were performed using the Discover module employing the constant valence force field (CVFF) and calculations were run on an Origin 2000 Silicon Graphics Fuel Server. The 2.9-Å crystallographic structure of the N-terminal and D1 ATPase domain of murine p97, PDB coordinates, 1E32 (Zhang et al. 2000), was used as starting coordinates for all calculations performed on p97WT ND1 and p97R155P ND1. The crystallographic water molecules as well as the bound ADP were removed and hydrogen atoms were added at the normal ionization state of the amino acids at pH 7.0. Atomic potentials were fixed to the CVFF atom types recommended by the software. To eliminate potential steric clashes, the initial structure was minimized by applying 1000 steps of steepest descents, followed by a conjugate gradient minimization, until a convergence of 0.001 kcal mol-1 Å2 was attained. The aforementioned procedure was repeated for the p97R155P ND1 mutant with the Arg155 to Pro mutation being introduced before energy minimization. These energy minimized structures were used as starting points for all subsequent modeling steps.

The initial minimized structures of p97WT ND1 and p97R155P ND1 were then subjected to a molecular dynamics simulated annealing protocol according to the following iterative procedure. The structure was heated to 1000 K over 5 ps, equilibrated at 1000 K for 3 ps, and then cooled down to 300 K in 5ps using an exponential rate constant (timtmp) of 0.7 ps for both the heating and cooling steps. The time step of the molecular dynamics simulations was set to 1 fs and a distance-dependent dielectric constant of 1 was applied to the system. During the simulated annealing protocol, the backbone atoms of the protein were tethered to their initial positions by applying a force constant of 1200 kcal mol-1 Å2. This force constant sufficiently restricts the protein backbone to limit local unfolding of secondary structural elements while allowing for subtle backbone movements that permit broad side-chain conformation exploration. Following each simulated annealing cycle the resulting cooled structures were subjected to a final energy minimization step involving 1000 steps of steepest descent followed by conjugate gradient minimization until a convergence of 0.01 kcal mol-1 Å2 was reached. This cycle was repeated 9 times and was performed in duplicate for a total simulation time of 260 ps yielding 20 minimized structures for p97WT ND1. The protocol was repeated for p97R155P ND1 resulting in 20 minimized conformations. Each minimized structure was subjected to a validation procedure in which the Val154 and Arg155 (or Pro155) positions, as well as Val166 and Thr168 positions were analyzed for proper atom contacts and geometry. The Cβ geometry, sidechain rotamers, Ramachandran angles, atomic clashes, and Cβ deviations were evaluated using the MolProbity software

developed by Richardson and coworkers (Lovell et al. 2003). Structural overlays for all validated conformations were generated using DeepView software version 4.0 (Guex and Peitsch 1997).

Protein Expression Vectors

p97WT ND1 (residues 1-480) expression vector was generated using murine p97 cDNA in the pBluescript SK+ vector (Dr. Fred Indig, National Institute on Aging/NIH, Baltimore, USA). The cDNA fragment encoding p97 amino acid residues 1 to 480 was amplified by PCR using primers: 5' AGCTCGAGAATGGCCTCTGGAGCCGAT 3', and 5' CCATATGTACCTTATCCA ATATCTTCCCAGGT 3', which contained the restriction sites, Xho I and Kpn I, respectively. The amplified cDNA product was inserted into the multiple cloning site of the pTrcHis2A (Invitrogen, Carlsband,CA) bacterial expression vector for COOH-terminal polyhistidine tagging. The p97R155P ND1 and p97A232E ND1 expression vectors were generated using site-directed mutagenesis of the pTrcHis2A-p97WT ND1 as previously described (Halawani et al. 2009). Full-length p97WT, p97R155P, p97A232E, and p97K524A expression vectors were previously described (Halawani et al. 2009). Casp6 recombinant expression vector, pET23b-Casp6-His, was kindly provided by Dr. Guy Salvesen (The Burnham Institute, La Jolla, CA, USA).

Recombinant Protein Expression and Purification

Full-length p97 proteins were expressed and purified as previously described (Halawani et al. 2009). p97ND1 protein variants were expressed in the Top10 *E.coli* strain using 2X YT growth media (16 g/L Tryptone, 10 g/L Yeast Extracts, 5 g/L NaCl). Briefly, overnight starter cultures were diluted 50X in growth media and incubated at 37°C with vigorous shaking. Culture were induced with 300 μM IPTG when the OD at 600 nm reached 0.6 and further grown for 4-5 hours. Cells were subsequently harvested by centrifugation (4,000 g for 20 minutes) and lysed in buffer A (20 mM HEPES pH 7.5, 300 mM NaCl, 5 mM $MgCl_2$, 2.5 mM DTT, and 20 mM imidazole), supplemented with 1 mg/ml lysozyme and complete protease inhibitors (Roche, Mississauga, ON). Following sonication and clearance by centrifugation at 26,000 g for 45 minutes, the supernatant was filtered with 0.2 μm filters (Millipore, Bedford, MA) and loaded on a Ni^{2+} affinity column (GE Healthcare Bio-sciences, Uppsala, Sweden) preequilibrated with buffer A. Following a first wash with 10 X column volume of buffer A, a second wash was performed using buffer B (20 mM HEPES pH 7.5, 300 mM NaCl, 5 mM $MgCl_2$, 2.5 mM DTT, and 35 mM imidazole). Elution was conducted using a 0-100% gradient between buffer C and buffer D (20 mM HEPES pH7.5, 300 mM NaCl, 5 mM $MgCl_2$, 2.5 mM DTT, and 500 mM imidazole) performed using 5 times column volume. Eluted proteins were subsequently dialyzed against buffer containing 20 mM HEPES pH 7.5, 150 mM NaCl, 5 mM $MgCl_2$, and 2.5 mM DTT, using the Slide-A-lyzer® dialysis cassettes with a molecular weight cut-off of 10 kDa (Fisher, Nepean, Ontario, Canada). Protein

concentrations were determined using the Bradford assay (BioRad, Mississauga, ON) and aliquoted proteins were snap frozen and stored at –80°C. Purifications were performed using the UKTA FPLC system (GE Healthcare Bio-sciences, Uppsala, Sweden).

Casp6 was expressed in the BL21(DE3)pLysS *E.coli* strain using a starter culture diluted 50 times in 2 times YT growth media (16 g/L Tryptone, 10 g/L Yeast Extracts, 5 g/L NaCl), 50 μM IPTG added at an OD at 600 nm of 0.6, and overnight expression at 16 °C. Subsequent cell lysis and purification steps were conducted as described above, except with the following buffers: lysis/equilibration buffer (50 mM Tris-HCL pH 8.0, 100 mM NaCl, and 10 mM imidazole supplemented with 1 mg/ml lysozyme), wash buffer (50 mM Tris-HCl pH 8.0, 500 mM NaCl, 10 mM imidazole), elution buffer (50 mM Tris-HCl pH 8.0, 100 mM NaCl using 10-500 mM imidazole gradient). Eluted proteins were dialyzed in buffer containing 50 mM Tris-HCl pH 8.0 and 100 mM NaCl exactly was described above. Protein concentrations were quantified using the Bradford assay (BioRad, Mississauga, ON). Caspase activity was verified using the fluorogenic substrate, AC-VEID-AFC (BioMol, Plymouth Meeting, PA, USA), as previously described (Zhang et al. 2000).

p97 proteolysis assays

The protein digestion reactions for p97ND1 or full-length protein variants were set in 50 μl reaction volumes using either HEPES (0.1 M HEPES, pH 7.5,

10% sucrose, 0.1% CHAPS, 10 mM DTT) or Stennicke's (20mM PIPES pH 7.4, 30 mM NaCl, 1 mM EDTA, 0.1% CHAPS, 10% sucrose, and 10 mM DTT) buffers. Reactions were prepared using the specified concentrations of p97 and Casp6 and incubated at 37°C for the indicated time periods. Reactions assessing the effect of ATP on p97 proteolysis were also supplemented with 5 mM $MgCl_2$. p97 proteolysis was detected using SDS-PAGE followed by either coomassie staining or western blot analysis. Western blotting was performed using a monoclonal anti-p97 antibody (1:1000 dilution) raised using a p97 fragment containing residues 9-130 (BD Transduction Laboratories™, San Jose, CA). Detection was performed with an HRP-conjugated secondary antibody and the chemilueminescence reagent ECL plus (GE Healthcare, Baie d'Urfé, QC, Canada). Signal visualization was conducted using the Storm 840 scanner (GE Healthcare, Baie d'Urfé, QC, Canada) or standard autoradiography.

Generation of an neopitope antibody for the *in vivo* detection Casp6 cleaved p97 N-terminal fragment.

Casp6 cleaved p97 (p97D179↓) neoepitope antibody was generated against p97 cleaved at the putative N-terminal consensus site 176VAPD179. Rabbit immunization was performed using the six amino acid peptide, 174CIVAPD179, N-terminally conjugated to the keyhole limpet hemocyanin (KLH) protein. A BLAST search was used to ensure the uniqueness of this peptide sequence to human p97. Peptide, synthesis, conjugation, immunization, bleed production and anti-sera collection were all performed in SIGMA GENOSYS

facilities (The Woodlands, TX, USA). The immunostaining was preformed as previously described (Guo et al. 2004)

4.6 Acknowledgement

We are very grateful for Jennifer Hammond for assistance with the immunohistochemistry, Dr. Steffen Albrecht (The Department of Pathology, McGill University, Montréal, QC, Canada) for guiding the interpretation of the immunohistochemical data. We would like to thank Dr. Guy Salvesen (The Burnham Institute, La Jolla, CA, USA) for providing the Casp6 recombinant expression construct. This work was supported by grants from the HFSP, Genome Canada, Silicon Kinetics and Genocean to ML and CIHR grant #MOP-81146 to ALB.

Table 4.1: Overall backbone RMSD analysis for p97WT ND1 or p97R155P ND1 versus the starting crystal structural coordinates of p97ND1.

RMSD	p97WT ND1(a)	p97 R155P ND1
Global[(c)]	1.8±0.6 Å	1.9±0.4 Å
Region 1 (Ala150 to Tyr173)	1.8±0.4 Å	2.0±0.5 Å
Region 2 (Phe163 to Tyr173)	1.7±0.7 Å	2.3±0.7 Å
Region 3 (Pro170 to Glu180)	2.1±0.1 Å	2.9±0.1 Å
Region 4 (Val57 to Glu66)	1.7±0.5 Å	2.2±0.5 Å

a. RMSD values for $p97^{WT}$ND1 based on 15 retained conformation. **b.** RMSD values for $p97^{R155P}$ND1 based on 19 retained conformation. **c.** Global RMSD values obtained from all 20 conformations for either $p97^{WT}$ND1or $p97^{R155P}$ND1.

Figure 4.1. Schematic comparison of the simulation annealing modeling of p97WT ND1 or p97R155P ND1. Overlay of retained conformers following analysis of simulated annealing molecular dynamics calculations of WT (**A**) and mutant Arg155Pro p97 (**B**) with the starting structural coordinates in green. The location of the mutated position and the Casp6 recognition site (176VAPD179) are indicated. Glu167 is shown in sticks representation.

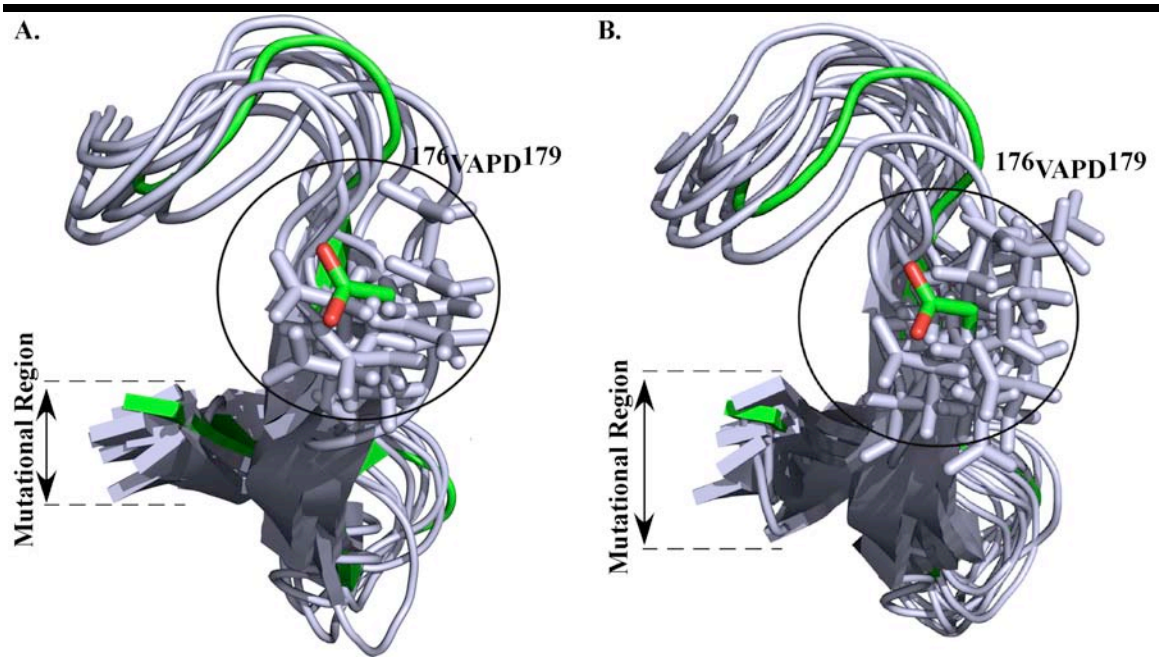
A.
176VAPD179
Mutational Region
B.
176VAPD179
Mutational Region

Figure 4.2. Schematic of p97 structural domains. Putative Casp6 cleavage sites indicated below the domain where they localize. Abbreviations: ab; antibody, N; amino-terminal domain, L1; linker-1, D1; D1 AAA+ Domain, L2; linker-2, D2; D2 AAA+ Domain, COOH; Carboxyl-terminal domain.

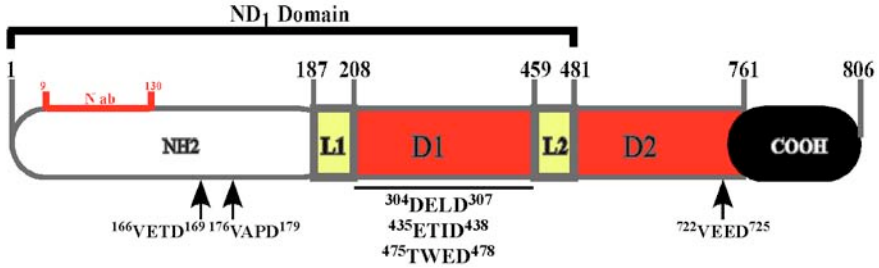
ND1 Domain
1
187
208
459
481
761
806
9
N ab
130
NH2
L1
D1
L2
D2
COOH
166VETD169 176VAPD179
304DELD307
435ETID438
475TWED478
722VEED725

Figure 4.3. Cleavage of IBMPFD-linked p97ND1 mutants by Casp6. A. Coomassie-blue staining of recombinant p97WT ND1 or IBMPFD-linked mutants. 5 μg of p97WT ND1, p97R155P ND1, or p97A232E ND1 were loaded on a 10 % gel and resolved by SDS-PAGE. **B & C.** Western blot analyses with a monoclonal antibody recognizing the N-domain of p97. The digests were set in Stennicke's buffer using ~ 67 nM p97 ND1 fragments and the indicated concentrations of Casp6. **D.** Quantitation of p97 ND1 cleavage in B. Quantitation reflects p97 cleavage by 213 nM Casp6. **E.** Coomassie-blue staining of ~67 nM recombinant p97WT ND1 or IBMPFD-linked mutants treated with the indicated concentration of Casp6. The digest were performed in Stennicke's buffer and resolved on a 10% SDS-PAGE gel.

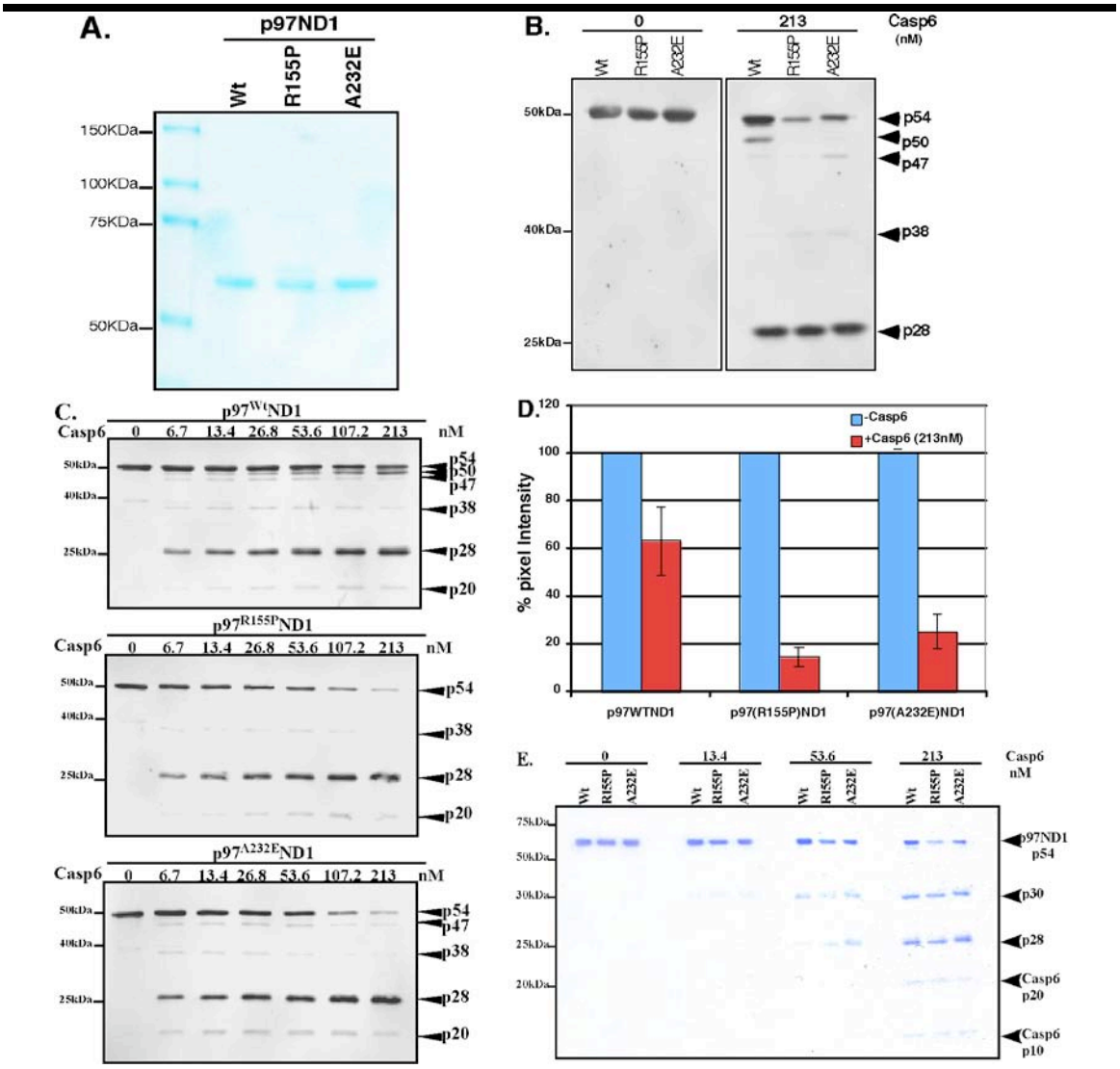
A.
p97ND1
Wt
R155P
A232E
150KDa
100KDa
75KDa
50KDa
B.
0
213
Casp6
(nM)
Wt
R155P
A232E
50kDa
40kDa
25kDa
p54
p50
p47
p38
p28
C.
p97WtND1
Casp6
0 6.7 13.4 26.8 53.6 107.2 213 nM
p97R155PND1
p97A232END1
p54
p50
p47
p38
p28
p20
D.
-Casp6
+Casp6 (213nM)
% pixel Intensity
p97WTND1
p97(R155P)ND1
p97(A232E)ND1
E.
75kDa
50kDa
30kDa
25kDa
20kDa
p97ND1
p54
p30
p28
Casp6
p20
Casp6
p10

Figure 4.4. ATP-dependent modulation of p97 ND1 cleavage by Casp6. A & B. Western blot analysis of ~ 67 nM p97 ND1 incubated with the indicated concentration of active Casp6 and ATP, in Stennicke's buffer.

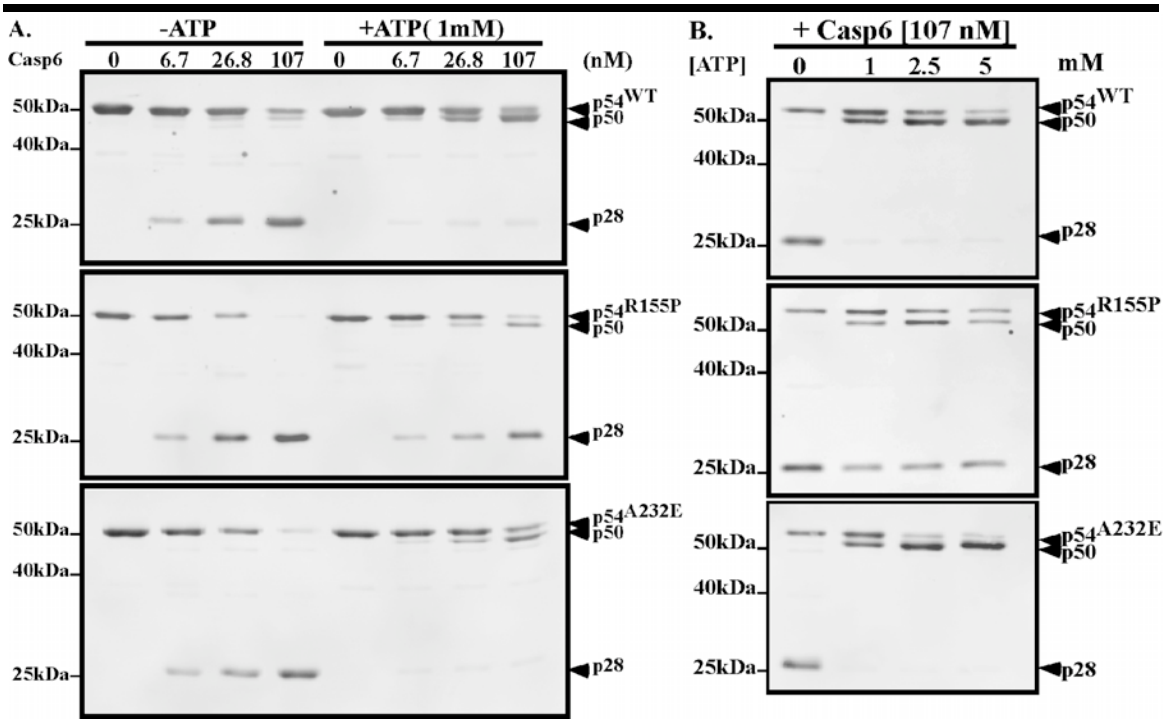
A.
-ATP
+ATP(1mM)
Casp6
0 6.7 26.8 107 0 6.7 26.8 107
(nM)
50kDa
40kDa
25kDa
p54WT
p50
p28
p54R155P
p50
p28
p54A232E
p50
p28
B.
+ Casp6 [107 nM]
[ATP]
0 1 2.5 5
mM
50kDa
40kDa
25kDa
p54WT
p50
p28
p54R155P
p50
p28
p54A232E
p50
p28

Figure 4.5. Susceptibility of full-length p97WT and IBMPFD-linked mutant variants to Casp6 -mediated proteolysis. A-D. Western blots of a time-course analysis of 100 nM of p97WT (A) , p97R155P (B), p97A232E (C), and p97K524A (D) cleaved with 300 nM of Casp6 in HEPES buffer, using a monoclonal anti-N-terminal antibody for p97.

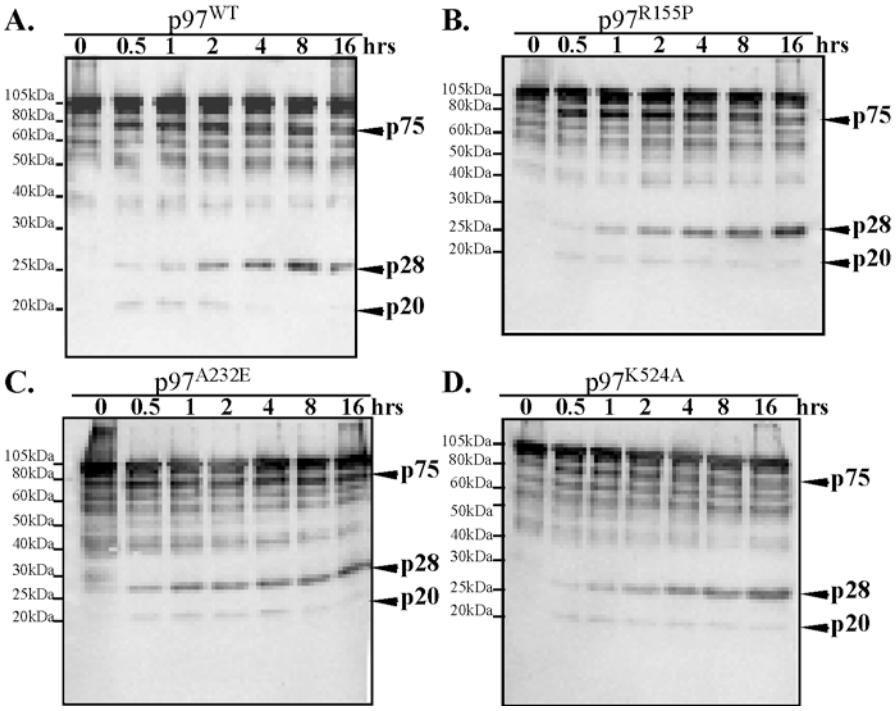
A.
p97WT
0 0.5 1 2 4 8 16 hrs
105kDa
80kDa
60kDa
50kDa
40kDa
30kDa
25kDa
20kDa
p75
p28
p20
B.
p97R155P
0 0.5 1 2 4 8 16 hrs
105kDa
80kDa
60kDa
50kDa
40kDa
30kDa
25kDa
20kDa
p75
p28
p20
C.
p97A232E
0 0.5 1 2 4 8 16 hrs
105kDa
80kDa
60kDa
50kDa
40kDa
30kDa
25kDa
20kDa
p75
p28
p20
D.
p97K524A
0 0.5 1 2 4 8 16 hrs
105kDa
80kDa
60kDa
50kDa
40kDa
30kDa
25kDa
20kDa
p75
p28
p20

Figure 4.6. Assessment of p97 cleavage in p97-linked FTD brains. Micrograph of healthy hippocampal brain sections (A) or p97-linked FTD frontal brain sections (B-C) carrying the p97R155C mutation immunostained with a neoepitope antibody against p97 cleaved at Asp179. The left panels represent 10 X magnification with a scale bar of 100 μm. The right panels represent 40 X magnification and a scale bar of 10 μm. Arrows point to unstained (white) and stained (black) neurons.

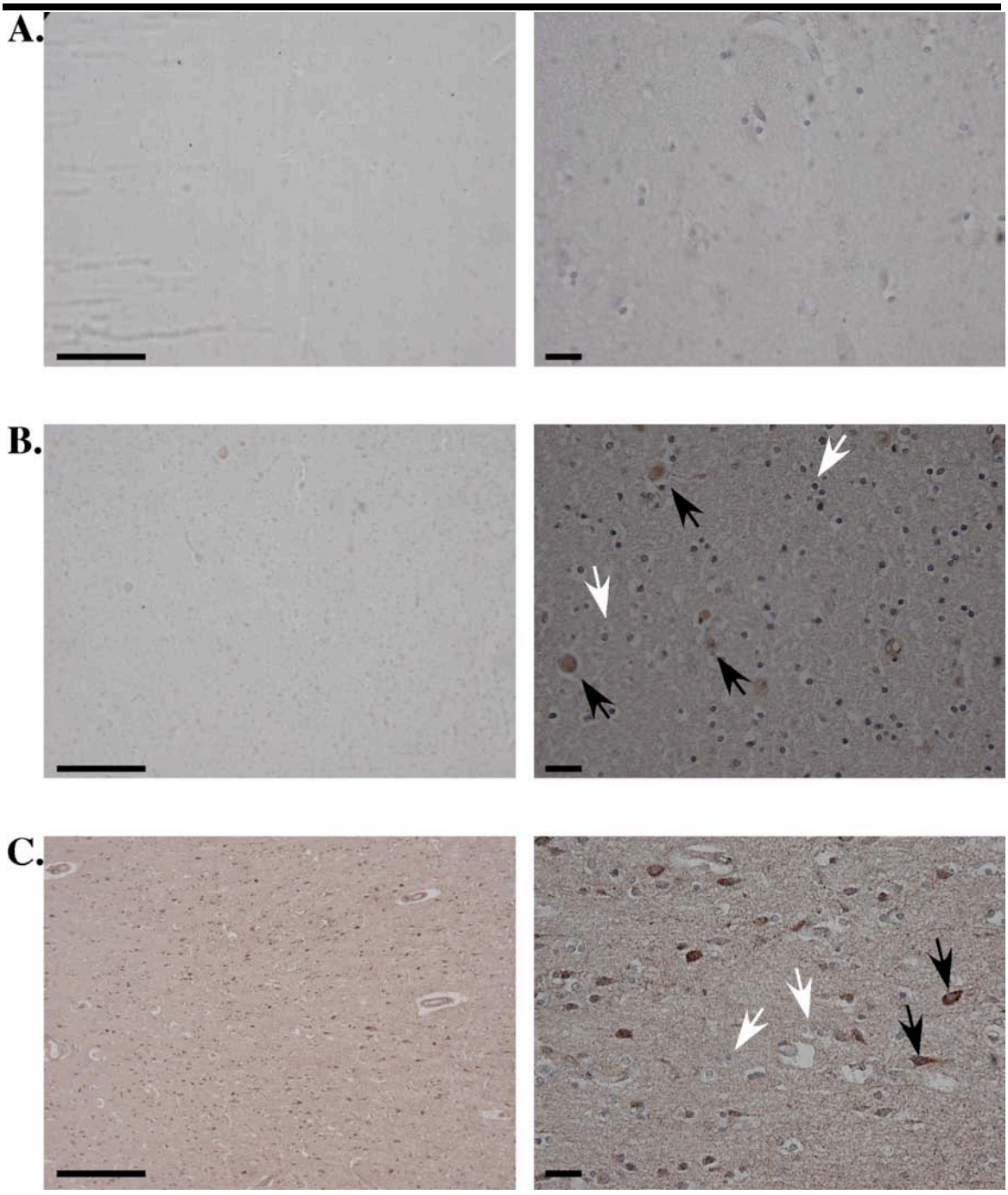
A.
B.
C.

Table S4.1 : *Residue geometry of Val154, Arg155, Val166, and Thr168 analyzed by MolProbity for each minimized simulated annealing conformer obtained for wild-type trial*

Conformer(a)	Residue	MolProbity Parameters			Validation (b)
		ϕ,ψ Quality Values (%)	Rotamer (%)	Cβ Deviation (Å)	
1	V154	favored (45.9)	2.5 (m)	0.12	√
	R155	favored (34.49)	0	0.082	Ä
	V166	allowed (1.03)	95 (t)	0.176	√
	T168	favored (29.34)	40.7 (p)	0.053	√
2	V154	favored (22.9)	5 (p)	0.188	√
	R155	favored (33.9)	0	0.151	Ä
	V166	allowed (0.9)	58.8 (t)	0.197	√
	T168	favored (39.0)	68.8 (p)	0.047	√
3	V154	favored (15.3)	3.6 (m)	0.123	√
	R155	favored (47.2)	27.1 (ptt180)	0.175	√
	V166	favored (15.4)	11.9 (p)	0.267	√
	T168	favored (37.9)	59.2 (p)	0.077	√
4	V154	favored (6.7)	59.2 (t)	0.07	√
	R155	favored (23.1)	0.1	0.227	Ä
	V166	favored (4.4)	58.2 (t)	0.157	√
	T168	favored (20.9)	91.1 (m)	0.066	√
5	V154	favored (23.8)	20 (t)	0.111	√
	R155	favored (34.5)	2.2 (mpt_?)	0.023	√
	V166	favored (2.7)	14.4 (p)	0.274	√
	T168	favored (34.9)	91.7 (m)	0.12	√
6	V154	favored (44.9)	86.2 (t)	0.084	√
	R155	favored (52.3)	6 (mmt_180)	0.037	√
	V166	allowed (1.41)	12 (p)	0.29	√
	T168	favored (13.2)	53.4 (m)	0.131	√
7	V154	favored (57.1)	55.6 (t)	0.082	√
	R155	favored (7.3)	5.4 (tmm_?)	0.099	√
	V166	allowed (1.1)	44 (t)	0.193	√
	T168	favored (12.2)	8.8 (t)	0.152	√
8	V154	favored (40.6)	60.1 (t)	0.098	√
	R155	favored (44.9)	58.7 (ttp85)	0.108	√
	V166	allowed (1.18)	97.5 (t)	0.179	√
	T168	favored (21.7)	4.9 (t)	0.172	√
9	V154	favored (24.1)	61.3 (t)	0.126	√
	R155	favored (20.8)	64.3 (mtt-85)	0.053	√
	V166	allowed (0.6)	47.5 (t)	0.206	√
	T168	favored (49)	10.7 (t)	0.147	√
10	V154	favored (60.4)	11.5 (p)	0.159	√
	R155	favored (40.3)	36.5 (mtt180)	0.046	√
	V166	allowed (0.68)	88.2 (t)	0.184	√
	T168	favored (38.5)	15.1 (t)	0.l43	√

a. Underlined conformation(s) were rejected due to unfavourable MolProbity analysis results. **b**. √ = all residue analysis criteria fell within acceptable MolProbity defaults; ƒ = residue criteria fell outside acceptable MolProbity defaults. **c**. Values in red signify residues with rotamer outliers as determined using the MolProbity software.

Table S4.2 : *Residue geometry of Val154, Arg155, Val166, and Thr168 analyzed by MolProbity* T168*for each minimized simulated annealing conformer obtained for wild-type trial.*

Conformer(a)	Residue	MolProbity Parameters			Validation (b)
		ϕ,ψ Quality Values (%)	Rotamer (%)	Cβ Deviation (Å)	
1	V154	favored (11.5)	75.6 (t)	0.12	√
	R155	favored (17.1)	87.4 (mtm-85)	0.042	√
	V166	favored (5.2)	9.6 (p)	0.271	√
	T168	favored (38.9)	50.5 (m)	0.069	√
2	V154	favored (17.7)	90 (t)	0.104	√
	R155	favored (47.2)	0	0.123	Ä
	V166	favored (16.8)	9.7 (p)	0.198	√
	T168	favored (47.4)	14.9 (t)	0.148	√
3	V154	favored (37.2)	7.8 (t)	0.119	√
	R155	favored (17.6)	7.8 (mpt_?)	0.058	√
	V166	allowed (0.72)	95.8 (t)	0.178	√
	T168	favored (41.3)	14.4 (t)	0.148	√
4	V154	favored (36.4)	8.1 (p)	0.191	√
	R155	favored (43.8)	15.2 (ptp180)	0.104	√
	V166	favored (13.4)	11.4 (p)	0.287	√
	T168	favored (36.4)	21.5 (p)	0.052	√
5	V154	favored (31.4)	7.3 (p)	0.203	√
	R155	favored (11.3)	81.1 (mtt85)	0.098	√
	V166	favored (3.33)	14.6 (p)	0.243	√
	T168	favored (47.3)	73.2 (p)	0.06	√
6	V154	favored (15.5)	7.1 (p)	0.187	√
	R155	favored (6.9)	6.8 (mpt?)	0.094	√
	V166	favored (8.9)	8.7 (p)	0.238	√
	T168	favored (18.3)	77.6 (p)	0.051	√
7	V154	favored (16.6)	9.1 (p)	0.178	√
	R155	favored (31.5)	33.1 (ptt180)	0.14	√
	V166	favored (8.8)	11.1 (p)	0.267	√
	T168	favored (21.3)	79.8 (m)	0.08	√
8	V154	favored (23.3)	9.4 (p)	0.187	√
	R155	favored (25.0)	6.3 (ppt?)	0.145	√
	V166	allowed (0.73)	54.4 (t)	0.208	√
	T168	favored (39.4)	73.4 (p)	0.071	√
9	V154	favored (42.5)	58.4 (t)	0.069	√
	R155	favored (40.8)	0	0.105	Ä
	V166	favored (2.8)	27.2 (m)	0.262	√
	T168	favored (52.2)	42.6 (p)	0.032	√
10	V154	favored (12.05)	70.2 (t)	0.134	√
	R155	favored (9.7)	8 (ptp180)	0.185	√
	V166	allowed (1.1)	80.4 (t)	0.202	√
	T168	favored (54.5)	72.8 (p)	0.056	√

a. Underlined conformation(s) were rejected due to unfavourable MolProbity analysis results. **b**. √ = all residue analysis criteria fell within acceptable MolProbity defaults; Ä = residue criteria fell outside acceptable MolProbity defaults. **c**. Values in red signify residues with rotamer outliers as determined using the MolProbity software.

Table S4.3: *Residue geometry of Val154, Arg155Pro, Val166, and Thr168 analyzed by MolProbity for each minimized simulated annealing conformer obtained for mutant trial 1.*

Conformer(a)	Residue	MolProbity Parameters			Validation (b)
		ϕ,ψ Quality Values (%)	Rotamer (%)	Cβ Deviation (Å)	
1	V154	Favored (34.1)	32.7 (t)	0.113	√
	R155P	Allowed (0.75)	74.1 (n)	0.057	√
	V166	Favored (4.4)	72.7 (t)	0.195	√
	T168	Favored (50.9)	33.3 (p)	0.043	√
2	V154	Favored (11.9)	16.5 (t)	0.105	√
	R155P	Favored (82.9)	59.4 (n)	0.06	√
	V166	Favored (14.2)	10.3 (p)	0.247	√
	T168	Favored (24.2)	41.2 (p)	0.063	√
3	V154	Favored (51)	1.4 (m)	0.094	√
	R155P	Favored (1.5)	52.3 (n)	0.094	√
	V166	Favored (10.8)	10.6 (p)	0.246	√
	T168	Favored (51.1)	73.3 (p)	0.067	√
4	V154	Favored (30.2)	40.4 (t)	0.114	√
	R155P	Favored (8.3)	45.9 (x)	0.064	√
	V166	Allowed (0.9)	12.7 (p)	0.295	√
	T168	Favored (19.9)	89.3 (m)	0.127	√
5	V154	Favored (18.8)	6.7 (p)	0.171	√
	R155P	Favored (8.5)	95.3 (n)	0.068	√
	V166	Favored (27.4)	13.0 (p)	0.248	√
	T168	Favored (35.9)	76.5 (p)	0.083	√
6	V154	Favored (7.3)	7.3 (p)	0.186	√
	R155P	Favored (56.3)	56.9 (n)	0.057	√
	V166	Favored (43.3)	7.5 (p)	0.185	√
	T168	Favored (51.7)	39.9 (p)	0.063	√
7	V154	Favored (33.4)	73.2 (t)	0.084	√
	R155P	Favored (45.5)	60.9 (n)	0.02	√
	V166	Allowed (1.1)	10.8 (p)	0.292	√
	T168	Favored (50.4)	68.8 (p)	0.077	√
8	V154	Favored (16.6)	46.8 (t)	0.073	√
	R155P	Favored (16)	47.2 (x)	0.06	√
	V166	Favored (11.9)	78.6 (t)	0.126	√
	T168	Favored (53.3)	80.7 (p)	0.045	√
9	V154	Favored (34.9)	32.5 (t)	0.077	√
	R155P	Favored (44.9)	73.6 (x)	0.022	√
	V166	Favored (15.7)	12 (p)	0.304	√
	T168	Favored (33.1)	67 (p)	0.032	√
10	V154	Favored (39.2)	8.9 (m)	0.196	√
	R155P	Favored (4.1)	38 (x)	0.086	√
	V166	Favored (2.3)	7.1 (p)	0.28	√
	T168	Favored (57.7)	68.6 (p)	0.037	√

a. Underlined conformation(s) were rejected due to unfavourable MolProbity analysis results. **b**. √ = all residue analysis criteria fell within acceptable MolProbity defaults; Ä = residue criteria fell outside acceptable MolProbity defaults. **c**. Values in red signify residues with rotamer outliers as determined using the MolProbity software.

Table S4.4: Residue geometry of Val154, Arg155Pro, Val166, and Thr168 analyzed by MolProbity for each minimized simulated annealing conformer obtained for mutant trial 2.

Conformer(a)	Residue	MolProbity Parameters			Validation (b)
		ϕ,ψ Quality Values (%)	Rotamer (%)	Cβ Deviation (Å)	
1	V154	Favored (19.1)	81.6 (t)	0.082	√
	R155P	Favored (6.4)	92.1 (n)	0.033	√
	V166	Favored (32.2)	35.9 (m)	0.245	√
	T168	Favored (46.6)	71.9 (p)	0.029	√
2	V154	Favored (96.3)	70.3 (t)	0.096	√
	R155P	Favored (2.1)	58.2 (n)	0.052	√
	V166	Allowed (1.9)	16.7 (m)	0.273	√
	T168	Favored (56.6)	27.1 (m)	0.054	√
3	V154	Favored (49.5)	4.9 (p)	0.192	√
	R155P	Favored (39.3)	86.6 (n)	0.023	√
	V166	Favored (0.7)	60.6 (t)	0.197	√
	T168	Favored (37.3)	76.1 (p)	0.029	√
4	V154	Favored (73.7)	11.8 (p)	0.194	√
	R155P	Favored (21.2)	70.5 (n)	0.059	√
	V166	Allowed (1.12)	92.5 (t)	0.207	√
	T168	Favored (61.5)	74.1 (p)	0.054	√
5	V154	Favored (47.9)	21.4 (t)	0.062	√
	R155P	Favored (8.8)	49.6 (n)	0.06	√
	V166	Allowed (0.67)	95.9 (t)	0.205	√
	T168	Favored (33.0)	74.4 (p)	0.028	√
6	V154	Favored (34.3)	9.6 (m)	0.123	√
	R155P	Favored (7.1)	49.3 (n)	0.042	√
	V166	Allowed (0.68)	67 (t)	0.176	√
	T168	Favored (54.5)	71.4 (p)	0.088	√
7	V154	Favored (4.1)	0	0.133	Ä
	R155P	Favored (43.5)	86.1 (n)	0.021	√
	V166	Allowed (0.54)	71.7 (t)	0.208	√
	T168	Favored (46.1)	61.1 (p)	0.041	√
8	V154	Favored (48.8)	3.4 (m)	0.117	√
	R155P	Favored (29.1)	82.3 (x)	0.025	√
	V166	Allowed (1)	98.6 (t)	0.211	√
	T168	Favored (23.8)	76.8 (p)	0.031	√
9	V154	Favored (77.4)	27.3 (t)	0.083	√
	R155P	Favored (27.2)	34.2 (n)	0.071	√
	V166	Favored (1.9)	13.6 (p)	0.288	√
	T168	Favored (51.1)	65.1 (p)	0.049	√
10	V154	Favored (11.2)	4.4 (m)	0.156	√
	R155P	Favored (9.1)	33.8 (n)	0.08	√
	V166	Favored (14.5)	10.9 (p)	0.23	√
	T168	Favored (61.9)	68.7 (p)	0.069	√

a. Underlined conformation(s) were rejected due to unfavourable MolProbity analysis results. **b**. √ = all residue analysis criteria fell within acceptable MolProbity defaults; Ä = residue criteria fell outside acceptable MolProbity defaults. **c**. Values in red signify residues with rotamer outliers as determined using the MolProbity software.

CHAPTER 5: Discussion

5.1 Summary of principal findings

IBMPFD perplexes the AAA field with the question of how IBMPFD-linked mutations severely impair p97 cell biological activities in adulthood while sparing its vital developmental roles. This thesis work demonstrates that IBMPFD-linked mutations are associated with subtle effects on p97 structure and biochemical activity and thus provides one explanation of how IBMPFD-linked mutations are tolerated during development, but not in ageing. It proposes that the additive effect of subtle structural defects combined with an elevation, rather than a loss, in p97 ATPase activity lead to degeneration, especially in tissue of post-mitotic origin such as skeletal muscles and the brain. Another obvious question is whether p97 function is compromised in more prevalent proteinopathies, such as AD, especially with the accumulation of polyubiquitinated proteins being a common denominator between IBMPFD and AD. This thesis used AD as an example of a common proteinopathy and demonstrated that p97 is proteolytically cleaved in AD. Abundant proteolytic processing of p97 was also demonstrated in IBMPFD affected neurons. In sum, this work presents the proteolytic processing of p97 as a novel mechanism for UPS impairment in neurodegeneration.

5.2 Contributions to the AAA protein field

5.2.1 Utilization of biochemical approaches in the characterization of IBMPFD-linked p97 mutants *in vitro*.

A major goal of this thesis is the elucidation of the structural and biochemical consequences of IBMPFD-linked p97 mutations—a goal which

necessitated the comparative characterization of recombinantly purified p97 wild-type and mutant complexes *in vitro*. The focus on the structural and biochemical defects represents a reductionist approach in investigating the problem of how IBMPFD-linked mutations induce their pathogenic effects *in vivo*. This reductionist approach allows the identification of the primary defects induced by the mutations, in the absence of the confounding variables usually encountered in more complex cell biological systems. For example, one major observation is that overexpression of IBMPFD-linked p97 mutants increase the accumulation of polyubiquitinated proteins, an outcome which may be caused by any one of several defects: (1) reduced interaction with proteasome recruitment factors downstream of p97, (2) increased association of p97 with its substrates and E3 ubiquitin ligases, (3) reduced p97-mediated deubiquitinating activity, (4) toxic gain-of-function leading to cellular protein denaturation, (5) failure in a UPS-independent function of p97 which leads to cytotoxicity and global impairment of the UPS. Another level of complexity is the fact that any given p97 mutation could lead to polyubiquitinated protein accumulation through any one of these pathways, as there is no evidence supporting a common mechanism for pathogenesis. Accordingly, the characterization of p97 *in vitro* will help address the question of whether the molecular consequences of the IBMPFD-linked mutations are similar.

5.2.2 Evidence for a bidirectional communication mode between the D2 ring and the N-domain of p97

This thesis work capitalizes on biochemical studies pioneered by Li and coworkers (Song et al. 2003; Wang et al. 2003; Wang et al. 2003) and identifies conformational defects in the D2 ring of two IBMPFD-linked p97 mutants p97R155P and p97A232E (Halawani et al. 2009). The fact that the mere substitution of a single amino acid residue within the N-domain or the D1 ring induces conformational changes in the D2 ring reinforces the dynamic nature of p97 inter-domain communication and supports a role for the N-D1 ring in the counter-regulation of D2 ring conformation. The fact that p97R155P displayed D2 conformational defects only in response to ATP binding suggests that conformational changes initiated in the D2 ring are relayed to the N-terminal domain and then back to the D2 ring. While p97R155P conformational defects were most evident following ATP binding, p97A232E D2 ring displayed conformational defects in both the unbound and ATP-bound states (Halawani et al. 2009). These findings provide further evidence for a mechanistic role for the D1 in the proper relay of conformational changes between the N-terminal domain and the D2 ring. Unlike the D2 ring, the D1 ring is very stable and displays high affinity for ADP (Wang et al. 2003; DeLaBarre and Brunger 2005). These properties are consistent with a role for the D1 ring in harnessing the chemical energy derived from the mechanical motions of the N-domain or the D2 ring, (DeLaBarre and Brunger 2005) whereby motions initiated in the N-terminal domain are relayed to the D2 ring and vice versa. Consequently, it is not

surprising that mutation of Ala232 is associated with a particularly severe phenotype (Watts et al. 2004), as it may alter the bidirectional communication between the N-terminal domain and the D2 ring. Accordingly, this thesis proposes that IBMPFD-linked p97 mutations induce their pathogenic effects by altering the communication of conformational changes between the N-terminal domain and the D2 ring. In support of this model, we found that the hydrophobicity of Trp476 within the D1-D2 linker is altered by both IBMPFD-linked p97 mutations (Halawani et al. 2009). Rouiller and coworkers reported that deletion of the N-terminal domain of p97 abolished all ATP-driven conformational change, without impairing its ATPase activity (Rouiller et al. 2002). These data provide evidence for the importance of the N-terminal domain in modulating p97 D2 ring conformation.

Validation of the bidirectional mode of p97 inter-domain communication requires detailed structural analysis of IBMPFD-linked p97 mutants. The data presented in this thesis suggests that a crystal structure of a p97 N-terminal deletion mutant would be necessary. Interestingly, the bidirectional communication mode predicts that deletion of the N-terminal domain would have consequences on D2 ring conformation and vice versa, however the crystal structure of the p97 N-D1 ring alone or in the context of full-length p97 show the same packing arrangement. Furthermore, the crystal structures of p97 in various nucleotide-binding states are very similar (DeLaBarre and Brunger 2005) and do not reveal much of the nucleotide-dependent conformational changes reported by

cryo-EM (Rouiller et al. 2000; Rouiller et al. 2002). Given these considerations, the resolution of conformational defects in the D2 ring of an N-terminal deletion mutant of p97 by X-ray crystallography may only be possible if the defects are drastic. More promising approaches include Cryo-EM and Small-angle X-ray Scattering (SAXS) which reveal the detailed surface structure of the hydrated p97 hexamer (Rouiller et al. 2000; Rouiller et al. 2002; Davies et al. 2005). Importantly, unlike X-ray crystallography, Cryo-EM and SAXS were both successfully used in the determination of p97 conformational changes during the ATPase cycle (Rouiller et al. 2000; Rouiller et al. 2002; Davies et al. 2005). Only the SAXS model compared conformational changes between full-length p97 and the ND1 ring, and in support of the bidirectional communication model, the assignment of the N-domain appears different (Davies et al. 2005). In full-length p97, the N-domain is coplanar with the D1 ring in all nucleotide-binding states, except the AMP-PNP state where it falls below the plane of the D1 ring (Davies et al. 2005). In contrast, in the absence of the D2 ring, the N-domain is positioned below the D1 ring irrespective of the nucleotide-binding state (Davies et al. 2005). Although, the D1 ring demonstrates ATPase activity in the absence of the D2 ring (Rouiller et al. 2002), these variations in the position of the N-domain support a role for the D2 ring in its regulation. Further substantiation of the bidirectional communication model requires comparison of the SAXS structure of the D2 ring in full-length p97 and an N-domain deletion mutant.

The data presented in this thesis also rationalize further detailed examination of p97WT and IBMPFD-linked mutants using both cryo-EM and SAXS. Cryo-EM allows the visualization of p97 conformational changes throughout its ATPase cycle, and a long with SAXS, these techniques can determine the precise dimensions of the D2 in wild-type or mutant p97. Our data predict that the D2 ring pore in IBMPFD-linked mutant p97 will be larger than its counter part in p97WT.

Given the link between the altered conformational state of the D2 ring and the increased ATPase activity, this thesis also proposes a novel role for p97 conformation in the counter-regulation of its ATPase activity. Conformational defects imposed by IBMPFD-linked p97 mutations may promote ATP-binding and hydrolysis, in spite of their substitution of residues neither implicated in ATP-binding, nor hydrolysis. However, it is important to note that the severity of the disease correlated with the conformational state of the D2 ring, and not the extent of the increase in p97 ATPase activity (Halawani et al. 2009). Accordingly, these data show the necessity of further characterizations of the effect of other IBMPFD-linked mutations on p97 D2 ring conformation, and whether the conformational defects of the D2 ring can be uncoupled from its ATPase activity.

5.2.3 Putative role of IBMPFD-linked mutations in modulating the flexibility of the N-domain.

This thesis work suggests that IBMPFD-linked p97 mutations increase the conformational flexibility of the N-domain: firstly, *in silico* simulation annealing modeling predicted greater flexibility in the conformation of the N-domain when Arg155 is substituted with a proline; and secondly, the N-domains of p97R155P and p97A232E both displayed increased susceptibility to Casp6 mediated proteolysis. However, the increased flexibility of the N-domain was only demonstrated for the ND1 mutant fragments and not the full-length p97 proteins. A possible explanation is that the bulk of the conformational defects observed in the N-domain are relayed to the D2 ring in the context of the full-length protein. Nevertheless, these results demonstrate the importance of further studies of N-domain motions using nuclear magnetic resonance. The increased flexibility of the N-domain, even in the context of the ND1 fragment, provides evidence for a role of IBMPFD-linked mutations in altering the conformational state of p97 and emphasizes the need for the validation of the proposed bidirectional communication model.

The finding that the N-domain displays increased flexibility in at least one IBMPFD-linked mutation (p97R155P ND1), merits discussion of its physiological role in the pathogenesis of IBMPFD. For other AAA proteins, N-domain motions are proposed to function in the dissociation of non-specific binding interactions in a crowded cellular milieu, and thereby the shielding of important substrate or adaptor binding sites within the D1 ring (Ishikawa et al. 2004; Cranz-Mileva et al. 2008). In the case of p97, the D1 domain is sufficient for mediating p97

disaggregation activity, and may therefore mediate p97 recognition of non-native protein structures (Song et al. 2007). It is possible that N-domain motions may regulate the accessibility and interaction of non-native proteins with the D1 ring. For example, in ERAD, the N-terminal domain recruits p97 to the retrotranslocation channel through binding VIMP and Ubx2 and may facilitate the binding and dissociation of misfolded proteins with the D1 ring as they emerge from the retrotranslocation channel. Accordingly, it is conceivable that the increased flexibility of the N-domain in mutant p97R155PND1 may reduce the disaggregation activity of the D1 ring by destabilizing or preventing its interaction with non-native proteins. Furthermore, if p97 chaperones its own disaggregation *in vitro* (Wang et al. 2003), then the self-aggregation behavior of IBMPFD-linked p97 mutants may be linked to the increased flexibility of the N-domain. An alternate non-mutually exclusive possibility is that the N-domain may regulate the extraction of denatured proteins from the D2 pore and that an increase in its flexibility may impair the dissociation of nonnative protein conformers from the p97 hexamer (Halawani and Latterich 2006). Impairment of this function may explain the accumulation of p97 containing protein inclusions in the muscles of patients diagnosed with p97-linked IBM (Watts et al. 2004).

5.2.4 The energetic costs of elevated ATPase activity in IBMPFD-linked p97 mutants may be compensatory to defective substrate processing.

This thesis presents evidence that IBMPFD-linked mutations increase the energetic costs of p97 biochemical activities by increasing its ATPase activity.

p97, as well as the majority of AAA proteins, differ from kinases and other P-loop ATPase by their low ATPase activity. Recently, it was also demonstrated that p97 ATPase activity was not necessary for its chaperone-like function against protein aggregation *in vitro (Song et al. 2007)*. These findings are inconsistent with a role for ATP-binding and hydrolysis in substrate disassembly or processing. To resolve the role of ATP in AAA protein function, Zhang and Wigley recently proposed that AAA proteins utilize ATP-binding in mediating the proper assembly of all component of large multi-protein complexes and ATP-hydrolysis in disassembling or cycling these components (Zhang and Wigley 2008). It is unclear how this model applies to p97 ATPase activity *in vitro*. It is plausible that p97 may chaperone against into own self-aggregation, especially considering its strong resistance to chemical or heat-induced denaturation *in vitro (Wang et al. 2003)*. Accordingly, we propose that the defective conformation of the D2 pore may compromise p97 function in the prevention of its own self-aggregation and thereby increase the demand for ATP-binding and hydrolysis in an attempt to release inappropriately bound complexes from the D2 ring. Interestingly, this thesis work also suggests that the D2 ring conformation is altered between residues Lys524 and Arg709, a region which encompasses a highly conserved motif comprised of an aromatic amino acid residue (Ar), Phe551, followed by a hydrophobic one (ϕ),Trp552. Work by DeLaBarre and colleagues have demonstrated the importance of the Ar-ϕ motif in substrate binding (DeLaBarre et al. 2006), and mutagenesis of its counterpart motif in the ClpX prokaryotic protease leads to loss of substrate grip and a compensatory

increase in ATPase activity (Martin et al. 2008). Therefore, the increased demand for ATP-binding and hydrolysis in IBMPFD-linked p97 mutants may be aimed at improving the efficiency of substrate dislocation within the D2 ring. Further biochemical studies utilizing synaptotagmin I, the only physiological substrate known to bind to the Ar-ϕ motif (DeLaBarre et al. 2006), are necessary to substantiate the link between substrate processing and ATPase activity in the IBMPFD-linked p97 mutants.

5.2.5 Utilization of a neoepitope antibody for the characterization of p97 proteolytic cleavage *in vivo*.

This thesis work developed an important tool for investigating p97 proteolysis *in vitro*. The strategy involved the synthesis and characterization of an neoepitope antibody for the specific detection of p97 cleavage at Asp179. Using this antibody, this thesis demonstrates neuronal proteolysis of p97 in AD and p97-linked FTD, but not in healthy control brains. This powerful technique allows the detection of mild p97 cleavage in specific brain regions and the precise identification of affected neurons. Alternate techniques such as immunoblotting for p97 cleavage in brain lysates may compromise detection in two ways: (1) p97 cleavage may be localized to specific neurons or specialized brain regions and might be diluted to beyond detection; and (2) the lysis process involves the release of functional proteases from healthy neighboring neurons which may lead to the destabilization of the p97 cleaved fragments. Furthermore, immunohistochemical detection of p97 proteolysis allows the determination of

whether the neurons containing cleaved p97 also accumulate polyubiquitinated proteins and active Casp6. Importantly, positive immunoreactivity with the anti-p97 neoepitope antibody may provide indirect evidence of UPS dysfunction in disease and development. Determination of whether the extent of p97 cleavage correlates with the accumulation of polyubiquitinated proteins in pathological situations is essential, especially considering the potential utilization of the neoepitope antibody as a quantitative marker for UPS dysfunction in neurodegeneration.

5.2.6 Regulated N-terminal proteolysis as a putative mechanism for p97 anti-aggregation activity in neurodegeneration.

Although AD and p97-linked FTD are classified as different diseases, p97 proteolysis was evident in both, a fact which raises the question of whether p97 is cleaved in all forms of neurodegeneration. Interestingly, proteinopathies are almost always accompanied by UPS dysfunction, and neurodegeneration is not an exception. Considering the role of the D1 ring in protein disaggregation, and the fact that N-terminal proteolysis increases the accessibility of the D1 ring, it is possible that p97 N-terminal proteolysis may represent a cellular mechanism for coping with increased protein aggregation or misfolding. This coping mechanism, if prolonged and unregulated, may lead to UPS dysfunction and the subsequent accumulation of polyubiquitinated proteins. Moreover, the N-terminal domain of p97 encompasses a nuclear localization sequence which may facilitate its retrotranslocation to the nucleus. The mere overexpression of the N-terminal

domain is also associated with increased proteolytic degradation of endogenous p97 and the generation of fragment similar in size to these produced by apoptotic caspases 3 and 7. These results suggest that overexpression of the N-terminal domain of p97 may lead to cytotoxicity. Interestingly, a caspase-8 generated osteopontin fragment localizes to the nucleus and leads to cell death through the upregulation of p53 transcriptional activity (Kim et al. 2009). Further studies are necessary to substantiate if Casp6 mediated proteolysis of p97 is also responsible for the increased transcriptional activity of p53 in Alzheimer disease (Cenini et al. 2008).

The view that p97 proteolysis is a coping mechanism in the clearance of protein aggregation poses the question of what triggers the proteinopathy in the first place. In Alzheimer disease, Casp6 activity is strongly implicated in hippocampal neurodegeneration (Guo et al. 2004; Albrecht et al. 2007) and may therefore mediate p97 proteolysis *in vivo*. In p97-linked FTD, it is possible that dysfunction in p97 mediated cell biological reactions as a result of the IBMPFD-linked mutations may lead to robust caspase activation and extensive neurodegeneration prior to the presentation of the proteinopathy.

5.3 Final statement

The elucidation of the biochemical mechanism mediating p97 inter-molecular communication is necessary for understanding the molecular pathogenesis of IBMPFD. Understanding how the interplay between ATP-binding and hydrolysis, conformational changes, and adaptor-binding mediates p97 cell biological activities is ever more pressing considering its involvement in neurodegeneration. Further studies on the possible role of regulated N-terminal proteolysis in unleashing p97 anti-aggregation activity are of paramount importance and may help establish the molecular pathogenesis of IBMPFD.

References

Abujarour, R. J., S. Dalal, et al. (2005). "p97 Is in a complex with cholera toxin and influences the transport of cholera toxin and related toxins to the cytoplasm." J Biol Chem **280**(16): 15865-71.

Acharya, U., R. Jacobs, et al. (1995). "The formation of Golgi stacks from vesiculated Golgi membranes requires two distinct fusion events." Cell **82**(6): 895-904.

Albrecht, S., M. Bourdeau, et al. (2007). "Activation of caspase-6 in aging and mild cognitive impairment." Am J Pathol **170**(4): 1200-9.

Alder, N. N., Y. Shen, et al. (2005). "The molecular mechanisms underlying BiP-mediated gating of the Sec61 translocon of the endoplasmic reticulum." J Cell Biol **168**(3): 389-99.

Alexandru, G., J. Graumann, et al. (2008). "UBXD7 binds multiple ubiquitin ligases and implicates p97 in HIF1alpha turnover." Cell **134**(5): 804-16.

Alvarez, R. B. S., Zachary; Engel, W. King; Askansas, Valerie (1998). New Autosomal-Dominant Inclusion-Body Myopathy (AD-IBM) with Many Congophilic Muscle Nuclei that Contain Paired-Helical Filaments (PHFs) Composed of Phosphorylated Tau. American Academy of Neurology 50th Annual Meeting, Minneapolis, MN, Neurology.

Ao, W. and D. Pilgrim (2000). "Caenorhabditis elegans UNC-45 is a component of muscle thick filaments and colocalizes with myosin heavy chain B, but not myosin heavy chain A." J Cell Biol **148**(2): 375-84.

Arai, T., I. R. Mackenzie, et al. (2009). "Phosphorylated TDP-43 in Alzheimer's disease and dementia with Lewy bodies." Acta Neuropathol **117**(2): 125-36.

Askanas, V. and W. K. Engel (2005). "Sporadic inclusion-body myositis: a proposed key pathogenetic role of the abnormalities of the ubiquitin-proteasome system, and protein misfolding and aggregation." Acta Myol **24**(1): 17-24.

Askanas, V. and W. K. Engel (2006). "Inclusion-body myositis: a myodegenerative conformational disorder associated with Abeta, protein misfolding, and proteasome inhibition." Neurology **66**(2 Suppl 1): S39-48.

Bai, S., J. Zha, et al. (2008). "Tumor necrosis factor receptor-associated factor 6 is an intranuclear transcriptional coactivator in osteoclasts." J Biol Chem **283**(45): 30861-7.

Baker, M., I. R. Mackenzie, et al. (2006). "Mutations in progranulin cause tau-negative frontotemporal dementia linked to chromosome 17." Nature **442**(7105): 916-9.

Bays, N. W., R. G. Gardner, et al. (2001). "Hrd1p/Der3p is a membrane-anchored ubiquitin ligase required for ER-associated degradation." Nat Cell Biol **3**(1): 24-9.

Bersano, A., R. Del Bo, et al. (2007). "Inclusion body myopathy and frontotemporal dementia caused by a novel VCP mutation." Neurobiol Aging.

Beuron, F., T. C. Flynn, et al. (2003). "Motions and negative cooperativity between p97 domains revealed by cryo-electron microscopy and quantised elastic deformational model." J Mol Biol **327**(3): 619-29.

Beyer, A. (1997). "Sequence analysis of the AAA protein family." Protein Sci **6**(10): 2043-58.

Bouwmeester, T., A. Bauch, et al. (2004). "A physical and functional map of the human TNF-alpha/NF-kappa B signal transduction pathway." Nat Cell Biol **6**(2): 97-105.

Braun, S., K. Matuschewski, et al. (2002). "Role of the ubiquitin-selective CDC48(UFD1/NPL4)chaperone (segregase) in ERAD of OLE1 and other substrates." Embo J **21**(4): 615-21.

Briggs, L. C., G. S. Baldwin, et al. (2008). "Analysis of nucleotide binding to P97 reveals the properties of a tandem AAA hexameric ATPase." J Biol Chem **283**(20): 13745-52.

Bruderer, R. M., C. Brasseur, et al. (2004). "The AAA ATPase p97/VCP interacts with its alternative co-factors, Ufd1-Npl4 and p47, through a common bipartite binding mechanism." J Biol Chem **279**(48): 49609-16.

Burgess, T. L., Y. Qian, et al. (1999). "The ligand for osteoprotegerin (OPGL) directly activates mature osteoclasts." J Cell Biol **145**(3): 527-38.

Cairns, N. J., M. Neumann, et al. (2007). "TDP-43 in familial and sporadic frontotemporal lobar degeneration with ubiquitin inclusions." Am J Pathol **171**(1): 227-40.

Cao, K., R. Nakajima, et al. (2003). "The AAA-ATPase Cdc48/p97 regulates spindle disassembly at the end of mitosis." Cell **115**(3): 355-67.

Caruso, M. E., S. Jenna, et al. (2008). "GTPase-mediated regulation of the unfolded protein response in Caenorhabditis elegans is dependent on the AAA+ ATPase CDC-48." Mol Cell Biol **28**(13): 4261-74.

Carvalho, P., V. Goder, et al. (2006). "Distinct ubiquitin-ligase complexes define convergent pathways for the degradation of ER proteins." Cell **126**(2): 361-73.

Cenini, G., R. Sultana, et al. (2008). "Elevated levels of pro-apoptotic p53 and its oxidative modification by the lipid peroxidation product, HNE, in brain from subjects with amnestic mild cognitive impairment and Alzheimer's disease." J Cell Mol Med **12**(3): 987-94.

Chamoux, E., J. Couture, et al. (2009). "The p62 P392L mutation linked to Paget's disease induces activation of human osteoclasts." Mol Endocrinol.

Choi, J., A. I. Levey, et al. (2004). "Oxidative modifications and down-regulation of ubiquitin carboxyl-terminal hydrolase L1 associated with idiopathic Parkinson's and Alzheimer's diseases." J Biol Chem **279**(13): 13256-64.

Clary, D. O., I. C. Griff, et al. (1990). "SNAPs, a family of NSF attachment proteins involved in intracellular membrane fusion in animals and yeast." Cell **61**(4): 709-21.

Cranz-Mileva, S., F. Imkamp, et al. (2008). "The flexible attachment of the N-domains to the ClpA ring body allows their use on demand." J Mol Biol **378**(2): 412-24.

Cummings, J. L. (2000). "Cholinesterase inhibitors: A new class of psychotropic compounds." Am J Psychiatry **157**(1): 4-15.

Cundy, T., M. Hegde, et al. (2002). "A mutation in the gene TNFRSF11B encoding osteoprotegerin causes an idiopathic hyperphosphatasia phenotype." Hum Mol Genet **11**(18): 2119-27.

Dai, R. M., E. Chen, et al. (1998). "Involvement of valosin-containing protein, an ATPase Co-purified with IkappaBalpha and 26 S proteasome, in ubiquitin-proteasome-mediated degradation of IkappaBalpha." J Biol Chem **273**(6): 3562-73.

Davies, J. M., A. T. Brunger, et al. (2008). "Improved structures of full-length p97, an AAA ATPase: implications for mechanisms of nucleotide-dependent conformational change." Structure **16**(5): 715-26.

Davies, J. M., H. Tsuruta, et al. (2005). "Conformational changes of p97 during nucleotide hydrolysis determined by small-angle X-Ray scattering." Structure **13**(2): 183-95.

DeLaBarre, B. and A. T. Brunger (2003). "Complete structure of p97/valosin-containing protein reveals communication between nucleotide domains." Nat Struct Biol **10**(10): 856-63.

DeLaBarre, B. and A. T. Brunger (2005). "Nucleotide dependent motion and mechanism of action of p97/VCP." J Mol Biol **347**(2): 437-52.

DeLaBarre, B., J. C. Christianson, et al. (2006). "Central pore residues mediate the p97/VCP activity required for ERAD." Mol Cell **22**(4): 451-62.

Deng, L., C. Wang, et al. (2000). "Activation of the IkappaB kinase complex by TRAF6 requires a dimeric ubiquitin-conjugating enzyme complex and a unique polyubiquitin chain." Cell **103**(2): 351-61.

Desagher, S., A. Osen-Sand, et al. (2001). "Phosphorylation of bid by casein kinases I and II regulates its cleavage by caspase 8." Mol Cell **8**(3): 601-11.

Diaz, R., L. S. Mayorga, et al. (1989). "Vesicle fusion following receptor-mediated endocytosis requires a protein active in Golgi transport." Nature **339**(6223): 398-400.

Dickson, D. W., A. Wertkin, et al. (1990). "Ubiquitin immunoelectron microscopy of dystrophic neurites in cerebellar senile plaques of Alzheimer's disease." Acta Neuropathol **79**(5): 486-93.

Djamshidian, A., J. Schaefer, et al. (2009). "A novel mutation in the VCP gene (G157R) in a german family with inclusion-body myopathy with paget disease of bone and frontotemporal dementia." Muscle Nerve **39**(3): 389-91.

Doss-Pepe, E. W., E. S. Stenroos, et al. (2003). "Ataxin-3 interactions with rad23 and valosin-containing protein and its associations with ubiquitin chains and the proteasome are consistent with a role in ubiquitin-mediated proteolysis." Mol Cell Biol **23**(18): 6469-83.

Duran, A., M. Serrano, et al. (2004). "The atypical PKC-interacting protein p62 is an important mediator of RANK-activated osteoclastogenesis." Dev Cell **6**(2): 303-9.

Eisenberg, I., N. Avidan, et al. (2001). "The UDP-N-acetylglucosamine 2-epimerase/N-acetylmannosamine kinase gene is mutated in recessive hereditary inclusion body myopathy." Nat Genet **29**(1): 83-7.

Erdmann, R., F. F. Wiebel, et al. (1991). "PAS1, a yeast gene required for peroxisome biogenesis, encodes a member of a novel family of putative ATPases." Cell **64**(3): 499-510.

Forman, M. S., I. R. Mackenzie, et al. (2006). "Novel ubiquitin neuropathology in frontotemporal dementia with valosin-containing protein gene mutations." J Neuropathol Exp Neurol **65**(6): 571-81.

Frohlich, K. U., H. W. Fries, et al. (1991). "Yeast cell cycle protein CDC48p shows full-length homology to the mammalian protein VCP and is a member of a protein family involved in secretion, peroxisome formation, and gene expression." J Cell Biol **114**(3): 443-53.

Fuentes-Prior, P. and G. S. Salvesen (2004). "The protein structures that shape caspase activity, specificity, activation and inhibition." Biochem J **384**(Pt 2): 201-32.

Galluzzi, L., S. A. Aaronson, et al. (2009). "Guidelines for the use and interpretation of assays for monitoring cell death in higher eukaryotes." Cell Death Differ **16**(8): 1093-107.

Gitcho, M. A., J. Strider, et al. (2009). "VCP mutations causing frontotemporal lobar degeneration disrupt localization of TDP-43 and induce cell death." J Biol Chem.

Gnann, A., J. R. Riordan, et al. (2004). "Cystic fibrosis transmembrane conductance regulator degradation depends on the lectins Htm1p/EDEM and the Cdc48 protein complex in yeast." Mol Biol Cell **15**(9): 4125-35.

Gohda, J., T. Akiyama, et al. (2005). "RANK-mediated amplification of TRAF6 signaling leads to NFATc1 induction during osteoclastogenesis." Embo J **24**(4): 790-9.

Goldfarb, L. G. and M. C. Dalakas (2009). "Tragedy in a heartbeat: malfunctioning desmin causes skeletal and cardiac muscle disease." J Clin Invest **119**(7): 1806-13.

Gotz, J. and L. M. Ittner (2008). "Animal models of Alzheimer's disease and frontotemporal dementia." Nat Rev Neurosci **9**(7): 532-44.

Grou, C. P., A. F. Carvalho, et al. (2009). "The peroxisomal protein import machinery--a case report of transient ubiquitination with a new flavor." Cell Mol Life Sci **66**(2): 254-62.

Guenther, B., R. Onrust, et al. (1997). "Crystal structure of the delta' subunit of the clamp-loader complex of E. coli DNA polymerase III." Cell **91**(3): 335-45.

Guex, N. and M. C. Peitsch (1997). "SWISS-MODEL and the Swiss-PdbViewer: an environment for comparative protein modeling." Electrophoresis **18**(15): 2714-23.

Guo, H., S. Albrecht, et al. (2004). "Active caspase-6 and caspase-6-cleaved tau in neuropil threads, neuritic plaques, and neurofibrillary tangles of Alzheimer's disease." Am J Pathol **165**(2): 523-31.

Guo, H., D. Petrin, et al. (2006). "Caspase-1 activation of caspase-6 in human apoptotic neurons." Cell Death Differ **13**(2): 285-92.

Guyant-Marechal, L., A. Laquerriere, et al. (2006). "Valosin-containing protein gene mutations: clinical and neuropathologic features." Neurology **67**(4): 644-51.

Halawani, D. and M. Latterich (2006). "p97: The cell's molecular purgatory?" Mol Cell **22**(6): 713-7.

Halawani, D., A. C. LeBlanc, et al. (2009). "Hereditary inclusion body myopathy-linked p97/VCP mutations in the N domain and the D1 ring modulate p97/VCP ATPase activity and D2 ring conformation." Mol Cell Biol **29**(16): 4484-94.

Hauser, M. A., S. K. Horrigan, et al. (2000). "Myotilin is mutated in limb girdle muscular dystrophy 1A." Hum Mol Genet **9**(14): 2141-7.

Hinderlich, S., I. Salama, et al. (2003). "Distal myopathy with rimmed vacuoles is allelic to hereditary inclusion body myopathy." Neurology **61**(1): 145; author reply 145.

Hirabayashi, M., K. Inoue, et al. (2001). "VCP/p97 in abnormal protein aggregates, cytoplasmic vacuoles, and cell death, phenotypes relevant to neurodegeneration." Cell Death Differ **8**(10): 977-84.

Hiruma, Y., N. Kurihara, et al. (2008). "A SQSTM1/p62 mutation linked to Paget's disease increases the osteoclastogenic potential of the bone microenvironment." Hum Mol Genet **17**(23): 3708-19.

Hocking, L., F. Slee, et al. (2000). "Familial Paget's disease of bone: patterns of inheritance and frequency of linkage to chromosome 18q." Bone **26**(6): 577-80.

Hoppe, T., G. Cassata, et al. (2004). "Regulation of the myosin-directed chaperone UNC-45 by a novel E3/E4-multiubiquitylation complex in C. elegans." Cell **118**(3): 337-49.

Hoppe, T., K. Matuschewski, et al. (2000). "Activation of a membrane-bound transcription factor by regulated ubiquitin/proteasome-dependent processing." Cell **102**(5): 577-86.

Hosokawa, N., I. Wada, et al. (2001). "A novel ER alpha-mannosidase-like protein accelerates ER-associated degradation." EMBO Rep **2**(5): 415-22.

Huang, Y., J. Niwa, et al. (2006). "Calcium-sensing receptor ubiquitination and degradation mediated by the E3 ubiquitin ligase dorfin." J Biol Chem **281**(17): 11610-7.

Hubbers, C. U., C. S. Clemen, et al. (2007). "Pathological consequences of VCP mutations on human striated muscle." Brain **130**(Pt 2): 381-93.

Hughes, A. E., S. H. Ralston, et al. (2000). "Mutations in TNFRSF11A, affecting the signal peptide of RANK, cause familial expansile osteolysis." Nat Genet **24**(1): 45-8.

Hutton, M., C. L. Lendon, et al. (1998). "Association of missense and 5'-splice-site mutations in tau with the inherited dementia FTDP-17." Nature **393**(6686): 702-5.

Huyton, T., V. E. Pye, et al. (2003). "The crystal structure of murine p97/VCP at 3.6A." J Struct Biol **144**(3): 337-48.

Ii, K., H. Ito, et al. (1997). "Immunocytochemical co-localization of the proteasome in ubiquitinated structures in neurodegenerative diseases and the elderly." J Neuropathol Exp Neurol **56**(2): 125-31.

Ikai, N. and M. Yanagida (2006). "Cdc48 is required for the stability of Cut1/separase in mitotic anaphase." J Struct Biol **156**(1): 50-61.

Indig, F. E., J. J. Partridge, et al. (2004). "Werner syndrome protein directly binds to the AAA ATPase p97/VCP in an ATP-dependent fashion." J Struct Biol **146**(1-2): 251-9.

Ishigaki, S., N. Hishikawa, et al. (2004). "Physical and functional interaction between Dorfin and Valosin-containing protein that are colocalized in ubiquitylated inclusions in neurodegenerative disorders." J Biol Chem **279**(49): 51376-85.

Ishikawa, T., M. R. Maurizi, et al. (2004). "The N-terminal substrate-binding domain of ClpA unfoldase is highly mobile and extends axially from the distal surface of ClpAP protease." J Struct Biol **146**(1-2): 180-8.

Iyer, L. M., K. S. Makarova, et al. (2004). "Comparative genomics of the FtsK-HerA superfamily of pumping ATPases: implications for the origins of chromosome segregation, cell division and viral capsid packaging." Nucleic Acids Res **32**(17): 5260-79.

Jang, M., B. C. Park, et al. (2008). "Mining of caspase-7 substrates using a degradomic approach." Mol Cells **26**(2): 152-7.

Janiesch, P. C., J. Kim, et al. (2007). "The ubiquitin-selective chaperone CDC-48/p97 links myosin assembly to human myopathy." Nat Cell Biol **9**(4): 379-90.

Jarosch, E., C. Taxis, et al. (2002). "Protein dislocation from the ER requires polyubiquitination and the AAA-ATPase Cdc48." Nat Cell Biol **4**(2): 134-9.

Jentsch, S. and S. Rumpf (2007). "Cdc48 (p97): a "molecular gearbox" in the ubiquitin pathway?" Trends Biochem Sci **32**(1): 6-11.

Ju, J. S., S. E. Miller, et al. (2008). "Impaired protein aggregate handling and clearance underlie the pathogenesis of p97/VCP-associated disease." J Biol Chem **283**(44): 30289-99.

Kadokura, A., T. Yamazaki, et al. (2009). "Regional distribution of TDP-43 inclusions in Alzheimer disease (AD) brains: Their relation to AD common pathology." Neuropathology.

Kadono, Y., F. Okada, et al. (2005). "Strength of TRAF6 signalling determines osteoclastogenesis." EMBO Rep **6**(2): 171-6.

Kaneko-Oshikawa, C., T. Nakagawa, et al. (2005). "Mammalian E4 is required for cardiac development and maintenance of the nervous system." Mol Cell Biol **25**(24): 10953-64.

Keck, S., R. Nitsch, et al. (2003). "Proteasome inhibition by paired helical filament-tau in brains of patients with Alzheimer's disease." J Neurochem **85**(1): 115-22.

Kerr, J. F., A. H. Wyllie, et al. (1972). "Apoptosis: a basic biological phenomenon with wide-ranging implications in tissue kinetics." Br J Cancer **26**(4): 239-57.

Kim, H. J., H. J. Lee, et al. (2009). "Intracellular cleavage of osteopontin by caspase-8 modulates hypoxia/reoxygenation cell death through p53." Proc Natl Acad Sci U S A.

Kimonis, V. E., E. Fulchiero, et al. (2008). "VCP disease associated with myopathy, Paget disease of bone and frontotemporal dementia: review of a unique disorder." Biochim Biophys Acta **1782**(12): 744-8.

Kimonis, V. E., M. J. Kovach, et al. (2000). "Clinical and molecular studies in a unique family with autosomal dominant limb-girdle muscular dystrophy and Paget disease of bone." Genet Med **2**(4): 232-41.

Kimonis, V. E., S. G. Mehta, et al. (2008). "Clinical studies in familial VCP myopathy associated with Paget disease of bone and frontotemporal dementia." Am J Med Genet A **146A**(6): 745-57.

Klaiman, G., N. Champagne, et al. (2009). "Self-activation of Caspase-6 in vitro and in vivo: Caspase-6 activation does not induce cell death in HEK293T cells." Biochim Biophys Acta **1793**(3): 592-601.

Klaiman, G., T. L. Petzke, et al. (2008). "Targets of caspase-6 activity in human neurons and Alzheimer disease." Mol Cell Proteomics **7**(8): 1541-55.

Klein, J. B., M. T. Barati, et al. (2005). "Akt-mediated valosin-containing protein 97 phosphorylation regulates its association with ubiquitinated proteins." J Biol Chem **280**(36): 31870-81.

Kobayashi, N., Y. Kadono, et al. (2001). "Segregation of TRAF6-mediated signaling pathways clarifies its role in osteoclastogenesis." Embo J **20**(6): 1271-80.

Kobayashi, T., K. Tanaka, et al. (2002). "Functional ATPase activity of p97/valosin-containing protein (VCP) is required for the quality control of endoplasmic reticulum in neuronally differentiated mammalian PC12 cells." J Biol Chem **277**(49): 47358-65.

Koegl, M., T. Hoppe, et al. (1999). "A novel ubiquitination factor, E4, is involved in multiubiquitin chain assembly." Cell **96**(5): 635-44.

Kondo, H., C. Rabouille, et al. (1997). "p47 is a cofactor for p97-mediated membrane fusion." Nature **388**(6637): 75-8.

Koonin, E. V., Y. I. Wolf, et al. (2000). "Protein fold recognition using sequence profiles and its application in structural genomics." Adv Protein Chem **54**: 245-75.

Kothe, M., Y. Ye, et al. (2005). "Role of p97 AAA-ATPase in the retrotranslocation of the cholera toxin A1 chain, a non-ubiquitinated substrate." J Biol Chem **280**(30): 28127-32.

Kunau, W. H., A. Beyer, et al. (1993). "Two complementary approaches to study peroxisome biogenesis in Saccharomyces cerevisiae: forward and reversed genetics." Biochimie **75**(3-4): 209-24.

LaFevre-Bernt, M. A. and L. M. Ellerby (2003). "Kennedy's disease. Phosphorylation of the polyglutamine-expanded form of androgen receptor regulates its cleavage by caspase-3 and enhances cell death." J Biol Chem **278**(37): 34918-24.

Lamothe, B., A. Besse, et al. (2007). "Site-specific Lys-63-linked tumor necrosis factor receptor-associated factor 6 auto-ubiquitination is a critical determinant of I kappa B kinase activation." J Biol Chem **282**(6): 4102-12.

Lamothe, B., W. K. Webster, et al. (2007). "TRAF6 ubiquitin ligase is essential for RANKL signaling and osteoclast differentiation." Biochem Biophys Res Commun **359**(4): 1044-9.

Landsverk, M. L., S. Li, et al. (2007). "The UNC-45 chaperone mediates sarcomere assembly through myosin degradation in Caenorhabditis elegans." J Cell Biol **177**(2): 205-10.

Latterich, M. (2006). "p97 adaptor choice regulates organelle biogenesis." Dev Cell **11**(6): 755-7.

Latterich, M., K. U. Frohlich, et al. (1995). "Membrane fusion and the cell cycle: Cdc48p participates in the fusion of ER membranes." Cell **82**(6): 885-93.

Latterich, M. and R. Schekman (1994). "The karyogamy gene KAR2 and novel proteins are required for ER-membrane fusion." Cell **78**(1): 87-98.

Laurin, N., J. P. Brown, et al. (2001). "Paget disease of bone: mapping of two loci at 5q35-qter and 5q31." Am J Hum Genet **69**(3): 528-43.

Laurin, N., J. P. Brown, et al. (2002). "Recurrent mutation of the gene encoding sequestosome 1 (SQSTM1/p62) in Paget disease of bone." Am J Hum Genet **70**(6): 1582-8.

Lavoie, C., E. Chevet, et al. (2000). "Tyrosine phosphorylation of p97 regulates transitional endoplasmic reticulum assembly in vitro." Proc Natl Acad Sci U S A **97**(25): 13637-42.

LeBlanc, A., H. Liu, et al. (1999). "Caspase-6 role in apoptosis of human neurons, amyloidogenesis, and Alzheimer's disease." J Biol Chem **274**(33): 23426-36.

LeBlanc, A. C. (2005). "The role of apoptotic pathways in Alzheimer's disease neurodegeneration and cell death." Curr Alzheimer Res **2**(4): 389-402.

Leipe, D. D., E. V. Koonin, et al. (2003). "Evolution and classification of P-loop kinases and related proteins." J Mol Biol **333**(4): 781-815.

Lepper, C., S. J. Conway, et al. (2009). "Adult satellite cells and embryonic muscle progenitors have distinct genetic requirements." Nature **460**(7255): 627-31.

Li, J. and J. Yuan (2008). "Caspases in apoptosis and beyond." Oncogene **27**(48): 6194-206.

Li, P., D. Nijhawan, et al. (1997). "Cytochrome c and dATP-dependent formation of Apaf-1/caspase-9 complex initiates an apoptotic protease cascade." Cell **91**(4): 479-89.

Lilley, B. N. and H. L. Ploegh (2004). "A membrane protein required for dislocation of misfolded proteins from the ER." Nature **429**(6994): 834-40.

Lindsten, K., F. M. de Vrij, et al. (2002). "Mutant ubiquitin found in neurodegenerative disorders is a ubiquitin fusion degradation substrate that blocks proteasomal degradation." J Cell Biol **157**(3): 417-27.

Liu, J., M. Aoki, et al. (1998). "Dysferlin, a novel skeletal muscle gene, is mutated in Miyoshi myopathy and limb girdle muscular dystrophy." Nat Genet **20**(1): 31-6.

Livingstone, M., H. Ruan, et al. (2005). "Valosin-containing protein phosphorylation at Ser784 in response to DNA damage." Cancer Res **65**(17): 7533-40.

Lomaga, M. A., W. C. Yeh, et al. (1999). "TRAF6 deficiency results in osteopetrosis and defective interleukin-1, CD40, and LPS signaling." Genes Dev **13**(8): 1015-24.

Lovell, S. C., I. W. Davis, et al. (2003). "Structure validation by Calpha geometry: phi,psi and Cbeta deviation." Proteins **50**(3): 437-50.

Lucas, G. J., S. G. Mehta, et al. (2006). "Evaluation of the role of Valosin-containing protein in the pathogenesis of familial and sporadic Paget's disease of bone." Bone **38**(2): 280-5.

Luo, S., C. Vacher, et al. (2005). "Cdk5 phosphorylation of huntingtin reduces its cleavage by caspases: implications for mutant huntingtin toxicity." J Cell Biol **169**(4): 647-56.

Madeo, F., E. Frohlich, et al. (1997). "A yeast mutant showing diagnostic markers of early and late apoptosis." J Cell Biol **139**(3): 729-34.

Madeo, F., J. Schlauer, et al. (1998). "Tyrosine phosphorylation regulates cell cycle-dependent nuclear localization of Cdc48p." Mol Biol Cell **9**(1): 131-41.

Madeo, F., E. Frohlich, et al. (1999). "Oxygen stress: a regulator of apoptosis in yeast." J Cell Biol **145**(4): 757-67.

Mahoney, J. A., J. A. Odin, et al. (2002). "The human homologue of the yeast polyubiquitination factor Ufd2p is cleaved by caspase 6 and granzyme B during apoptosis." Biochem J **361**(Pt 3): 587-95.

Malhotra, V., T. Serafini, et al. (1989). "Purification of a novel class of coated vesicles mediating biosynthetic protein transport through the Golgi stack." Cell **58**(2): 329-36.

Martin, A., T. A. Baker, et al. (2008). "Pore loops of the AAA+ ClpX machine grip substrates to drive translocation and unfolding." Nat Struct Mol Biol **15**(11): 1147-51.

Martinsson, T., N. Darin, et al. (1999). "Dominant hereditary inclusion-body myopathy gene (IBM3) maps to chromosome region 17p13.1." Am J Hum Genet **64**(5): 1420-6.

Martinsson, T., A. Oldfors, et al. (2000). "Autosomal dominant myopathy: missense mutation (Glu-706 --> Lys) in the myosin heavy chain IIa gene." Proc Natl Acad Sci U S A **97**(26): 14614-9.

Matsumoto, M., M. Yada, et al. (2004). "Molecular clearance of ataxin-3 is regulated by a mammalian E4." Embo J **23**(3): 659-69.

Meyer, H. H., H. Kondo, et al. (1998). "The p47 co-factor regulates the ATPase activity of the membrane fusion protein, p97." FEBS Lett **437**(3): 255-7.

Meyer, H. H., J. G. Shorter, et al. (2000). "A complex of mammalian ufd1 and npl4 links the AAA-ATPase, p97, to ubiquitin and nuclear transport pathways." Embo J **19**(10): 2181-92.

Meyer, H. H., Y. Wang, et al. (2002). "Direct binding of ubiquitin conjugates by the mammalian p97 adaptor complexes, p47 and Ufd1-Npl4." Embo J **21**(21): 5645-52.

Minetti, C., F. Sotgia, et al. (1998). "Mutations in the caveolin-3 gene cause autosomal dominant limb-girdle muscular dystrophy." Nat Genet **18**(4): 365-8.

Moir, D., S. E. Stewart, et al. (1982). "Cold-sensitive cell-division-cycle mutants of yeast: isolation, properties, and pseudoreversion studies." Genetics **100**(4): 547-63.

Moreira, E. S., T. J. Wiltshire, et al. (2000). "Limb-girdle muscular dystrophy type 2G is caused by mutations in the gene encoding the sarcomeric protein telethonin." Nat Genet **24**(2): 163-6.

Mori, H., J. Kondo, et al. (1987). "Ubiquitin is a component of paired helical filaments in Alzheimer's disease." Science **235**(4796): 1641-4.

Morishima-Kawashima, M., M. Hasegawa, et al. (1993). "Ubiquitin is conjugated with amino-terminally processed tau in paired helical filaments." Neuron **10**(6): 1151-60.

Mouysset, J., A. Deichsel, et al. (2008). "Cell cycle progression requires the CDC-48UFD-1/NPL-4 complex for efficient DNA replication." Proc Natl Acad Sci U S A **105**(35): 12879-84.

Muchir, A., G. Bonne, et al. (2000). "Identification of mutations in the gene encoding lamins A/C in autosomal dominant limb girdle muscular dystrophy with atrioventricular conduction disturbances (LGMD1B)." Hum Mol Genet **9**(9): 1453-9.

Muller, J. M., K. Deinhardt, et al. (2007). "Targeted deletion of p97 (VCP/CDC48) in mouse results in early embryonic lethality." Biochem Biophys Res Commun **354**(2): 459-65.

Nakagawa, N., M. Kinosaki, et al. (1998). "RANK is the essential signaling receptor for osteoclast differentiation factor in osteoclastogenesis." Biochem Biophys Res Commun **253**(2): 395-400.

Nakatsukasa, K., G. Huyer, et al. (2008). "Dissecting the ER-associated degradation of a misfolded polytopic membrane protein." Cell **132**(1): 101-12.

Neary, D., J. S. Snowden, et al. (1998). "Frontotemporal lobar degeneration: a consensus on clinical diagnostic criteria." Neurology **51**(6): 1546-54.

Neuber, O., E. Jarosch, et al. (2005). "Ubx2 links the Cdc48 complex to ER-associated protein degradation." Nat Cell Biol **7**(10): 993-8.

Neumann, M., I. R. Mackenzie, et al. (2007). "TDP-43 in the ubiquitin pathology of frontotemporal dementia with VCP gene mutations." J Neuropathol Exp Neurol **66**(2): 152-7.

Neuwald, A. F., L. Aravind, et al. (1999). "AAA+: A class of chaperone-like ATPases associated with the assembly, operation, and disassembly of protein complexes." Genome Res **9**(1): 27-43.

Nikolaev, A., T. McLaughlin, et al. (2009). "APP binds DR6 to trigger axon pruning and neuron death via distinct caspases." Nature **457**(7232): 981-9.

Noguchi, S., E. M. McNally, et al. (1995). "Mutations in the dystrophin-associated protein gamma-sarcoglycan in chromosome 13 muscular dystrophy." Science **270**(5237): 819-22.

Oda, Y., T. Okada, et al. (2006). "Derlin-2 and Derlin-3 are regulated by the mammalian unfolded protein response and are required for ER-associated degradation." J Cell Biol **172**(3): 383-93.

Ogura, T., S. W. Whiteheart, et al. (2004). "Conserved arginine residues implicated in ATP hydrolysis, nucleotide-sensing, and inter-subunit interactions in AAA and AAA+ ATPases." J Struct Biol **146**(1-2): 106-12.

Paget (1877). "On a form of chronic inflammation of bones (osteitis deformans)." Trans Med-Chir Soc **60**: 37-63.

Partridge, J. J., J. O. Lopreiato, Jr., et al. (2003). "DNA damage modulates nucleolar interaction of the Werner protein with the AAA ATPase p97/VCP." Mol Biol Cell **14**(10): 4221-9.

Perry, G., R. Friedman, et al. (1987). "Ubiquitin is detected in neurofibrillary tangles and senile plaque neurites of Alzheimer disease brains." Proc Natl Acad Sci U S A **84**(9): 3033-6.

Perry, G., P. Mulvihill, et al. (1989). "Immunochemical properties of ubiquitin conjugates in the paired helical filaments of Alzheimer disease." J Neurochem **52**(5): 1523-8.

Peters, J. M., M. J. Walsh, et al. (1990). "An abundant and ubiquitous homo-oligomeric ring-shaped ATPase particle related to the putative vesicle fusion proteins Sec18p and NSF." Embo J **9**(6): 1757-67.

Piccolo, F., S. L. Roberds, et al. (1995). "Primary adhalinopathy: a common cause of autosomal recessive muscular dystrophy of variable severity." Nat Genet **10**(2): 243-5.

Powell, K. S. and M. Latterich (2000). "The making and breaking of the endoplasmic reticulum." Traffic **1**(9): 689-94.

Pye, V. E., I. Dreveny, et al. (2006). "Going through the motions: the ATPase cycle of p97." J Struct Biol **156**(1): 12-28.

Rabouille, C., H. Kondo, et al. (1998). "Syntaxin 5 is a common component of the NSF- and p97-mediated reassembly pathways of Golgi cisternae from mitotic Golgi fragments in vitro." Cell **92**(5): 603-10.

Rabouille, C., T. P. Levine, et al. (1995). "An NSF-like ATPase, p97, and NSF mediate cisternal regrowth from mitotic Golgi fragments." Cell **82**(6): 905-14.

Ramadan, K., R. Bruderer, et al. (2007). "Cdc48/p97 promotes reformation of the nucleus by extracting the kinase Aurora B from chromatin." Nature **450**(7173): 1258-62.

Rape, M., T. Hoppe, et al. (2001). "Mobilization of processed, membrane-tethered SPT23 transcription factor by CDC48(UFD1/NPL4), a ubiquitin-selective chaperone." Cell **107**(5): 667-77.

Rebel, A., M. Basle, et al. (1980). "Bone tissue in Paget's disease of bone. Ultrastructure and Immunocytology." Arthritis Rheum **23**(10): 1104-14.

Richard, I., O. Broux, et al. (1995). "Mutations in the proteolytic enzyme calpain 3 cause limb-girdle muscular dystrophy type 2A." Cell **81**(1): 27-40.

Richly, H., M. Rape, et al. (2005). "A series of ubiquitin binding factors connects CDC48/p97 to substrate multiubiquitylation and proteasomal targeting." Cell **120**(1): 73-84.

Roberds, S. L., F. Leturcq, et al. (1994). "Missense mutations in the adhalin gene linked to autosomal recessive muscular dystrophy." Cell **78**(4): 625-33.

Rodighiero, C., B. Tsai, et al. (2002). "Role of ubiquitination in retro-translocation of cholera toxin and escape of cytosolic degradation." EMBO Rep **3**(12): 1222-7.

Rothballer, A., N. Tzvetkov, et al. (2007). "Mutations in p97/VCP induce unfolding activity." FEBS Lett **581**(6): 1197-201.

Rouiller, I., V. M. Butel, et al. (2000). "A major conformational change in p97 AAA ATPase upon ATP binding." Mol Cell **6**(6): 1485-90.

Rouiller, I., B. DeLaBarre, et al. (2002). "Conformational changes of the multifunction p97 AAA ATPase during its ATPase cycle." Nat Struct Biol **9**(12): 950-7.

Roy, L., J. J. Bergeron, et al. (2000). "Role of p97 and syntaxin 5 in the assembly of transitional endoplasmic reticulum." Mol Biol Cell **11**(8): 2529-42.

Rumpf, S. and S. Jentsch (2006). "Functional division of substrate processing cofactors of the ubiquitin-selective Cdc48 chaperone." Mol Cell **21**(2): 261-9.

Sanz, L., M. T. Diaz-Meco, et al. (2000). "The atypical PKC-interacting protein p62 channels NF-kappaB activation by the IL-1-TRAF6 pathway." Embo J **19**(7): 1576-86.

Sanz, L., P. Sanchez, et al. (1999). "The interaction of p62 with RIP links the atypical PKCs to NF-kappaB activation." Embo J **18**(11): 3044-53.

Saraste, M., P. R. Sibbald, et al. (1990). "The P-loop--a common motif in ATP- and GTP-binding proteins." Trends Biochem Sci **15**(11): 430-4.

Scaffidi, C., S. Kirchhoff, et al. (1999). "Apoptosis signaling in lymphocytes." Curr Opin Immunol **11**(3): 277-85.

Schroder, R., G. D. Watts, et al. (2005). "Mutant valosin-containing protein causes a novel type of frontotemporal dementia." Ann Neurol **57**(3): 457-61.

Schuberth, C. and A. Buchberger (2005). "Membrane-bound Ubx2 recruits Cdc48 to ubiquitin ligases and their substrates to ensure efficient ER-associated protein degradation." Nat Cell Biol **7**(10): 999-1006.

Schumacher, A., P. Friedrich, et al. (2009). "No association of common VCP variants with sporadic frontotemporal dementia." Neurobiol Aging **30**(2): 333-5.

Shcherbik, N. and D. S. Haines (2007). "Cdc48p(Npl4p/Ufd1p) binds and segregates membrane-anchored/tethered complexes via a polyubiquitin signal present on the anchors." Mol Cell **25**(3): 385-97.

Shirogane, T., T. Fukada, et al. (1999). "Synergistic roles for Pim-1 and c-Myc in STAT3-mediated cell cycle progression and antiapoptosis." Immunity **11**(6): 709-19.

Simonet, W. S., D. L. Lacey, et al. (1997). "Osteoprotegerin: a novel secreted protein involved in the regulation of bone density." Cell **89**(2): 309-19.

Skibinski, G., N. J. Parkinson, et al. (2005). "Mutations in the endosomal ESCRTIII-complex subunit CHMP2B in frontotemporal dementia." Nat Genet **37**(8): 806-8.

Sollner, T., M. K. Bennett, et al. (1993). "A protein assembly-disassembly pathway in vitro that may correspond to sequential steps of synaptic vesicle docking, activation, and fusion." Cell **75**(3): 409-18.

Sollner, T., S. W. Whiteheart, et al. (1993). "SNAP receptors implicated in vesicle targeting and fusion." Nature **362**(6418): 318-24.

Song, C., Q. Wang, et al. (2003). "ATPase activity of p97-valosin-containing protein (VCP). D2 mediates the major enzyme activity, and D1 contributes to the heat-induced activity." J Biol Chem **278**(6): 3648-55.

Song, C., Q. Wang, et al. (2007). "Characterization of the aggregation-prevention activity of p97/valosin-containing protein." Biochemistry **46**(51): 14889-98.

Spina, S., A. D. Van Laar, et al. (2008). "Frontotemporal dementia associated with a Valosin-Containing Protein mutation: report of three families." FASEB J. **22**(1_MeetingAbstracts): 58.4-.

Sreedharan, J., I. P. Blair, et al. (2008). "TDP-43 mutations in familial and sporadic amyotrophic lateral sclerosis." Science **319**(5870): 1668-72.

Stein, A., G. Weber, et al. (2009). "Helical extension of the neuronal SNARE complex into the membrane." Nature **460**(7254): 525-8.

Sutton, R. B., D. Fasshauer, et al. (1998). "Crystal structure of a SNARE complex involved in synaptic exocytosis at 2.4 A resolution." Nature **395**(6700): 347-53.

Tabaton, M., S. Cammarata, et al. (1991). "Ultrastructural localization of beta-amyloid, tau, and ubiquitin epitopes in extracellular neurofibrillary tangles." Proc Natl Acad Sci U S A **88**(6): 2098-102.

Thoms, S. (2002). "Cdc48 can distinguish between native and non-native proteins in the absence of cofactors." FEBS Lett **520**(1-3): 107-10.

Trabelsi, M., N. Kavian, et al. (2008). "Revised spectrum of mutations in sarcoglycanopathies." Eur J Hum Genet **16**(7): 793-803.

Tsai, B., Y. Ye, et al. (2002). "Retro-translocation of proteins from the endoplasmic reticulum into the cytosol." Nat Rev Mol Cell Biol **3**(4): 246-55.

Uchiyama, K., E. Jokitalo, et al. (2002). "VCIP135, a novel essential factor for p97/p47-mediated membrane fusion, is required for Golgi and ER assembly in vivo." J Cell Biol **159**(5): 855-66.

Uchiyama, K., E. Jokitalo, et al. (2003). "The localization and phosphorylation of p47 are important for Golgi disassembly-assembly during the cell cycle." J Cell Biol **161**(6): 1067-79.

Uchiyama, K. and H. Kondo (2005). "p97/p47-Mediated biogenesis of Golgi and ER." J Biochem **137**(2): 115-9.

Uchiyama, K., G. Totsukawa, et al. (2006). "p37 is a p97 adaptor required for Golgi and ER biogenesis in interphase and at the end of mitosis." Dev Cell **11**(6): 803-16.

Uryu, K., H. Nakashima-Yasuda, et al. (2008). "Concomitant TAR-DNA-binding protein 43 pathology is present in Alzheimer disease and corticobasal degeneration but not in other tauopathies." J Neuropathol Exp Neurol **67**(6): 555-64.

van Leeuwen, F. W., D. P. de Kleijn, et al. (1998). "Frameshift mutants of beta amyloid precursor protein and ubiquitin-B in Alzheimer's and Down patients." Science **279**(5348): 242-7.

Vandermoere, F., I. El Yazidi-Belkoura, et al. (2006). "The valosin-containing protein (VCP) is a target of Akt signaling required for cell survival." J Biol Chem **281**(20): 14307-13.

Vercammen, D., G. Brouckaert, et al. (1998). "Dual signaling of the Fas receptor: initiation of both apoptotic and necrotic cell death pathways." J Exp Med **188**(5): 919-30.

Waggoner, B., M. J. Kovach, et al. (2002). "Heterogeneity in familial dominant Paget disease of bone and muscular dystrophy." Am J Med Genet **108**(3): 187-91.

Walker, J. E., M. Saraste, et al. (1982). "Distantly related sequences in the alpha- and beta-subunits of ATP synthase, myosin, kinases and other ATP-requiring enzymes and a common nucleotide binding fold." Embo J **1**(8): 945-51.

Wang, Q., C. Song, et al. (2005). "Multifunctional roles of the conserved Arg residues in the second region of homology of p97/valosin-containing protein." J Biol Chem **280**(49): 40515-23.

Wang, Q., C. Song, et al. (2003). "Hexamerization of p97-VCP is promoted by ATP binding to the D1 domain and required for ATPase and biological activities." Biochem Biophys Res Commun **300**(2): 253-60.

Wang, Q., C. Song, et al. (2004). "Molecular perspectives on p97-VCP: progress in understanding its structure and diverse biological functions." J Struct Biol **146**(1-2): 44-57.

Wang, Q., C. Song, et al. (2003). "D1 ring is stable and nucleotide-independent, whereas D2 ring undergoes major conformational changes during the ATPase cycle of p97-VCP." J Biol Chem **278**(35): 32784-93.

Wang, Y., A. Satoh, et al. (2004). "VCIP135 acts as a deubiquitinating enzyme during p97-p47-mediated reassembly of mitotic Golgi fragments." J Cell Biol **164**(7): 973-8.

Warren, G. (1993). "Membrane partitioning during cell division." Annu Rev Biochem **62**: 323-48.

Watts, G. D., D. Thomasova, et al. (2007). "Novel VCP mutations in inclusion body myopathy associated with Paget disease of bone and frontotemporal dementia." Clin Genet **72**(5): 420-6.

Watts, G. D., J. Wymer, et al. (2004). "Inclusion body myopathy associated with Paget disease of bone and frontotemporal dementia is caused by mutant valosin-containing protein." Nat Genet **36**(4): 377-81.

Webb, M. R. (1992). "A continuous spectrophotometric assay for inorganic phosphate and for measuring phosphate release kinetics in biological systems." Proc Natl Acad Sci U S A **89**(11): 4884-7.

Weidman, P. J., P. Melancon, et al. (1989). "Binding of an N-ethylmaleimide-sensitive fusion protein to Golgi membranes requires both a soluble protein(s) and an integral membrane receptor." J Cell Biol **108**(5): 1589-96.

Weihl, C. C., S. Dalal, et al. (2006). "Inclusion body myopathy-associated mutations in p97/VCP impair endoplasmic reticulum-associated degradation." Hum Mol Genet **15**(2): 189-99.

Weihl, C. C., S. E. Miller, et al. (2007). "Transgenic expression of inclusion body myopathy associated mutant p97/VCP causes weakness and ubiquitinated protein inclusions in mice." Hum Mol Genet **16**(8): 919-28.

Weihl, C. C., P. Temiz, et al. (2008). "TDP-43 accumulation in inclusion body myopathy muscle suggests a common pathogenic mechanism with frontotemporal dementia." J Neurol Neurosurg Psychiatry **79**(10): 1186-9.

Whyte, M. P., S. E. Obrecht, et al. (2002). "Osteoprotegerin deficiency and juvenile Paget's disease." N Engl J Med **347**(3): 175-84.

Wojcik, C., M. Rowicka, et al. (2006). "Valosin-containing protein (p97) is a regulator of endoplasmic reticulum stress and of the degradation of N-end rule and ubiquitin-fusion degradation pathway substrates in mammalian cells." Mol Biol Cell **17**(11): 4606-18.

Wojcik, C., M. Yano, et al. (2004). "RNA interference of valosin-containing protein (VCP/p97) reveals multiple cellular roles linked to ubiquitin/proteasome-dependent proteolysis." J Cell Sci **117**(Pt 2): 281-92.

Wolf, Y. I., S. E. Brenner, et al. (1999). "Distribution of protein folds in the three superkingdoms of life." Genome Res **9**(1): 17-26.

Wooten, M. W., T. Geetha, et al. (2005). "The p62 scaffold regulates nerve growth factor-induced NF-kappaB activation by influencing TRAF6 polyubiquitination." J Biol Chem **280**(42): 35625-9.

Wooten, M. W., M. L. Seibenhener, et al. (2001). "The atypical protein kinase C-interacting protein p62 is a scaffold for NF-kappaB activation by nerve growth factor." J Biol Chem **276**(11): 7709-12.

Yasuda, H., N. Shima, et al. (1998). "Osteoclast differentiation factor is a ligand for osteoprotegerin/osteoclastogenesis-inhibitory factor and is identical to TRANCE/RANKL." Proc Natl Acad Sci U S A **95**(7): 3597-602.

Ye, Y., H. H. Meyer, et al. (2001). "The AAA ATPase Cdc48/p97 and its partners transport proteins from the ER into the cytosol." Nature **414**(6864): 652-6.

Ye, Y., H. H. Meyer, et al. (2003). "Function of the p97-Ufd1-Npl4 complex in retrotranslocation from the ER to the cytosol: dual recognition of nonubiquitinated polypeptide segments and polyubiquitin chains." J Cell Biol **162**(1): 71-84.

Ye, Y., Y. Shibata, et al. (2005). "Inaugural Article: Recruitment of the p97 ATPase and ubiquitin ligases to the site of retrotranslocation at the endoplasmic reticulum membrane." Proc Natl Acad Sci U S A **102**(40): 14132-8.

Ye, Y., Y. Shibata, et al. (2004). "A membrane protein complex mediates retro-translocation from the ER lumen into the cytosol." Nature **429**(6994): 841-7.

Yoshida, Y., E. Adachi, et al. (2005). "Glycoprotein-specific ubiquitin ligases recognize N-glycans in unfolded substrates." EMBO Rep **6**(3): 239-44.

Zhang, X., A. Shaw, et al. (2000). "Structure of the AAA ATPase p97." Mol Cell **6**(6): 1473-84.

Zhang, X. and D. B. Wigley (2008). "The 'glutamate switch' provides a link between ATPase activity and ligand binding in AAA+ proteins." Nat Struct Mol Biol **15**(11): 1223-7.

Zhang, Y., C. Goodyer, et al. (2000). "Selective and protracted apoptosis in human primary neurons microinjected with active caspase-3, -6, -7, and -8." J Neurosci **20**(22): 8384-9.

Zhong, X., Y. Shen, et al. (2004). "AAA ATPase p97/valosin-containing protein interacts with gp78, a ubiquitin ligase for endoplasmic reticulum-associated degradation." J Biol Chem **279**(44): 45676-84.

Zou, H., Y. Li, et al. (1999). "An APAF-1.cytochrome c multimeric complex is a functional apoptosome that activates procaspase-9." J Biol Chem **274**(17): 11549-56.

Appendix

Molecular Cell *22*, 713–717, June 23, 2006 ©2006 Elsevier Inc. DOI 10.1016/j.molcel.2006.06.003

p97: The Cell's Molecular Purgatory?

Minireview

Dalia Halawani[1] and Martin Latterich[1,*]
[1] Department of Anatomy and Cell Biology
McGill University
3640 University Street
Montreal, QC H3A 2B2
Canada

The multifunctional AAA-ATPase p97/VCP is one of the most extensively studied members of this protein family, yet it presents the field with many perplexing questions surrounding its mechanism of substrate engagement and processing. Recent discoveries have unmasked a new purgatorial identity for this molecule in the ubiquitin-proteasome pathway, specifically its role in linking ubiquitylated substrates with competing ubiquitin conjugation and deconjugation machineries. Furthermore, biochemical studies surprisingly identify the C-terminal D2 ring as essential for substrate interaction, thus bringing p97 one step closer to its prokaryotic AAA protease relatives.

p97 (also called VCP in mammals and Cdc48p in yeast) is a prominent member of the magnesium-dependent Walker P loop AAA-ATPases. It functions as a homohexamer with two AAA cassettes forming stacked rings, which couple coordinated ATP-hydrolysis cycles to conformational changes of the hexamer (reviewed in Pye et al. [2006]). Originally identified as a biochemical requirement for organelle assembly membrane fusion reactions, p97 rapidly emerged as a biochemical and genetic component in additional cellular pathways, including the processing of membrane-associated precursors of transcription factors, endoplasmic reticulum-associated degradation (ERAD), cell cycle regulation, and DNA repair (Wang et al., 2004). The well-established requirement for p97 activity in the retrotranslocation of ERAD substrates strongly hints at a mechanistic role in ubiquitylated substrate extraction and subsequent delivery to the proteasome. However, this ascribed function is in striking contrast with its apparent role in organelle membrane fusion, which implicates p97 in substrate deubiquitylation rather than degradation (Uchiyama and Kondo, 2005). A number of recent studies now establish a novel paradigm by which p97 plays a purgatorial (deciding) role in regulating the ubiquitylation status of protein substrates, which is consistent with the apparently differing biochemical functions previously observed.

Functional Cooperativity with E3 Ubiquitin Ligases

p97 employs a bipartite mechanism in substrate recruitment involving direct recognition of misfolded domains and indirect interaction with ubiquitylated moieties (Ye et al., 2003). A commonly conceived notion is that substrates must first be processed by the ubiquitin-conjugation machinery prior to recognition and recruitment by ubiquitin-dependent adaptors. Emerging data, however, point to an active role for p97 in substrate recognition and presentation to ubiquitin ligases. Cdc48p, the yeast ortholog of p97, is able to function in a novel ubiquitin-fusion degradation pathway, along with its binary partner, Ufd1p/Npl4p, and the specialized E3/E4 ligase Ufd2p. These proteins form a stable complex that catalyzes the extension of oligo-ubiquitylated chains. Importantly, complex stability appears contingent on the simultaneous assembly of all components, hinting that p97/Cdc48p may mediate substrate presentation to the ubiquitin conjugation machinery (Richly et al., 2005). Consistently, several recent reports highlight functional interactions between p97 and various E3 ligases (Table 1), including ERAD-linked $SCF^{fbs1,2}$ (Skp1p/cullin/F box protein), and Dorfin, a RING-IBR ligase that is elevated in neurodegenerative conditions (Ishigaki et al., 2004; Yoshida et al., 2005). For example, SCF employs two F box protein receptors (fbs1 and fbs2) to link misfolded N glycosylated ERAD substrates to p97. Surprisingly, active ATP hydrolysis by the p97 D2 ring is necessary for Fbs1-mediated substrate recognition, suggesting that p97 is mechanistically required prior to $SCF^{fbs1,2}$ complex recruitment. Similarly, an ATPase-deficient p97 mutant abolishes Dorfin-mediated recognition and ubiquitylation of superoxide dismutase-1 (SOD-1). Therefore, it appears that substrate accessibility to p97 is a prerequisite for coupling E3 ligase activity to select target substrates.

The mechanistic basis of p97 participation in substrate ubiquitylation remains elusive. The fact that Cdc48p interaction with ubiquitylated substrates and Ufd2p is concomitantly reduced in *ufd1-2* and *npl4-1* mutant strains indicates that some target substrate must first be recruited by adaptor proteins prior to E3 complex assembly (Richly et al., 2005). Given that Ufd2p has an unusual role in catalyzing the elongation of preassembled oligo-ubiquitylated chains, it is possible that to ensure the timely degradation of "expired" proteins p97 may couple an extraction step with the multiubiquitylation process, whereby target substrates are already oligo-ubiquitylated and present as an integral part of a larger macromolecular assembly. Remarkably, Cdc48p has been shown to restrict the length of Ufd2p-assembled ubiquitin chains in vitro. This is especially important considering that the length of the multiubiquitin chain has a modulating effect on the efficiency of recognition and degradation by the 20S proteasome. Once processed, arrested degradation substrates are then channeled to the trimeric Ufd2p/Dsk2p/Rad23p complex, which in turn mediates their transfer from Cdc48p to the proteasome (Richly et al., 2005). Whether ubiquitylation is indeed coupled to substrate extraction during retrotranslocation or is an actual prerequisite is hitherto unclear. The fact that the retrotranslocation of pro-α factor does not depend on p97 function suggests that the retrotranslocation process functions in the absence of p97 but that ubiquitylated substrates need to be concomitantly extracted and processed by the membrane-associated p97 complex (Lee et al., 2004).

*Correspondence: martin.latterich@mcgill.ca

Table 1. p97-Interacting Ubiquitin Modification Enzymes and Their Associated Cellular Pathways

Process	E3 Ligase	Interaction	Substrate	Adaptors	Reference
Quality Control (ERAD)	Hrd1p (RING-H2)	Complex Ubx2p mediated	Carboxypeptidase Y (CPY*), MHC class I, Hmg2p	Ufd1p/Npl4p	(Schuberth and Buchberger, 2005; Neuber et al., 2005)
	Ufd2p (U box)	Direct	Spt23p	Ufd1p/Npl4p	(Richly et al., 2005)
	AMFR/gp78 (RING-H2)	Direct	CD3delta	N/A	(Zhong et al., 2004)
	$SCF^{fbs1,2}$ (RING Complex)	Complex	B1 integrin, N glycosylated proteins	N/A	(Yoshida et al., 2005)
	Dorfin (RING-IBR)	Direct	Calcium sensing receptor (CaR)	N/A	(Huang et al., 2006)
UPS	Yeast Ufd2p (U box)	Direct	Ub-Proβgal, Ub-ProtA, Ub-GST	Ufd1p/Npl4p	(Richly et al., 2005)
	Mammalian E4B	Direct	Ataxin-3	N/A	(Matsumoto et al., 2004)
	Dorfin (RING-IBR)	Direct	Superoxide dismutase-1 (SOD1)	N/A	(Ishigaki et al., 2004)
Process	Deubiquitylating Enzyme	Interaction	Substrate	Adaptors	Reference
ERAD UPS	Yeast Otu1p	Direct	Spt23p	Ufd1p/Npl4p, Ufd3p, Shp1p*	(Rumpf and Jentsch, 2006)
UPS	Ataxin-3	Direct	Ub-Proβgal	N/A	(Doss-Pepe et al., 2003)
Membrane Fusion	Mammalian VCIP135	Direct	Unidentified	p47	(Uchiyama and Kondo, 2005)

An asterisk (*) represents unidentified substrates. Abbreviation: N/A, not assessed.

Making Purgatorial Decisions

Just as it is able to interact with the ubiquitin conjugation machinery, Cdc48p is now identified as a constituent of distinct complexes that either inhibit E3 interaction or actively deubiquitylate the substrate. Strikingly, both Ufd2p and the WD40-motif protein Ufd3p compete for interaction with Cdc48p and share the same docking site on its C-terminal domain, with Ufd3p having preferentially the higher binding affinity (Rumpf and Jentsch, 2006). Consequently, depending on the cofactor associated with the complex, Cdc48p can either promote or inhibit the ubiquitylation process for a common substrate. For example, the degradation of Ub-proline-β-galactosidase is accelerated with Ufd2p overexpression but conversely repressed by Ufd3p upregulation. Similarly, an Ufd3p deletion mutant, containing only its Cdc48p binding site, dominantly inhibits the degradation of model UFD substrates. Better yet, even if the substrate is already ubiquitylated, $Cdc48p^{Ufd1/Npl4}$ is able to assemble a deubiquitylating complex with both Otu1p, a member of the Ovarian Tumor family with an ubiquitin-hydrolase activity, and Ufd3p. This complex, in turn, competes with Ufd2p in the processing of its well-characterized substrate in the *OLE* pathway, the transmembrane transcription factor Spt23p. Therefore, depending on the cellular metabolic demands, Cdc48p is able to participate in opposing functions, which can either involve the ubiquitylation and activation of Spt23p or its deubiquitylation and stabilization on the ER membrane. Interestingly, in addition to Cdc48p activity, the common denominator in this process is the requirement of the Ufd1p/Npl4p heterodimer, which helps bridge Cdc48p to its substrate (Rumpf and Jentsch, 2006).

These findings together establish a novel role for p97/Cdc48p in regulating substrate turnover and raise more questions surrounding the underlying biochemical basis of its mechanism. The fact that p97 is considerably more abundant than its partners suggests that cofactor expression, stability, or localization may all be important determinants of the identity of the assembled complexes. Alternatively, p97 and its cofactors may be subject to a dynamic posttranslational modification process that determines the identity of the assembled complex within pockets of cellular microdomains and according to specific metabolic demands. This would not be surprising considering that the cell cycle-dependent phosphorylation of p47 by Cdc2 regulates its localization on the ER and Golgi membranes and may subsequently affect its interaction with p97 (Uchiyama and Kondo, 2005). Similarly, AKT-mediated phosphorylation regulates p97 interaction with ubiquitylated substrates, although it is unclear whether this is a direct effect on substrate binding or a mere consequence of abolishing cofactor binding (Klein et al., 2005). Furthermore, p97 may also assume the role of a protein-proofing chaperone that is coevolved to alleviate the metabolic pressures of protein synthesis and degradation. Depending on conformational recoverability, a crucial decision must be made to either ubiquitylate and degrade or deubiquitylate and recycle target substrates (Figure 1). A better mechanistic understanding of p97 function, especially its potential role in protein unfolding or complex disassembly, is evermore pressing considering the scope and complexity of its interaction with the ubiquitin modification machinery.

Structural Clues to a Biochemical Function

The p97 N-terminal domain possesses multiple features that confer its unique ability to interact with a multitude of highly diverse proteins, with some sharing no underlying structural or functional commonality. One feature is its extension and flexibility with respect to the

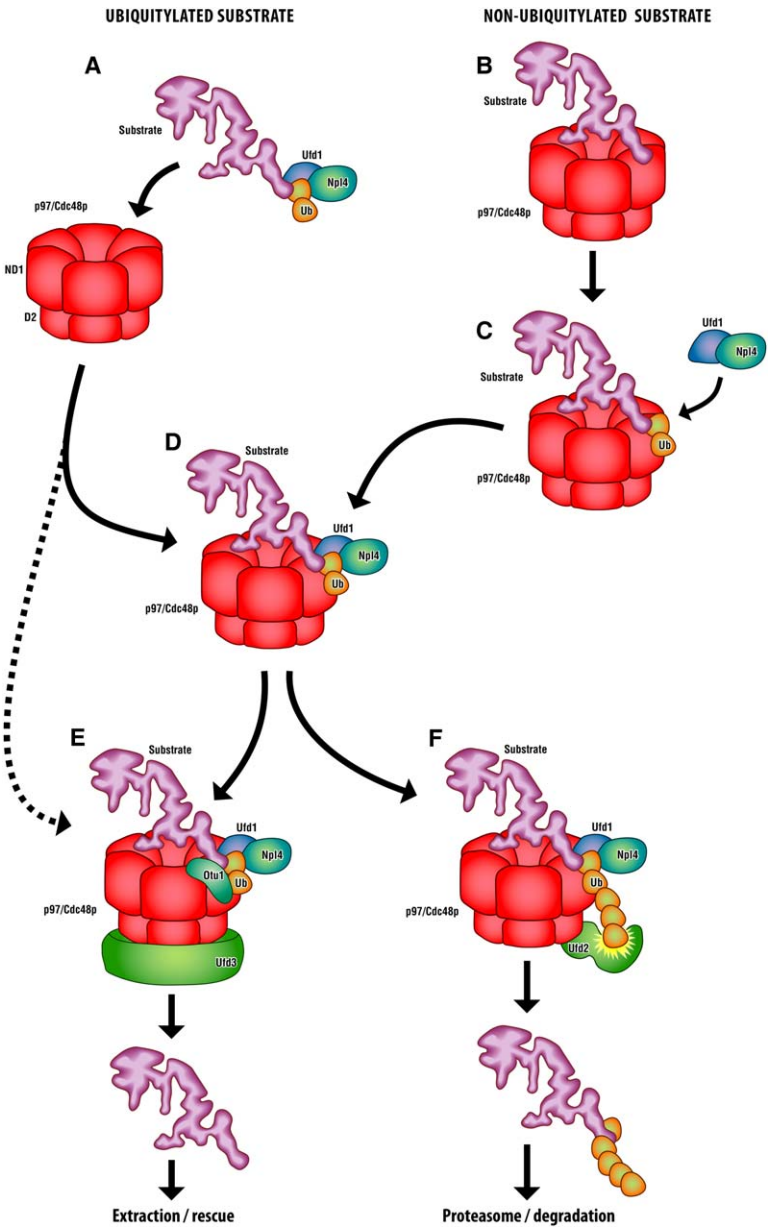

Figure 1. Proposed Mechanisms for p97/Cdc48p Substrate Recognition and Processing

Oligoubiquitylated substrates are first recruited to p97/Cdc48p via its diverse adaptors (A). Alternatively, p97/Cdc48p can bind to misfolded proteins (B) and oligoubiquitylated substrates (C) directly and chaperone against their aggregation. Once the substrate is bound (D), complex will stabilize on the binding of either an E4 ligase, which catalyzes substrate ubiquitylation (F), or a deubiquitylating complex (Otu1p/Ufd3p), which subsequently removes the attached ubiquitin moieties (E). Ubiquitylated substrates, depending on the type of attached ubiquitin moieties, can be channeled for degradation or, like deubiquitylated substrates, extracted and released into the cytosol.

anchoring D1 ring, a property that enables the hexamer to survey its surrounding environment and trap potential substrates. This domain maintains its flexibility in all nucleotide states, except during the transitional state of ATP hydrolysis when complex dissociation is thought to occur. Structurally, the N-terminal domain forms two equally sized subdomains, encompassing a distal double-Ψ β barrel and a proximal β clam fold, with a hydrophobic interphase that functions as protein binding groove (Pye et al., 2006). The contribution of this protein binding cleft to p97 function has only been demonstrated for adaptor binding, specifically the Ubx-UBA containing protein p47 (Beuron et al., 2006; Dreveny et al., 2004), but not substrate engagement, although its deletion abolishes substrate recognition (Ye et al., 2003). Mechanistically, misfolded protein substrates could associate with the N-terminal end of some p97 protomers through their exposed hydrophobic surfaces, whereas adaptors could still occupy other protomers. Although this may still hold, in a recent issue of *Molecular Cell*, DeLaBarre et al. (2006) surprisingly demonstrate the involvement of the D2 ring in substrate binding and propose an in-house mechanism for substrate processing.

By exploiting the homology between p97 and the proteasomal Rpt regulatory proteins, DeLaBarre et al. (2006) identified two loops (residues Arg586/Arg599 and Trp551/Phe552) guarding the aperture of the D2 ring as essential for substrate interaction. Comparison with AAA Rpt proteins is rationalized in their ability to mimic p97 function in ERAD by directly extracting misfolded substrates from the ER retrotranslocation channel. Importantly, conspicuous evidence from previous studies hints at D2 involvement in substrate interaction and processing. Cryo-EM images of p97 in different nucleotide occupancy states show drastic conformational

changes in the D2 ring, portrayed as cycles of perforation and constriction in the bottom pore (Rouiller et al., 2002). Furthermore, D2 ATP binding mutant, but not the D1 mutant, traps ERAD substrates, thus hinting at D2 involvement in substrate interaction with the hexamer (Ye et al., 2003, 2005). This is certainly not the first report of substrate recognition via an AAA-ATPase ring, as bacterial ClpX also employs its distal processing ring in substrate recognition (Ortega et al., 2002). Furthermore, VAT in *Thermoplasma acidophilum* mobilizes hydrophobic residues in the D1 ring during binding and remodeling in vitro substrates (Gerega et al., 2005).

Although no unfoldase activity has been demonstrated for p97 in vitro, it now appears that a calcium sensor for synaptic neurotransmission, synaptotagmin-1, could be a physiological candidate for a putative p97 unfoldase function (DeLaBarre et al., 2006). Synaptotagmin-1 crosslinks specifically to D2 lysine 565, indicating that it does indeed interact with residues at the distal end. Mutations affecting the D2 loops Arg586/Arg599 and Phe552 all lead to severe attenuation of p97 ATPase activity, disruption of its cooperativity, and impairment in ERAD function as measured by the accumulation of TCRα-GFP reporter. A key p97 mutation essential for the interpretation of these results is Trp551, which exhibits wild-type level ATPase activity and kinetics and yet demonstrates a pronounced defect in ERAD. This behavior, combined with reduced coimmunoprecipitation and crosslinking with synaptotagmin-1, suggests that Trp551 is essential for substrate binding and that ERAD impairment can be attributed to the abolition of substrate binding. Although this model is indeed attractive, caution must be taken in its interpretation. p97 interacts with a wide array of cofactors, which may have modulating effects on its ATPase activity. For instance, both Ufd2p and Ufd3p dock at the C-terminal domain of a substrate-occupied Cdc48p complex; however, their effect on its ATPase activity is unclear (Richly et al., 2005; Rumpf and Jentsch, 2006). p47, however, binds to the N-terminal domain and inhibits its ATPase activity. A plausible alternative scenario is that synaptotagmin-1 may stimulate p97 activity, subsequently enabling its interaction with a yet unidentified substrate at the N-terminal end of the complex. Synaptotagmin-1 could then represent a membrane receptor for the recruitment of p97 activity.

Although these findings pose the possibility of D2 involvement in substrate binding, the molecular mechanism of substrate processing remains to be elucidated. Thus far, multiple models have been proposed based on structural parallels to other AAA proteins. In the "molecular-ratchet" model, p97 utilizes ATP-powered conformational changes in propelling substrates that latch on its N-terminal domain, akin to the proposed role of Hsp104. This model is substantiated by the dynamic full-length communication of the structural changes accompanying ATP hydrolysis from the D2 ring to the N-terminal end. For p97-p47 interaction, ATP-dependent conformational changes in the D2 rings are communicated to the N-terminal domain through the D1-D2 and N-D1 linker regions, where highly conserved glycine residues are thought to be indispensable for this process. Consequently, the interacting p97 and p47 domains together form a propeller-like structure, which relocalizes

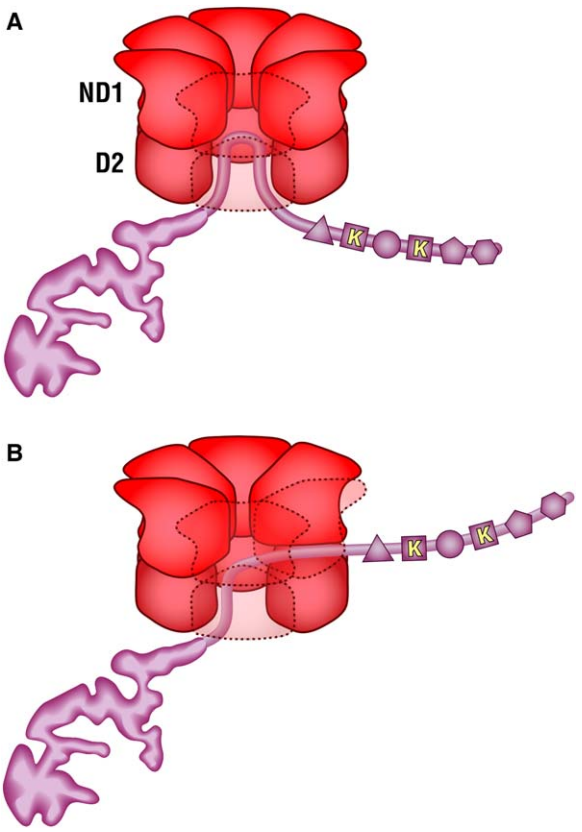

Figure 2. The "Denaturation-Collar" Model for D2-Mediated Substrate Processing

DeLaBarre et al. (2006) propose the D2 ring as an entry port. Guarding the D2 pore is an arginine double ring (Arg586/Arg599) and, thus, the collar, which provides a guanidyl-rich environment theoretically sufficient for unwinding tertiary structures. Once denatured, the substrate is either funneled back through the entry port (A) or threaded through transient pores are the D1/D2 interphase (B).

the arrangement of p47 UBA domain relative to the p97 hexamer. The stoichiometry of p47 to p97 is finally resolved at 0.5 to 1 in vitro, although its contribution to the in vivo formation of these propeller densities or the in vitro inhibition of p97 ATPase activity remains unclear (Beuron et al., 2006).

DeLaBarre and colleagues now introduce the "denaturation-collar" model in which secondary structures are unfolded through the guanidyl-rich denaturing milieu of the arginine double ring (Arg586/Arg599) that guards the D2 pore (DeLaBarre et al., 2006). Subsequently, substrates are either threaded out through transient grooves at the D1/D2 interphase or reversibly channeled out from the entry port (Figure 2). In contrast to other AAA proteins, which thread substrates through their symmetry axis, p97 has a narrow D1 pore that is unlikely able to accommodate a polypeptide chain. In this case, the D1 ring function seems to be limited to correct hexameric assembly and proper interprotomer communication. Furthermore, this model does not rule out the mechanistic involvement of the N-terminal domain and adaptor proteins in substrate recruitment to the C-terminal pore or substrate release from the D2 ring.

Although it is obvious that both models pose very different molecular mechanisms in substrate extraction;

the denaturation-collar model is the first to propose a mechanism coupling substrate extraction to an internal unfoldase function. Reconstitution of this process in vitro should aid in addressing the mechanistic details, particularly the remaining question of whether substrates are internally processed or externally remodeled. Furthermore, one tempting question is whether this proposed role in protein remodeling is evolutionarily exploited by E3 ligases in order to improve substrate accessibility and the efficiency of protein degradation. Alternatively, without an intrinsic unfoldase activity, p97 could assume the role of a cochaperone for substrate recognition and a platform for the assembly of ubiquitin modifying enzymes.

Selected Reading

Beuron, F., Dreveny, I., Yuan, X., Pye, V.E., McKeown, C., Briggs, L.C., Cliff, M.J., Kaneko, Y., Wallis, R., Isaacson, R.L., et al. (2006). EMBO J. *25*, 1967–1975.

DeLaBarre, B., Christianson, J.C., Kopito, R.R., and Brunger, A.T. (2006). Mol. Cell *22*, 451–462.

Doss-Pepe, E.W., Stenroos, E.S., Johnson, W.G., and Madura, K. (2003). Mol. Cell. Biol. *23*, 6469–6483.

Dreveny, I., Kondo, H., Uchiyama, K., Shaw, A., Zhang, X., and Freemont, P.S. (2004). EMBO J. *23*, 1030–1039.

Gerega, A., Rockel, B., Peters, J., Tamura, T., Baumeister, W., and Zwickl, P. (2005). J. Biol. Chem. *280*, 42856–42862.

Huang, Y., Niwa, J., Sobue, G., and Breitwieser, G.E. (2006). J. Biol. Chem. *281*, 11610–11617.

Ishigaki, S., Hishikawa, N., Niwa, J., Iemura, S., Natsume, T., Hori, S., Kakizuka, A., Tanaka, K., and Sobue, G. (2004). J. Biol. Chem. *279*, 51376–51385.

Klein, J.B., Barati, M.T., Wu, R., Gozal, D., Sachleben, L.R., Jr., Kausar, H., Trent, J.O., Gozal, E., and Rane, M.J. (2005). J. Biol. Chem. *280*, 31870–31881.

Lee, R.J., Liu, C.W., Harty, C., McCracken, A.A., Latterich, M., Romisch, K., DeMartino, G.N., Thomas, P.J., and Brodsky, J.L. (2004). EMBO J. *23*, 2206–2215.

Neuber, O., Jarosch, E., Volkwein, C., Walter, J., and Sommer, T. (2005). Nat. Cell Biol. *7*, 993–998.

Ortega, J., Lee, H.S., Maurizi, M.R., and Steven, A.C. (2002). EMBO J. *21*, 4938–4949.

Pye, V.E., Dreveny, I., Briggs, L.C., Sands, C., Beuron, F., Zhang, X., and Freemont, P.S. (2006). J. Struct. Biol.. Published online Mar 29, 2006. 10.1016/j.jsb.2006.03.003.

Richly, H., Rape, M., Braun, S., Rumpf, S., Hoege, C., and Jentsch, S. (2005). Cell *120*, 73–84.

Rouiller, I., DeLaBarre, B., May, A.P., Weis, W.I., Brunger, A.T., Milligan, R.A., and Wilson-Kubalek, E.M. (2002). Nat. Struct. Biol. *9*, 950–957.

Rumpf, S., and Jentsch, S. (2006). Mol. Cell *21*, 261–269.

Schuberth, C., and Buchberger, A. (2005). Nat. Cell Biol. *7*, 999–1006.

Uchiyama, K., and Kondo, H. (2005). J. Biochem. (Tokyo) *137*, 115–119.

Wang, Q., Song, C., and Li, C.C. (2004). J. Struct. Biol. *146*, 44–57.

Ye, Y., Meyer, H.H., and Rapoport, T.A. (2003). J. Cell Biol. *162*, 71–84.

Ye, Y., Shibata, Y., Kikkert, M., van Voorden, S., Wiertz, E., and Rapoport, T.A. (2005). Proc. Natl. Acad. Sci. USA *102*, 14132–14138.

Yoshida, Y., Adachi, E., Fukiya, K., Iwai, K., and Tanaka, K. (2005). EMBO Rep. *6*, 239–244.

MOLECULAR AND CELLULAR BIOLOGY, July 2008, p. 4261–4274 Vol. 28, No. 13
0270-7306/08/$08.00+0 doi:10.1128/MCB.02252-07
Copyright © 2008, American Society for Microbiology. All Rights Reserved.

GTPase-Mediated Regulation of the Unfolded Protein Response in *Caenorhabditis elegans* Is Dependent on the AAA$^+$ ATPase CDC-48▽†

Marie-Elaine Caruso,[1] Sarah Jenna,[1]‡ Marion Bouchecareilh,[2] David L. Baillie,[3] Daniel Boismenu,[4] Dalia Halawani,[5] Martin Latterich,[5] and Eric Chevet[1,2,6]*

Department of Surgery, McGill University, Montreal, QC, Canada[1]; INSERM, U889, Team Avenir, Bordeaux, France[2]; Department of Molecular Biology and Biochemistry, Simon Fraser University, Burnaby, BC, Canada[3]; McGill University and Génome Quebec Innovation Centre, Montreal, QC, Canada[4]; Faculty of Pharmacy, University of Montreal, Montreal, QC, Canada[5]; and University Bordeaux 2, Bordeaux, France[6]

Received 20 December 2007/Returned for modification 7 January 2008/Accepted 10 April 2008

When endoplasmic reticulum (ER) homeostasis is perturbed, an adaptive mechanism is triggered and named the unfolded protein response (UPR). Thus far, three known UPR signaling branches (IRE-1, PERK, and ATF-6) mediate the reestablishment of ER functions but can also lead to apoptosis if ER stress is not alleviated. However, the understanding of the molecular mechanisms integrating the UPR to other ER functions, such as membrane traffic or endomembrane signaling, remains incomplete. We consequently sought to identify new regulators of UPR-dependent transcriptional mechanisms and focused on a family of proteins known to mediate, among other, ER-related functions: the small GTP-binding proteins of the RAS superfamily. To this end, we used transgenic UPR reporter *Caenorhabditis elegans* strains as a model to specifically silence small-GTPase expression. We show that the Rho subfamily member CRP-1 is an essential component of UPR-induced transcriptional events through its physical and genetic interactions with the AAA$^+$ ATPase CDC-48. In addition, we describe a novel signaling module involving CRP-1 and CDC-48 which may directly link the UPR to DNA remodeling and transcription control.

The endoplasmic reticulum (ER) is an organelle found in eukaryotic cells, which is mainly involved in calcium sequestration, lipid biosynthesis and translation, folding, and transport of secretory proteins (9). These functions require specialized and integrated molecular machines (7). Most of the proteins distributed in organelles of the secretory pathway, expressed at the cell surface or secreted, transit through the ER before reaching their final destination. Indeed, polypeptide chains, translated on ER membrane-bound ribosomes, are first translocated into the ER lumen via the translocon and then processed through the ER folding machineries, which include a chaperone component (e.g., BiP or GRP94), a posttranslational modification machinery (e.g., N glycosylation with the oligosaccharyl transferase complex, S-S bound formation with the protein disulfide isomerases), and a quality control component (e.g., calnexin, UDP-glucose:glycoprotein glucosyltransferase). Proteins which do not acquire a correct conformation are retained in the ER by ER-specific quality control mechanisms and are consequently granted further folding attempts. If this fails again, terminally misfolded proteins are degraded via the ER-associated degradation (ERAD) machinery (9).

Under basal conditions, these integrated mechanisms maintain the ER protein load in equilibrium with ER's folding and export capacities. However, if one of those components is dysfunctional, the entire chain reaction is perturbed and ER homeostasis is disrupted. This leads to an increased amount of improperly folded proteins, which accumulate within the ER. As a mechanism for adaption to this phenomenon, cells have evolved the unfolded protein response (UPR), which aims at restoring ER homeostasis (38, 41) by (i) attenuating protein translation, (ii) increasing ER folding capacity, (iii) increasing ERAD capacity, and (iv) triggering cell death if ER homeostasis is not restored. This stress response is regulated by the activation of three ER resident proximal sensors, which constitute the three arms of the UPR: inositol-requiring enzyme 1 (IRE-1), activating transcription factor 6 (ATF-6), and protein kinase RNA-like ER kinase (PERK) (38, 41).

Another mechanism regulating ER content is mediated by the export machinery. For instance, activation of the UPR was shown to induce the expression of the small G protein SAR-1, a member of the COPII protein complex (28, 40, 43). Moreover, expression of a dominant negative SAR-1 induces the accumulation of proteins in the ER (28, 40, 43), probably leading to the saturation of ER folding capacity. In addition to the role of SAR-1 in the regulation of ER protein load, other GTPases of the RAS superfamily were found to play a role in either organelle maintenance/biogenesis (2, 24) or endomembrane signaling (33–35).

These observations led us to postulate that small GTP binding proteins of the RAS superfamily may represent a master regulatory component of ER homeostasis. To test this hypothesis, we investigated the involvement of these GTPases in the activation of the UPR using RNA interference (RNAi) in *Caenorhabditis elegans*. This experimental system constitutes a

* Corresponding author. Mailing address: Team Avenir, INSERM U889, Université Bordeaux 2, 146 rue Léo Saignat, 33076 Bordeaux, France. Phone: 33 (0)5 57 57 92 53. Fax: 33 (0)5 56 51 40 77. E-mail: eric.chevet@u-bordeaux2.fr.

† Supplemental material for this article may be found at http://mcb.asm.org/.

‡ Present address: Dept. of Chemistry, UQAM, Montreal, QC, Canada.

▽ Published ahead of print on 5 May 2008.

Downloaded from mcb.asm.org at McGill Univ on January 19, 2010

powerful model in which the three UPR arms are conserved and which contains over 60 conserved GTPases of the RAS superfamily. Based on the analysis of a GTPase family subset, our results indicate the specific roles of members of the Rho family of GTPases in the transcriptional activation of UPR target genes. We found that this is possibly regulated through the presence of CRP-1 in a complex with the AAA^+ ATPase CDC-48. We demonstrate physical and genetic interactions between CRP-1 and CDC-48 and consequently delineate a novel signaling component physically linking ER stress and transcriptional regulation in metazoans.

MATERIALS AND METHODS

***C. elegans* strains.** The wild-type strain N2 (Bristol) was used as the reference strain. Knockout mutant alleles *ok685* (*crp-1*$^{-/-}$; Y32F6B.3), *gk186* (*atm-1*$^{-/-}$; Y48G1BL.2), *tm544* (*cdc-48.1*$^{-/-}$; C06A1.1), *ok275* (*pek-1*$^{-/-}$; F46C3.1), and *ok551* (*atf-6*$^{-/-}$; F45E6.2) were obtained from the *Caenorhabditis* Genetics Center at the University of Minnesota. *promoter*::*gfp* reporter strains BC10700 (ZK632.6), BC13719 (F48E3.3), BC11945 (F43E2.8), BC10066 (C15H9.6), BC13607 (B0403.4), BC10371 (C53B4.7A), BC14636 (B0285.9), and BC10178 (C55B6.2) were obtained from the British Columbia *C. elegans* Gene Expression Consortium. *C. elegans* animals were maintained at 20°C under standard culture conditions and fed with OP50 unless otherwise mentioned (5).

Drug induction and GFP quantification. ER stress level was measured using transgenic worms expressing green fluorescent protein (GFP) under the control of various ER stress promoters. Synchronized L1 populations expressing the different ER stress GFP reporters were grown on standard nematode growth medium (NGM) plates. L4 stage worms were then transferred on NGM plates containing dimethyl sulfoxide as control, 5 μg/ml tunicamycin (TM), 5 mM L-azetidine-2-carboxylic acid (AZC), 1 mM dithiothreitol (DTT), or 1 μM thapsigargin (TG) for 5 h at 20°C. Fluorescence quantification was performed using two different methods. Entire worm populations were analyzed using the Copas Biosort (Union Biometrica) (11), which provided an average fluorescence level for the entire worm population ($n \geq 1{,}000$). These results were correlated with an observation-based counting method using fluorescence microscopy in which worms were classified in three groups of (i) low, (ii) medium, and (iii) high levels of fluorescence. At least 100 worms were counted per strain and condition in triplicate by at least two independent investigators. Moreover, to validate the counting methodology, a blinded evaluation of fluorescence was correlated with an immunoblot using anti-GFP antibodies on worm lysates. As expected, the highest signal observed by immunoblotting correlated with the highly fluorescent worm population.

Tissue localization. Expression profiles were analyzed using GFP-reporter transgenic worms (19). Following a 5-h treatment with 5 μg/ml TM at 20°C, living worms were mounted on agarose pads in M9 buffer containing 1 mM levamisole (Sigma). Fluorescence emission from living worms was observed using an Axiovert-200 microscope (Zeiss), and images were analyzed using Northern Eclipse, version 6.0 (Empix Imaging, Mississauga, Ontario, Canada).

RNAi. All RNAi experiments were carried out using a feeding procedure described previously (21). RNAi constructs were either cloned from a *C. elegans* cDNA library (de novo) or retrieved from the *C. elegans* ORFeome collection, version 1.1 (37), using the Gateway technology (Invitrogen). For primers used for de novo cloning, see Table S1 in the supplemental material. GTPase open reading frames (ORFs), without ATG, and approximately 500 base pairs of the *cdc-48.1* (C06A1.1) and *xbp-1* (R74.3) genes were amplified by PCR using Platinum *Taq* high-fidelity DNA polymerase (Invitrogen) and the following amplification scheme: denaturation at 94°C for 40 s, annealing at 60°C for 40 s, and elongation at 72°C for 1 min for 35 cycles. These PCR products were polyethylene glycol precipitated and recombined into pDONR201 using the Gateway BP Clonase (Invitrogen). These entry clones were subsequently recombined, using LR Clonase, into Gateway-compatible pL4440 vector and transformed into HT115(DE3) bacteria. Isolated transformant bacteria were grown for 12 h at 37°C in Luria-Bertani medium supplemented by 100 μg/ml ampicillin. Bacteria were spotted on NGM plates containing 1 mM IPTG (isopropyl-β-D-thiogalactopyranoside) and 100 μg/ml ampicillin, dried, and induced overnight at room temperature. Synchronized L1 worm populations were transferred to these plates and treated for three days. L4 worms were then transferred to new RNAi plates containing or not 5 μg/ml TM, and fluorescence levels were analyzed as described above, following 5 hours of incubation at 20°C.

ORF cloning, expression, and pull-down affinity purification. Recombinant *C. elegans* GST–CRP-1 and GST–CDC-42 and mouse His_6–p97/VCP/CDC-48 (which displays 76% identity with CeCDC-48) proteins were expressed in *Escherichia coli* as previously described (8, 23) and purified using glutathione-Sepharose 4B or nickel-nitrilotriacetic acid (NTA)-agarose, respectively. The ORFs encoding CDC-48.1, CDC648.2, and HIM-6 were amplified by reverse transcription-PCR (RT-PCR) using the indicated primers (see Table S1 in the supplemental material) from *C. elegans* total RNA. The amplified PCR products were cloned by recombination into the pDONR201 vector using the Gateway technology (Invitrogen). The entry vectors generated were then used to recombine the specific ORFs into His_6-Nterm or Strep tag-Nterm prokaryotic expression vectors. These were then transformed into DH5a bacteria. Five individual colonies were picked and pooled, and plasmid DNA was amplified and transformed into BL21 cells. Recombinant proteins were produced in BL21 cells following a 3-h induction using either 1 mM IPTG or 0.2 μg/ml tetracycline. Protein lysates were either directly frozen or directly subjected to affinity purification as recommended by the manufacturers. For one set of experiments (see Fig. 4), we used bacterial lysate expressing recombinant proteins. In these conditions, GST–CRP-1 or GST–CDC-42 (in equal amounts) was mixed with mouse His_6–p97/VCP/CDC-48-expressing bacterial lysate and the mixture was incubated for 2 hours at 4°C. GST pull-down was then carried out on bacterial lysate using glutathione-Sepharose 4B resin (GE Biosciences). Following incubation for an additional hour at 4°C, beads were washed six times with phosphate-buffered saline and resolved by sodium dodecyl sulfate-polyacrylamide gel electrophoresis (SDS-PAGE). Proteins were revealed using Coomassie blue R250 staining. His_6 pull-down was carried out on N2 or *crp-1*$^{-/-}$ (*ok685*) allele strains mixed with purified His_6–p97/VCP/CDC-48 proteins for 2 hours at 4°C. Complexes were purified using Ni-NTA-agarose (Qiagen) and resolved by SDS-PAGE. Gels were then transferred on nitrocellulose membranes and subjected to standard immunoblot protocols using either mouse anti-p97/VCP/CDC-48 (Abnova) or hen anti-CRP-1 antibodies (HyperOmics Farma, Inc., Montreal, QC, Canada). For the other set of experiments (see Fig. 5), purified proteins (1 μg) were incubated with 10 mM Tris, pH 7.4, and 100 mM NaCl (in the presence or not of 10 μM GTP and ATP) for 2 h at 4°C and pulled down with beads for 45 min under rotation at 4°C. Following five washes using the same buffer as above but containing 0.5% Triton X-100, the beads were resuspended in 2× Laemmli sample buffer, resolved by electrophoresis, and immunoblotted using anti-glutathione *S*-transferase (GST; Cellular Signaling) or anti-Strep tag (Qiagen) antibodies.

CRP-1 pull-down analyses. Worm protein extracts were prepared as previously described (19). Briefly, worms were washed five times using M9 medium to remove bacteria and suspended in homogenization buffer (15 mM HEPES, pH 7.6, 10 mM KCl, 0.1 mM EDTA, 0.5 mM EGTA, 44 mM sucrose, 1 mM DTT, protease inhibitor cocktail [Roche]) and sonicated, and the resulting lysate was cleared by centrifugation at 13,500 rpm for 15 min at 4°C. GST pull-down assays were performed on total worm lysate precleared with glutathione-Sepharose beads bound to GST or Ni-NTA beads to remove all nonspecific binding. Precleared lysates were then mixed with purified GSP–CRP-1 on glutathione-Sepharose 4B or His_6–p97/VCP/CDC-48 on Ni-NTA beads and incubated for 2 h at 4°C. After five washes, beads were suspended using 2× Laemmli buffer and proteins were resolved by SDS-PAGE. The resulting gel was stained using Coomassie blue R250 and processed for mass spectrometry (see methods in the supplemental material).

Data analyses. The human ortholog of each hit identified in the CRP-1 pull-down was retrieved from NCBI, ENSEMBL, or other large sequence repositories when existing or available. The corresponding list was then analyzed using the STRING suite (46, 47) to evaluate the potentially existing functional interactions between proteins found in the CRP-1 complex. We also added a subnetwork including the first-degree genetic or physical interactor of His_6–p97/VCP/CDC-48. The resulting scale-free functional interaction network was then annotated using the Medusa program (16).

TM sensitivity assay. N2 worms and mutant strains were treated using the alkaline hypochlorite method (0.5 M NaOH, H_2O, and 0.8% bleach) to isolate embryos. Eggs were hatched overnight in M9 medium (40 mM Na_2HPO_4, 20 mM KH_2PO_4, 8 mM NaCl, 20 mM NH_4Cl) to obtain an L1-synchronized population. L1 worms were transferred onto NGM plates containing various concentrations of TM (0, 2, 5, or 10 μg/ml) and seeded on HT115 cells expressing or not double-stranded RNA (dsRNA) for the target genes (see "RNAi" for conditions). The developmental stage was analyzed after 24 and 48 h at 20°C, and the percentages of L1 larvae and dead worms over the total population were determined and reported.

RT-PCR analyses. Worms (N2 or *crp-1*$^{-/-}$) were treated or not with 5 μg/ml TM and 2 mM DTT for 5 h or 10 mM NaN_3 for 90 min. They were then collected and lysed using Trizol (Invitrogen). Total RNA was then extracted as recom-

Downloaded from mcb.asm.org at McGill Univ on January 19, 2010

A

Gene name	Sequence name	GFP-reporter strains	Human orthologs	NCBI protein ID	e value	References
hsp-4	F43E2.8	BC11945	HSPA5 (BiP)	NP_005338.1	4.10E-269	Urano, 2002 Shen, 2001
ckb-2	B0285.9	BC14636	Choline/ethanolamine kinase	NP_005189.2	1.50E-28	Urano, 2002
hsp-3	C15H9.6	BC10066	HSPA5 (BiP)	NP_005338.1	4.20E-276	Urano, 2002 Shen, 2001
tag-320	B0403.4	BC13607	protein disulfide isomerase A6	NP_005733.1	3.90E-132	Urano, 2002
cnx-1	ZK632.6	BC10700	calnexin precursor	NP_001737.1	5.79E-127	
dnj-7	C55B6.2	BC10178	DnaJ	NP_006251.1	3.60E-114	Urano, 2002
	F48E3.3	BC13719	UDP-glucose:glycoprotein glucosyltransferase 2	NP_064506.2	3.90E-290	
bre-1	C53B4.7	BC10371	GDP-mannose 4,6 dehydratase	NP_001491.1	1.10E-128	Urano, 2002

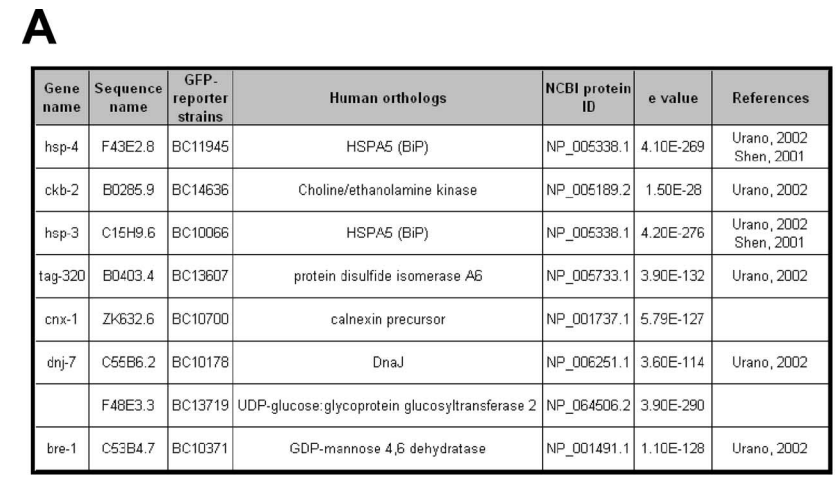

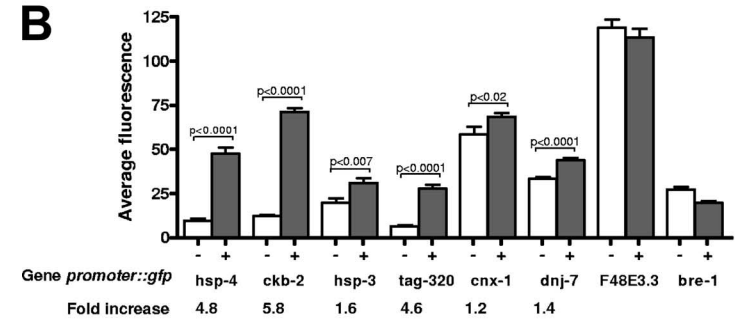

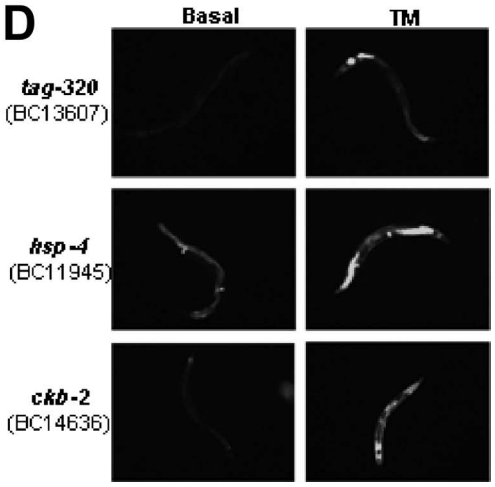

FIG. 1. Identification and characterization of powerful ER stress GFP reporter genes. (A) List of ER stress *promoter::gfp* reporter genes successfully constructed, with the strain name and the human ortholog information. (B) Fluorescence induction of the eight GFP reporter genes when treated with 5 μg/ml TM. Fluorescence level was quantified on entire transgenic worm populations (≥1,000 worms per conditions) using the Copas Biosort. The increase is the ratio between the average fluorescence under TM conditions compared to the basal fluorescence level of each strain. (C) Expression pattern of each GFP reporter strain in living animals. Intestine expression and neuronal expression are represented in light gray and dark gray, respectively. (D) Fluorescence microscopy pictures for the three strains with the highest increases in fluorescence (*tag-320*, *hsp-4*, and *ckb-2* strains) under basal conditions or after TM treatment.

mended by the manufacturer and reverse transcribed using the Superscript III kit (Invitrogen). PCR products were then amplified using the primers described in Table S1 in the supplemental material within the linear part of the amplification curve, resolved on agarose gels, and visualized following ethidium bromide staining. Transcript expression was normalized to that of *ama-1*.

RESULTS

ER stress-mediated activation of *hsp-4*, *ckb-2*, and *tag-320* promoters in *C. elegans* intestine. To study the implication of small G proteins of the RAS superfamily in the maintenance of ER homeostasis, we developed an experimental system allowing efficient and rapid ER stress detection. To this end, we used a *Caenorhabditis elegans*-based GFP reporter driven by UPR-responsive promoters. We selected these promoters based upon their previously reported activation upon ER stress using, for instance, microarray studies (6, 45). Practically, a putative promoter region of 2.5 kilobases cloned upstream of each target gene was fused to the GFP gene (*gfp*) cDNA. These constructs were used to generate transgenic worm lines expressing GFP under the control of putative UPR-induced promoters (11, 17, 27). The strains successfully created are listed in Fig. 1A. Also listed in this figure are the gene and sequence names as they appear in WormBase (http://www.wormbase.org/), as well as the names of the corresponding human orthologs. *hsp-4* and *hsp-3* are the two *C. elegans* homologs of the

Downloaded from mcb.asm.org at McGill Univ on January 19, 2010

mammalian ER chaperone GRP78/BiP gene. Expression of the GFP reporter under the control of endogenous promoters from both genes was previously shown to increase upon TM treatment (22), and these results were confirmed using our BC11945 (*phsp-4*::*gfp*) and BC10066 (*phsp-3*::*gfp*) strains (Fig. 1B). The six other GFP reporters used in our study expressed GFP under the control of various promoters: the ER protein disulfide isomerase-like protein-encoding gene (*ptag-320*::*gfp*), the heat shock protein p58 (DnaJ)-encoding gene (*pdnj-7*::*gfp*), the choline/ethanolamine kinase-encoding gene (*pckb-2*::*gfp*), and three genes involved in ER quality control, the calnexin (*pcnx-1*::*gfp*), UDP-glucose:glycoprotein glucosyltransferase 2 (*pF48E3.3*::*gfp*), and GDP-mannose-4,6-dehydratase (*pbre-1*::*gfp*) genes (Fig. 1A). To test whether these transgenic lines were able to activate the selected GFP reporters upon ER stress, we treated adult hermaphrodites with TM, an antibiotic that inhibits N glycosylation (15) and strongly induces the UPR. We measured and quantified GFP expression level using the Copas Biosort (Union Biometrica) (11, 20). This instrument is designed to perform multiparametric analyses of micrometric particles in a semiautomated manner. This allowed us to measure the average fluorescence emitted by a large population of transgenic worms (1,000 animals per conditions) in response to TM treatment. Fluorescence levels of *phsp-4*::*gfp* (BC11945), *pckb-2*::*gfp* (BC14636), *phsp-3*::*gfp* (BC10066), *ptag-320*::*gfp* (BC13607), *pcnx-1*::*gfp* (BC10700), and *pdnj-1*::*gfp* (BC10178) strains were significantly increased upon TM treatment, whereas those of the *pF48E3.3*::*gfp* (BC13719) and *pbre-1*::*gfp* (BC10371) strains were not (Fig. 1B).

To select the most appropriate GFP reporter strains for our study, we also analyzed, using fluorescence microscopy, GFP tissue expression profiles of the strains described above. Interestingly, *phsp-4*::*gfp*, *pckb-2*::*gfp*, *phsp-3*::*gfp*, and *ptag-320*::*gfp* reporters, shown to have the highest GFP expression, increased upon TM treatment 4.8-, 5.8-, 1.6-, and 4.6-fold, respectively, were expressed mainly in the intestine (Fig. 1C and D). In contrast, reporters such as *pcnx-1*::*gfp*, *pF48E3.3*::*gfp*, and *pbre-1*::*gfp*, which were less sensitive to TM, were principally expressed in the nervous system (Fig. 1C). Differences in GFP expression upon TM treatment may result from a greater sensitivity/accessibility of certain organs/cell types (for example, the intestine) and also the relative sizes of the organs. We therefore concluded that *phsp-4*::*gfp*, *pckb-2*::*gfp*, and *ptag-320*::*gfp* were the three most efficient reporters to detect and measure the ER stress-mediated transcriptional response.

ER stress-responsive promoters are specifically activated upon treatment with different ER stress inducers. To determine if the induction of fluorescence observed in the three most responsive GFP-reporter strains was TM specific, we treated transgenic animals using various chemicals known to induce ER stress in cultured mammalian cells. Worms were exposed to four different agents, including TM, that act differentially on the ER but ultimately lead to ER stress. AZC is a proline analogue which causes defects in protein conformation when integrated into the polypeptide chain (10). DTT is a reducing agent that affects the ER lumen oxidative environment (4), and, finally, TG is a Ca^{2+}-ATPase (SERCA) inhibitor that causes ER Ca^{2+} depletion (39). As shown in Fig. 2, the three GFP reporter strains tested responded differentially to the four ER stress inducers selected. In our experimental setup, TM was the strongest ER stress inducer for the *pckb-2*::*gfp*, *phsp-4*::*gfp*, and *ptag-320*::*gfp* strains with, respectively, 78%, 80%, and 22% of the worm population expressing a high level of fluorescence following a 5-hour treatment. AZC and DTT had mainly the same impact on the three reporters, with almost 49% of worms expressing high fluorescence in the *pckb-2*::*gfp* strain, 28% in the *phsp-4*::*gfp* strain, and less than 20% in the *ptag-320*::*gfp* strain. Finally, TG had a higher level of fluorescence induction in the *pckb-2*::*gfp* strain, with 61% of the worm population expressing high fluorescence. These results show that *pckb-2*::*gfp* is the reporter which presents the highest and most homogenous response to diverse ER stress treatments. In addition, they indicate that, in our experimental settings, TM represents the most universal ER stress inducer. For these reasons, we selected the *pckb-2*::*gfp* reporter to identify, using RNAi, new ER signaling regulators and TM to induce ER stress in *C. elegans*.

CRP-1 expression is necessary for a TM-induced ER stress transcriptional response. In an attempt to identify small GTP-binding proteins involved in ER stress signaling events, we subjected the *pckb-2*::*gfp* reporter strain to RNAi treatments targeting specific GTPases (Table 1). Variations were measured using fluorescence microscopy, under basal conditions or following a 5-hour treatment with TM. Three controls were used to evaluate RNAi efficiency and specificity. *pckb-2*::*gfp* reporter worms were treated with an empty RNAi vector, an RNAi vector against GFP, or RNAi vectors containing GTPase coding sequences but for which production of dsRNA was not induced by IPTG (see Materials and Methods). These controls supported the validity and efficacy of our experimental system.

Based on the current knowledge on small GTPases of the RAS superfamily in *C. elegans*, we focused on 13 *C. elegans* GTPases whose mammalian orthologs were either localized in the ER or along the secretory pathway and/or known to regulate ER-related functions (Table 1). RNAi treatment targeting these GTPases revealed that they could be divided into four different categories according to their effect on the activation of the *ckb-2* promoter under basal conditions or upon TM exposure (Table 1). The first category contained most of the GTPases tested (8/13), which did not have any effect on *pckb-2*::*gfp* activation. The second category contained GTPases for which RNAi-mediated silencing led to a severe phenotype such as L1 arrest of lethality and for which GFP expression could not be measured in adult worms. Two GTPases, RAB-1 and RAB-7, were found to be in this category and were excluded from further analysis (Table 1).

The two other categories included GTPases for which alteration of expression levels had significant effects on ER stress-mediated *pckb-2*::*gfp* activation under basal conditions or following treatment. Representative results obtained for these GTPases are shown in Fig. 3A. In the third category, we identified one GTPase, SAR-1, whose silencing led to an activation of *pckb-2*::*gfp* under basal conditions. This is consistent with the previous observations that SAR-1 was implicated in membrane transport from the ER to the Golgi apparatus (43). In addition, our results suggest that disruption of this transport would inhibit protein progression from the ER (43) and consequently induce the UPR. The fourth category contains two GTPases, CDC-42 and CRP-1, whose silencing prevented

Downloaded from mcb.asm.org at McGill Univ on January 19, 2010

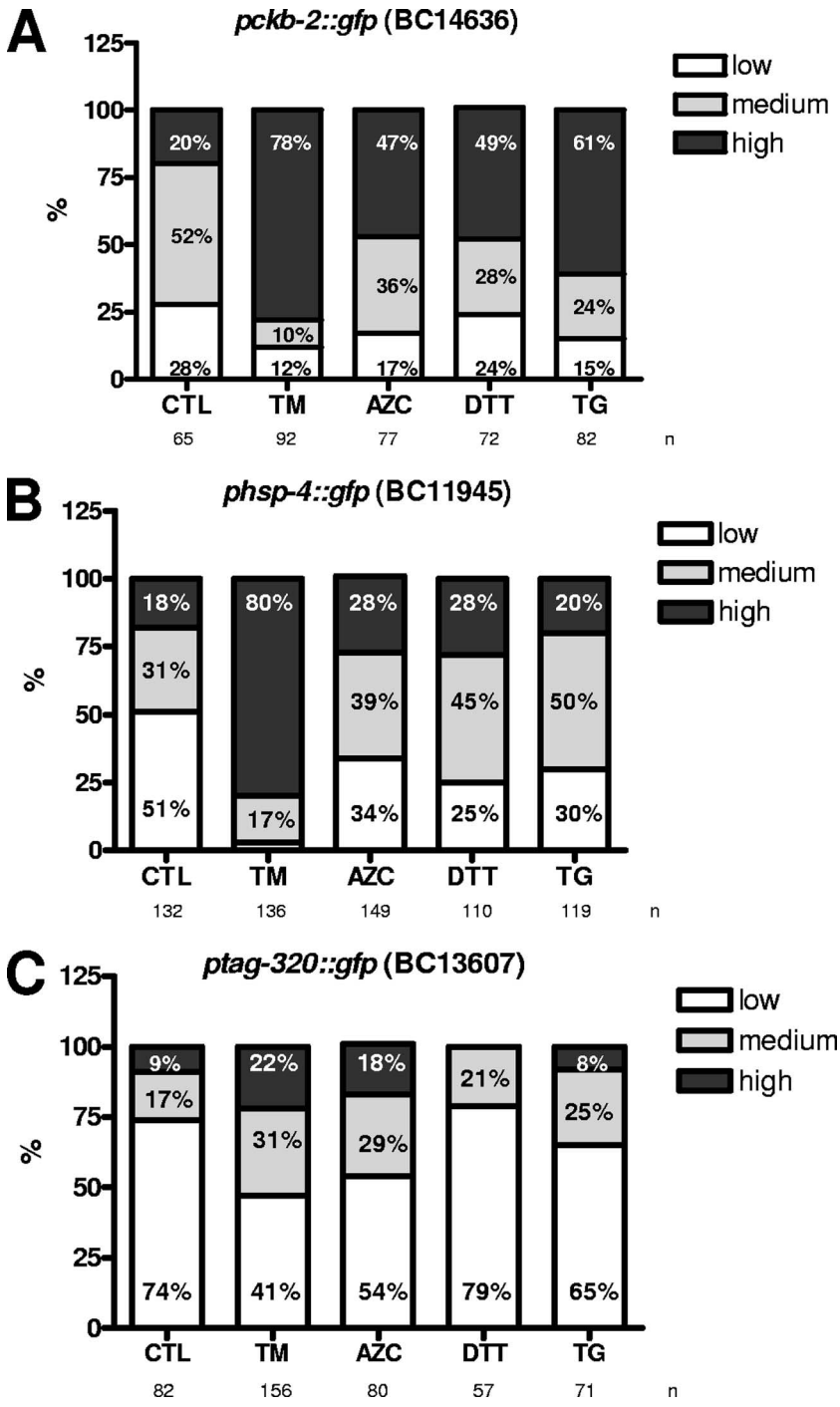

FIG. 2. ER stressors TM, AZC, DTT, and TG act differentially on the three most responsive GFP reporter strains. Populations of (A) *pckb-2*::*gfp* (BC14636), (B) *phsp-4*::*gfp* (BC11945), and (C) *ptag-320*::*gfp* (BC13607) strains were treated with 5 μg/ml TM, 10 μM AZC, 2 mM DTT, and 5 μM TG for 5 hours and visualized and quantified using a fluorescence microscope. The percentage of worms with a low, medium, or high level of fluorescence was plotted against the different chemicals. Experiments were performed at least twice in duplicate. CTL, control.

pckb-2::*gfp* activation after TM exposure. CDC-42 is a small GTPase that regulates actin dynamics and has also been involved in Golgi-to-ER vesicle trafficking events in mammalian cells (25). CRP-1 is a small G protein which clustered with the Rho subfamily according to its amino acid sequence and showed 45% identity to CDC-42 (19) (Table 1). We previously showed that CRP-1 is implicated in the regulation of membrane trafficking in intestinal cells (19) and that CRP-1 RNAi specifically targets CRP-1 expression (see Fig. S1 in the supplemental material). Quantification of total fluorescence of a worm population clearly showed that *crp-1* silencing significantly led to a reduced activation of the *pckb-2*::*gfp* reporter

Downloaded from mcb.asm.org at McGill Univ on January 19, 2010

TABLE 1. Characteristics of the GTPases selected for the first screen and their effect on *pckb-2*::*gfp* reporter activation[a]

Phenotype	WormBase ID[b]	Designation	Subcellular localization[c]	Functions related to the ER (reference)
No effect	C44C11.1	RAS-1	Endomembrane (ER/G)	Intracellular protein transport, ER signal transduction (33)
	F53G12.1	RAB-11.1	TGN recycling/exocytic compartment	Membrane fusion, vesicular trafficking
	F54C9.10	ARL-1	TGN/G	Membrane fusion and traffic
	F53F10.4	UNC-108	ER/*cis*-G	Endocytosis, membrane fusion, vesicular trafficking
	W01H2.3	RAB-37	Secretory granules	Vesicle exocytosis
	ZK792.6	LET-60	Endomembrane (ER/G)	Intracellular protein transport, ER signal transduction (33)
	C27B7.8	RAP-1	G	Membrane fusion, vesicular trafficking
	F45E4.1	ARF-1.1	G/ERGIC/TGN	Mitotic Golgi fragmentation, vesicular trafficking
Severe developmental defects	C39F7.4	RAB-1	ER/*cis*-G	Intracellular vesicle trafficking
	W03C9.3	RAB-7	ER/LE/endosome	Endosomal traffic, vesicular trafficking
Induction of basal ER stress	ZK180.4	SAR-1	ER	ER-to-Golgi protein transport
ER stress inhibition	R07G3.1	CDC-42	ER/G	Cell polarity, protein trafficking
	Y32F6B.3	CRP-1	TGN/RE	Membrane trafficking, cell polarity (19)

[a] *pckb-2*::*gfp* reporter worms were treated with selected GTPase RNAi vectors and exposed or not to TM for 5 hours. The consequence of GTPase silencing on the activation of *ckb*-2 promoters was measured using a fluorescence microscope, and GTPases were classified according to their effect on this reporter into four categories.
[b] ID, identification.
[c] G, Golgi apparatus; TGN, *trans*-Golgi network; ERGIC, ER-Golgi intermediate compartment; LE, late endosomes; RE, recycling endosomes.

under ER stress conditions (Fig. 3B). Our results suggest that both CRP-1 and CDC-42 may be specifically involved in the transmission/establishment of ER stress signals in *C. elegans*.

CRP-1 interacts with CDC-48. To investigate the mechanisms by which CRP-1 may contribute to *pckb-2*::*gfp* induction upon TM treatment, we sought to characterize CRP-1 molecular partners. To this end, we performed a CRP-1 GST pull-down on *C. elegans* total protein extracts followed by SDS-PAGE and mass spectrometry analysis. We identified 20 proteins with various functions, out of which one, the ATPase CDC-48.1 (C06A1.1), which is orthologous to the transitional ER AAA^+ ATPase P97/VCP/CDC-48, was previously reported to display ER-related specific functions (Fig. 4A; see Table S2 in the supplemental material). In addition, although a Mascot search indicated that the hit corresponded to CDC-48.1, the peptides identified by de novo sequencing were common to both CDC-48.1 and CDC-48.2.

CDC-48 has been implicated in the ERAD pathway and in ER membrane fusion (13) and has been identified as a regulator of the ER stress response (48). We confirmed the interaction between CRP-1 and CDC-48 using both GST–CRP-1 and the mouse His_6–P97/VCP/CDC-48 fusion protein expressed in *E. coli*. In this experiment, *E. coli* lysates containing either GST–CRP-1 or GST–CDC-42 were mixed with His_6–P97/VCP/CDC-48-containing lysate followed by pull-down using glutathione-Sepharose beads. As shown in Fig. 4B, P97/VCP/CDC-48 was found in the CRP-1 complex, thus confirming the mass spectrometry analyses. Interestingly, no interaction between P97/VCP/CDC-48 and CDC-42 was detected under these conditions (Fig. 4B). The reverse experiment was also carried out using N2 and CRP-$1^{-/-}$ (allele *ok685*) (19) worm lysates, which were pulled-down using His_6-P97/VCP/CDC48 immobilized on Ni-agarose beads (Fig. 4B). As expected, a complex between P97/VCP/CDC-48 and CRP-1 was observed in wild-type animals but not in the CPR-$1^{-/-}$ worm lysates. The hypothesis supporting a functional interaction between CRP-1 and CDC-48 was also reinforced using *cdc-48.1* silencing in *pckb-2*::*gfp* reporter worms. As observed for *crp-1*, reduction of *cdc-48.1* expression led to an inhibition of TM-induced *pckb-2*::*gfp* reporter activation (Fig. 4C). This phenotype suggests that *pckb-2*::*gfp* activation by TM requires both CRP-1 and CDC-48.1.

Among the proteins identified by mass spectrometry, two other hits presented some interest. Indeed, ATM-1 (Y48G1BL.2) and HIM-6 (T04A11.6) are, respectively, an ortholog of the human protein kinase ATM and the human Bloom syndrome helicase (BLM), a RecQ-like ATP-dependent DNA helicase. BLM was shown to be a direct substrate of ATM, and both proteins are required for optimal repair during DNA replication (1, 36). Recently, p97/VCP/CDC-48 was also shown to be a direct substrate of ATM kinase, but the physiological function of this interaction remains unclear (26). Finally, it was shown that p97/VCP/CDC-48 interacted with another RecQ helicase, WRN, and modulated its localization and functions (18). As a consequence, we postulated that we might have purified a complex of proteins implicated in DNA repair, DNA remodeling, or transcriptional processes and containing at least CRP-1, CDC-48, and ATM-1.

Using the STRING program suite (http://string.embl.de/), a database for the retrieval of known and predicted gene/proteins interactions (46, 47), we built a network based on the human orthologs of the *C. elegans* proteins identified in the CRP-1 GST pull-down (Fig. 4D, white nodes; see Table S3 in the supplemental material). Interestingly, 9 out of the 20 proteins identified by mass spectrometry (Fig. 4D, white nodes) were found to belong to a specific subnetwork implicated in DNA processes (Fig. 4D, black nodes) and including the transcriptional activator p53, ATM, BLM, and P97/VCP/CDC-48. In contrast, none of the proteins found in complex with CRP-1 belonged to the other p97/VCP/CDC-48 subnetwork functionally related to ERAD or membrane fusion (Fig. 4D, gray nodes). In addition, when we attempted to identify other po-

Downloaded from mcb.asm.org at McGill Univ on January 19, 2010

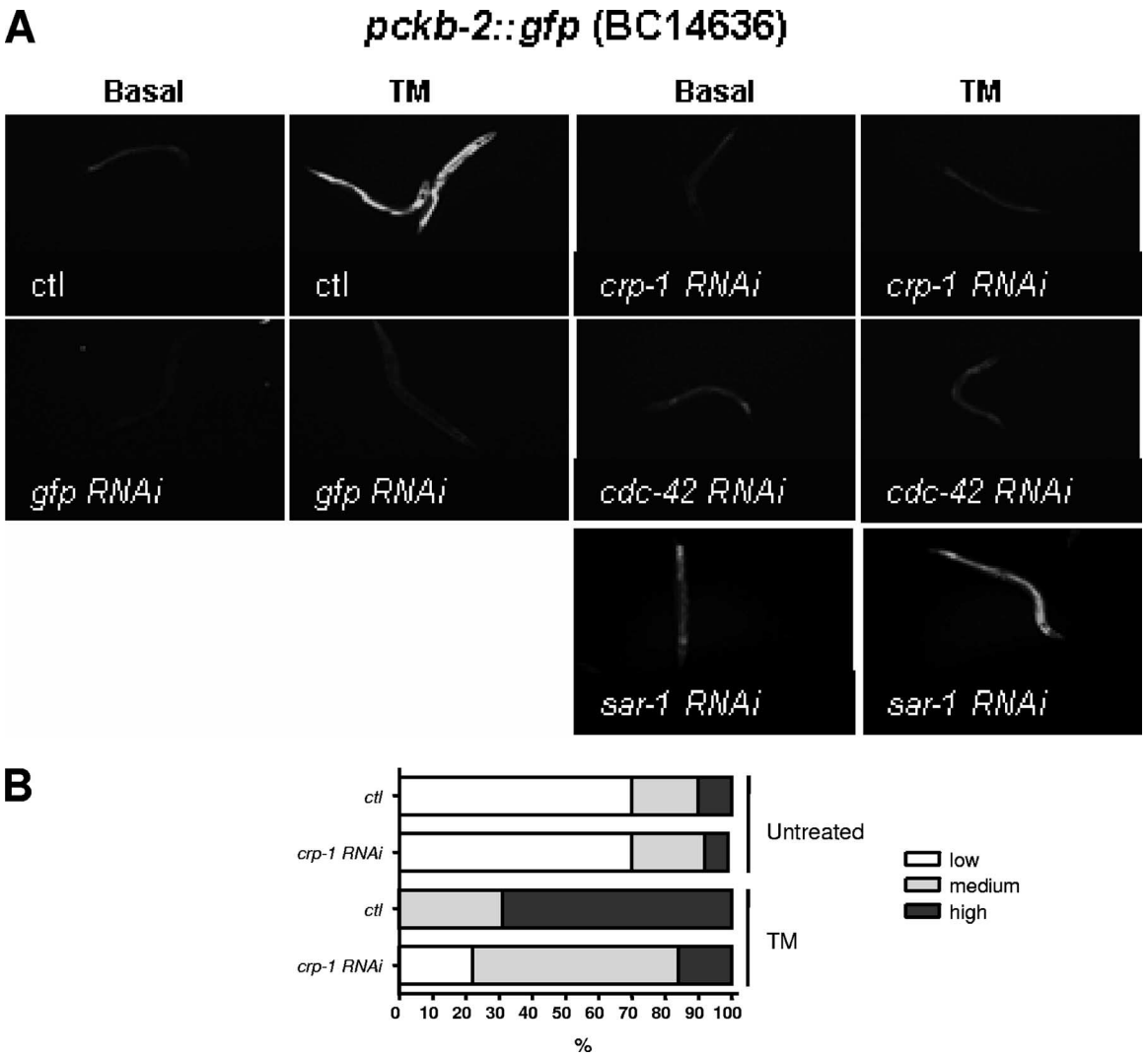

FIG. 3. Effect of *crp-1*, *cdc-42*, and *sar-1* silencing on *ckb-2* promoter activation upon ER stress. (A) Qualitative microscopic pictures for two controls (no RNAi induction [ctl] or GFP RNAi) and three GTPases that gave the most significant results for *pckb-2*::*gfp* reporter activation (encoded by *crp-1*, *cdc-42*, and *sar-1*). (B) Quantification of fluorescence induction of *pckb-2*::*gfp* subjected or not to *crp-1* RNAi and exposed or not to 5 μg/ml TM.

tential functional networks in which proteins found in the CRP-1 GST pull-down could be enriched, no significant other group could be generated (data not shown). This specific functional enrichment further supported the idea that CRP-1 might interact with a protein complex implicated in DNA remodeling/transcription.

Physical interactions regulating the complex including CRP-1, CDC-48, and HIM-6. To further evaluate the relevance of a protein complex including CRP-1, HIM-6, and CDC-48, we evaluated the in vitro interactions between these three proteins. To this end, we used the previously described GST–CRP-1 as well as bacterial recombinant HIM-6 and CDC-48.1, both N-terminally tagged by either six histidine residues or a Strep tag and produced as described in Materials and Methods. We established the existence of six possible interactions to be tested in vitro. We first tested the direct interactions between CRP-1 and HIM-6 and between CRP-1 and CDC-48.1. As shown in Fig. 5A, CRP-1 did not directly bind to HIM-6 but, as expected from the results obtained in Fig. 4, directly interacted with CDC-48.1 (similar results were obtained with CDC-48.2 [data not shown]). We then evaluated the association between HIM-6 and CDC-48.1. To this end, six-His-tagged CDC-48.1 or HIM-6 was incubated in the presence of Strep-tagged HIM-6 or CDC-48.1, respectively; the mixture was then pulled-down using Ni-NTA-agarose beads and immunoblotted using anti-Strep tag antibodies. These experiments revealed that HIM-6 directly associated with CDC-48.1 (Fig. 5B). This result was not that surprising, as P97, the mammalian ortholog of CDC-48, binds to the Werner syndrome RecQ helicase, which is homologous to BLM, the mammalian ortholog of HIM-6. In an attempt to test for the existence of a ternary complex, we incubated GST–CRP-1 with Strep-tagged HIM-6 and increasing concentrations of His_6–CDC-48.1 (Fig. 5C). The mixture was then subjected to a pull-down using glutathione-Sepharose beads and immunoblotted using anti-Strep tag antibodies. The analysis revealed the existence of a

Downloaded from mcb.asm.org at McGill Univ on January 19, 2010

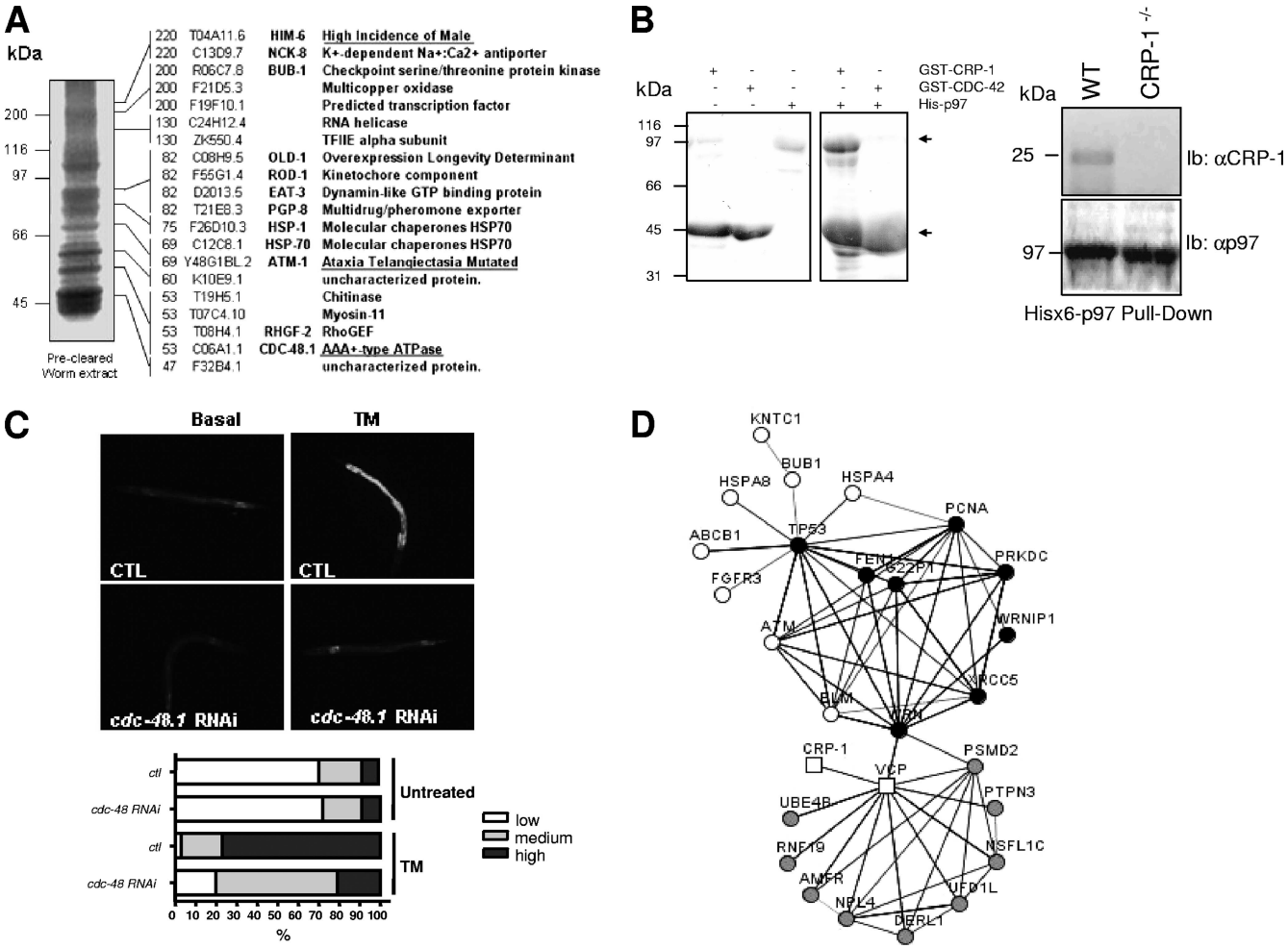

FIG. 4. CRP-1 interacts with a protein complex which includes CDC-48.1 and ATM-1. (A) SDS-PAGE of the GST–CRP-1 pull-down performed on precleared worm lysate, followed by mass spectrometry analysis (right). Peptides identified were annotated using the WormBase (http://www.wormbase.org/) sequence name as well as the *Caenorhabditis* Genetic Center (http://www.cbs.umn.edu/CGC/) three-letter name. (B, left) GST pull-down using GST–CRP-1 or GST–CDC-42 and mouse His_6-p97/VCP/CDC-48 recombinant proteins expressed in bacteria and resolved on SDS-PAGE gel stained with Coomassie blue R250. (Right) His_6-p97/VCP/CDC-48 pull-down was performed on wild-type (WT) (N2) or *crp-1*$^{-/-}$ total worm extract followed by immunoblot analysis using anti (α)-CRP-1 antibodies (HyperOmics Farma, Inc.) or anti-p97 antibodies. (C) Transcriptional regulation of *pckb-2*::*gfp* reporter by *cdc-48*. *pckb-2*::*gfp* transgenic worms were subjected or not to *cdc-48.1* RNAi as described in Materials and Methods. Following exposure to TM, *pckb-2*::*gfp* activation was visualized and quantified using fluorescence microscopy. (D) STRING network representation of the known and predicted interactions between proteins identified by mass spectrometry (white), VCP (p97/VCP/CDC-48) first-interacting proteins (gray), and ATM-1 first-interacting proteins (black). The edges are representative of the various interaction types available through STRING. Circles and squares are indicative of human and *C. elegans* genes, respectively (see also Table S3 in the supplemental material).

ternary complex comprising CRP-1, HIM-6, and CDC-48, with the last bridging the two others (Fig. 5C). This allowed us to build an interaction model where CRP-1 is in complex with HIM-6 through interaction with CDC-48. In this model, ATM-1 could play a regulatory role by phosphorylating both CDC-48 and HIM-6 since the mammalian orthologs of these proteins are established ATM substrates (26).

***C. elegans* resistance to ER stress is controlled though genetic interactions between *crp-1*, *cdc-48.1*, and *atm-1*.** To evaluate the functional relevance of such a complex, we hypothesized that CRP-1, CDC-48.1, and ATM-1 could constitute a functional protein complex involved in an ER stress-mediated transcriptional regulatory pathway. We then postulated that mutations in these proteins would cause defects in their ER stress-adaptive capacity. Consequently, we tested the susceptibility of wild-type and knockout strains subjected to treatments with increasing TM concentrations. Under basal conditions, wild-type worms (N2) as well as *crp-1* (*ok685*), *cdc-48.1* (*tm544*), and *atm-1* (*gk186*) knockout strains developed normally and the growth rate of wild-type (N2) worms was not affected until the concentration of TM reached 5 μg/ml (Fig. 6A and B). At this concentration, less than 20% of the N2 worms failed to develop to adults. In contrast, *crp-1*$^{-/-}$, *atm-1*$^{-/-}$, and to a lesser extent *cdc-48*.1$^{-/-}$ knockout strains were more sensitive to TM than N2 worms (Fig. 6A and B). At 2 μg/ml of TM, more than 60% of all the *crp-1*$^{-/-}$ mutants and 30% of the *atm-1*$^{-/-}$ mutants were arrested at the L1 larval stages compared to less than 1% of wild-type worms. *Cdc-*

Downloaded from mcb.asm.org at McGill Univ on January 19, 2010

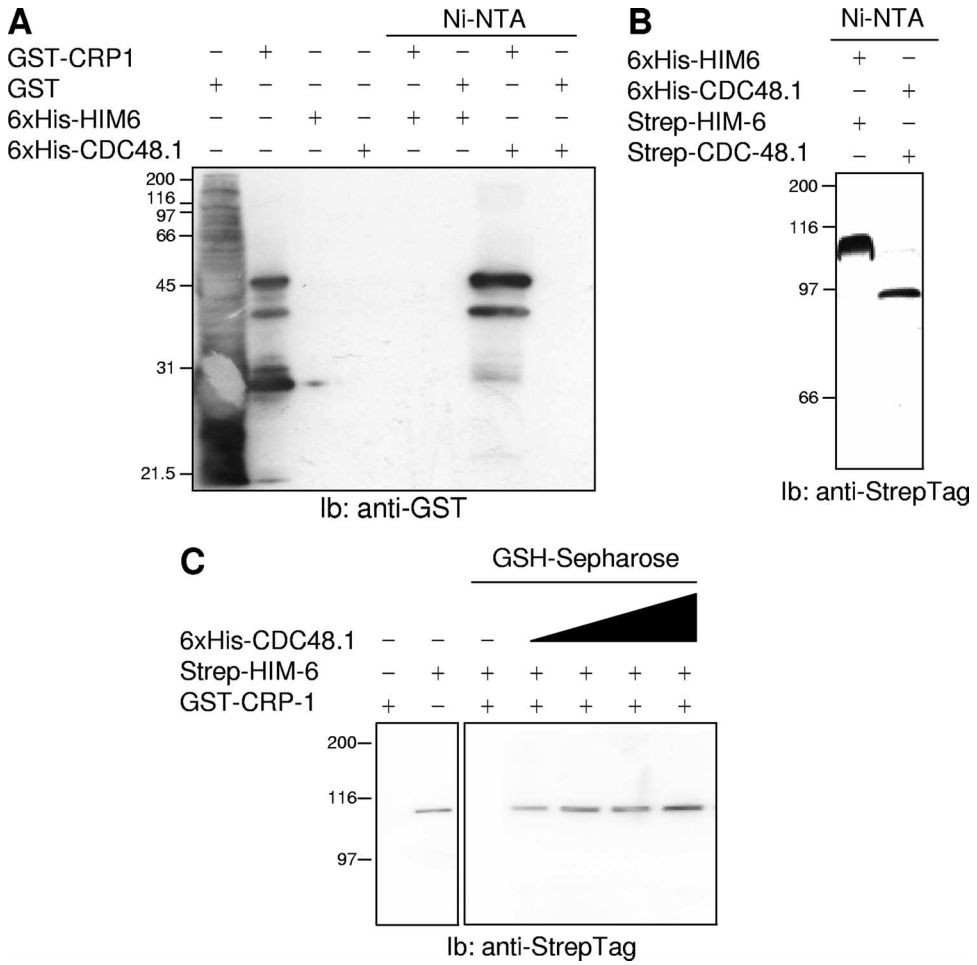

FIG. 5. Physical interactions between CRP-1, HIM-6, and CDC-48. (A) Binary interactions between CRP-1 and either His_6–HIM-6 or His_6–CDC-48. The purified proteins were pulled-down using Ni-NTA-agarose beads, and the presence of GST–CRP-1 was revealed by immunoblotting (Ib) using anti-GST antibodies. (B) Binary interactions between His_6–CDC-48.1 and Strep-tagged HIM-6 or His_6–HIM-6 and Strep-tagged CDC-48.1 following purification of the complex by Ni-NTA-agarose beads and analysis by immunoblotting using anti-Strep tag antibodies. (C) Ternary complex including CRP-1, HIM-6, and CDC-48.1. Increasing concentrations of His_6–CDC-48.1 were added to an equimolar mixture of GST–CRP-1 and Strep-tagged HIM-6. Following 1 h of incubation on ice, the complex was pulled-down using glutathione-Sepharose beads and the presence of HIM-6 in the complex was evaluated by immunoblotting using anti-Strep tag antibodies.

48.1$^{-/-}$ mutants displayed a similar phenotype at a 5-μg/ml concentration of TM, where 70% of *cdc-48.1*$^{-/-}$ mutants failed to develop to adults compared to 20% of wild-type animals. These results suggest that *crp-1*, *cdc-48.1*, and *atm-1* are required for worm adaptation to stress conditions and for larva development.

To further investigate this observation, we aimed at establishing functional interactions between these three genes. Identification of genetic interactions is a useful way to investigate functional relationships between two genes. Consequently, we subjected *atm-1*$^{-/-}$ and *cdc-48.1*$^{-/-}$ knockout strains to RNAi treatment targeting *crp-1* and measured the resistance of these double mutants to TM. Interestingly, in both conditions, reduction of *crp-1* expression suppressed the hypersensitivity of *cdc-48*$^{-/-}$ and *atm-1*$^{-/-}$ mutants to TM (Fig. 6C). Indeed, when sujected to 5 μg/ml *crp-1* RNAi, a *cdc-48.1*$^{-/-}$ mutant exhibited development rates similar to that of N2 worms, with 80% of the animals developing normally. In a similar manner, exposure to 2-μg/ml *crp-1* silencing of an *atm-1*$^{-/-}$ mutant led to better resistance to TM and 90% of the animals were able to develop to adult stages. An attenuating phenotype was also observed when the *atm-1*$^{-/-}$ strain was subjected to *cdc-48.1* RNAi (Fig. 6D). These results show that *crp-1*, *atm-1*, and *cdc-48* interact genetically and may then have antagonistic functions with respect to an ER stress signaling event occurring upon TM treatment. In addition, these results led us propose the existence of an alternative, ERAD-independent p97/VCP/CDC-48 pathway. Indeed, this protein may associate with a functional complex containing CRP-1 and ATM-1 to regulate the transcriptional level of UPR-induced genes (Fig. 6) in a manner similar to that occurring in the IRE-1/XBP-1 axis (see Fig. S2 in the supplemental material).

Genetic interactions between CRP-1 and the UPR components. In an attempt to further dissect the role of CRP-1 in the ER stress response, we analyzed using RT-PCR the expression of seven genes, *hsp-4*, *srp-7*, *dnj-27*, *cht-1*, *ckb-2*, *F22E5.6*, and *xbp-1*, that were previously reported to be specifically regulated by the UPR (42, 45). These genes were selected on the basis of

Downloaded from mcb.asm.org at McGill Univ on January 19, 2010

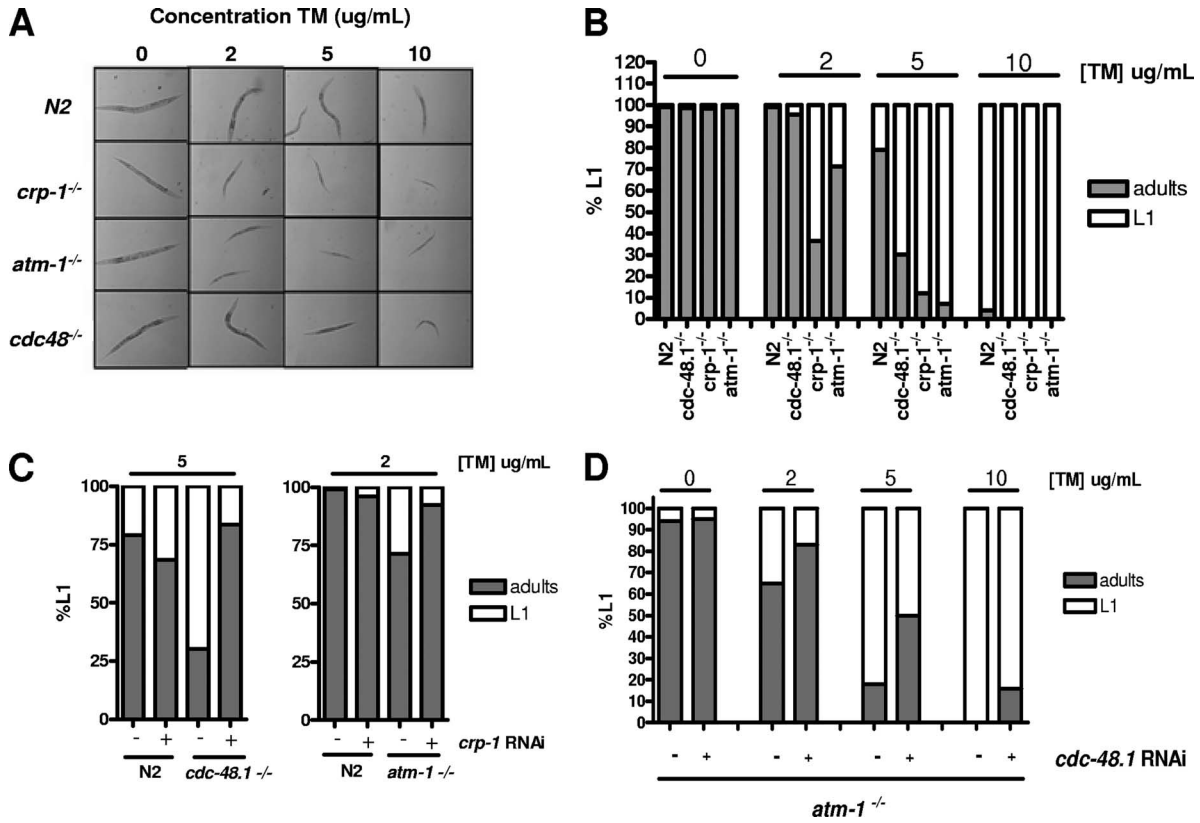

FIG. 6. *crp-1*$^{-/-}$, *atm-1*$^{-/-}$, and *cdc-48.1*$^{-/-}$ mutants are hypersensitive to TM and interact genetically. (A) Pictures showing the average sizes of wild-type (N2) and mutant worms when exposed to different concentrations of TM. (B) The percentage of progeny arrested in the L1 stage of development was plotted against the different concentrations of TM for the wild-type worms (N2) and *cdc-48.1*$^{-/-}$ (tm544), *crp-1*$^{-/-}$ (ok685), and *atm-1*$^{-/-}$ (gk186) mutants. (C and D) The percentage of progeny arrested in L1 stages of development was plotted against the different concentrations of TM for *cdc-48.1*$^{-/-}$ and *atm-1*$^{-/-}$ mutants subjected of not to *crp-1* RNAi (C) and for the *atm-1*$^{-/-}$ mutant subjected of not to *cdc-48* RNAi (D).

two transcriptome analyses (42, 45). The expression of the corresponding mRNAs was normalized using the expression levels of *ama-1*, previously reported not to be a UPR target (22). To evaluate the expression levels of the mRNAs, N2 or *crp-1*$^{-/-}$ worms were treated with TM, DTT (oxidative stress), or sodium azide (hypoxia) as described in Materials and Methods. Interestingly, the absence of CRP-1 did not significantly affect the expression levels of *srp-7*. More importantly, a differential response was observed for the other genes, with attenuated expression in *crp-1*$^{-/-}$ worms of *xbp-1* and *ckb-2* and increased expression of *hsp-4* and *F22E5.6* (Fig. 7 A and B). The response also varied depending on the stress applied to the worms, as observed in Fig. 2. In addition, we assessed the effect on the splicing of *xbp-1* mRNA of the above-mentioned stresses. mRNA splicing was slightly attenuated upon TM treatment in *crp-1*$^{-/-}$ animals but remained unchanged upon treatment with other stressors (Fig. 7C; $P < 0.02$).

As the above-selected genes were found to be downstream of PEK-1/IRE1 (*F22E5.6*), ATF-6/IRE-1 (*cht-1*, *xbp-1*), or IRE1 (*srp-7*, *dnj-27*, *hsp-4*, *ckb-2*) signaling, our next objective was to evaluate the genetic interactions between *crp-1* and the three proximal ER stress sensors, PEK-1, ATF-6, and IRE-1. To this end, *pek-1*$^{-/-}$ and *atf-6*$^{-/-}$ worms were subjected to *crp-1* RNAi and treated or not with increasing concentrations of TM (2 or 5 μg/ml). To evaluate the genetic interaction between *crp-1* and *ire-1*, the opposite experiment was performed: we used *crp-1*$^{-/-}$ animals and subjected them to *xbp-1* RNAi. This experiment was carried out since the *ire-1*$^{-/-}$ strain showed a developmental defect in the early stage and was very sensitive to TM. Interestingly, *crp-1* silencing did not significantly affect the sensitivity of *pek-1*$^{-/-}$ animals to TM (Fig. 8A and B). In contrast, when *crp-1* was silenced in *atf-6*$^{-/-}$ animals, the worms turned out to be less sensitive to TM treatment than nonsilenced animals, thus suggesting that CRP-1 may function synergistically with ATF-6 to transduce adaptive signals (Fig. 8C). Interestingly, this phenomenon correlates with the observed up-regulation of total *xbp-1* mRNA in *crp-1*$^{-/-}$ animals upon TM treatment, as *xbp-1* was previously described as a transcriptional target of ATF-6.

DISCUSSION

ER stress is a physiological response that occurs in normal processes such as plasma cell differentiation (31), insulin secretion by pancreatic beta cells (14), and cytokinesis (3). In addition, it can be activated in the course of environmental perturbation and diseases (14, 29, 31). Although the molecular entities and mechanisms involved in the activation and trans-

Downloaded from mcb.asm.org at McGill Univ on January 19, 2010

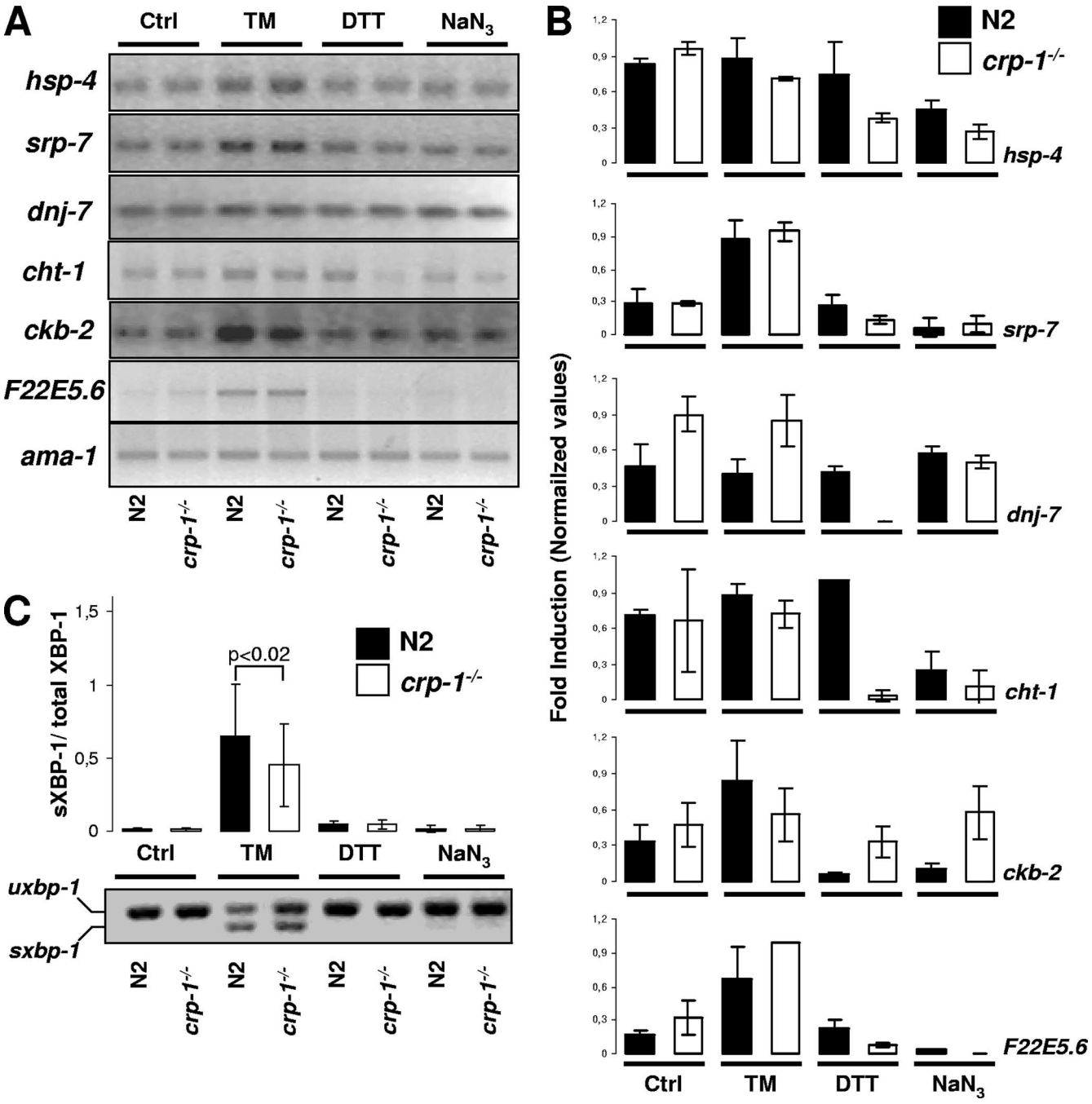

FIG. 7. CRP-1-dependent regulation of the UPR transcriptional response. (A) Evaluation of the expression of the UPR target genes *hsp-4*, *srp-7*, *dnj-7*, *cht-1*, *ckb-2*, and *F22E5.6* by RT-PCR analysis on mRNA isolated from worms treated or not with 5 μg/ml TM or 2 mM DTT for 5 h or 10 mM sodium azide for 90 min. PCR products are visualized following resolution by agarose gel electrophoresis, staining with ethidium bromide, and UV transillumination. Ctrl, control. (B) Quantification of the gels presented in panel A. Values relative to the expression of a control mRNA (*ama-1*) are reported and were obtained following normalization. The graphs represent the averages of three independent experiments ± standard deviations (SD). (C) Assessment of *xbp-1* mRNA splicing using RT-PCR on mRNA collected as described above. PCR products are visualized followed resolution by agarose gel electrophoresis, staining with ethidium bromide, and UV transillumination (bottom). The graph shows the quantification of spliced *xbp-1* mRNA (sXBP-1)/spliced plus unspliced *xbp-1* mRNA (total XBP-1) as deduced from three independent experiments ± SD.

mission of ER stress signals have been really well characterized in the past 10 years (30, 38, 41), the existence of regulatory pathways remains to be investigated.

In an attempt to identify novel regulators of the UPR, we characterized eight GFP reporters to allow rapid and efficient detection of ER stress in living *C. elegans*. Only two reporters, *pF48E3.3*::*gfp* and *pbre-1*::*gfp*, were not responsive to TM. Besides a per se nonresponsiveness to ER stress, the lack of

Downloaded from mcb.asm.org at McGill Univ on January 19, 2010

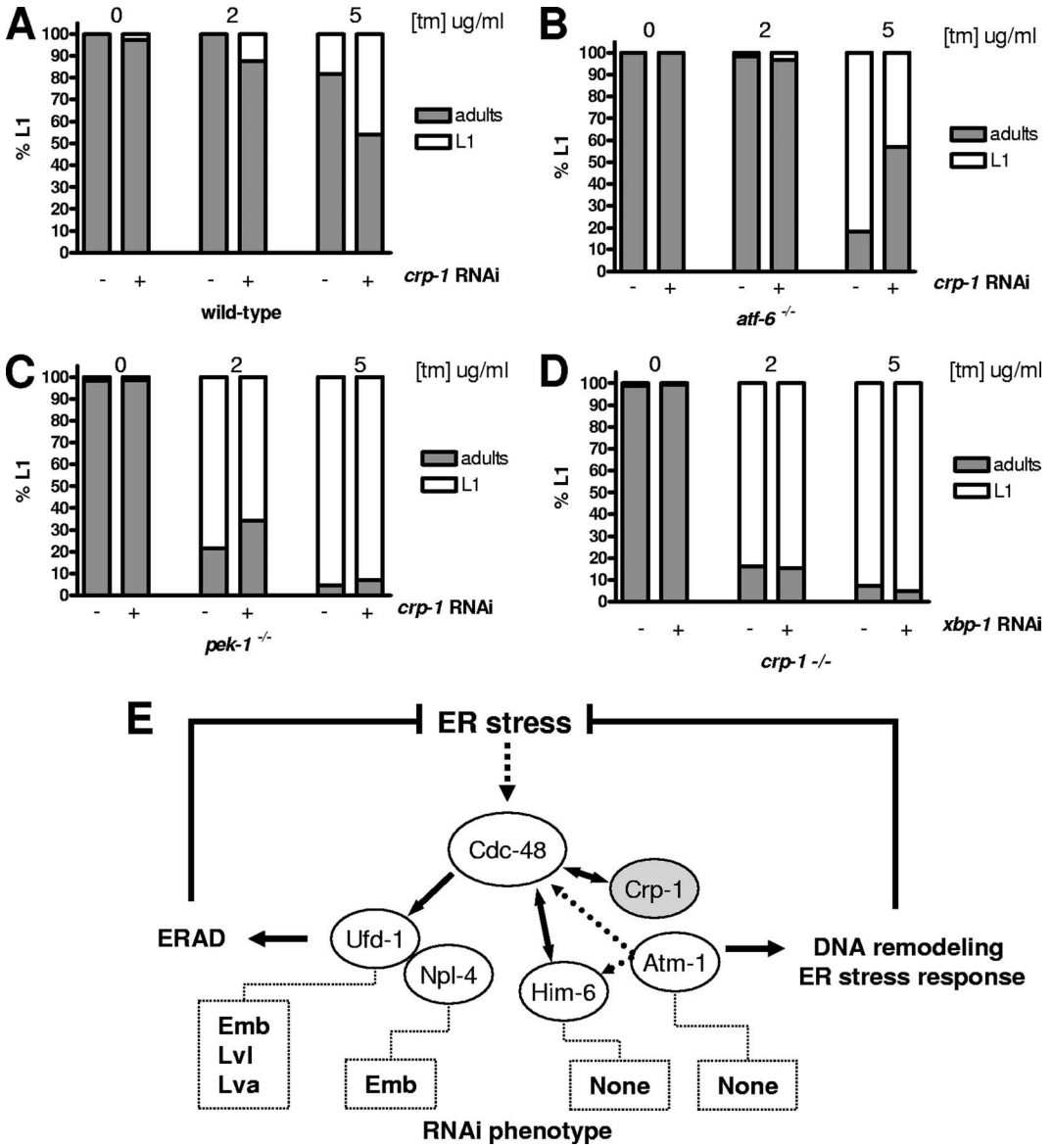

FIG. 8. Genetic interaction map linking *crp-1* and the UPR proximal sensors. (A to C) The percentage of progeny arrested in the L1 stage of development was plotted against different concentrations of TM (2 or 5 μg/ml) for N2 (A), *pek-1*$^{-/-}$ (B), and *atf-6*$^{-/-}$ (C) animals subjected or not to *crp-1* RNAi. (D) The percentage of progeny arrested in the L1 stage of development was plotted against different concentrations of TM (2 or 5 μg/ml) for *crp-1*$^{-/-}$ animals subjected to *xbp-1* RNAi. (E) Schematic representation of CDC-48-dependent pathways proposed to explain the implication of CRP-1, HIM-6, and ATM-1 in the regulation of ER homeostasis during stress condition through DNA remodeling/transcriptional processes.

induction of these two reporters could be attributed to (i) gene expression exclusively in tissues or cells that are less exposed to TM, (ii) fluorescence levels too low to be detected using the Copas Biosort, or finally (iii) the region cloned to construct the GFP reporter not including all the regulatory elements required for promoter activation. We selected three specific reporters that were highly induced upon ER stress and displayed major intestinal expression. Interestingly, the activation of the different reporter construct-selected promoters was dependent on the ER stress inducer (TM, AZC, DTT, or TG) used for our experiment, supporting the conservation in *C. elegans* of a UPR machinery known to be extremely complex and multimodular in mammals (42). To provide functional insights into regulatory mechanisms taking place during UPR activation, we used a reverse genetic approach combining gene silencing and analysis of in vivo GFP reporters upon basal and ER stress conditions. At first, we evaluated the role of 13 GTPases either localized in the ER or along the secretory pathway or implicated in ER-related function to increase the chances of affecting ER stress signaling. The silencing of most of the GTPases did not show any effect on the reporter. Even if the entire reading frames were used to perform the RNAi, we could not exclude the possibility that these negative observations may result from RNAi inefficiency in degrading target mRNAs.

Downloaded from mcb.asm.org at McGill Univ on January 19, 2010

Indeed, many factors can dramatically reduce the effectiveness of an RNAi experiment. First, dsRNA introduced into the worms might not be abundant enough to completely degrade the target mRNA. This is particularly true for mRNAs that are highly expressed or which have a low turnover (long half-life). The tissue localization of the GTPase mRNA is also an important factor to consider. Since the GFP reporter used in our experiments was mainly expressed in the worm intestine, GTPases expressed in other tissues might have a lower impact on the activation of this promoter.

Our experimental approach allowed us to identify three GTPases, namely, SAR-1, CDC-42, and CRP-1, as important regulators of ER stress signaling under either basal or stress conditions. Indeed silencing of SAR-1, which belongs to the COPII complex, led to the activation of ER stress under basal conditions. This observation could be explained by the required presence of SAR-1 for protein progression from the ER; the resulting protein accumulation may be sufficient to saturate ER folding capacity and lead to ER stress.

On the other hand, silencing of CDC-42 and CRP-1 prevented TM-induced *pckb-2*::*gfp* activation. These proteins are two homologous member of the Rho subfamily of GTPases. We then sought to investigate the molecular mechanisms responsible for this observation. To this end, CRP-1-interacting partners were characterized by CRP-1–GST pull-down followed by mass spectrometry analysis. Integration of these data to a STRING-based (46, 47) functional network representation of CRP-1 partners showed that most of the hits identified were involved in transcriptional and DNA-monitoring/repair processes. We showed that the transcription-regulatory role of CRP-1 also required a direct interaction with the AAA^+ ATPase CDC-48.1. It is noteworthy that both genetic and physical interactions between GTPases of the RAS superfamily and AAA ATPases have been reported in the literature to be relevant to specific physiological and pathological mechanisms (12, 44).

CDC-48 is a mostly cytosolic chaperone involved in several cellular pathways, such as organelle maintenance through homotypic membrane fusion of the ER, Golgi apparatus, and nuclear envelope, and degradation of misfolded proteins via ERAD (13). This protein is homologous to the mammalian P97/VCP/CDC-48, which is also found in the nucleus and directly binds to the RecQ domain of Werner syndrome helicase (WRN) (18, 32). Interestingly, when we characterized CRP-1-interacting proteins, we found the *C. elegans* Bloom syndrome helicase homolog HIM-6, which shows a RecQ domain conserved with that of WRN. Moreover, in the complex, we also detected the ATM-1 kinase, which is known to phosphorylate BLM and VCP in mammalian systems (26). We confirmed that CRP-1 can directly interact with CDC-48 in vitro but not with HIM-6. The CRP-1/HIM-6 complex was made possible by the presence of CDC-48, which bridges those proteins (Fig. 5). The role of ATM-1 in this complex remains to be further investigated. However, as BLM (the HIM-6 mammalian ortholog) and P97/VCP (the CDC-48 mammalian ortholog) are both ATM substrates, this kinase may represent a key regulatory component of the DNA remodeling/transcriptional functions of the complex. As a consequence, we believe that CDC-48 might act as a scaffold to create a new functional complex between HIM-6, CRP-1, and possibly ATM-1, which could in turn activate/inactivate specific transcriptional programs, as evidenced in Fig. 7A and B.

In addition, we propose a novel role for P97/VCP/CDC-48 in the regulation of ER stress. Indeed, this protein could function in parallel (and perhaps independently) to ERAD because (i) none of the CRP-1-interacting partners found in the P97/VCP/CDC-48 functional subnetwork were implicated in ERAD and membrane fusion (Fig. 5D), (ii) these two events are known to occur in different subcellular compartments, with ERAD occurring mainly in the cytosol, whereas the mechanisms identified here are believed to take place in the nucleus, and finally (iii) silencing of P97/VCP/CDC-48-interacting partners involved in ERAD (NPL-4 and UFD-1) leads to lethal phenotypes, which is not the case for HIM-6 and ATM-1 (Fig. 6). The last observation may rely on the fact that either the CDC-48-dependent transcriptional program activated in response to ER stress is dispensable or redundant mechanisms can compensate for the absence of HIM-6 (e.g., WRN-1) or ATM-1 (e.g., ATL-1).

In addition to this evidence, we have demonstrated that *crp-1* genetically interacted with *atf-6*, as the absence of CRP-1 decreased the sensitivity of ATF-6-deficient but not PEK-1-deficient worms to TM (Fig. 8). This suggested that, similar what that occurs in the IRE-1/XBP-1 axis (see Fig. S2 in the supplemental material), the CRP-1/CDC-48/HIM-6 complex is implicated in the regulation of subsets of genes required for ER stress adaptation. This phenomenon could potentially be explained by the substantial redistribution of CRP-1 from punctate structures to more-diffuse areas, which is observed upon TM treatment (see Fig. S3 in the supplemental material). Although the subcellular localization of the complex and its dynamics remain to be fully investigated, our data suggest that TM treatment may alter the localization of CRP-1 and CDC-48 to promote their nuclear localization (see Fig. S3 in the supplemental material) (32) by a yet-undetermined mechanism. In this compartment, a ternary complex between CRP-1, CDC-48, and HIM-6 may form to promote DNA remodeling/gene transcription control. This complex may then be regulated by the activation of the ATM-1 pathway (stabilized or destabilized), as suggested by the observation, made by Partridge and colleagues, that in mammalian cells DNA damage, an ATM activator, promotes the dissociation of the RecQ helicase WRN from the CDC-48 ortholog P97/VCP (32).

Our results unravel the existence of a novel pathway dependent on the GTP binding protein CRP-1 and the AAA+ ATPase CDC-48 which controls a specific UPR-mediated transcriptional response to promote cell adaptation to ER stress. This pathway may be dependent on DNA remodeling mechanisms, as indicated by the complex formed by CRP-1, CDC-48, and the RecQ DNA helicase HIM-6, and may be activated independently of ERAD (Fig. 8E).

ACKNOWLEDGMENTS

We thank A. Higa-Nishiyama for help with confocal microscopy and O. Pluquet, V. Moreau, M. Dominguez, and P. Legembre for critical reading of the manuscript. We also thank the *Caenorhabditis* Genetics Center for *C. elegans* strains.

This work was supported by grants from the Fond de Recherche en Santé du Québec, INSERM (Avenir), and a Marie Curie reintegration grant to E.C. M.E.C. was a recipient of a FRNTQ Ph.D. studentship.

Downloaded from mcb.asm.org at McGill Univ on January 19, 2010

REFERENCES

1. **Ababou, M., S. Dutertre, Y. Lecluse, R. Onclercq, B. Chatton, and M. Amor-Gueret.** 2000. ATM-dependent phosphorylation and accumulation of endogenous BLM protein in response to ionizing radiation. Oncogene **19:** 5955–5963.
2. **Altan-Bonnet, N., R. Sougrat, and J. Lippincott-Schwartz.** 2004. Molecular basis for Golgi maintenance and biogenesis. Curr. Opin. Cell Biol. **16:**364–372.
3. **Bicknell, A. A., A. Babour, C. M. Federovitch, and M. Niwa.** 2007. A novel role in cytokinesis reveals a housekeeping function for the unfolded protein response. J. Cell Biol. **177:**1017–1027.
4. **Braakman, I., J. Helenius, and A. Helenius.** 1992. Manipulating disulfide bond formation and protein folding in the endoplasmic reticulum. EMBO J. **11:**1717–1722.
5. **Brenner, S.** 1974. The genetics of *Caenorhabditis elegans*. Genetics **77:**71–94.
6. **Calfon, M., H. Zeng, F. Urano, J. H. Till, S. R. Hubbard, H. P. Harding, S. G. Clark, and D. Ron.** 2002. IRE1 couples endoplasmic reticulum load to secretory capacity by processing the XBP-1 mRNA. Nature **415:**92–96.
7. **Caruso, M. E., and E. Chevet.** 2007. Systems biology of the endoplasmic reticulum stress response. Subcell. Biochem. **43:**277–298.
8. **Caruso, M. E., S. Jenna, S. Beaulne, E. H. Lee, A. Bergeron, C. Chauve, P. Roby, J. F. Rual, D. E. Hill, M. Vidal, R. Bosse, and E. Chevet.** 2005. Biochemical clustering of monomeric GTPases of the Ras superfamily. Mol. Cell. Proteomics **4:**936–944.
9. **Chevet, E., P. H. Cameron, M. F. Pelletier, D. Y. Thomas, and J. J. Bergeron.** 2001. The endoplasmic reticulum: integration of protein folding, quality control, signaling and degradation. Curr. Opin. Struct. Biol. **11:**120–124.
10. **Chevet, E., C. A. Jakob, D. Y. Thomas, and J. J. Bergeron.** 1999. Calnexin family members as modulators of genetic diseases. Semin. Cell Dev. Biol. **10:**473–480.
11. **Dupuy, D., N. Bertin, C. A. Hidalgo, K. Venkatesan, D. Tu, D. Lee, J. Rosenberg, N. Svrzikapa, A. Blanc, A. Carnec, A. R. Carvunis, R. Pulak, J. Shingles, J. Reece-Hoyes, R. Hunt-Newbury, R. Viveiros, W. A. Mohler, M. Tasan, F. P. Roth, C. Le Peuch, I. A. Hope, R. Johnsen, D. G. Moerman, A. L. Barabasi, D. Baillie, and M. Vidal.** 2007. Genome-scale analysis of in vivo spatiotemporal promoter activity in *Caenorhabditis elegans*. Nat. Biotechnol. **25:**663–668.
12. **Evans, K., C. Keller, K. Pavur, K. Glasgow, B. Conn, and B. Lauring.** 2006. Interaction of two hereditary spastic paraplegia gene products, spastin and atlastin, suggests a common pathway for axonal maintenance. Proc. Natl. Acad. Sci. USA **103:**10666–10671.
13. **Halawani, D., and M. Latterich.** 2006. p97: the cell's molecular purgatory? Mol. Cell **22:**713–717.
14. **Harding, H. P., and D. Ron.** 2002. Endoplasmic reticulum stress and the development of diabetes: a review. Diabetes **51**(Suppl. 3)**:**S455–S461.
15. **Hemming, F. W.** 1982. Control and manipulation of the phosphodolichol pathway of protein N-glycosylation. Biosci. Rep. **2:**203–221.
16. **Hooper, S. D., and P. Bork.** 2005. Medusa: a simple tool for interaction graph analysis. Bioinformatics **21:**4432–4433.
17. **Hunt-Newbury, R., R. Viveiros, R. Johnsen, A. Mah, D. Anastas, L. Fang, E. Halfnight, D. Lee, J. Lin, A. Lorch, S. McKay, H. M. Okada, J. Pan, A. K. Schulz, D. Tu, K. Wong, Z. Zhao, A. Alexeyenko, T. Burglin, E. Sonnhammer, R. Schnabel, S. J. Jones, M. A. Marra, D. L. Baillie, and D. G. Moerman.** 2007. High-throughput in vivo analysis of gene expression in *Caenorhabditis elegans*. PLoS Biol. **5:**e237.
18. **Indig, F. E., J. J. Partridge, C. von Kobbe, M. I. Aladjem, M. Latterich, and V. A. Bohr.** 2004. Werner syndrome protein directly binds to the AAA ATPase p97/VCP in an ATP-dependent fashion. J. Struct. Biol. **146:**251–259.
19. **Jenna, S., M. E. Caruso, A. Emadali, D. T. Nguyen, M. Dominguez, S. Li, R. Roy, J. Reboul, M. Vidal, G. N. Tzimas, R. Bosse, and E. Chevet.** 2005. Regulation of membrane trafficking by a novel Cdc42-related protein in *Caenorhabditis elegans* epithelial cells. Mol. Biol. Cell **16:**1629–1639.
20. **Jenna, S., and E. Chevet.** 2007. High-throughput RNAi in *Caenorhabditis elegans*—from molecular phenotypes to pathway analysis, p. 158. *In* M. Latterich (ed.), RNAi. Taylor and Francis, New York, NY.
21. **Kamath, R. S., A. G. Fraser, Y. Dong, G. Poulin, R. Durbin, M. Gotta, A. Kanapin, N. Le Bot, S. Moreno, M. Sohrmann, D. P. Welchman, P. Zipperlen, and J. Ahringer.** 2003. Systematic functional analysis of the *Caenorhabditis elegans* genome using RNAi. Nature **421:**231–237.
22. **Kapulkin, W. J., B. G. Hiester, and C. D. Link.** 2005. Compensatory regulation among ER chaperones in *C. elegans*. FEBS Lett. **579:**3063–3068.
23. **Lavoie, C., E. Chevet, L. Roy, N. K. Tonks, A. Fazel, B. I. Posner, J. Paiement, and J. J. Bergeron.** 2000. Tyrosine phosphorylation of p97 regulates transitional endoplasmic reticulum assembly in vitro. Proc. Natl. Acad. Sci. USA **97:**13637–13642.
24. **Lazarow, P. B.** 2003. Peroxisome biogenesis: advances and conundrums. Curr. Opin. Cell Biol. **15:**489–497.
25. **Luna, A., O. B. Matas, J. A. Martinez-Menarguez, E. Mato, J. M. Duran, J. Ballesta, M. Way, and G. Egea.** 2002. Regulation of protein transport from the Golgi complex to the endoplasmic reticulum by CDC42 and N-WASP. Mol. Biol. Cell **13:**866–879.
26. **Matsuoka, S., B. A. Ballif, A. Smogorzewska, E. R. McDonald III, K. E. Hurov, J. Luo, C. E. Bakalarski, Z. Zhao, N. Solimini, Y. Lerenthal, Y. Shiloh, S. P. Gygi, and S. J. Elledge.** 2007. ATM and ATR substrate analysis reveals extensive protein networks responsive to DNA damage. Science **316:**1160–1166.
27. **McKay, S. J., R. Johnsen, J. Khattra, J. Asano, D. L. Baillie, S. Chan, N. Dube, L. Fang, B. Goszczynski, E. Ha, E. Halfnight, R. Hollebakken, P. Huang, K. Hung, V. Jensen, S. J. Jones, H. Kai, D. Li, A. Mah, M. Marra, J. McGhee, R. Newbury, A. Pouzyrev, D. L. Riddle, E. Sonnhammer, H. Tian, D. Tu, J. R. Tyson, G. Vatcher, A. Warner, K. Wong, Z. Zhao, and D. G. Moerman.** 2003. Gene expression profiling of cells, tissues, and developmental stages of the nematode *C. elegans*. Cold Spring Harbor Symp. Quant. Biol. **68:**159–169.
28. **Memon, A. R.** 2004. The role of ADP-ribosylation factor and SAR1 in vesicular trafficking in plants. Biochim. Biophys. Acta **1664:**9–30.
29. **Moenner, M., O. Pluquet, M. Bouchecareilh, and E. Chevet.** 2007. Integrated endoplasmic reticulum stress responses in cancer. Cancer Res. **67:**10631–10634.
30. **Mori, K.** 2004. Unfolded protein response as a quality control mechanism of proteins. Tanpakushitsu Kakusan Koso **49:**992–997. (In Japanese.)
31. **Otsu, M., and R. Sitia.** 2007. Diseases originating from altered protein quality control in the endoplasmic reticulum. Curr. Med. Chem. **14:**1639–1652.
32. **Partridge, J. J., J. O. Lopreiato, Jr., M. Latterich, and F. E. Indig.** 2003. DNA damage modulates nucleolar interaction of the Werner protein with the AAA ATPase p97/VCP. Mol. Biol. Cell **14:**4221–4229.
33. **Philips, M. R.** 2005. Compartmentalized signalling of Ras. Biochem. Soc. Trans. **33:**657–661.
34. **Philips, M. R.** 2004. Sef: a MEK/ERK catcher on the Golgi. Mol. Cell **15:**168–169.
35. **Quatela, S. E., and M. R. Philips.** 2006. Ras signaling on the Golgi. Curr. Opin. Cell Biol. **18:**162–167.
36. **Rao, V. A., A. M. Fan, L. Meng, C. F. Doe, P. S. North, I. D. Hickson, and Y. Pommier.** 2005. Phosphorylation of BLM, dissociation from topoisomerase IIIα, and colocalization with γ-H2AX after topoisomerase I-induced replication damage. Mol. Cell. Biol. **25:**8925–8937.
37. **Reboul, J., P. Vaglio, J. F. Rual, P. Lamesch, M. Martinez, C. M. Armstrong, S. Li, L. Jacotot, N. Bertin, R. Janky, T. Moore, J. R. Hudson, Jr., J. L. Hartley, M. A. Brasch, J. Vandenhaute, S. Boulton, G. A. Endress, S. Jenna, E. Chevet, V. Papasotiropoulos, P. P. Tolias, J. Ptacek, M. Snyder, R. Huang, M. R. Chance, H. Lee, L. Doucette-Stamm, D. E. Hill, and M. Vidal.** 2003. *C. elegans* ORFeome version 1.1: experimental verification of the genome annotation and resource for proteome-scale protein expression. Nat. Genet. **34:**35–41.
38. **Ron, D., and P. Walter.** 2007. Signal integration in the endoplasmic reticulum unfolded protein response. Nat. Rev. Mol. Cell Biol. **8:**519–529.
39. **Sabala, P., M. Czarny, J. P. Woronczak, and J. Baranska.** 1993. Thapsigargin: potent inhibitor of Ca^{2+} transport ATP-ases of endoplasmic and sarcoplasmic reticulum. Acta Biochim. Pol. **40:**309–319.
40. **Saloheimo, M., H. Wang, M. Valkonen, T. Vasara, A. Huuskonen, M. Riikonen, T. Pakula, M. Ward, and M. Penttila.** 2004. Characterization of secretory genes *ypt1*/*yptA* and *nsf1*/*nsfA* from two filamentous fungi: induction of secretory pathway genes of *Trichoderma reesei* under secretion stress conditions. Appl. Environ Microbiol. **70:**459–467.
41. **Schroder, M., and R. J. Kaufman.** 2005. The mammalian unfolded protein response. Annu. Rev. Biochem. **74:**739–789.
42. **Shen, X., R. E. Ellis, K. Sakaki, and R. J. Kaufman.** 2005. Genetic interactions due to constitutive and inducible gene regulation mediated by the unfolded protein response in *C. elegans*. PLoS Genet. **1:**e37.
43. **Takeuchi, M., T. Ueda, K. Sato, H. Abe, T. Nagata, and A. Nakano.** 2000. A dominant negative mutant of sar1 GTPase inhibits protein transport from the endoplasmic reticulum to the Golgi apparatus in tobacco and *Arabidopsis* cultured cells. Plant J. **23:**517–525.
44. **Tanaka, H., H. Fujita, H. Katoh, K. Mori, and M. Negishi.** 2002. Vps4-A (vacuolar protein sorting 4-A) is a binding partner for a novel Rho family GTPase, Rnd2. Biochem. J. **365:**349–353.
45. **Urano, F., M. Calfon, T. Yoneda, C. Yun, M. Kiraly, S. G. Clark, and D. Ron.** 2002. A survival pathway for *Caenorhabditis elegans* with a blocked unfolded protein response. J. Cell Biol. **158:**639–646.
46. **von Mering, C., M. Huynen, D. Jaeggi, S. Schmidt, P. Bork, and B. Snel.** 2003. STRING: a database of predicted functional associations between proteins. Nucleic Acids Res. **31:**258–261.
47. **von Mering, C., L. J. Jensen, M. Kuhn, S. Chaffron, T. Doerks, B. Kruger, B. Snel, and P. Bork.** 2007. STRING 7–recent developments in the integration and prediction of protein interactions. Nucleic Acids Res. **35:**D358–D362.
48. **Wojcik, C., M. Rowicka, A. Kudlicki, D. Nowis, E. McConnell, M. Kujawa, and G. N. DeMartino.** 2006. Valosin-containing protein (p97) is a regulator of endoplasmic reticulum stress and of the degradation of N-end rule and ubiquitin-fusion degradation pathway substrates in mammalian cells. Mol. Biol. Cell **17:**4606–4618.

Downloaded from mcb.asm.org at McGill Univ on January 19, 2010

Retrovirology

BioMed Central

Research

Open Access

Requirements for the selective degradation of CD4 receptor molecules by the human immunodeficiency virus type 1 Vpu protein in the endoplasmic reticulum

Julie Binette[1,2], Mathieu Dubé[1,2], Johanne Mercier[1], Dalia Halawani[3], Martin Latterich[4] and Éric A Cohen*[1,2]

Address: [1]Laboratory of Human Retrovirology, Institut de Recherches Cliniques de Montréal, 110 Avenue des Pins Ouest, Montreal, Quebec H2W 1R7, Canada, [2]Department of Microbiology and Immunology, Université de Montréal, 2900, Édouard-Montpetit, Montreal, Quebec H3T 1J4, Canada, [3]Department of Anatomy and Cell Biology, McGill University, 3640 University Street Montreal, Quebec H3A 2B2, Canada and [4]Faculty of Pharmacy, Université de Montréal, 2900, Édouard-Montpetit, Montreal, Quebec H3T 1J4, Canada

Email: Julie Binette - julie.binette@ircm.qc.ca; Mathieu Dubé - mathieu.dube@ircm.qc.ca; Johanne Mercier - johanne.mercier@ircm.qc.ca; Dalia Halawani - dhalawani@yahoo.com ; Martin Latterich - mlatterich@pharmacogenomics.ca; Éric A Cohen* - eric.cohen@ircm.qc.ca

* Corresponding author

Published: 15 October 2007

Retrovirology 2007, **4**:75 doi:10.1186/1742-4690-4-75

Received: 23 July 2007
Accepted: 15 October 2007

This article is available from: http://www.retrovirology.com/content/4/1/75

© 2007 Binette et al; licensee BioMed Central Ltd.
This is an Open Access article distributed under the terms of the Creative Commons Attribution License (http://creativecommons.org/licenses/by/2.0), which permits unrestricted use, distribution, and reproduction in any medium, provided the original work is properly cited.

Abstract

Background: HIV-1 Vpu targets newly synthesized CD4 receptor for rapid degradation by a process reminiscent of endoplasmic reticulum (ER)-associated protein degradation (ERAD). Vpu is thought to act as an adaptor protein, connecting CD4 to the ubiquitin (Ub)-proteasome degradative system through an interaction with β-TrCP, a component of the $SCF^{\beta\text{-}TrCP}$ E3 Ub ligase complex.

Results: Here, we provide direct evidence indicating that Vpu promotes *trans*-ubiquitination of CD4 through recruitment of $SCF^{\beta\text{-}TrCP}$ in human cells. To examine whether Ub conjugation occurs on the cytosolic tail of CD4, we substituted all four Ub acceptor lysine residues for arginines. Replacement of cytosolic lysine residues reduced but did not prevent Vpu-mediated CD4 degradation and ubiquitination, suggesting that Vpu-mediated CD4 degradation is not entirely dependent on the ubiquitination of cytosolic lysines and as such might also involve ubiquitination of other sites. Cell fractionation studies revealed that Vpu enhanced the levels of ubiquitinated forms of CD4 detected in association with not only the ER membrane but also the cytosol. Interestingly, significant amounts of membrane-associated ubiquitinated CD4 appeared to be fully dislocated since they could be recovered following sodium carbonate salt treatment. Finally, expression of a transdominant negative mutant of the AAA ATPase Cdc48/p97 involved in the extraction of ERAD substrates from the ER membrane inhibited Vpu-mediated CD4 degradation.

Conclusion: Taken together, these results are consistent with a model whereby HIV-1 Vpu targets CD4 for degradation by an ERAD-like process involving most likely poly-ubiquitination of the CD4 cytosolic tail by $SCF^{\beta\text{-}TrCP}$ prior to dislocation of receptor molecules across the ER membrane by a process that depends on the AAA ATPase Cdc48/p97.

Background

CD4 is a 55-kDa class I integral membrane glycoprotein that serves as the primary co-receptor for human immunodeficiency virus type 1 (HIV-1) entry into cells [1]. CD4 consists of a large lumenal domain, a transmembrane portion, and a 38-residues cytoplasmic tail. It is expressed primarily on the surface of a subset of T lymphocytes that recognizes major histocompatibility complex (MHC) class II-associated peptides and plays a major role in the development and maintenance of the immune system.

Despite the critical role played by CD4 during HIV-1 entry, it is well established that HIV-1 down-regulates cell surface expression of its cognate receptor (reviewed in reference [2]). It is believed that this process prevents superinfection and promotes production of fully infectious virions [3,4]. Down-regulation of CD4 in HIV-1-infected cells is mediated through different independent mechanisms involving the activity of three viral proteins: Nef, Env and Vpu. Early in infection, Nef removes CD4 molecules that are already present at the cell surface by enhancing their endocytosis and subsequent degradation in lysosomes [5]. At later stages of the infection, the envelope precursor gp160, through its high receptor binding affinity and inefficient vesicular transport [6], sequesters newly synthesized CD4 in the endoplasmic reticulum (ER) in the form of Env-CD4 complexes and prevents its transport and maturation to the cell surface [7]. The accessory protein Vpu induces a rapid degradation of newly synthesized CD4 molecules bound to gp160 in the ER [8].

Vpu is an 81-amino acids class I integral membrane protein of 16 kDa that is unique to HIV-1 and simian immunodeficiency virus isolated from chimpanzee (SIVcpz) and a few other monkey species ([9-11] and reviewed in reference [12]). The protein consists of an N-terminal hydrophobic membrane anchor domain of 27 amino acids and a charged C-terminal hydrophilic domain of 54 residues that extends into the cytoplasm [13]. This cytosolic domain contains a highly conserved dodecapeptide sequence encompassing residues 47–58 which comprises a pair of serine residues (S52 and S56) that are phosphorylated by casein kinase II [14,15]. Besides its ability to mediate the rapid degradation of CD4 molecules complexed with Env gp160 in the ER, Vpu was also found to promote efficient release of progeny HIV-1 viruses in different human cell types, including T cells and macrophages, by a mechanism that appears to involve the inactivation of a putative host cell factor that restricts viral particle release in a cell-type dependent manner [10,16-19].

From a mechanistic point of view, HIV-1 Env is not absolutely required for Vpu-mediated CD4 degradation. The role of Env appears to be limited to its ability to retain CD4 in the ER, given that efficient CD4 degradation can be observed in the absence of Env as long as CD4 is retained in the ER through the presence of an ER retention sequence or treatment of cells with Brefeldin A (BFA), a fungal metabolite known to block protein sorting from the ER to the Golgi apparatus [20]. The degradation of CD4 mediated by Vpu involves multiple steps that are initiated by the direct physical binding of Vpu to the cytoplasmic tail of CD4 in the ER [21]. Although the binding of Vpu to CD4 is necessary to induce CD4 degradation, it is not sufficient. Indeed, studies aimed at identifying Vpu partners by two-hybrid screens led to the identification of a host cellular co-factor, β-TrCP, which plays a critical role in Vpu-mediated CD4 degradation by interacting with Vpu in a phosphorylation-dependent manner [22]. The human F-box protein β-TrCP functions as a substrate recognition receptor for the multi-subunit ubiquitin ligase (E3) $SCF^{\beta\text{-}TrCP}$ involved in the ubiquitin (Ub) conjugating pathway (reviewed in reference [23]). The interaction between Vpu and β-TrCP is essential for Vpu-mediated CD4 degradation since substitution mutations of Vpu phospho-acceptor sites, S52 and S56, prevent association with β-TrCP and abolish the effect of Vpu on CD4 turnover [22]. These findings have established a link between the machinery responsible for the ubiquitination of proteins destined for degradation by the proteasome and the enhanced CD4 turnover in presence of Vpu. Indeed, further lines of evidence for an involvement of the Ub-proteasome system in Vpu-mediated CD4 degradation were also reported: 1) Vpu-mediated CD4 degradation is not observed in a mammalian cell line expressing a temperature-sensitive Ub activating enzyme (E1), a key component of the machinery involved in the covalent attachment of Ub to target proteins [24]; 2) over-expression of a mutant Ub (Ub K48/R), which prevents the formation of poly-Ub chains, impairs Vpu-mediated CD4 degradation [24]; 3) Vpu-mediated CD4 degradation is inhibited by specific proteasome inhibitors [24].

Vpu-induced CD4 degradation is reminiscent of ER-associated protein degradation (ERAD), a quality control process in the ER that ensures that only proteins with a native folded conformation leave the organelle for other destinations across the secretory pathway [25]. Misfolded proteins that cannot reach their native state are transferred from the ER to the cytosol by a multi-step process called retro-translocation or dislocation which is thought to involve pore complexes formed by proteins such as Derlin-1 [26,27] or by multi-spanning transmembrane E3 ligases such as Hrd1 [28]. ERAD substrates exposed to the cytosol are acted upon by ER-associated components of the Ub conjugation machinery, extracted from the ER membrane by the AAA ATPase Cdc48/p97 and its associated cofactors Ufd1p and Np14p and degraded by the 26 S proteasome (reviewed in reference [25]). This cellular

pathway has been co-opted by some viruses to selectively destroy cellular proteins required for immune defense of the host. For example, two human cytomegalovirus (HCMV) proteins, US2 and US11, are able to target newly synthesized class I MHC (MHC-I) heavy chains (HC) for dislocation from the ER, leading to complete extraction of MHC-I HC from the ER membrane into the cytosol followed by proteasomal destruction [29,30]. Most ERAD substrates are poly-ubiquitinated while undergoing dislocation although the details of recognition, timing and post-translational modification of dislocation substrates can vary depending on the substrates [31-33].

Although part of the molecular machinery that is recruited by Vpu to target CD4 for degradation is reasonably well defined, several aspects of Vpu-mediated CD4 degradation still remain unclear. In particular, direct evidence of CD4 ubiquitination in presence of Vpu in human cells has not been demonstrated. Furthermore, it is unclear whether ER-associated CD4 encounters the cytoplasmic proteasome by a process involving dislocation of CD4 molecules across the ER membrane as described for ERAD substrates. Finally, the role of CD4 ubiquitination in processes underlying Vpu-mediated CD4 degradation remains to be specified. Meusser and Sommer have reconstituted the process of Vpu-mediated CD4 degradation in *Saccharomyces cerevisiae* by expressing human CD4 together with Vpu and human β-TrCP and have provided evidence suggesting that Vpu-mediated proteolysis strictly relies on ubiquitination of CD4 at cytosolic lysine residues prior to export of receptor molecules from the ER membrane [34].

In this study, we have analyzed the process of Vpu-mediated CD4 degradation in human cells. The data presented here provide evidence suggesting that Vpu promotes ubiquitination of CD4 cytosolic tail by $SCF^{\beta\text{-}TrCP}$ and mediates dislocation of the viral receptor across the ER membrane in human cells by a process that might depend on the AAA ATPase Cdc48/p97. Interestingly, in contrast to previous results, Vpu-mediated CD4 degradation and ubiquitination were not found to be entirely dependent on cytosolic lysine residues, raising the possibility that ubiquitination at sites other than lysines might also be involved.

Results

Poly-ubiquitination of CD4 is required for Vpu-mediated CD4 degradation

In order to study processes involved in Vpu-mediated CD4 degradation, we established a transient expression system whereby CD4 and Vpu are expressed *in trans* in SV40-transformed human embryonic kidney fibroblasts (HEK 293T) cells. CD4- and Vpu-expressing cells were treated with BFA in order to retain CD4 in the ER before and during metabolic labeling. Pulse-chase radio-labeling analysis followed by immunoprecipitation with anti-CD4 antibodies was performed to ensure that CD4 was specifically degraded by Vpu in this system. Fig. 1 reveals that CD4 turnover was significantly accelerated in presence of

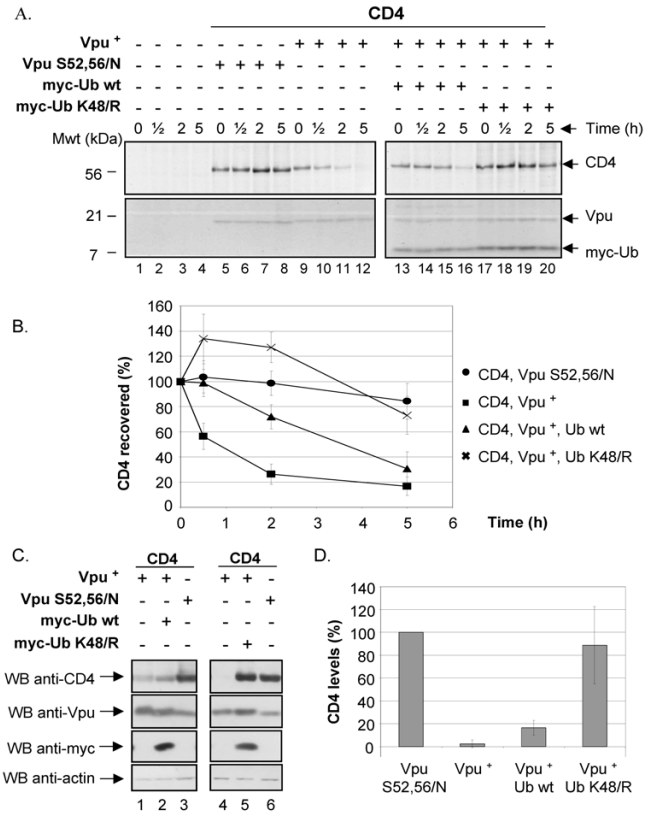

Figure 1

Poly-ubiquitination of CD4 is required for Vpu-mediated CD4 degradation. A. HEK 293T cells were mock-transfected or co-transfected with 1.5 μg of SVCMV CD4 wt and 8 μg of SVCMV Vpu+ (Vpu+) or the phosphorylation-defective Vpu mutant SVCMV Vpu S52,56/N (Vpu S52,56/N). In parallel, CD4/Vpu transfectants were co-transfected with 8 μg of plasmids encoding his(6)/c-myc-Ub wt (myc-Ub wt) or the TDN mutant of ubiquitin his(6)/c-myc-Ub K48/R (myc-Ub K48/R). Transfected cells were treated with BFA, pulse-labeled with [^{35}S]methionine and [^{35}S]cysteine and chased with complete media for the indicated time intervals. Cells were then lysed and immunoprecipitated sequentially with anti-CD4 monoclonal and polyclonal antibodies first and then with anti-Vpu and anti-myc antibodies. B. Using quantitative scanning of CD4 bands from three independent experiments, the percentage of CD4 remaining over time as compared to time 0 is plotted for each transfection. C. HEK 293T cells were mock-transfected or co-transfected as described in A. Cell transfectants were treated for two hours with BFA prior to lysis. Steady state levels of CD4, actin and tagged ubiquitin were analysed by western-blot. D. Quantitative analysis from three independent experiments showing the level of CD4 relative to CD4 expressed with Vpu S52,56/N (arbitrarily set at 100%) for each transfectant.

Vpu. Furthermore, the effect of Vpu on CD4 was specific since expression of a phospho-acceptor sites mutant, Vpu S52,56/N, which is unable to interact with the E3 Ub ligase complex $SCF^{\beta\text{-}TrCP}$ [22] did not mediate CD4 degradation (Fig. 1A, compare lanes 5–8 with lanes 9–12 and Fig. 1B). Moreover, as previously reported [24,35], addition of specific proteasome inhibitor, such as MG-132, to HEK 293T cells expressing CD4 and Vpu inhibited Vpu-mediated CD4 degradation (data not shown).

We also tested whether poly-ubiquitination of CD4 was required for Vpu-mediated CD4 degradation in HEK 293T cells. For this purpose, we co-expressed CD4 and Vpu with a N-terminal his(6)/c-myc tagged form of wild-type (wt) Ub or a N-terminal his(6)/c-myc tagged form of a transdominant negative (TDN) mutant of Ub, Ub K48/R, that is unable to form poly-Ub chains required for proteasomal degradation [36]. This Ub mutant acts as a chain terminator in the process of poly-ubiquitination since the Ub-acceptor lysine residue at position 48 is mutated for an arginine. In agreement with previous reported data [24], results of Fig. 1A (compare lanes 9–12 with lanes 17–20) and B reveal that expression of tagged-Ub K48/R markedly reduced the rate of Vpu-mediated CD4 degradation, thus suggesting that poly-ubiquitination of CD4 via K48 linkage of Ub moieties was required for Vpu-mediated CD4 degradation. Although expression of wt tagged-Ub had some attenuating effect on Vpu-mediated CD4 degradation (compare lanes 13–16 with lanes 9–12 and Fig. 1B), it was clearly less pronounced than with the TDN tagged-Ub K48/R mutant. In that regard, wt tagged Ub has been previously reported to decrease the rate of degradation of some substrate by the Ub-proteasome system given that fusion of the his-myc tag at the N-terminal of Ub renders poly-Ub-protein conjugates less recognizable by the proteasome [37]. All of these results were also confirmed by analyzing steady-state levels of CD4 by western-blot in Vpu-expressing HEK 293T cells (Fig. 1C and 1D). Overall, these results provide evidence that this expression system in HEK 293T cells supports an efficient degradation of CD4 that is Vpu-specific, depends on the recruitment of β-TrCP, necessitates an active proteasome and requires poly-ubiquitination of CD4.

Vpu induces ubiquitination of CD4 molecules

Having established that over-expression of Ub K48/R inhibited Vpu-mediated CD4 degradation in HEK 293T cells, we investigated whether we could isolate and directly detect ubiquitinated forms of CD4 that are expected to accumulate under these conditions. Towards this goal, we first analyzed CD4 expression at steady state in Vpu/CD4 HEK 293T transfectants in presence or absence of tagged-Ub K48/R (Fig. 2A). In these experiments, transfected cells were treated with BFA during 2 h prior to lysis to retain newly synthesized CD4 in the ER.

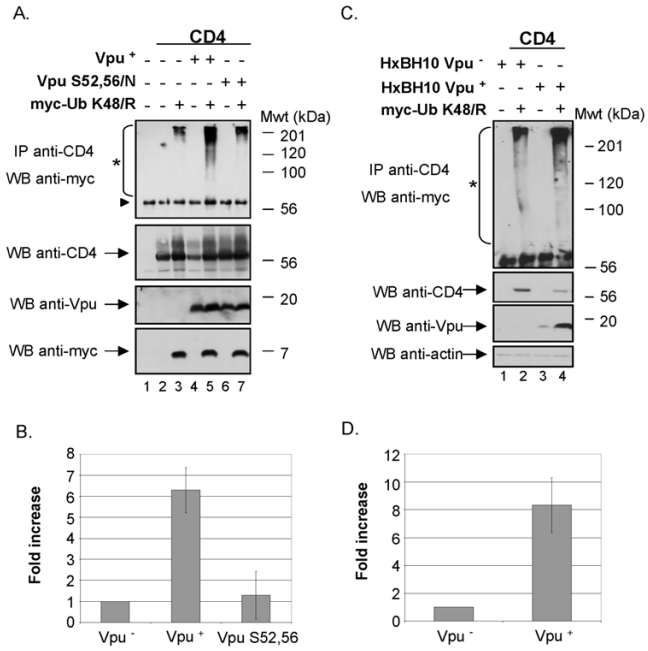

Figure 2

Effect of Vpu on CD4 ubiquitination. A. Vpu-mediated ubiquitination of CD4 wt when CD4 is retained in the ER through treatment with BFA. HEK 293T cells were mock-transfected or co-transfected with 1 μg of SVCMV CD4 wt, 8 μg of SVCMV Vpu+ or the phosphorylation-defective Vpu mutant SVCMV Vpu S52,56/N and 8 μg of the TDN mutant his(6)/c-myc-Ub K48/R. Samples were then treated as described in the materials and methods section. CD4 molecules were immunoprecipitated with anti-CD4 polyclonal antibodies prior to western-blot analysis with anti-myc monoclonal antibodies. (triangle) indicates the position of the heavy chains of anti-CD4 antibodies. B. Quantitative analysis of ubiquitinated CD4 conjugates. (asterisk) represents the area of the autoradiogram that was used for quantitation of CD4-Ub conjugates. The histogram shows the relative levels of ubiquitinated CD4 conjugates in presence or absence of a functional Vpu. Relative CD4-Ub conjugate levels were evaluated by quantitation of the signal detected in the area delineated on the autoradiogram relative to total CD4 as determined by quantitation of the band detected with the anti-CD4 antibodies on whole cell lysate. The relative level of ubiquitinated CD4 detected in absence of Vpu was arbitrarily set at 1. The data represent results from seven experiments. C. Vpu-mediated ubiquitination of CD4 wt in condition where CD4 is retained in the ER through binding with HIV-1 Env. HEK 293T cells were mock-transfected or co-transfected with 1 μg of pHIV CD4 wt, 10 μg of provirus encoding Vpu^- (HxBH10-vpu^-) or Vpu^+ (HxBH10-vpu^+) and 20 μg of his(6)/c-myc-Ub K48/R. Samples were then treated as in A but in absence of BFA. D. Quantitative analysis showing the relative levels of ubiquitinated CD4 detected in two independent experiments. Relative levels of ubiquitinated CD4 conjugates were determined as described in B.

Fig. 2A reveals that CD4 levels at steady-state were significantly reduced in presence of Vpu (compare lanes 2 and 4). As expected, expression of tagged-Ub K48/R suppressed the effect of Vpu on CD4 and re-established the amounts of CD4 to levels comparable to those detected in absence of Vpu (compare lanes 5 and 2). To detect CD4-Ub conjugates, cell lysates were first immunoprecipitated with anti-CD4 polyclonal antibodies and the resulting CD4-containing immunocomplexes were subsequently analyzed for the presence of CD4-Ub conjugates by western-blot using anti-myc antibodies. Ubiquitinated forms of CD4 were detected as a typical smear in presence of Vpu (lane 5). Although background high molecular weight ubiquitinated forms of CD4 could still be detected in absence of Vpu (lane 3) or in presence of the non-functional Vpu S52,56/N mutant (lane 7), their levels were not as elevated as in presence of wt Vpu (lane 5). Indeed, quantitative analysis revealed that levels of CD4-Ub conjugates were approximately 6-fold higher in presence than in absence of a functional Vpu (Fig. 2B). The detection of a smear of high molecular weight proteins in presence of Vpu is suggestive of poly-ubiquitination of CD4. Poly-ubiquitination is still possible even if Ub K48/R is over-expressed because cells are expressing endogenous wt Ub that can initiate poly-Ub chains before a molecule of Ub K48/R can prematurely terminate the chain.

Finally, we examined whether we could extend this enhancing effect of Vpu on CD4 ubiquitination to a more physiological system where CD4 is retained in the ER through the formation of complexes with Env glycoproteins instead of BFA treatment. In this system, initially described by Willey and co-workers [20], Vpu and Env glycoproteins are co-expressed from a proviral construct while CD4, that is under HIV-1 long terminal repeat control (pHIV CD4) [24], is expressed only in cells expressing Vpu and Env. Results of Fig. 2C and 2D show that even in a system where CD4 is naturally retained in the ER through binding to HIV-1 Env, Vpu expression increases substantially (approximately 8-fold) the level of CD4 molecules undergoing ubiquitination (compare the levels of CD4-Ub conjugates in lanes 4 and 2 (upper panel) relative to their respective CD4 steady state levels (lower panel) and Fig. 2D).

Overall these results indicate that Vpu promotes poly-ubiquitination of CD4 molecules that are targeted for degradation by the proteasome through the recruitment of the $SCF^{\beta\text{-}TrCP}$ E3 Ub ligase.

Vpu-mediated CD4 degradation and ubiquitination are not strictly dependent on CD4 cytosolic lysines

CD4 contains four potential Ub acceptor lysine residues in its cytoplasmic domain. To determine whether ubiquitination of the cytosolic tail was required for Vpu-mediated CD4 degradation, we analyzed a CD4 mutant, CD4 KRcyto, in which all four cytoplasmic lysine residues were replaced by arginines. The stability of CD4 wt and CD4 KRcyto was first assessed in cells expressing a provirus encoding either wt Vpu (HxBH10-vpu$^+$) or Vpu S52,56/D (HxBH10-vpu S52,56/D) as described above in Fig. 2C. Results of Fig. 3A clearly show that both CD4 wt and CD4 KRcyto were unstable in Vpu expressing cells as observed by the decreased recovery of CD4 molecules over the chase period (lanes 9–12 and lanes 13–16). Quantification of CD4 turnover over several experiments indicated an attenuation of the degradation kinetic of CD4 KRcyto as compared to CD4 wt but the protein was clearly susceptible to Vpu-induced degradation (Fig. 3B). In contrast, both CD4 wt and CD4 KRcyto remained stable over the entire 7 h chase period in cells expressing the phosphorylation mutant Vpu S52,56/D (Fig. 3A, lanes 1–4 and lanes 5–8 and Fig. 3B).

Given that previous studies had shown that Vpu-mediated CD4 degradation strictly relied on cytosolic lysine residues in mammalian cells and yeast [24,34], we analyzed the steady-state levels of CD4 wt or CD4 KRcyto in HEK 293T expressing Vpu$^+$ or Vpu$^-$ provirus by western-blot. Similar to what we found in pulse-chase experiments, we repeatedly observed a difference in sensitivity to Vpu-mediated degradation between CD4 wt and CD4 KRcyto (Fig. 3C, compare lanes 14 and 16 with lanes 10 and 12 and Fig. 3D, right panel) but clearly, the absence of cytosolic Ub acceptor lysine residues was not entirely preventing the effect of Vpu on CD4 degradation. Similar results were also obtained when steady-state levels of CD4 wt and CD4 KRcyto were analyzed in BFA-treated HEK 293T cells expressing Vpu$^+$ or Vpu$^-$ provirus lacking Env (Fig. 3C, compare lanes 2 and 4 with lanes 6 and 8, and Fig. 3D, left panel).

Given that Vpu was reported to interact with the cytoplasmic tail of CD4 in a region (EKKT, residues 416–419 of CD4) that encompasses some of the lysine residues mutated in the CD4 KRcyto mutant (K417, K418), we further tested whether this difference in susceptibility to Vpu-mediated CD4 degradation could be explained by a diminished ability of CD4 KRcyto to associate with Vpu. Binding experiments were performed as described in materials and methods using the Vpu S52,56/N mutant, which binds CD4 as efficiently as Vpu wt but is unable to mediate CD4 degradation [21]. Results from these experiments reveal that CD4 KRcyto associates with Vpu at least as efficiently as CD4 wt, thus ruling-out that the decreased sensitivity of CD4 KRcyto to Vpu-mediated degradation results from reduced Vpu binding efficiency [Additional file 1]. These results were also confirmed by immunoprecipitation of CD4 followed by western-blot using anti-Vpu antibodies (data not shown).

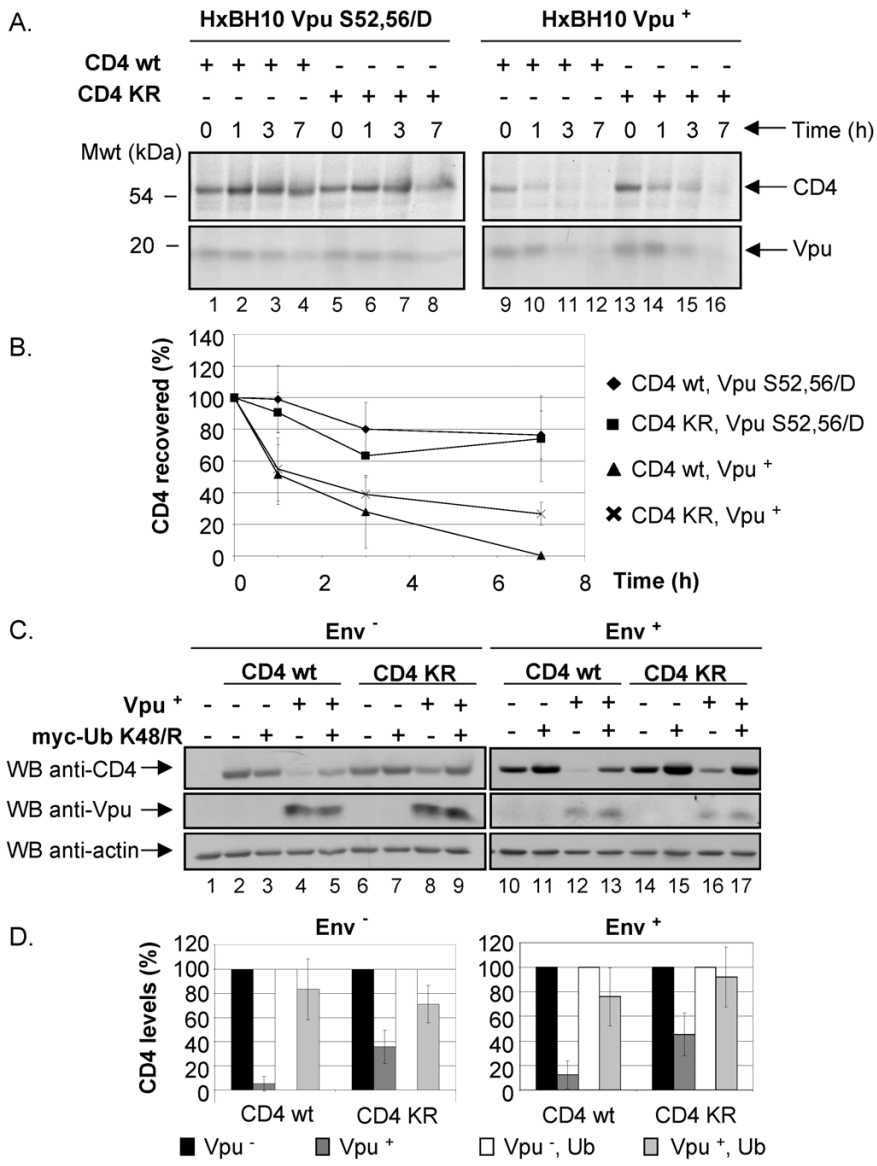

Figure 3

Effect of Vpu on CD4 molecules lacking lysine residues in the cytoplasmic tail. A. Analysis of CD4 wt and CD4 KRcyto turnover in presence or absence of functional Vpu by pulse-chase labeling and immunoprecipitation. HEK 293T cells were mock-transfected or co-transfected with 2 μg of pHIV CD4 wt or pHIV CD4 KRcyto and 20 μg of provirus encoding Vpu^+ ($HxBH10\text{-}vpu^+$) or phosphorylation-defective Vpu mutant (HxBH10-vpu S52,56/D). Cells were pulse-labeled with [^{35}S]methionine and [^{35}S]cysteine and chased in complete medium for the indicated time intervals. Cells were then lysed and immunoprecipitated sequentially with anti-CD4 antibodies first (polyclonal and monoclonal) and then with anti-Vpu antibodies. B. Using quantitative scanning of CD4 bands from two independent experiments, the percentage of CD4 remaining over time as compared to time 0 is plotted for each transfection. C. Effect of Vpu on steady-state CD4 wt and CD4 KRcyto levels. HEK 293T cells were mock-transfected or co-transfected with 1 μg of pHIV CD4 wt or pHIV CD4 KRcyto and 10 μg of proviruses encoding Vpu^- or Vpu^+ in addition to 25 μg of the his(6)/c-myc-Ub K48/R expressor. In the left panel (Env^-), a similar experiment was performed except that HEK 293T cells were co-transfected with 10 μg of envelope-defective provirus ($HxBc2\text{-}pr^-$, vpu^-, env^- or $HxBH10\text{-}pr^-$, vpu^+, env^-) and treated with BFA for 2 h prior to lysis. Cell lysates were then treated as described in the materials and methods section. D. Quantitative analysis of steady-state CD4 levels. CD4 levels in presence of absence of his(6)/c-myc-Ub K48/R were arbitrarily set at 100%. The levels of CD4 in presence of Vpu are shown relative to the corresponding controls. These results are representative of the data obtained in three independent experiments for Env^- and five independent experiments for Env^+.

Given that CD4 KRcyto was still susceptible to Vpu-mediated degradation, we next evaluated whether CD4 KRcyto could undergo ubiquitination in presence of Vpu. To optimize the recovery of CD4-Ub conjugates, Vpu/CD4 or Vpu/CD4 KRcyto HEK 293T transfectants were made to co-express the TDN Ub K48/R mutant. Analysis of CD4-Ub and CD4 KRcyto-Ub conjugates levels in presence or absence of Vpu was performed as described above for Fig. 2B. Fig. 4A reveals that even though CD4 KRcyto is less susceptible to Vpu-mediated degradation as compared to CD4 wt (compare lanes 1 and 3 with lanes 5 and 7, middle panel), it still undergoes enhanced ubiquitination in presence of Vpu (compare lane 6 and lane 8). However, it is important to note that the relative level of recovered CD4 KRcyto-Ub conjugates was decreased as compared to CD4-Ub conjugates. In fact, quantitative analysis of ubiquitinated CD4 conjugate levels reveals that Vpu enhanced ubiquitination of CD4 KR by approximately 3-fold while it increased ubiquitination of wt CD4 by 8-fold. Altogether, these results suggest that lysine residues in the cytosolic domain of CD4 are not absolutely essential for ubiquitination and degradation of the viral receptor in presence of Vpu. Even-though optimal Vpu-mediated CD4 ubiquitination most probably involves cytosolic lysine residues there must be other sites that are also targeted during Vpu-induced ubiquitination.

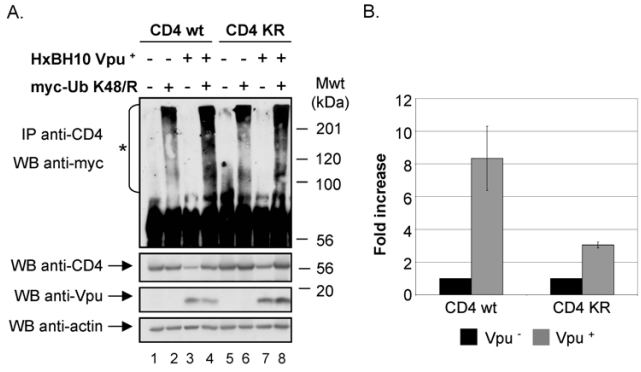

Figure 4

Effect of Vpu on CD4 KRcyto poly-ubiquitination. A. HEK 293T cells were mock-transfected or co-transfected with 1 μg of pHIV CD4 wt or pHIV CD4 KRcyto, 10 μg of provirus encoding Vpu^- (HxBH10-vpu^-) or Vpu^+ (HxBH10-vpu^+) and 25 μg of the TDN mutant of Ub his(6)/c-myc-Ub K48/R. Transfected cells were not treated with BFA prior to lysis. Samples were then treated as described in the materials and methods. B. Quantitative analysis of the relative levels of ubiquitinated CD4 conjugates for CD4 wt and CD4 KRcyto in two independent experiments. (asterisk) represents the area of the autoradiogram that was used for the quantitation of CD4-Ub conjugates. Relative levels of ubiquitinated CD4 conjugates were determined as described in Fig. 2B.

Vpu-mediated CD4 degradation involves the dislocation of ubiquitinated CD4 conjugates across the ER membrane

To examine whether CD4 undergoes a process of dislocation across the ER membrane during Vpu-mediated degradation, we conducted subcellular fractionation studies. To optimize recovery and detection of dislocated forms of CD4 targeted for degradation by the cytosolic proteasome, we performed these cell fractionation experiments in conditions where CD4 degradation was inhibited by over-expression of the TDN Ub K48/R mutant. BFA-treated HEK 293T cells expressing CD4/Ub K48/R and Vpu or CD4/Ub K48/R alone were fractionated by mechanical lysis into membrane and cytosolic fractions and each resulting fraction was directly analyzed for the presence of CD4, Vpu and membrane or cytosolic markers, such as calnexin and actin respectively, by western-blot as described in materials and methods. Furthermore, the presence of poly-ubiquitinated forms of CD4 in membrane or cytosolic fractions was determined by immunoprecipitation/western-blot analysis. In contrast to Fig. 2 and 4 and because of technical reasons, ubiquitinated CD4 molecules were detected in these experiments by performing immunoprecipitation using anti-Myc antibodies followed by western-blot using anti-CD4 antibodies. As expected, Vpu and calnexin were detected exclusively in association with membrane fractions (Fig. 5A, lane 5 for Vpu and lanes 1, 3, 5 and 7 for calnexin) whereas actin (lanes 2, 4, 6, 8) or Ub (lanes 4, 6, 8) were recovered in a very large proportion in the cytosolic fractions, thus demonstrating that the fractionation procedure was almost free of membrane or cytosolic contaminations. CD4 molecules were found in the membrane fraction in presence or absence of Vpu (lanes 3 and 5). We could repeatedly recover and detect CD4-Ub conjugates, represented as a smear signal, predominantly in the membrane fraction but also in the cytosolic fraction in absence and in presence of Vpu (Fig. 5A); in some instances, depending on the experiments, we also detected discrete high molecular bands in addition to the smear signal [lane 5 of Additional file 2A and lane 6 of Additional file 2B]. Interestingly, the absolute signal associated with membrane and cytosolic fractions was always more intense in presence than in absence of Vpu (Fig. 5A, compare lanes 3, 5 and 7 as well as lanes 4, 6 and 8, upper panel). The specific levels of CD4-Ub conjugates associated with membrane and cytosolic fractions in absence and in presence of Vpu were calculated relative to the amount of CD4 detected directly by western-blot. As shown in Fig. 5B, quantitative analysis revealed that in presence of Vpu there was approximately a six-fold increase in membrane-associated CD4-Ub conjugate levels relative to the negative control without Vpu (Vpu^-); in the cytosolic fractions, the levels of CD4-Ub conjugates detected in presence of Vpu were approximately two-fold higher relative to the Vpu^- control (Fig. 5B).

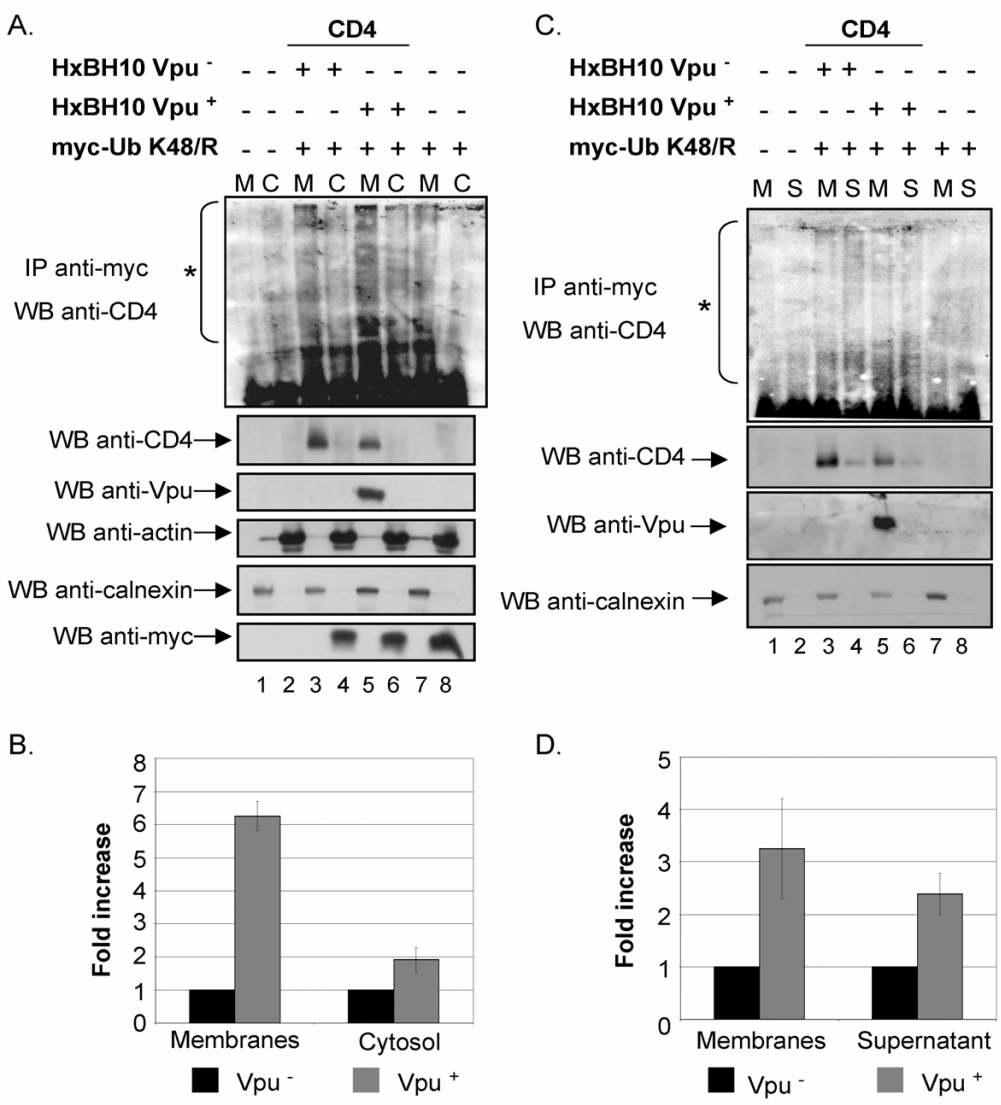

Figure 5

Vpu-mediated CD4 degradation involves dislocation of ubiquitinated CD4 conjugates from the ER membrane to the cytosol. HEK 293T cells were mock-transfected or co-transfected with 1 μg of pHIV CD4 wt, 10μg of envelope-defective provirus (HxBc2-pr$^-$, vpu$^-$, env$^-$ or HxBH10-pr$^-$, vpu$^+$, env$^-$) and 15 μg of his(6)/c-myc-Ub K48/R expression plasmid where indicated. Cells were treated with BFA for 2 h before mechanical lysis. CD4-Ub conjugates were immunoprecipitated with anti-myc monoclonal antibodies prior to western-blot analysis with anti-CD4 polyclonal antibodies while control proteins in each fraction were revealed by western-blot. Actin and calnexin were used as cytosolic and membrane controls, respectively. A. Membrane (M) and cytosolic (C) fractions were separated and treated as described in the materials and methods section. B. Quantitative analysis of the relative amounts of ubiquitinated CD4 molecules present in each fraction relative to the amounts measured in absence of Vpu (arbitrarily set at 1). (asterisk) represents the area of the autoradiogram that was used for the quantitation of CD4-Ub conjugates. Non-specific background signal detected in lanes 7 and 8 was subtracted. Relative levels of ubiquitinated CD4 conjugates were determined as described in the legend of Fig. 2B. Error bars reflect standard deviations from duplicate independent experiments. C. Membrane (M) fractions were treated with Na_2CO_3 (pH 11) as described in materials and methods. Treated membrane and supernatant (S) were subsequently recovered by centrifugation. Fractions were analyzed as described above in A. D. Quantitative analysis of the relative amounts of ubiquitinated CD4 molecules (as described in the legend of Fig. 2B) present in each fraction relative to the amounts measured in absence of Vpu (arbitrarily set at 1). (asterisk) represents the area that was used for the quantitation of CD4-Ub conjugates. Non-specific background signal detected in lanes 7 and 8 was subtracted. Error bars reflect standard deviations from duplicate independent experiments.

To determine whether membrane-associated CD4-Ub conjugates represent CD4 molecules that are still embedded in the membrane while undergoing dislocation or if some of these conjugates are fully dislocated but stay tethered to the cytosolic face of the membrane, we treated membrane fractions with 100 mM sodium carbonate at basic pH (pH 11) (Fig. 5C) and analyzed the treated membrane and resulting supernatant for the presence of CD4-Ub conjugates as described in Fig. 5A. Salt-wash at basic pH (Na_2CO_3) but not at neutral pH (NaCl) was previously shown to remove peripheral proteins that are associated with membranes [38]. In this experiment, Vpu (Fig. 5C, lane 5) and calnexin (lanes 1, 3, 5 and 7) were exclusively recovered in the membrane fractions after Na_2CO_3 treatment, thus confirming that the integrity of microsomes was maintained during the procedure. Surprisingly, we repeatedly detected small amounts of CD4 in the salt-wash supernatant (lanes 4 and 6, WB anti-CD4 panel) that perhaps represent population of CD4 molecules that are dislocated prior to ubiquitination. Quantitative analysis of the relative CD4-Ub conjugates signal associated with membrane and supernatant fractions revealed that approximately 50% of the membrane-associated signal could be salt washed at basic pH (Fig. 5C, compare lane 3 to lane 4 and lane 5 to lane 6), thus indicating that part of the membrane-associated CD4-Ub signal represents dislocated ubiquitinated forms of CD4 that are associated with the cytosolic face of the membrane. Importantly, in presence of Vpu we detected a 2-3-fold increase in the relative levels of CD4-Ub conjugates associated with the treated membrane fraction and salt-washed supernatant (Fig. 5D). As expected, control experiments where membranes were washed with sodium chloride at neutral pH (pH 7) did not lead to any recovery of CD4-Ub in the supernatant [Additional file 2A]. Conversely, treatment of membranes with RIPA-DOC lysis buffer solubilized CD4-Ub conjugates, which were detected almost completely in the supernatant [Additional file 2B]. As expected, in both conditions the absolute levels of detected CD4-Ub conjugates was more elevated in presence than in absence of Vpu. Overall, these results suggest that Vpu targets CD4 for cytosolic proteasomal degradation by enhancing dislocation of receptor molecules across the ER membrane.

Expression of a transdominant negative mutant of p97 inhibits Vpu-mediated CD4 degradation

To further confirm that Vpu-mediated CD4 degradation involves a dislocation step, we examined the implication of the Cdc48/p97 ATPase in this process. Mammalian p97 plays an important role in dislocation of ERAD substrates presumably by binding poly-ubiquitinated substrates in conjunction with its cofactors, including Ufd1 and Npl4 [39], and mediating a process of extraction that is energy-dependent [40]. The p97 protein has two ATPase domains and mutants affected in their ability to bind or hydrolyze ATP are no longer able to perform their function in retrotranslocation [41]. We took advantage of a well-described p97 TDN ATP binding mutant (p97 AA) [41] and tested its effect on Vpu-mediated CD4 degradation. HEK 293T cells were co-transfected with expression plasmids encoding CD4, Vpu and FLAG-tagged p97 wt or FLAG-tagged p97 TDN mutant and the levels of CD4 were analyzed at steady-state by western-blot. As shown in Fig. 6, expression of the p97 TDN mutant strongly inhibited Vpu-mediated CD4 degradation while wt p97 had no significant inhibitory effect on Vpu ability to degrade CD4 (compare lanes 3 and 5 with lanes 2 and 4). These results were also confirmed by pulse-chase labeling experiments where CD4 turnover was evaluated in presence of Vpu and the p97 TDN mutant or wt p97 (data not shown). Since p97 is directly involved in the dislocation of several ERAD substrates, these results provide additional evidence suggesting that Vpu targets the CD4 receptor for cytosolic proteasomal degradation by a process that involves a dislocation step across the ER membrane.

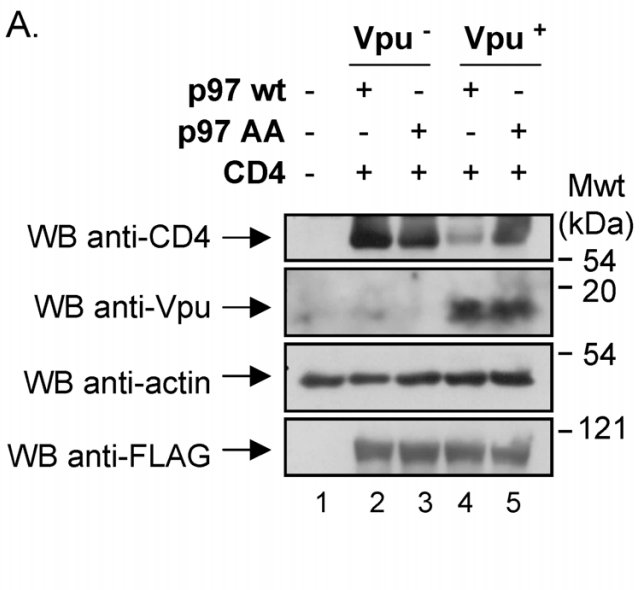

Figure 6
Effect of a TDN mutant of p97 on Vpu-mediated CD4degradation. HEK 293T cells were mock-transfected or co-transfected with 1.5 μg of SVCMV CD4 wt, 12 μg of SVCMV Vpu^- or Vpu^+ and 1 μg of an expression plasmid encoding a FLAG-tagged version of p97 wt or the TDN mutant p97 AA. Cells were treated with BFA for 2 h prior to lysis. Cell lysates were then analyzed by western-blot as described in materials and methods. These results are representative of the data obtained in two independent experiments.

Discussion

In the present study, we have conducted a detailed analysis of processes involved in the ER-associated degradation of CD4 receptor molecules induced by the HIV-1 Vpu accessory protein in human cells. Using a TDN mutant of Ub, Ub K48/R, which acts as a poly-Ub chain terminator, we have confirmed previous findings [24] suggesting that poly-ubiquitination of CD4 is required for Vpu-mediated CD4 degradation (Fig. 1). Based on these observations, we attempted to directly detect ubiquitinated forms of CD4, which are expected to accumulate under conditions where Ub K48/R is over-expressed. A similar approach was successfully used to facilitate the isolation and detection of substrates of the Ub pathway such as APOBEC3G in presence of HIV-1 Vif [42]. Under these conditions, we could demonstrate an increased accumulation of high molecular weight CD4-Ub conjugates, typical of poly-ubiquitinated protein targets, in presence of Vpu (Fig. 2). Direct detection of ubiquitinated forms of CD4 in presence of Vpu was achieved both in conditions where CD4 retention in the ER was produced through short treatment of cells with BFA or through formation of Env/CD4 complexes, thus demonstrating that both systems could be used to analyze Vpu-mediated CD4 degradation. Some high molecular weight ubiquitinated CD4 conjugates could be detected in absence or presence of a non functional Vpu mutant unable to recruit the $SCF^{\beta\text{-}TrCP}$ E3 ligase complex, except that their levels were significantly lower than those found in presence of Vpu. It is likely that ubiquitinated CD4 conjugates detected at steady-state in absence of Vpu or in presence of inactive Vpu represent intermediates resulting from the relatively low but normal degradation of misfolded CD4 molecules that occurs through the ERAD pathway in condition of transient ectopic over-expression. Together, these findings provide direct evidence that Vpu promotes *trans*-ubiquitination of CD4 through recruitment of the $SCF^{\beta\text{-}TrCP}$ complex in human cells.

CD4, as a type 1 integral membrane protein, consists of a 38-amino acid cytosolic domain that contains four lysine residues (amino acid positions: K411, KK417-418, and K428) that could serve as acceptor sites for ubiquitination. Ubiquitin conjugation of lysine residues accessible from the cytosol through recruitment of the specific $SCF^{\beta\text{-}TrCP}$ E3 ligase complex by Vpu may represent a very early step in the process of CD4 degradation and precede the transport of the viral receptor through the ER membrane for proteolytic degradation by the cytosolic proteasome. To investigate the role of cytosolic lysine residues in Vpu-mediated CD4 degradation, we used a CD4 mutant in which all four lysines were replaced by arginine residues. In contrast to earlier observations made in HeLa cells [24], replacement of lysine residues in the CD4 cytoplasmic tail did not strictly prevent CD4 degradation by Vpu in HEK 293T cells. In our conditions, even though we detected a significant difference in the protein turnover (Fig. 3A–B) as well as in the steady-state levels (Fig. 3C–D) of CD4 KRcyto and CD4 wt in presence of Vpu, our data also revealed that CD4 KRcyto was still susceptible to Vpu-mediated CD4 degradation. These results suggest that ubiquitination of the cytosolic tail at lysine acceptor sites by the $SCF^{\beta\text{-}TrCP}$ E3 ligase is not strictly required for Vpu-mediated CD4 degradation and, therefore, does not appear to constitute an essential early signal that triggers CD4 targeting to the cytosolic proteasome. Given that poly-ubiquitination of CD4 appears to be required for Vpu-mediated CD4 degradation (Fig. 1), our findings raise the possibility that ubiquitination may occur at sites other than cytosolic lysines. Consistent with this possibility, CD4 molecules lacking cytosolic lysine Ub acceptor sites (CD4 KRcyto) are still capable of undergoing ubiquitination in presence of Vpu, albeit to levels that are lower than wt CD4 (Fig. 4). One possible explanation for Vpu-mediated ubiquitination of cytosolic lysine-less CD4 is that a partial dislocation of the receptor N-termini to the cytosolic side may be required, so that lysine residues in the lumenal domain of CD4 may be accessible for ubiquitination by the cytosolic ubiquitination machinery recruited by Vpu. In that regard, in the specific case of HCMV US2-induced ERAD of MHC-I HC, the replacement of cytosolic tail lysine residues did not affect MHC-I HC dislocation and degradation while internal lysine residues were found to be required for these processes. These results have raised the possibility that US2 could induce a partial dislocation of part of the heavy chain into the cytosol, resulting in cytosolic deposition of lumenal lysine residues [43]. Although, this possibility cannot be completely excluded at this point for Vpu-mediated CD4 degradation, we believe that this scenario is unlikely since replacement of cytosolic lysine residues led to an attenuation of CD4 degradation and to a substantial decrease of CD4 ubiquitination by the $SCF^{\beta\text{-}TrCP}$ E3 ligase (Fig. 4); these observations suggests that Vpu-mediated CD4 degradation involves most probably ubiquitination of the receptor cytosolic tail.

An alternative explanation for the ubiquitination and degradation of cytosolic tail lysine-less CD4 molecules by Vpu is that ubiquitination may occur via non-lysine residues. Interestingly, recent evidence indicate that the mouse gamma herpesvirus (γ-HSV) mK3 E3 Ub ligase, which targets nascent MHC-I HC for degradation by ERAD, mediates ubiquitination via serine, threonine or lysine on the HC tail, each of which was found to be sufficient to induce rapid degradation of HC [44]. The γ-HSV mK3 E3 Ub ligase was found to have the ability to mediate the formation of ester bonds that covalently linked Ub to serine or threonine in the tail of the HC substrate. Unlike MIR 1 (also called kK3), an E3 ligase of Kaposi's sarcoma-

associated herpesvirus that requires cysteine residues to ubiquitinate MHC-I [45], a cysteine residue in the HC tail was not required for HC to be a substrate for mK3-induced ubiquitination and degradation. Interestingly, the CD4 cytoplasmic tail contains three serine, three threonine and four cysteine residues in addition to four lysines that could potentially serve as ubiquitin acceptor sites. Vpu-mediated ubiquitination of CD4 cytosolic tail at serine, threonine, cysteine or lysine ubiquitin acceptor sites would obviate the need for a partial dislocation of CD4 before ubiquitination and would suggest a vectorial exit of CD4 from the ER in presence of Vpu. On the basis of these novel findings, a systematic analysis of the role of cytosolic serine, threonine, cysteine and lysine residues in Vpu-mediated CD4 ubiquitination and degradation is warranted.

Our cell fractionation studies reveal that Vpu promoted dislocation of CD4 across the ER membrane since levels of poly-ubiquitinated CD4 molecules found associated with membrane and cytosolic fractions were found to be significantly increased in presence of Vpu (Fig. 5A–B). Furthermore, larger amounts of membrane-associated CD4-Ub conjugates, which likely represent exported ubiquitinated CD4 intermediates still attached to the cytosolic surface of the membrane, were recovered following salt wash treatment in presence of Vpu (Fig. 5D). These cytosolic- and membrane-associated poly-ubiquitinated CD4 molecules represent very likely substrates for the cytosolic 26 S proteasome. Importantly, the process underlying Vpu-mediated CD4 degradation appears to depend on the AAA ATPase Cdc48/p97 since over-expression of a TDN mutant of p97 inhibits efficiently the degradation of the receptor (Fig. 6). Although we cannot rule-out that the effect of the p97 TDN mutant might be indirect, we believe that this result combined with the subcellular fractionation studies provide evidence consistent with a model whereby Vpu targets CD4 for cytosolic proteasomal degradation by a process involving dislocation of the receptor across the ER membrane.

Our findings contrast in part with observations made by Meusser and Sommer in *S. cerevisiae* where they have reconstituted the process of Vpu-mediated CD4 degradation by expressing human CD4 together with Vpu and human β-TrCP [34]. They found that Vpu-mediated proteolysis of CD4 involved dislocation of ubiquitinated intermediates in the cytosol as we found in the present study. However, in their reconstituted biological system this process relied strictly on prior ubiquitination of CD4 at cytosolic lysine residues. Their findings based on data obtained in yeast display one basic difference compared to our results, which indeed suggest that the process of CD4 degradation mediated by Vpu involves a dislocation of CD4 across the ER membrane that is not entirely dependent on prior ubiquitination of CD4 at cytosolic lysine Ub acceptor sites. Even though cytosolic lysine-less CD4 molecules displayed a substantial reduction of Vpu-mediated ubiquitination, they were still substrate susceptible to Vpu-mediated degradation. This apparent discrepancy may reflect differences between human cells and yeast where indeed the CD4 receptor is not normally expressed. Indeed, human CD4, which is a stable protein when expressed in mammalian cells, was found to be rapidly degraded in yeast in the absence of Vpu. On the other hand, we cannot rule-out that Vpu-mediated degradation and ubiquitination of cytosolic lysine-less CD4 may indeed represent a forced pathway used by substrate having no available lysine residues in the cytoplasmic tail. Nevertheless, both studies provide evidence suggesting that Vpu-mediated ubiquitination of the CD4 cytosolic tail represents an early signal triggering dislocation of receptor molecules across the ER membrane for proteolysis by the cytosolic proteasome.

The recruitment of an E3 ubiquitin ligase complex by Vpu that is distinct from those used in classical ERAD raises the possibility that Vpu might target CD4 to a distinct ERAD pathway. Interestingly, three major pathways of ERAD are now emerging, including ERAD-C, ERAD-L and more recently ERAD-M [46-48]. These pathways, which were mostly characterized in *S. cerevisiae*, are involved in the degradation of substrates that display misfolded cytosolic, lumenal or transmembrane domains, respectively. Even though these pathways have been found to involve ER-associated dislocation and ubiquitination machineries of different protein composition, they all appear to rely on the presence of the Cdc48/p97 ATPase complex [49]. It is believed that the ERAD-M and ERAD-C pathways involve dislocation of substrate membrane-anchored portion to the cytosol before the lumenal domain whereas in the ERAD-L pathway the lumenal domain of the misfolded substrate is dislocated first through a channel before the membrane-anchored portion is released in the cytosol. The situation is thought to be similar in mammalian cells but less is known about the different protein complexes involved in the different ERAD pathways. Interestingly, the well-characterized degradation of MHC-I HC by the HCMV proteins US11 and US2 involve different protein complexes and distinct requirements for cytoplasmic lysine residues for dislocation, ubiquitination and degradation. Indeed, MHC-I HC degradation by HCMV US11 involves the recruitment of Derlin-1 [26,27] whereas US2 does not need this interaction to mediate degradation of MHC-I HC [26]. The specific ERAD pathway recruited by Vpu to target the CD4 receptor for degradation by the proteasome remains to be identified. More studies in this area will not only shed light on the molecular mechanism underlying Vpu-mediated CD4 degradation but will also

enhance our understanding of ER-associated protein quality control pathway in mammalian cells.

Conclusion

Our data provide evidence supporting a model whereby HIV-1 Vpu targets CD4 to the ubiquitin-proteasome degradative machinery by a process involving most likely poly-ubiquitination of the CD4 cytosolic tail by the $SCF^{\beta\text{-}TrCP}$ E3 ligase prior to dislocation of CD4 through the ER membrane. Given that lysine residues in the cytosolic domain of CD4 are not absolutely essential for ubiquitination and degradation of the viral receptor in presence of Vpu, there might be sites, other than lysines, that are also targeted during Vpu-induced CD4 ubiquitination.

Methods

DNA constructions

SVCMV CD4 was constructed by inserting a XbaI-XbaI cDNA fragment encoding CD4 into the corresponding sites of the expression vector SVCMV expa as described previously [50]. Plasmid pHIV CD4 KRcyto has already been described [24] and is a kind gift from Dr. Klaus Strebel (NIAID, NIH, Bethesda). The four cytoplasmic lysine residues of CD4 were replaced by arginines in pHIV CD4 KRcyto. pHIV CD4 was constructed by inserting a NheI-BamHI fragment from the CD4 cDNA derived from the pT4B expression plasmid [51] into the corresponding sites of pHIV CD4 KRcyto plasmid, thus creating the wild-type (wt) counterpart of pHIV CD4 KRcyto. The plasmid SVCMV CD4 KRcyto was constructed by subcloning a PCR-generated fragment from pHIV CD4 KRcyto into SVCMV CD4.

The Vpu expression plasmid, SVCMV Vpu has been described previously [52]. SVCMV Vpu S52,56/N expressing the corresponding Vpu substitution mutant was generated by PCR-based site-directed mutagenesis as described previously [53].

HxBH10-vpu$^+$ (LTR-gag$^+$, pol$^+$, vif$^+$, vpr$^-$, tat$^+$, rev$^+$, vpu$^+$, env$^+$, nef-LTR) and HxBH10-vpu$^-$ (LTR-gag$^+$, pol$^+$, vif$^+$, vpr$^-$, tat$^+$, rev$^+$, vpu$^-$, env$^+$, nef-LTR) are two isogenic infectious molecular clones of HIV-1 that differ only in their ability to express Vpu [16]. The phosphorylation mutant of Vpu, HxBH10-vpu S52,56/D, was created from HxBH10-vpu$^+$ using PCR-based mutagenesis. HxBc2-pr$^-$, vpu$^-$, env$^-$ was obtained by replacing the SalI-BamHI fragment of HxBc2-pr$^-$, vpu$^-$ [54] with the corresponding fragment from HxBc2-vpu$^-$, env-fs [55]. HxBH10-pr$^-$, vpu$^+$, env$^-$ was obtained by replacing the SalI-BamHI fragment of HxBH10-pr$^-$, vpu$^+$ with the corresponding fragment from HxBH10-vpu$^+$, env-fs [55].

The expression plasmids pCW7 and pCW8 encoding wt Ub and the Ub K48/R transdominant negative (TDN) mutant respectively, have been described previously [56] and were kindly provided by Dr. Ron Kopito (Department of Biological Sciences, Stanford University, Stanford). They both encode N-terminal his(6)/c-myc tagged forms of yeast Ub, which is almost identical to the mammalian counterpart. The plasmids encoding the FLAG-tagged versions of p97 wt and the TDN mutant p97AA were kindly provided by Dr. Martin Latterich (Faculty of Pharmacy, Université de Montréal, Montreal). The TDN p97AA mutant was described previously [40]. The nucleotide sequence of all plasmids was confirmed by automatic DNA sequencing.

Cell lines and transfections

SV40-transformed human embryonic kidney fibroblasts (HEK 293T) were obtained from the American Type Culture Collection (ATCC, Rockville, MD) and cultured in Dulbecco's modified Eagle medium (Wisent Inc., Saint-Bruno, QC) supplemented with 5% of fetal bovine serum (FBS) (Wisent Inc.) (DMEM+5%). For transfections, 100-mm petri dishes were seeded with 1 or 2 million cells and cultured overnight in DMEM+5%. Cells were then co-transfected with a mixture of the indicated DNA plasmids by the calcium-phosphate method.

Antibodies and chemical compounds

The anti-CD4 (OKT4) and anti-myc (9E10) monoclonal antibodies were derived from ascitic fluids of Balb/c mice that were injected with the OKT4 or 9E10 hybridoma respectively. The OKT4 and 9E10 hybridomas were obtained from the ATCC. Rabbit polyclonal anti-CD4 (CD4 H-370) antibodies were purchased from Santa Cruz Biotechnology Inc. (Santa Cruz, CA). Rabbit anti-Vpu serum was raised by immunization of rabbits with a synthetic peptide corresponding to amino acids 73–81 of the HIV-1 BH10 Vpu protein [9]. Rabbit polyclonal anti-actin, anti-calnexin and anti-FLAG (M2) antibodies as well as BFA were obtained from Sigma Chemical Co (Saint-Louis, MO). BFA was stored as a stock solution of 10 mM in ethanol at -20°C. MG-132 was purchased from Peptide International (Louisville, KY) and was stored as a 10 mM stock solution in DMSO at -20°C.

Metabolic labeling and radio-immunoprecipitation

Pulse-chase analysis of CD4 degradation experiments were all performed 48 hours post-transfection. Transfected cells were starved in methionine-free DMEM+5% in the presence of 10 μM BFA for 30 min before labeling. Cells were then pulse-labeled for 30 min with 800 μCi/ml of [^{35}S]methionine and [^{35}S]cysteine ([^{35}S] Protein Labeling mix, Perkin Elmer, Waltham, MA) and chased in complete DMEM+5% supplemented with 10 μM BFA. At the indicated time periods, radio-labeled cells were lysed in radio-immunoprecipitation assay (RIPA-DOC) buffer (140 mM NaCl, 8 mM Na_2HPO_4, 2 mM NaH_2PO_4, 1%

Nonidet-P40, 0.5% sodium dodecyl sulfate, 1.2 mM deoxycholate (DOC), pH 7.2) supplemented with a cocktail of protease inhibitors (Complete, Roche Diagnostics, Laval, QC). For CD4 degradation experiments where Vpu was expressed from HxBH10 provirus, no BFA was added since CD4 ER retention was achieved through HIV-1 Env glycoproteins.

CD4-Vpu binding experiments were performed 48 hours post-transfection. Transfected cells expressing CD4 and a phosphorylation mutant of Vpu (Vpu S52,56/N) were first starved in methionine-free DMEM+5% for 30 min. Cells were then labeled for 2.5 h with 400 μCi/ml of [^{35}S]methionine and [^{35}S]cysteine and lysed in CHAPS buffer (50 mM Tris, 5 mM EDTA, 100 mM NaCl, 0.5% CHAPS, pH 7.2) supplemented with a cocktail of protease inhibitors.

Following lysis, labeled protein lysates were sequentially immunoprecipitated with anti-CD4 OKT4 monoclonal antibodies only (for binding experiments) or a mixture of OKT4 and CD4 H-370 antibodies (for CD4 degradation experiments) and subsequently with a rabbit anti-Vpu serum as described previously [57]. When indicated, anti-myc antibodies (9E10) were mixed with anti-Vpu antibodies in order to detect his(6)/c-myc Ub fusion proteins. Immunoprecipitates were resolved on a 12.5% SDS-poly-acrylamide tricine gel and analyzed by autoradiography. Scanning of the autoradiograms was performed on an AGFA Duoscan T1200 scanner. Densitometric analysis of autoradiograms was performed with Image Quant 5.0 from Molecular Dynamics (Sunnyvale, CA).

Protein analysis by immunoprecipitation and western-blots

All experiments were performed 48 h post-transfections. For experiments using SVCMV expressor plasmids to express CD4 and Vpu proteins or experiments using protease and envelope deficient proviruses (HxBH10 pr$^-$, env$^-$), cells were pre-treated with 10 μM BFA for 2 h when indicated prior to lysis with 0.5%-1% Nonidet-P40 (10 mM Tris, 250 mM glucose, 1 mM EDTA, 0.5–1% Nonidet-P40, pH 7.6) for 30 min on ice. When HxBH10 was used to express Vpu, no BFA was added to the cells. Cell lysates were obtained after centrifugation at 10,000 g in a microcentrifuge for 30 min at 4°C. A sample of each lysate was run directly on 12.5% SDS-poly-acrylamide tricine gel. For detection of ubiquitinated CD4 conjugates, the remaining portion was immunoprecipitated with anti-CD4 polyclonal antibodies (CD4 H-370) and analyzed on an 8% SDS-poly-acrylamide tricine gel. Proteins were then electro-blotted over-night in a Bio-Rad Trans Blot Cell on a 0.45 μm pore size nitrocellulose membrane (Bio-Rad Laboratories, Mississauga, ON) and specific proteins were revealed by western-blotting using anti-CD4 polyclonal antibodies (1:1,000 dilution), anti-Vpu polyclonal antibodies (1:1,000 dilution), anti-actin polyclonal antibodies (1:1,200 dilution), anti-myc monoclonal antibodies (1:1,500 dilution) or anti-FLAG antibodies (1:2,000 dilution) diluted in PBS containing 0.02% sodium azide (NaN_3). Ubiquitinated forms of CD4 were revealed by western-blotting the membrane containing the anti-CD4 immunoprecipitates with anti-myc monoclonal antibodies. Bound antibodies were then probed with horse-radish peroxidase-linked anti-rabbit (1:7,000 dilution) or anti-mouse (1:6,000 dilution) antibodies, washed extensively and revealed using a standard enhanced chemiluminescence (ECL) detection system.

Cell fractionation and salt wash experiment

Forty-eight hours post-transfection, HEK 293T cells were treated with 10 μM BFA for 2 h, washed in cold PBS, resuspended in 500 μl of hypotonic buffer (10 mM Tris, 250 mM glucose, 1 mM EDTA) and incubated on ice for 30 min. Cells were then lysed mechanically with a type B Dounce homogeneizer on ice (70 strokes). Cell lysates were centrifuged twice at 250 g in a microcentrifuge at 4°C for 15 min to eliminate unlysed cells and then centrifuged at 10,000 g for 30 min at 4°C to isolate the membrane fraction. The supernatant (cytosolic fraction) was ultra-centrifuged at 100,000 g at 4°C for 1.5 h to eliminate remaining membrane contaminants and then adjusted with lysis buffer (10 mM Tris, 250 mM glucose, 1 mM EDTA, 4% Nonidet-P40, pH 7.6) to a final concentration of 1% Nonidet-P40. The pellet (membrane fraction) of the 10,000 g centrifugation was washed with the hypotonic buffer 4 times prior to lysis in 1% Nonidet-P40 lysis buffer. After lysis, a sample of each fraction was run directly on 12.5% SDS-poly-acrylamide tricine gel while the remaining portion was immunoprecipitated first with anti-myc 9E10 monoclonal antibodies before analysis on an 8% SDS-poly-acrylamide tricine gel. Analysis of proteins in lysates was performed as described above while detection of ubiquitinated CD4 conjugates was performed by western-blotting using anti-CD4 polyclonal antibodies. Polyclonal anti-calnexin antibodies were diluted 1:7,000.

For the salt wash experiment, the cytosolic fraction was discarded and the membrane fraction was either treated with 100 μl of Na_2CO_3 (100 mM, pH 11), NaCl (100 mM) or with RIPA-DOC lysis buffer during 10 min on ice. After treatment, samples were centrifuged at 10,000 g for 30 min at 4°C to isolate the membrane fraction (M) and the supernatant (S) was recovered and adjusted to a final volume of 1 ml with 1% Nonidet-P40 lysis buffer. The remaining membrane fraction was lysed with 1 ml of 1% Nonidet-P40 lysis buffer. Each fraction was then analyzed as described above.

Competing interests

The author(s) declare that they have no competing interests.

Authors' contributions

JB designed and performed all the experiments and contributed to the writing of the manuscript. MD provided reagents, participated in the design of some experiments and in the revision of the manuscript. JM participated in the execution of several experiments. DH and ML provided original reagents. EAC conceived the study, participated to data analysis and contributed to the writing of the manuscript. All authors read and approved the final manuscript.

Additional material

Additional file 1

Analysis of Vpu binding to CD4 wt or CD4 KRcyto. HEK 293T cells were mock-transfected, co-transfected with 1.5 μg of SVCMV CD4 wt or SVCMV CD4 KRcyto and 12 μg of a plasmid encoding a phosphorylation-defective Vpu mutant (SVCMV Vpu S52,56/N) or with 12 μg of SVCMV Vpu S52.56/N alone. Cells were labeled with [^{35}S]methionine and [^{35}S]cysteine, lysed and sequentially immunoprecipitated with anti-CD4 OKT4 monoclonal antibodies first to observe bound Vpu and then with anti-Vpu antibodies to recover the unbound Vpu proteins. B. Quantitative analysis of the bands in A showing the percentage of binding of CD4 KRcyto to Vpu S52,56/N relative to CD4 wt (arbitrary set at 100%). Error bars reflect standard deviations from duplicate independent experiments.

Click here for file
[http://www.biomedcentral.com/content/supplementary/1742-4690-4-75-S1.pdf]

Additional file 2

Salt-wash experiment controls. HEK 293T cells were mock-transfected or co-transfected with 1 μg of pHIV CD4 wt, 10 μg of envelope-defective provirus (HxBc2-pr$^-$, vpu$^-$, env or HxBH10-pr$^-$, vpu$^+$, env$^-$) and 15 μg of his(6)/c-myc-Ub K48/R expression plasmid where indicated. Cells were treated with BFA for 2 h prior to mechanical lysis. Membrane (M) were treated with either NaCl (pH 7.0) (panel A.) or RIPA-DOC (panel B.) as described in materials and methods. The treated membranes (M) and supernatants (S) were subsequently isolated by centrifugation. CD4-Ub conjugates were immunoprecipitated with anti-myc monoclonal antibodies prior to western-blot using anti-CD4 polyclonal antibodies whereas control proteins in each fraction were directly revealed by western-blot. Calnexin was used as a membrane-associated protein control. (asterisk) represents the area of the autoradiogram that we considered as poly-ubiquitinated CD4 molecules.

Click here for file
[http://www.biomedcentral.com/content/supplementary/1742-4690-4-75-S2.pdf]

Acknowledgements

We want to thank Klaus Strebel for kindly providing the pHIV CD4 KRcyto plasmid, and Ron Kopito for the kind gift of pCW7 and pCW8 ubiquitin expressors.

This work was performed by JB in partial fulfillment of her doctoral thesis and was supported by grants from the Canadian Institutes of Health Research (CIHR) (MOP-14228) and from the Fonds de la Recherche en Santé du Québec (FRSQ) to EAC. JB and MR are the recipients of studentships from the FRSQ and the CIHR strategic training program in cancer research, respectively. EAC holds the Canada Research Chair in Human Retrovirology.

References

1. Klatzmann D, Champagne E, Chamaret S, Gruest J, Guetard D, Hercend T, Gluckman JC, Montagnier L: **T-lymphocyte T4 molecule behaves as the receptor for human retrovirus LAV.** *Nature* 1984, **312:**767-768.
2. Levesque K, Finzi A, Binette J, Cohen EA: **Role of CD4 receptor down-regulation during HIV-1 infection.** *Curr HIV Res* 2004, **2:**51-59.
3. Levesque K, Zhao YS, Cohen EA: **Vpu exerts a positive effect on HIV-1 infectivity by down-modulating CD4 receptor molecules at the surface of HIV-1-producing cells.** *J Biol Chem* 2003, **278:**28346-28353.
4. Wildum S, Schindler M, Munch J, Kirchhoff F: **Contribution of Vpu, Env, and Nef to CD4 down-modulation and resistance of human immunodeficiency virus type 1-infected T cells to superinfection.** *J Virol* 2006, **80:**8047-8059.
5. Schwartz O, Dautry-Varsat A, Goud B, Marechal V, Subtil A, Heard JM, Danos O: **Human immunodeficiency virus type 1 Nef induces accumulation of CD4 in early endosomes.** *J Virol* 1995, **69:**528-533.
6. Willey RL, Bonifacino JS, Potts BJ, Martin MA, Klausner RD: **Biosynthesis, cleavage, and degradation of the human immunodeficiency virus 1 envelope glycoprotein gp160.** *Proc Natl Acad Sci USA* 1988, **85:**9580-9584.
7. Crise B, Buonocore L, Rose JK: **CD4 is retained in the endoplasmic reticulum by the human immunodeficiency virus type 1 glycoprotein precursor.** *J Virol* 1990, **64:**5585-5593.
8. Willey RL, Maldarelli F, Martin MA, Strebel K: **Human immunodeficiency virus type 1 Vpu protein regulates the formation of intracellular gp160-CD4 complexes.** *J Virol* 1992, **66:**226-234.
9. Cohen EA, Terwilliger EF, Sodroski JG, Haseltine WA: **Identification of a protein encoded by the vpu gene of HIV-1.** *Nature* 1988, **334:**532-534.
10. Strebel K, Klimkait T, Martin MA: **A novel gene of HIV-1, vpu, and its 16-kilodalton product.** *Science* 1988, **241:**1221-1223.
11. Huet T, Cheynier R, Meyerhans A, Roelants G, Wain-Hobson S: **Genetic organization of a chimpanzee lentivirus related to HIV-1.** *Nature* 1990, **345:**356-359.
12. Binette J, Cohen EA: **Recent advances in the understanding of HIV-1 Vpu accessory protein functions.** *Curr Drug Targets Immune Endocr Metabol Disord* 2004, **4:**297-307.
13. Maldarelli F, Chen MY, Willey RL, Strebel K: **Human immunodeficiency virus type 1 Vpu protein is an oligomeric type I integral membrane protein.** *J Virol* 1993, **67:**5056-5061.
14. Schubert U, Schneider T, Henklein P, Hoffmann K, Berthold E, Hauser H, Pauli G, Porstmann T: **Human-immunodeficiency-virus-type-1-encoded Vpu protein is phosphorylated by casein kinase II.** *Eur J Biochem* 1992, **204:**875-883.
15. Friborg J, Ladha A, Gottlinger H, Haseltine WA, Cohen EA: **Functional analysis of the phosphorylation sites on the human immunodeficiency virus type 1 Vpu protein.** *J Acquir Immune Defic Syndr Hum Retrovirol* 1995, **8:**10-22.
16. Terwilliger EF, Cohen EA, Lu YC, Sodroski JG, Haseltine WA: **Functional role of human immunodeficiency virus type 1 vpu.** *Proc Natl Acad Sci USA* 1989, **86:**5163-5167.
17. Klimkait T, Strebel K, Hoggan MD, Martin MA, Orenstein JM: **The human immunodeficiency virus type 1-specific protein vpu is required for efficient virus maturation and release.** *J Virol* 1990, **64:**621-629.
18. Varthakavi V, Smith RM, Bour SP, Strebel K, Spearman P: **Viral protein U counteracts a human host cell restriction that inhibits HIV-1 particle production.** *Proc Natl Acad Sci USA* 2003, **100:**15154-15159.
19. Schubert U, Clouse KA, Strebel K: **Augmentation of virus secretion by the human immunodeficiency virus type 1 Vpu protein is cell type independent and occurs in cultured human**

primary macrophages and lymphocytes. *J Virol* 1995, **69:**7699-7711.
20. Willey RL, Maldarelli F, Martin MA, Strebel K: **Human immunodeficiency virus type 1 Vpu protein induces rapid degradation of CD4.** *J Virol* 1992, **66:**7193-7200.
21. Bour S, Schubert U, Strebel K: **The human immunodeficiency virus type 1 Vpu protein specifically binds to the cytoplasmic domain of CD4: implications for the mechanism of degradation.** *J Virol* 1995, **69:**1510-1520.
22. Margottin F, Bour SP, Durand H, Selig L, Benichou S, Richard V, Thomas D, Strebel K, Benarous R: **A novel human WD protein, h-beta TrCp, that interacts with HIV-1 Vpu connects CD4 to the ER degradation pathway through an F-box motif.** *Mol Cell* 1998, **1:**565-574.
23. Fuchs SY, Spiegelman VS, Kumar KG: **The many faces of beta-TrCP E3 ubiquitin ligases: reflections in the magic mirror of cancer.** *Oncogene* 2004, **23:**2028-2036.
24. Schubert U, Anton LC, Bacik I, Cox JH, Bour S, Bennink JR, Orlowski M, Strebel K, Yewdell JW: **CD4 glycoprotein degradation induced by human immunodeficiency virus type 1 Vpu protein requires the function of proteasomes and the ubiquitin-conjugating pathway.** *J Virol* 1998, **72:**2280-2288.
25. Meusser B, Hirsch C, Jarosch E, Sommer T: **ERAD: the long road to destruction.** *Nat Cell Biol* 2005, **7:**766-772.
26. Lilley BN, Ploegh HL: **A membrane protein required for dislocation of misfolded proteins from the ER.** *Nature* 2004, **429:**834-840.
27. Ye Y, Shibata Y, Yun C, Ron D, Rapoport TA: **A membrane protein complex mediates retro-translocation from the ER lumen into the cytosol.** *Nature* 2004, **429:**841-847.
28. Gauss R, Sommer T, Jarosch E: **The Hrd1p ligase complex forms a linchpin between ER-lumenal substrate selection and Cdc48p recruitment.** *EMBO J* 2006, **25:**1827-1835.
29. Wiertz EJHJ, Tortorella D, Bogyo M, Yu J, Mothes W, Jones TR, Rapoport TA, Ploegh HL: **Sec61-mediated transfer of membrane protein from the endoplasmic reticulum to the proteasome for destruction.** *Nature* 1996, **384:**432-438.
30. Wiertz EJHJ, Jones TR, Sun L, Bogyo M, Geuze HJ, Ploegh HL: **The Human Cytomegalovirus US11 Gene Product Dislocates MHC Class I Heavy Chains from the Endoplasmic Reticulum to the Cytosol.** *Cell* 1996, **84:**769-779.
31. Yang M, Omura S, Bonifacino JS, Weissman AM: **Novel aspects of degradation of T cell receptor subunits from the endoplasmic reticulum (ER) in T cells: importance of oligosaccharide processing, ubiquitination, and proteasome-dependent removal from ER membranes.** *J Exp Med* 1998, **187:**835-846.
32. Furman MH, Loureiro J, Ploegh HL, Tortorella D: **Ubiquitinylation of the cytosolic domain of a type I membrane protein is not required to initiate its dislocation from the endoplasmic reticulum.** *J Biol Chem* 2003, **278:**34804-34811.
33. Shamu CE, Flierman D, Ploegh HL, Rapoport TA, Chau V: **Polyubiquitination is required for US11-dependent movement of MHC class I heavy chain from endoplasmic reticulum into cytosol.** *Mol Biol Cell* 2001, **12:**2546-2555.
34. Meusser B, Sommer T: **Vpu-mediated degradation of CD4 reconstituted in yeast reveals mechanistic differences to cellular ER-associated protein degradation.** *Mol Cell* 2004, **14:**247-258.
35. Fujita K, Omura S, Silver J: **Rapid degradation of CD4 in cells expressing human immunodeficiency virus type 1 Env and Vpu is blocked by proteasome inhibitors.** *J Gen Virol* 1997, **78(Pt 3):**619-625.
36. Chau V, Tobias JW, Bachmair A, Marriott D, Ecker DJ, Gonda DK, Varshavsky A: **A multiubiquitin chain is confined to specific lysine in a targeted short-lived protein.** *Science* 1989, **243:**1576-1583.
37. Ellison MJ, Hochstrasser M: **Epitope-tagged ubiquitin. A new probe for analyzing ubiquitin function.** *J Biol Chem* 1991, **266:**21150-21157.
38. Doolman R, Leichner GS, Avner R, Roitelman J: **Ubiquitin is conjugated by membrane ubiquitin ligase to three sites, including the N terminus, in transmembrane region of mammalian 3-hydroxy-3-methylglutaryl coenzyme A reductase.** *J Biol Chem* 2004, **279:**38184-38193.
39. Meyer HH, Shorter JG, Seemann J, Pappin D, Warren G: **A complex of mammalian ufd1 and npl4 links the AAA-ATPase, p97, to ubiquitin and nuclear transport pathways.** *EMBO J* 2000, **19:**2181-2192.
40. Ye Y, Meyer HH, Rapoport TA: **The AAA ATPase Cdc48/p97 and its partners transport proteins from the ER into the cytosol.** *Nature* 2001, **414:**652-656.
41. Ye Y, Meyer HH, Rapoport TA: **Function of the p97-Ufd1-Npl4 complex in retrotranslocation from the ER to the cytosol: dual recognition of nonubiquitinated polypeptide segments and polyubiquitin chains.** *J Cell Biol* 2003, **162:**71-84.
42. Mehle A, Strack B, Ancuta P, Zhang C, McPike M, Gabuzda D: **Vif overcomes the innate antiviral activity of APOBEC3G by promoting its degradation in the ubiquitin-proteasome pathway.** *J Biol Chem* 2004, **279:**7792-7798.
43. Hassink GC, Barel MT, Van Voorden SB, Kikkert M, Wiertz EJ: **Ubiquitination of MHC class I heavy chains is essential for dislocation by human cytomegalovirus-encoded US2 but not US11.** *J Biol Chem* 2006, **281:**30063-30071.
44. Wang X, Herr RA, Chua WJ, Lybarger L, Wiertz EJ, Hansen TH: **Ubiquitination of serine, threonine, or lysine residues on the cytoplasmic tail can induce ERAD of MHC-I by viral E3 ligase mK3.** *J Cell Biol* 2007, **177:**613-624.
45. Cadwell K, Coscoy L: **Ubiquitination on nonlysine residues by a viral E3 ubiquitin ligase.** *Science* 2005, **309:**127-130.
46. Huyer G, Piluek WF, Fansler Z, Kreft SG, Hochstrasser M, Brodsky JL, Michaelis S: **Distinct machinery is required in Saccharomyces cerevisiae for the endoplasmic reticulum-associated degradation of a multispanning membrane protein and a soluble luminal protein.** *J Biol Chem* 2004, **279:**38369-38378.
47. Vashist S, Ng DT: **Misfolded proteins are sorted by a sequential checkpoint mechanism of ER quality control.** *J Cell Biol* 2004, **165:**41-52.
48. Carvalho P, Goder V, Rapoport TA: **Distinct ubiquitin-ligase complexes define convergent pathways for the degradation of ER proteins.** *Cell* 2006, **126:**361-373.
49. Ismail N, Ng DT: **Have you HRD? Understanding ERAD is DOAble!** *Cell* 2006, **126:**237-239.
50. Yao XJ, Friborg J, Checroune F, Gratton S, Boisvert F, Sekaly RP, Cohen EA: **Degradation of CD4 induced by human immunodeficiency virus type 1 Vpu protein: a predicted alpha-helix structure in the proximal cytoplasmic region of CD4 contributes to Vpu sensitivity.** *Virology* 1995, **209:**615-623.
51. Maddon PJ, Littman DR, Godfrey M, Maddon DE, Chess L, Axel R: **The isolation and nucleotide sequence of a cDNA encoding the T cell surface protein T4: a new member of the immunoglobulin gene family.** *Cell* 1985, **42:**93-104.
52. Yao XJ, Gottlinger H, Haseltine WA, Cohen EA: **Envelope glycoprotein and CD4 independence of vpu-facilitated human immunodeficiency virus type 1 capsid export.** *J Virol* 1992, **66:**5119-5126.
53. Tiganos E, Friborg J, Allain B, Daniel NG, Yao XJ, Cohen EA: **Structural and functional analysis of the membrane-spanning domain of the human immunodeficiency virus type 1 Vpu protein.** *Virology* 1998, **251:**96-107.
54. Gottlinger HG, Dorfman T, Cohen EA, Haseltine WA: **Vpu protein of human immunodeficiency virus type 1 enhances the release of capsids produced by gag gene constructs of widely divergent retroviruses.** *Proc Natl Acad Sci USA* 1993, **90:**7381-7385.
55. Lavallee C, Yao XJ, Ladha A, Gottlinger H, Haseltine WA, Cohen EA: **Requirement of the Pr55gag precursor for incorporation of the Vpr product into human immunodeficiency virus type 1 viral particles.** *J Virol* 1994, **68:**1926-1934.
56. Ward CL, Omura S, Kopito RR: **Degradation of CFTR by the ubiquitin-proteasome pathway.** *Cell* 1995, **83:**121-127.
57. Tiganos E, Yao XJ, Friborg J, Daniel N, Cohen EA: **Putative alpha-helical structures in the human immunodeficiency virus type 1 Vpu protein and CD4 are involved in binding and degradation of the CD4 molecule.** *J Virol* 1997, **71:**4452-4460.